Titre: Title:	Improvement of the Reliability of Field Permeability Tests
Auteur: Author:	Lu Zhang
Date:	2018
Type:	Mémoire ou thèse / Dissertation or Thesis
Référence: Citation:	Zhang, L. (2018). Improvement of the Reliability of Field Permeability Tests [Thèse de doctorat, École Polytechnique de Montréal]. PolyPublie. https://publications.polymtl.ca/3183/

UNIVERSITÉ DE MONTRÉAL

IMPROVEMENT OF THE RELIABILITY OF FIELD PERMEABILITY TESTS

LU ZHANG

DÉPARTEMENT DES GÉNIES CIVIL, GÉOLOGIQUE ET DES MINES

ÉCOLE POLYTECHNIQUE DE MONTRÉAL

THÈSE PRÉSENTÉE EN VUE DE L'OBTENTION

DU DIPLÔME DE PHILOSOPHIAE DOCTOR

(GÉNIE MINÉRAL)

JUILLET 2018

UNIVERSITÉ DE MONTRÉAL

ÉCOLE POLYTECHNIQUE DE MONTRÉAL

Cette thèse intitulée :

IMPROVEMENT OF THE RELIABILITY OF FIELD PERMEABILITY TESTS

présentée par : ZHANG Lu

en vue de l'obtention du diplôme de : Philosophiae Doctor

a été dûment acceptée par le jury d'examen constitué de :

M. SILVESTRI Vincenzo, Ph. D., président

M. CHAPUIS Robert P., D. Sc. A., membre et directeur de recherche

M. MBONIMPA Mamert, Ph. D., membre

M. KARA Redha, Ph. D., membre externe

DEDICATION

I dedicate the dissertation to my family and Chao.

ACKNOWLEDGEMENTS

First of all, I would like to give my highest respect and appreciation to my supervisor Robert P. Chapuis. My Ph. D. study is coming to an end, but I can still clearly recall the first day I stepped into his office, where we talked my study situation and future plan for the first time. During the four years, he taught me easy ways to plot clear scientific graphs, helped me improve writing skills, answered my simple (sometimes maybe stupid) questions, encouraged me to attend conferences and competitions, and provided me various inspirations. He set a good model for my research career, meanwhile, gave adequate spaces for me to do research. I always received his gentle words and smiles, which encouraged me during the entire study. All of the guidance and memories are a great treasure to my life.

I also appreciate the jury members, Prof. Silvestri, Prof. Mbonimpa, and Mr. Kara for their time to read the dissertation and their useful comments. I am grateful to my colleague and co-author, Vahid Marefat, for his assistance in the lab and field tests, suggesstion and advices for the writing of the papers. My thanks also go to the technician of our Hydrogeology and Mining Environment laboratory, Noura, for preparing the test equipment. I am thankful to Prof. Li Li., my college and friend Pengyu, Ali, Karim, Dominique, my friends Wenxi and Shibo for your help and good times we spent.

I would like to thank the China Scholarship Council to provide the four-year financial support for my study. And many thanks to the Natural Sciences and Engineering Research Council of Canada (NSERC) for sponsoring the research on field equipment and field permeability tests.

I feel deeply indebted to all of my family members and friends far away in China, especially my dear parents Xiaolin Ma and Zexue Zhang, little brother Yu Zhang, and my best friends Xiao Yu and Yuanyuan Feng. Without your support and love, I cannot have peace of mind in my study abroad. I express my deep love and gratitude to my husband Chao Xu. Thanks for your care and support in daily life and during my study. You always bring laughters and happiness to me during the tough times, and back me up when I feel inconfident. Finally, thank you, my little special person, for giving me an opportunity to be a mom. You are such a surprise and impetus during the writing of my dissertation.

RÉSUMÉ

Les essais de perméabilité in situ sont faciles à réaliser dans un seul puits de surveillance (MW) et produisent peu de perturbation du sol in situ. Les valeurs de *K* locales in situ sont obtenues à partir de deux méthodes d'essais de perméabilité in situ, c'est-à-dire des tests à différence de charge constante (CH) et à différence de charge variable (VH). Pour les couches aquifères homogènes et isotropes, la valeur moyenne locale de *K* dans plusieurs puits peut être représentative de la valeur *K* du sol car l'effet d'échelle est négligeable. Les théories des méthodes d'essai et d'interprétation sont parvenues à maturité. Cependant, des opérations sur le terrain non idéales et des MWs mal installés peuvent produire des erreurs qui influent grandement sur les résultats des essais. Par conséquent, les valeurs *K* obtenues sont moins précises. Utiliser des valeurs *K* inexactes peut affecter l'évaluation de nombreux problèmes pratiques tels que les fuites et la stabilité des barrages, l'infiltration dans les champs d'épandage, le transport des contaminants dans les eaux souterraines etc. Par conséquent, l'étude s'est concentrée sur la quantification des conditions imparfaites qui n'ont pas été discutées auparavant et l'amélioration de la fiabilité des essais de perméabilité in situ, afin de fournir analytiquement, expérimentalement et numériquement des évaluations précises de la valeur *K*. Les imperfections ont été causées par des défauts d'étalonnage et de surveillance des transducteurs de pression, des directions opposées de l'eau traversant la zone d'injection d'eau, différents types d'essais et méthodes d'interprétation utilisés et des modèles numériques inappropriés.

Des essais de perméabilité in situ ont été effectués dans des puits de surveillance installés dans des nappes captives situés dans trois sites d'essai. Le premier site est un système aquifère à échelle réduite construit en laboratoire, homogène et isotrope. Il a un volume de 3.05 m x 2.44 m x 1.22 m et se compose d'une nappe libre supérieure, sus-jacent à un aquitard, et d'une nappe captive dans le fond. Un nombre total de 24 MWs a été installé dans l'aquifère de sable à nappe captive, qui n'ont pas de filtre installé autour de la crépine. Le second site est situé à Sorel-Tracy avec une superficie de 150 m x 150 m, hétérogène avec des stratifications compliquées en profondeur. Un puits de pompage et 44 MWs ont été installés dans l'aquifère de sable à nappe captive de 3.5 m d'épaisseur. La distance moyenne entre deux MWs est de 30 m à l'exception de la zone autour du puits de pompage. Le troisième site est à Lachenaie, qui contient neuf sites

d'étude avec trois types de MWs installés à différentes profondeurs des strates. Les MWs testés ont pénétré dans l'aquifère de roche de schiste à nappe captive à une profondeur de plus de 6 m.

Les essais CH, également connue sous le nom d'essais de débit constant, ont été effectués à l'aide d'une pompe péristaltique jusqu'à ce que le niveau d'eau dans le tuyau MW atteigne une stabilisation. Les essais VH ont débuté par le changement soudain d'un volume d'eau dans le tuyau et la réponse subséquente du niveau d'eau a été enregistrée dans le temps. La variation du niveau d'eau pendant les essais a été surveillée par une paire de transducteurs de pression absolue (PT) et de transducteur de pression atmosphérique (APT), qui sont des outils de surveillance plus précis et plus efficaces que d'autres outils de mesure. L'importance de l'étalonnage de PT seul a été bien reconnue, mais peu de chercheurs et de praticiens ont évalué l'importance de l'étalonnage et de la surveillance synchrone de la paire PT-APT. Les abaissements des essais CH et des différences de hauteur hydraulique des essais VH sont souvent obtenus par soustraction directe de la lecture courante PT (t) et du PT (*pré-test*) initial, ce qui revient à négliger la variation de pression d'air pendant l'essai.

Par conséquent, la thèse présente d'abord l'approche pour calibrer les transducteurs de pression sur le bureau des utilisateurs, afin d'évaluer leurs erreurs d'étalonnage systématiques. La paire PT-APT a ensuite été utilisée pour enregistrer les résultats d'essais CH et VH de courte durée dans 14 puits qui surveillaient la nappe captive à échelle réduite en laboratoire et un essai à niveau remontant de longue durée dans l'argile de Lachenaie. L'influence de la surveillance synchronisée pour la paire PT-APT, sur des données de test à court et à long terme a été quantifiée. Les résultats montrent que l'étalonnage doit être mis en œuvre pour chaque paire de PT et APT avant les essais in situ. A l'exception d'un test à charge variable très rapide, la fluctuation atmosphérique avec le temps joue un rôle important dans les résultats des essais, et donc le suivi synchronisé de la paire est nécessaire pour tous les essais.

Chaque essai de perméabilité in situ peut être réalisé avec un flux entrant de l'aquifère dans le MW ou sortant du MW vers l'aquifère, ce qui donne quatre types d'essais: les essais de décharge et d'injection (CH), et les essais à niveau montant et descendant (VH). Pour les MW parfaitement installés et développés, les mêmes valeurs de K devraient être données par des essais de deux écoulements opposés en raison de leurs mécanismes physiques identiques. Cependant, l'état de la crépine et du filtre peut empirer au fil du temps, après divers essais in situ et prélèvements d'eau

souterraine. Les théories ont été discutées précédemment mais les résultats pratiques des deux façons de conduire les essais CH et VH dans le même MW ont rarement été comparées par les praticiens. En outre, les gens comparaient et expliquaient rarement les deux méthodes d'essai communément utilisées: les essais de décharge et à niveau montant, et les essais d'injection et à niveau descendant du point de vue expérimental.

Dans la thèse, les essais d'injection et de décharge de type CH ont été effectués en injectant constamment de l'eau dans et en évacuant de l'eau à partir d'un seul MW, respectivement, pour générer une différence de charge hydraulique constante (état stationnaire). L'essai à niveau descendant a été effectué en ajoutant instantanément un volume d'eau, et pour un essai à niveau remontant, une écope ou une tige solide a été utilisée pour créer un déclin soudain du niveau d'eau. Tous les types d'essais ont été réalisés dans 33 puits de surveillance (MW) installés dans les trois sites. Les résultats des essais avec les flux entrants et sortants de divers cas indiquent des écarts dans les valeurs *K* pour le même MW. Bien que les MW aient été développés peu après leur installation, un certain colmatage de l'écran/du filtre ou de l'érosion interne du filtre/ du sol adjacent se produit pendant les essais. De plus, les *K* (essai CH), fréquemment inférieurs aux *K* (essai VH), sont considérés comme plus précis car l'essai CH implique un plus grand volume de sol et dure plus longtemps. Des recommandations pratiques ont également été fournies pour le choix de la méthode d'essai.

Dans certains cas de terrain, les praticiens n'ont pas accordé suffisamment d'attention au mécanisme de départ de l'essai VH: ils ont négligé le changement soudain de colonne d'eau et fait une analyse VH de la phase de récupération après une période de pompage relativement longue (essai CH). Les méthodes de Hvorslev et du graphique de vitesse, qui sont utilisées pour interpréter l'essai VH, ont été utilisées pour analyser ces données de récupération. L'application a donné deux résultats anormaux: (1) la forme du graphe de vitesse est dispersée ou courbe au lieu d'être droite, et (2) les valeurs K_{VH} déterminées par les méthodes d'interprétation d'essai VH ne sont pas équivalentes aux valeurs K_{CH} par la méthode d'interprétation d'essai CH (solution de Lefranc). La thèse a théoriquement prouvé que les méthodes d'interprétation pour l'essai VH sont applicables aux données de l'essai de récupération après un essai CH. Les anomalies dans le graphique de vitesse et les différences dans les valeurs K_{CH} et K_{VH} sont dues à une mauvaise installation des MWs. Pour deux cas de MW bien installés, le diagramme de vitesse présentait des droites et les valeurs de K_{CH} et K_{VH} étaient très proches.

En variante, les essais de perméabilité in situ peuvent être réalisés de manière numérique, ce qui permet de visualiser et de quantifier les propriétés de l'écoulement et du flux au cours d'un essai à tout moment. Fréquemment, le rayon d'influence du MW est inconnu, ce qui entraîne des difficultés à définir la distance radiale limite *R* du modèle de l'aquifère. Une valeur *R* élevée peut ne pas être représentative car le taux de pompage pour un essai à CH dans des conditions de terrain est faible et le rayon d'influence sera donc faible. Cela augmente aussi considérablement le temps de calcul car le drainage non saturé prend beaucoup de temps. De plus, les facteurs de forme numérique (*c*) dans la littérature précédente ont été obtenus pour les conditions d'équilibre de l'essai CH seulement, et dans des conditions saturées uniquement, alors que les essais CH et VH sont effectués dans la pratique dans des zones saturées et parfois non saturées.

Ainsi, les moyens numériques pour simuler les essais CH et VH dans les nappes libres via le code d'éléments finis Seep/W ont été présentés, car les nappes libres présentent un fort potentiel de contamination. Les valeurs *c* ont été déduites numériquement en régime permanent et transitoire (soit pour un essai CH ou VH), en considérant l'écoulement non saturé de l'aquifère. L'essai CH a atteint l'état d'équilibre après une condition transitoire, qui a été simulée de deux façons: on a appliqué soit une différence de charge constante soit un débit constant comme condition aux limites de la crépine. L'essai VH était totalement en état transitoire. Deux séries de modèles d'aquifères équipés de MW ont été analysées et comparées; les MWs ont soit un filtre ou non. En outre, les influences de la distance radiale limite de la limite externe, les dimensions et les positions de la zone d'injection d'eau, et les types de matériaux aquifères sur les valeurs numériques *c* ont été étudiées. Les valeurs *R* représentatives pour chaque type de modèle d'essai ont également été déterminées.

ABSTRACT

Field permeability tests are easy to be performed in a single monitoring well (MW) and yield little disturbance to in-situ soil. The local *K* values in situ are obtained from two methods of field permeability tests, i.e., constant-head (CH) and variable-head (VH) tests. For homogeneous and isotropic aquifer layers, the average local values of *K* in several wells can be representative of the *K* value of the soil because the scale effect is negligible. The theories of the test and interpretation methods are mature; however, non-ideal field operations and poorly installed MWs may yield some errors, which greatly influence the test results. As a result, the derived *K* values are less accurate. Using inaccurate *K* values may affect the assessment in many practical problems like seepage and stability of dams, infiltration from disposal fields, contamination transport in groundwater etc. Therefore, the study focused on quantifying imperfect conditions which have not been discussed before and improving the reliability of the field permeability tests, in order to analytically, experimentally and numerically provide accurate assessments for the *K* value. The imperfections were caused by incorrect calibration and monitoring of pressure transducers, opposite directions of water flowing through the water injection zone, different test types and interpretation methods we used, and inappropriate numerical models.

Field permeability tests were conducted in monitoring wells installed in confined aquifers located in three test sites. The first site is a reduced-scale aquifer system built in the laboratory, which is homogeneous and isotropic. It has a volume of 3.05 m x 2.44 m x 1.22 m and consists of an upper unconfined aquifer, overlying an aquitard, and a confined aquifer in the bottom. A total number of 24 MWs were installed in the confined sand aquifer, which have no filter pack installed around the screen. The second site is located in Sorel-Tracy with an area of 150 m x 150 m, which is heterogeneous with complicated stratifications in depth. A pumping well and 44 MWs were installed in the confined sand aquifer of 3.5 m in thickness. The average distance between two MWs is 30 m except for the area around the pumping well. The third one is in Lachenaie, which contains nine study sites with 3 types of MWs installed at different depths in the strata. The tested MWs penetrated in the confined shale rock aquifer by a depth over 6 m.

The CH tests, also known as constant flow rate tests, were performed using a peristaltic pump until the water level in the MW pipe reached stabilization. The VH tests were started by the sudden change of a volume of water in the pipe and the subsequent water level response was

recorded against time. The variation in water level during the tests was monitored by a pair of absolute pressure transducer (PT) and atmospheric pressure transducer (APT), which are more accurate and efficient monitoring tools compared to other measurement approaches. The importance of calibration of PT alone has been well recognized, however, few researchers and practitioners valued the importance of calibration and synchronous monitoring of the PT-APT pair. The drawdowns of the CH tests and hydraulic head differences of the VH tests are often obtained by the direct subtraction of current PT (*t*) and the initial PT (*pre-test*), which means that the variation in air pressure is neglected during the test.

Therefore, the thesis first presents the approach to calibrate the pressure transducers on users' desk, in order to assess their systematic calibration errors. The PT-APT pair was then used to register test data during short-duration CH and VH tests performed in 14 wells monitoring the reduced-scale confined aquifer in the lab and a long-duration rising-head test in Lachenaie clay. The influence of synchronized monitoring for the PT-APT pair, on short- and long-term test data, was quantified. The results show that the calibration must be implemented for each pair of PT and APT before the field tests. Except for a very rapid variable-head test, the atmospheric fluctuation with time plays a significant role in the test results, and thus the synchronized monitoring of the pair is necessary for all tests.

Each test method of the field permeability tests can be carried out with either an inward flow from aquifer to pipe or outward flow from pipe to aquifer, which yields four test types: discharge and injection tests (CH), and rising- and falling-head tests (VH). For perfectly installed and developed MWs, same *K* values should be given by tests of two opposite flows due to their identical physical mechanisms. However, the condition of the well screen and filter pack may deteriorate over time, after various field tests and groundwater samplings. The theories were discussed previously but the practical results of the two ways to conduct the CH- and VH-tests have been rarely compared by the practitioners in the same MW. In addition, people rarely compared and explained the two commonly used test methods: discharge and rising-head tests, and injection and falling-head tests from the experimental aspect.

In the thesis, CH injection and discharge tests were performed by constantly injecting water into and discharging water from a single MW, respectively, to generate a constant hydraulic head difference (steady state). The falling-head test was conducted by instantaneously adding a volume

of water and for a rising-head test, a bailer or solid rod was used to create a sudden water level decline. All types of tests were conducted in 33 monitoring wells (MWs) installed in the three sites. The test results with inward and outward flows of various cases indicated discrepancies in K values for the same MW. Although the MWs were developed soon after their installation, some clogging of the screen/filter pack or internal erosion of the filter pack/adjacent soil occurs during the tests. Moreover, the K values (CH tests), frequently lower than the K values (VH tests), are considered to be more accurate because the CH test involves a larger soil volume and lasts longer. Some practical recommendations were also provided for the choice of test method.

In some field cases, the practitioners did not pay enough attention to the mechanism of the VH test: they neglected the sudden change in water column and considered the recovery phase after a relatively long pumping period (a CH test) as a VH test. The Hvorslev and velocity graph methods, which are used to interpret the VH test, were employed to analyze those recovery data. The application yielded two abnormal results: (1) the shape of the velocity graph is scattered or curved instead of being straight, and (2) the K_{VH} values determined by the VH test interpretation methods are not equivalent to the K_{CH} values by the CH test interpretation method (Lefranc's solution). The thesis theoretically proved that the interpretation methods for the VH test are applicable to the CH recovery test data. The abnormality in velocity plot and discrepancies in K_{CH} and K_{VH} values were found to be due to the poor installation of MWs. For two cases of MWs in good conditions, the velocity plot presented straight lines and the values of K_{CH} and K_{VH} were very close.

Alternatively, the field permeability tests can be performed in numerical ways, by which the seepage and flux properties during a test at any time may be visualized and quantified. Frequently, the influence radius of the MW is unknown, which causes difficulties in defining the boundary radial distance R of the aquifer model. A large R value may not be representative because the pumping rate for a CH test in field conditions is small and thus the influence radius will be small. It also greatly increases the computation time because unsaturated drainage takes a very long time. Additionally, the numerical shape factors (c) in previous literature were obtained for steady-state conditions of the CH test only, and for saturated conditions only, however, both CH and VH tests are performed in practice and for geometries with unsaturated seepage.

Thus, the numerical ways to simulate the CH and VH tests in unconfined aquifers via the finite element code Seep/W were presented, because the unconfined aquifers have a high potential for being contaminated. The *c* values were deduced numerically under steady- and transient-states (either for a CH or VH test), considering unsaturated seepage of the aquifer. The CH test reached steady-state after a transient condition, which was silumated in two ways: applied with either a constant head difference or a constant flow rate as the boundary condition of the screen. The VH test was totally in transient condition. Two series of aquifer models equipped with MWs were analyzed and compared; they either have a filter pack or not. Additionally, the influences of boundary radial distance of the external boundary, dimensions and positions of the water injection zone, and aquifer material types on the numerical *c* values were studied. The representative *R* values for each type of test model were also determined.

TABLE OF CONTENTS

LIST OF TABLES

LIST OF FIGURES

LIST OF SYMBOLS AND ABBREVIATIONS

a	Constant
A	Summation over the area of an element
A	Dimensionless coefficient determined by a function of L/r_w
APT	Atmospheric pressure transducer
b	Thickness of confined aquifer, saturated thickness of unconfined aquifer (m)
b	Constant
B	Dimensionless coefficient determined by a function of L/r_w
[*B*]	Gradient matrix
c	shape factor (cm or m)
C	Coefficient of consolidation, parameter equals S_{inj}/c.
[*C*]	Element hydraulic conductivity matrix
C	Dimensionless coefficient determined by a function of L/r_w
C_U	Coefficient of uniformity
CH	Constant-head
d	Diameter of MW pipe/borehole casing, distance from water level to the bottom of the water injection zone (mm or cm)
d_{10}	Effective size/ size at 10% passing (cm)
d_{60}	Size at 60% passing (cm)
D	Diameter of the cavity/water injection zone (cm)
D_a	Average diameter of the tapered cavity/water injection zone (cm)
e	Void ratio
f	Slope
h	Hydraulic head (cm or m)

H	Apparent hydraulic head difference, mean head difference of two consecutive measurements (cm or m)
$\{H\}$	Vector of nodal heads
dH, ΔH	Increment of head difference
H_1, H_2, H_3	Three different applied hydraulic head difference
H_c	Constant hydraulic head difference between the initial and stabilized piezometric levels in the well, applied hydraulic head (m)
H_e	Head at end of time increment (m)
H_i	Initial hydraulic head difference, head at the initiation of time increment (cm or m)
H_0	Piezometric error (cm or m)
H_j, H_{j+1}	Two consecutive head difference measurements (cm or m)
H_p	Limit of hydraulic head difference (m)
H_r	Real hydraulic head difference (cm or m)
K	Hydraulic conductivity (cm/s or m/s)
$[K]$	Element characteristic matrix
K_1	Hydraulic conductivity of the screen (m/s)
K_2	Hydraulic conductivity of the filter materials (m/s)
K_{23}	Hydraulic conductivity of the created filter zone (m/s)
K_3	Hydraulic conductivity of the soil (m/s)
K_{sat}	Saturated hydraulic conductivity (cm/s or m/s)
K_{CH}	Hydraulic conductivity calculated by the interpretation method of CH test (Lefranc's solution) (m/s)
K_{VH}	Hydraulic conductivity calculated by the interpretation methods of VH test (m/s)
K_{VH1}	Hydraulic conductivity calculated by the semi-log graph method (m/s)

K_{VH2}	Hydraulic conductivity calculated by the velocity graph method with the entire velocity plot (m/s)
K_{VH2}'	Hydraulic conductivity calculated by the velocity graph method with the straight portion of velocity plot (m/s)
K_{VH3}	Hydraulic conductivity calculated by the optimized semi-log graph method (m/s)
L	Length of cavity/water injection zone, summation over the edge of an element (cm or m)
m_w	Slope of θ versus u_w:
$[M]$	Element mass matrix
MW	Monitoring well
$<N>$	Vector of interpolation function
P, P_1, P_2	Slope
PL	Piezometric level
PT	Pressure transducer
Q	Constant pumping/discharge/injection flow rate, steady-state outflow rate (m^3/s)
$\{Q\}$	Element applied flux vector
Q_e	Nodal flux at end of the time increment (m^3/s)
Q_{inj}	Water flow rate into the pipe/borehole casing (m^3/s)
Q_s, Q_{soil}	Water flow rate through the injection zone/soil (m^3/s)
r	Distance from the center of pumping well to the center MW or piezometer (m)
r_1, r_2	Distance from the center of pumping well to the center of MW1 and MW2 (m)
r_c	Radius of MW pipe/borehole casing (cm)
r_w	Radius of cavity/water injection zone (cm)
R	Boundary radial distance (m)
R_0	Radius of influence (m)

s	Drawdown (m)
s_1, s_2	Drawdowns in MW1 and MW2 (m)
Δs	Drawdown difference per log cycle of t (m)
s'	Residual drawdown (m)
$\Delta s'$	Residual drawdown difference per log cycle of t/t' (m)
S	Storativity, surface area of the injection zone
S_{inj}	Cross-sectional area of MW pipe/borehole casing (cm^2)
S_s	Specific storativity
t	Elapsed time (s)
t_j, t_{j+1}	Two consecutive time measurements (s)
dt, Δt	Increment of time (s)
t'	Time from the beginning of recovery test (s)
t_i	Initial time (s)
T	Transmissivity (m^2/s), time factor
u, u_w	Pore water pressure (kPa)
Δu	Excess pore water pressure (kPa)
u_i	Initial pore water pressure (kPa)
v	Relative velocity calculated by two consecutive measurements (m/s)
V	Steady-state outflow volume (m^3)
VH	Variable-head
W(u)	Well function of pumping period
W(u')	Well function of residual period
z	Elevation (m)
δ_0	Mean systematic error of the pressure sensor (cm)

θ	Volumetric water content
γ_w	Unit weight of water (kN/m^3)
λ	Ratio of horizontal and vertical hydraulic conductivities, storage term for a transient seepage equals to $m_w\gamma$

CHAPTER 1 INTRODUCTION

1.1 Context and motivation

Hydraulic conductivity, *K*, represents the ability of water moving through porous materials (Todd and Mays, 2005). Three ways including empirical approaches, laboratory experiments, and in-situ tests are normally used to obtain the saturated *K* value. To estimate the hydraulic conductivity empirically, many predictive equations were proposed based on the grain size distribution, porosity and other properties of the soil, reviewed by Chapuis (2012a). In the laboratory, the saturated *K* values of granular soils can be determined with either a constant or falling head test in a rigid-wall or flexible-wall (triaxial cell) permeameter. The detailed specifications are included in ASTM standards (ASTM D2434, 2006; ASTM D5084, 2016). The pumping and field permeability tests are performed to evaluate the in-situ *K* values.

Knowledge of the in-situ *K* values of aquifers is critical for many hydrogeological, geotechnical, and environmental problems, such as seepage through dams and their foundations, infiltration from disposal fields, and monitoring groundwater contamination (Chapuis, Soulié and Sayegh, 1990). Pumping test is considered to be the most reliable test to estimate the hydraulic conductivity due to its slightest disturbance in soil properties in the field (Todd and Mays, 2005). It is performed by constantly discharging a pumping well and observing the water level in the controlled well and several piezometers at different distances (e.g., Chapuis 1999a; Kruseman and Ridder, 1994). However, a pumping test is not always justified or even possible. If there is only a single monitoring well (MW), piezometer or borehole casing, the local hydraulic conductivity may be determined by field permeability tests of constant-head (CH) and variable-head (VH). The *K* values assessed by different types of tests may provide different values due to the scale effect. For homogeneous aquifer, however, the scale effect is insignificant and can be neglected (Chapuis et al., 2005a; Dallaire, 2004).

The research focuses on the field permeability tests in monitoring wells (MWs), which is easier to be achieved than the pumping test. Although the theories of the tests are well developed, the field manipulation details can significantly affect test results (Canadian Geotechnical Society, 1985; Chapuis et al., 1990; Milligan, 1975). Thus, the research dedicates effort to studying the

effects of several error sources on the derived hydraulic conductivities and providing practical recommendations to improve the reliability of the field permeability tests.

CH and VH tests were conducted in the monitoring wells installed in a large sand box (a reduced-scale aquifer system) and two field sites in Sorel and Lachenaie. All tests were conducted with two opposite water flows. The water flowing from aquifer to well pipe was defined an inward flow, caused by a water withdrawal from the MW. The injection of water into the pipe generates an outward water flow from pipe to aquifer. The screens of the MW pipe are located in the confined aquifer layer, where the pore water pressure is greater than the atmospheric pressure.

The water level position versus time during a test is registered by an absolute pressure transducer (PT) and an atmospheric pressure transducer (APT). The PT measures the total pressure acting on its sensor, including the water column and atmospheric pressure above the sensor. To obtain the true water column height above the sensor, the barometric pressure obtained by an APT should be subtracted from the PT reading. The transducer converts water or barometric pressure into a height of water column, and the built-in datalogger outputs the registered data in the unit of cm directly.

The calibration method for different PT-APT pairs is firstly proposed, to assess their accuracy. The influence of the variations in barometric pressure on the derived K value during short-term tests in a sand aquifer is then examined. Additionally, the influence on the recovery of a long-term rising-head test in clay is analyzed.

The CH tests were performed by discharging or injecting a single constant flow rate from or into the riser pipe until the water level reaches stabilization. After shutting off the pump, the water level in the riser pipe slowly returned to the pre-test static water level. The pumping rates were automatically controlled by the peristaltic pump and monitored using a burette and a stopwatch during the test. The CH tests with outward and inward water flows were termed injection and discharge tests, respectively. Water-level rises and drawdowns were registered by a pair of PT and APT every 15 seconds.

Compared to the continuously constant water flow, the VH tests (slug tests), were initiated with a sudden change of water volume in the pipe by a quick addition (falling-head) or removal (rising-head) of water, and the subsequent water level response was recorded over time. However, some practitioners were not aware of this “sudden” water level change. They considered the recovery

period after a long-time groundwater sampling/discharging (CH test) as a VH test and employed the interpretation methods of VH tests to analyze the recovery test data. The abnormalities in test plots aroused our interest. Therefore, *K* values interpreted by CH and VH solutions were compared, where the discrepancies indicate a poor installation of MW. Moreover, the connections between the interpretation approaches for VH and CH tests were explained.

In the project, the falling-head test was conducted by quickly adding a volume of water. The rising-head test was started with a solid rod in the reduced-scale sand aquifer and Sorel site, and a bailer in Lachenaie site. The PT and APT were synchronized to take readings with a 2-second interval.

The theories of the field permeability test method have been well-developed. The CH test data were interpreted by the Lefranc's solution (CAN/BNQ 250-135, 2014) to obtain the local *K* values, which may be different from the hydraulic conductivity in a large scale (AFNOR NF P94-132, 2000). The time-drawdown method (Cooper and Jacob, 1946) was used to interpret the transient state of the CH test for which equilibrium had not been reached. The VH test data were interpreted using the semi-log graph method (Hvorslev, 1951). If the semi-log plot is curved, the piezometric correction must be made by the velocity graph method (Chapuis, Paré and Lavallée, 1981) or the *Z-t* method (Chiasson, 2005, 2012). The *K* values obtained from different tests and interpretation methods were compared and discussed.

Theoretically, injection and discharge tests should provide close *K* values, so do falling- and rising-head tests, because the manipulations and physical mechanisms of each two types of the tests are identical except that the water flow directions are opposite. If sediments at the bottom of the pipe are carried by an outward flow, clogging of the well screen may occur and thereby decrease the permeability of soil. Also, erosion may appear in the gravel pack resulting from an inward flow that carries fine particles, and hence a higher *K* value is attained. To check the possibility of these situations, the tests with opposite flows were conducted in succession, and the *K* values were compared.

The two types of field permeability tests in unconfined aquifers were modelled with the finite element code Seep/W, to study the seepage property and numerical values of shape factors, *c*, in the target aquifer. The code solves the seepage and conservation equations based on functions related to the pore water pressure. The models are axisymmetric, where the soil, filter material,

and pipe are homogeneous and isotropic. The unsaturated portions were fully defined for all materials. The lower boundaries of the unconfined aquifers were impervious, and the screen and far boundary conditions were specified for various cases.

The numerical simulation of CH tests was achieved in two ways, to apply either a constant head difference or a constant flow rate on the screen. The steady-state and transient analyses of the CH test were studied, whereas the entire VH test was in the transient state. Four variables including 11 boundary radial distances, 15 different soils properties, 4 different lengths of water injection zones, 3 different positions for the water injection zones were analyzed, to study their influences on the *c* values derived from the numerical CH and VH tests. Additionally, numerical *c* values were compared with the theoretical ones.

1.2 Research question and objectives

Despite the development, all field operations yield not-so-perfect conditions. If the monitoring wells or the field operations are not perfect, the hydraulic conductivity obtained is less accurate. The imperfections like hydraulic fractures, hydraulic short circuits, clogging, piezometric errors, selection of shape factors, etc. contribute to the inaccurate estimation of hydraulic properties of the aquifer. In addition, the errors caused by pressure transducers, opposite directions of water flows, different test types and interpretation methods may affect the reliability of test results. Therefore, it is essential to check these errors and remove or minimize them, in order to improve the reliability of field permeability tests.

The research is a continuous improvement to previous research on the reliability of the field permeability tests. It aims to study and quantify non-ideal conditions that have not been discussed and to provide practical recommendations and accurate assessments for the hydraulic parameters from experimental, analytical and numerical aspects.

To achieve the goal, several specific objectives are listed as follows,

1. Remove the systematic error caused by barometric variation during the test by calibrating and synchronously monitoring each PT-APT pair.

2. Examine how the PT-APT calibration and synchronous monitoring, during a test, influences the test data accuracy and the resulting *K* value.

3. Check the conditions of the screen and filter pack by conducting the field permeability tests of two opposite flows (i.e., rising- and falling-head tests, discharge and injection tests) in each MW.

5. Find the reason for the discrepancy of *K* values between CH and VH tests in the same MW by studying the connection of the interpretation methods of the two types of tests.

4. Verify the reliability of field hydraulic conductivity by comparing the results of CH and VH tests and provide practical recomendations for the choice of test method.

6. Simulate the CH and VH tests via numerical code, through which numerical values of shape factors of various cases are evaluated and the proper boundary radial distance of the aquifer model are determined.

1.3 Dissertation structure

The dissertation consists of seven chapters. Chapter 1 introduced the background of the research, based on which the objectives were proposed. Chapter 2 will present a critical review of previous work most related to the research. Chapter 3 will be devoted mainly to the description of the influence of barometric calibration and PT pair monitoring on the field permeability tests. Chapter 4 will compare CH and VH tests with two opposite flow directions in the confined aquifers of three different sites, which indicates the condition of screen clogging and filter pack erosion. Chapter 5 will provide theoretical and experimental evidence of the application of VH interpretation methods on the CH recovery tests. Chapter 6 will focus on the assessment of numerical shape factors under various conditions via the numerical code. Chapter 7 will provide a general discussion on the results. The last Chapter 8 will draw a conclusion for the entire study and discuss the limitations to provide useful inspirations for future research.

CHAPTER 2 LITERATURE REVIEW

2.1 Pressure transducer calibration

The three major types of sensors to gauge the water level in wells were sorted as float recorders, pressure transducers, and acoustic devices (Ritchey, 1986). Due to the limitation of traditional water level measuring devices (floats and acoustic devices) in small diameter (≤ 10 cm) wells, the potential of the application of electrical pressure transducers in water level measurement was initially proposed by Shuter and Johnson (1961). Afterwards, different types of pressure transducers based on the electrical method were designed and evaluated by researchers (e.g., Clark, Germond and Bennett, 1983; Holbo, Harr and Hyde, 1975; MacVicar and Walter, 1984; Keeland, Dowd and Hardegree,1997), in order to determine the pressure on the submerged stationary probe. Combined with electronic data recorders, the pressure transducers have been developed to be capable of collecting continuous water level or pressure data from wells (Freeman et al., 2004). A pressure transducer linked to a data logger or display device can be used in an aquifer test in the open well and is necessary for the test in a closed well where manual measuring method is unable to provide frequent measurements (ASTM D4044, 2015). It provides rapid measurements of water-level variations and can be programmed to register at different frequencies.

Down and Williams (1989) mentioned that if individual calibration for the pressure transducer is not carried out, large measurement errors will occur due to the unique response characteristics of each transducer. Their datalogger gave voltage outputs for the soil suction measurements. The calibration curve was plotted as suction versus millivolt sensor output, which is a linear response with a correlation coefficient of 1.0. The similar calibration process was implemented in the laboratory by Keeland et al. (1997) for the measurements of water levels in wells. The laboratory and field calibrations displayed straight calibration lines with correlation coefficients close to 1.0. Freeman et al. (2004) and ISO (2009) established guides on selection, installation, and operation of the submersible pressure transducers. Freeman et al. (2004) introduced various types of pressure transducers, used in wells, piezometers, soil-moisture tensiometers, and surface water gages, in the application of water resources. They pointed out the source of errors in commonly-used linear calibrations and proposed a temperature-corrected transducer calibration which

reduces residual error to 0.03% of full-scale output or less. It was suggested that users should recalibrate the PTs and determine their performance before exploiting them in the field. ISO (2009) specified in the scope of automated pressure transducer methods in measuring the water level in a well based on the work of Freeman et al. (2004). The calibration procedure for the individual pressure transducer is the same as previously mentioned.

For an absolute pressure transducer used in field permeability test, the real water column is the subtraction of barometric pressure from the total pressure measured. The necessity of calibration of individual pressure transducers was well recognized. ASTM D4050 (2014) regulated that the single pressure sensor should be checked before using in the field by raising and lowering a measured distance in the well. Meanwhile, the verification of the sensor readings periodically with a steel tape is required. However, little literature valued the significance of barometric pressure in the calibration process of the pressure transducer. Chapuis (2009a) indicated that atmospheric pressure is one of the reasons to affect the accuracy of the readings of pressure sensors. The noteworthy variations in barometric pressure have been mentioned in the test of checking accuracy and drift properties of pressure transducers, and it was pointed out that an industry-wide standard should be developed (Sorensen and Butcher, 2011). Zhang, Chapuis and Marefat (2015, 2018a) used field permeability test data in sand and clay to show the important influence of calibration and synchronous monitoring of atmospheric pressure on the water level measurements.

2.2 In-situ tests for soil permeability

In situ, the field permeability tests in a single well, piezometer, or borehole casing (AFNOR NF P94-132, 1992; ASTM D4044, 2015; CAN/BNQ 2501-135, 2501-130, 2014; ISO 22282-2, 2012) yield the local hydraulic conductivity, *K*. On a larger scale, the hydraulic parameters of transmissivity *T* and storativity S are determined by a pumping test, where a pumping well and several piezometers/ monitoring wells are needed to measure the water levels (Chapuis, 1999a; Kruseman, 1994; Todd and Mays, 2005). Compared to the laboratory tests, in-situ or field tests for soil permeability involve a larger soil volume and consider the macrostructure effects better (Olson and Daniel, 1981). As a result, they are preferred for saturated soils. In-situ tests for permeability were classified in several different ways, and the same test may have altered names. They are summarized herein to avoid confusing the readers.

2.2.1 Aquifer tests

The pumping and slug tests are collectively called aquifer test in textbooks of hydrogeology (Fetter, 2001; Istok and Dawson, 1991). The term “aquifer test”, in a narrow sense, refers in particular to the pumping test. In pumping tests, groundwater is either pumped into or from the pumping well at a constant flow rate, which corresponds to an injection or withdrawal test (ASTM D4050, 2014), shown in Figure 2.1a and b. When the pump is stopped, the water levels in the pumping well and piezometers start to return to the original water levels before the test, which is a recovery test. It provides reliable test data and examines the results of the pumping test independently (Kruseman, 1994). If the pumping rate is increased periodically, it is a step-drawdown test, which is able to assess the well performance (Istok and Dawson, 1991; Kruseman 1994) and evaluate the hydraulic conductivity when each step reaches equilibrium (Zhang et al., 2015).

The slug test, as its name suggests, is performed by abruptly adding or removing of a slug of water in a single injection or withdrawal well and water levels in the well are monitored subsequently, which corresponds to the slug injection and withdrawal test, respectively (Istok and Dawson, 1991). The sudden change of water volume can also be achieved by quick insertion or removal of a mechanical “slug,” or rapid increase or decrease of air pressure in the well (Chapuis, 2012b). Several ways to initiate a slug test were discussed in ASTM D4044 (2015). The slug test has overdamped or underdamped responses of water level, depending on the water mass in the well and the hydraulic properties of the aquifer (Van der Kamp, 1976). In overdamped cases (Chapuis, 1998; Cooper, Bredehoeft and Papadopulos, 1967; Hvorslev, 1951), the water level returns to equilibrium in an approximately exponential way after slugging. If the water level oscillates around the equilibrium level, the test is underdamped, which yields transmissivity and storativity (Kipp, 1985; Ross, 1985; Uffink, 1984; Van der Kamp, 1976) or only K values (McElwee, 2001; McElwee and Zenner, 1998; Zurbuchen, Zlotnik and Butler, 2002). The slug test was also called variable-head (VH) test in geotechnical engineering (e.g., Cassan, 2005; Chapuis, 1999b; Chapuis and Chenaf, 2003a; Monnet, 2015; Reynolds, 2015).

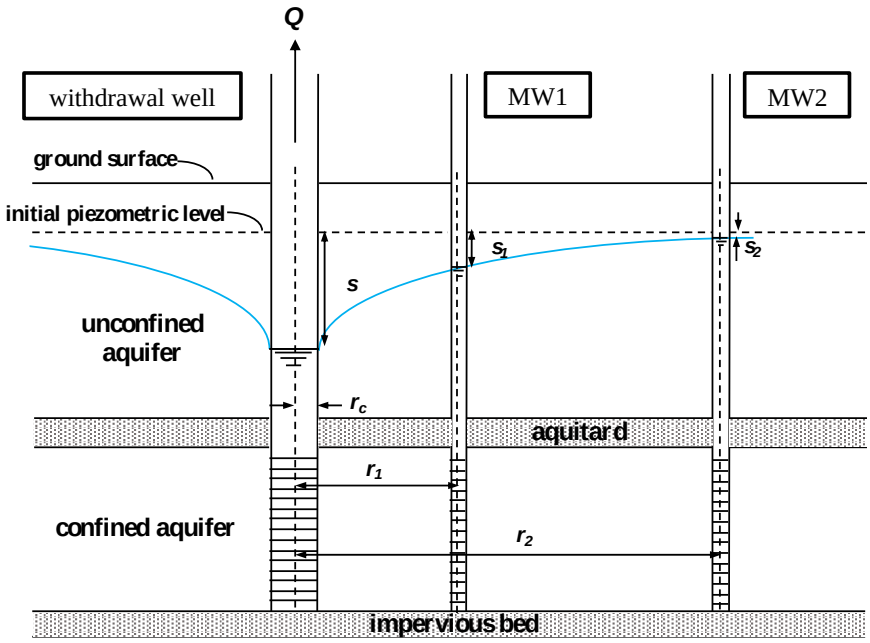

(a) withdrawal test

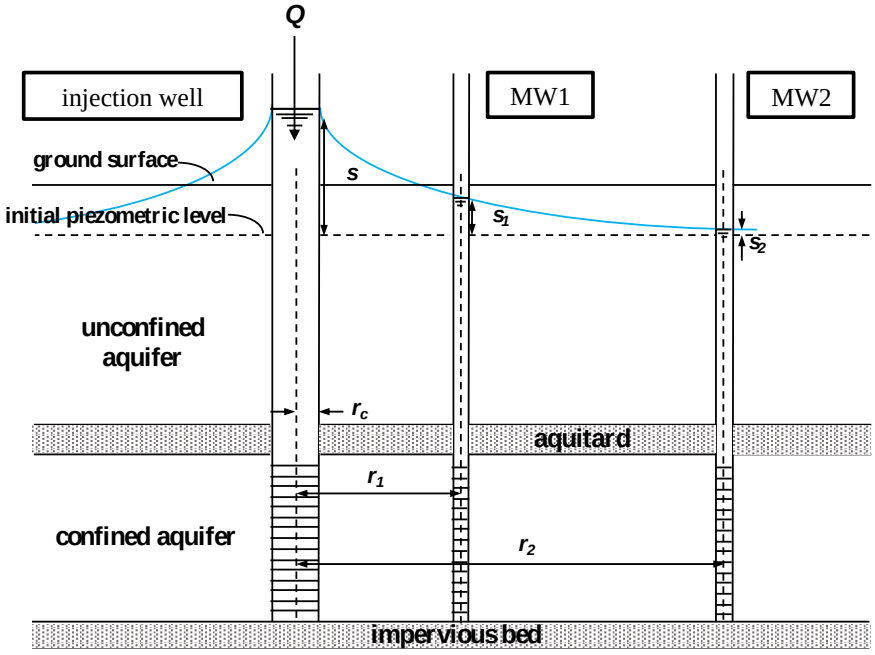

(b) injection test

Figure 2.1: Schematic of pumping tests

For the tight formations that have very low permeabilities, the duration of pumping test is inordinately long. The slug test was suggested and its duration can be shortened by using a pipe

of small radius (Bredehoeft and Papadopulos, 1980). However, the radius will be too small to put into practice if the permeability of the formation is extremely low, like the tightly compacted clays, shales, basalts, and salt formations that are used for the disposal of hazardous wastes. Several modified slug test methods were provided to shorten the test duration by pressurizing a volume of water into the formation (Bredehoeft and Papadopulos, 1980; Neuzil, 1982).

2.2.2 Field permeability tests

The constant-head (CH) and variable-head (VH) tests in casing borehole were first proposed by the French civil engineer Lefranc (1936, 1937), known as the Lefranc test. It is a reliable test method to obtain the local *K* value when the pumping test is not available for homogeneous and isotropic aquifers (Houti's course note), included in several textbooks (Cassan, 1980, 2005; Monnet, 2015) and the French, International and Canadian standards (AFNOR NF P94-132, 1992, 2000; CAN/BNQ 2501-135, 2014; ISO 22282-2, 2012). It was also used to assess the groutability of the soil ground (Bell, 2004; Cambefort, 1987) and the anisotropy coefficient of the aquifer (Cassan, 2000; Lafhaj and Shahrour, 2004).

The test consists of generating a water flow with a constant or variable water head into a cavity of a given shape, named lantern, at the bottom of a borehole and observing the variations of the water level (Cassan, 2005). Three methods of the Lefranc test were described in the Canadian standard (CAN/BNQ 2501-135, 2014): 1) the constant-head test; 2) the variable falling-head test; 3) the variable rising-head test. The first way to conduct a constant-head (CH) test is to add or remove water continuously to maintain a constant water level in the well casing until the flow rate becomes nearly constant (Cassan, 2005; Monnet, 2015). It is easier to do the test with a constant flow rate, which is the second way to achieve a constant head difference, sometimes also called a constant-rate test (Cassan, 2005; ISO 22282-2, 2012). The two ways of the CH test are presented in Figures 2.2a, b. The CH tests of injecting and discharging at a constant rate until an equilibrium is reached were named CH injection and discharge tests (Zhang, Chapuis and Marefat, 2018b). The variable-head (VH) test herein is equivalent to the previously mentioned slug test initiated by filling or removing the water in the drill casing. The falling- and rising-head tests refer to slug-injection (baildown or slug-out) and slug-withdrawal (slug-in) tests, respectively. The variable-head test was not applicable in highly pervious formations in previous

times because the test is so fast that manual measurements may be impossible to take. With the pressure transducer, which is able to record with 0.5s intervals, the test is achievable.

Besides the borehole casing (Chapuis, 2001; Chapuis and Chenaf, 2003a), the CH and VH test methods could also be applied in driven permeameters (Chapuis and Chenaf, 2010), monitoring wells/piezometers (e.g., Chapuis, 1998; Zhang et al., 2018a, b), or double-packer permeameters (Mathias and Butler, 2007). The water of tests in driven casing seeps through either the end of the drill casing (CAN/BNQ 2501-130, 2014) or the cylindrical gravel pack below the driving shoe (CAN/BNQ 2501-135, 2014). They were collectively named the field permeability tests. Compared to the aquifer pumping test, the implementation of the CH test is faster and necessary equipment is reduced, and the test can be done as the geotechnical investigation progresses. However, it is less popular, which may be because that it has not been standardized in the US.

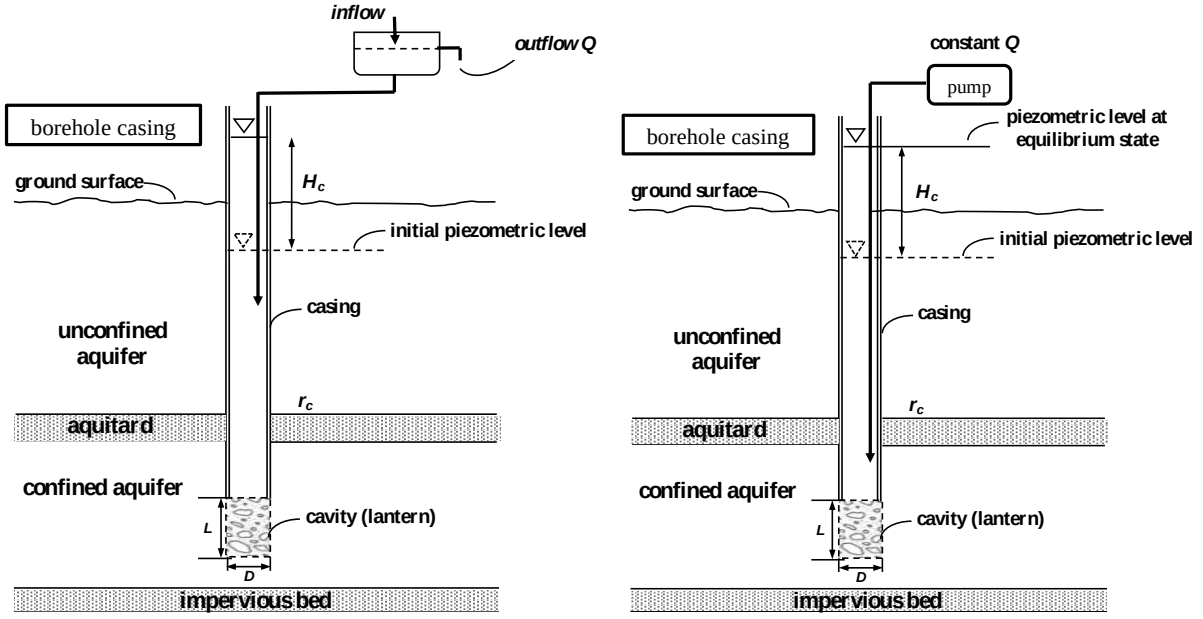

(a) maintain a constant hydraulic head until reach a steady-state flow

(b) inject water at a constant rate until reach a constant head (constant-flow test)

Figure 2.2: Two ways to conduct the CH test

2.3 Field permeability test interpretation

2.3.1 Results of the field permeability test

ISO 22282-2 (2012) illustrated three examples of the test results for the CH tests conducted in two ways and the VH tests. Figure 2.3 (a) presents the results of a CH test performed with a water injection at a constant flow rate. After some time, the hydraulic head of the test stabilizes. In fact, when injecting, there is a fairly rapid variation in the head while the water has not yet begun to permeate into the soil. Then the flow remains constant gradually, and the head increases or decreases regularly to stabilize at a level so that the flow through the wall of the cavity is equal to the injected flow, which indicates that steady state is reached (Cassan, 2005). If the CH test is conducted by discharging water constantly, the plot will have a constant drawdown instead of the rising water head. Figure 2.3 (b) displays three plots of CH tests conducted by applying three different constant hydraulic heads. The volume of water supplied or extracted are registered against time until the steady-state flow is achieved. The flow rate, the slope of the *V-t* curve, becomes constant after some variations. The VH test results are given in Figure 2.4, which refers to a falling-head test because the hydraulic head is decreasing with time. The head of a variable rising-head test increases with time.

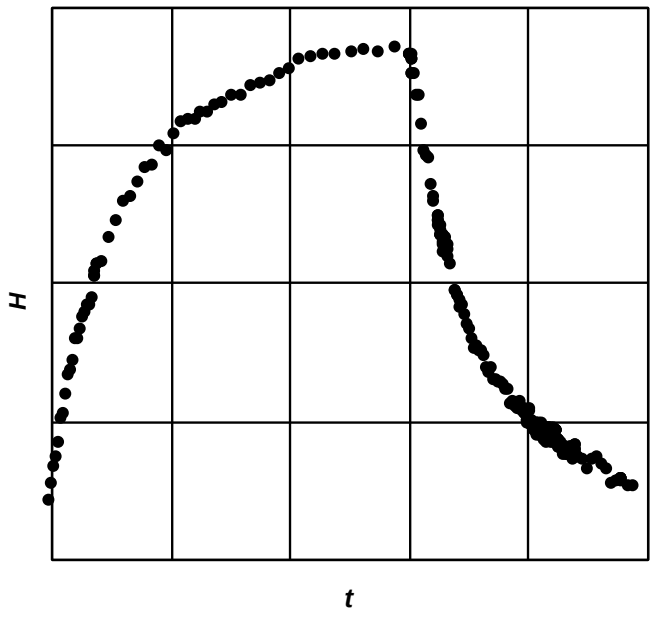

(a) a constant-head test by injecting water at a constant rate

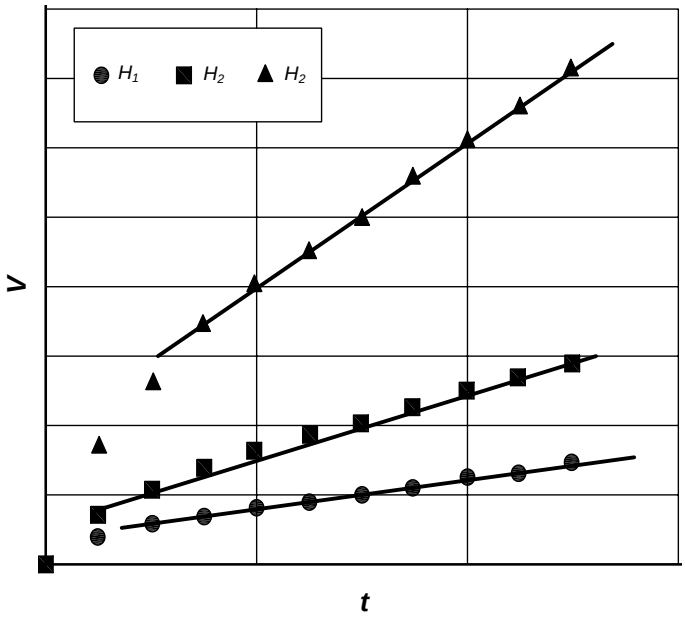

(b) constant-head tests by maintaining three constant hydraulic heads (from ISO 22282-2 2012)

Figure 2.3: Examples of test results of constant-head tests

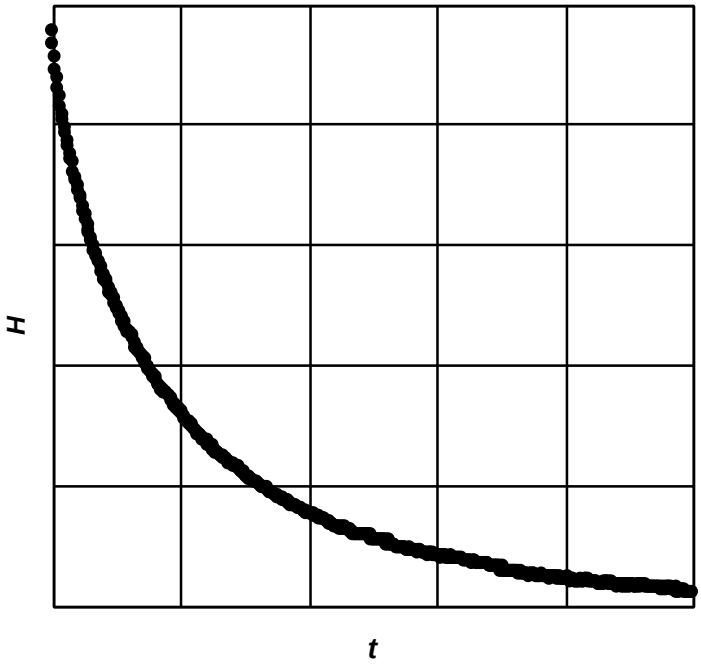

Figure 2.4: Example of test result of a variable-head test (from ISO 22282-2 2012)

2.3.2 Interpretation for constant-head test in granular soils

2.3.2.1 Lefranc's solution

The solution of the CH test at steady state was given by Lefranc (1936, 1937), which was referred by many researchers (e.g., United States Bureau of Reclamation, 1960, 1990; Benabdallah, 2010; Cassan 1980, 2000, 2005; Chapuis, 1999b, Chapuis et al. 1990; Dhouib et al., 1998; Lafhaj, 1998; Lafhaj and Shahrour 2002a, 2006; Rat, Laviron and Jorez, 1970) and normalized in several standards (AFNOR NF P94-132, 2000; CAN/BNQ 2501-135, 2014; ISO 22282-2, 2012).

The general equation of the field permeability test in steady state is similar to Darcy's, expressed as

$$Q = Q_s = cKH_c \tag{2.1}$$

where Q is the constant flow rate for the CH test that injects or discharges at a constant rate (Figure 2.2b), equal to the flow rate of water through the injection zone Q_s when the test reaches equilibrium, c is the shape factor, and H_c is the constant head difference between the initial and stabilized piezometric levels in the well.

The saturated hydraulic conductivity is then determined:

$$K = \frac{Q}{cH_c} \tag{2.2}$$

For the CH test that maintains a constant water level, the steady-state outflow rate Q (Figure 2.2a) can be calculated by the steady-state outflow volume V and the corresponding elapsed time t:

$$Q = \frac{V}{t} \tag{2.3}$$

The Equation 2.2 can be rewritten as:

$$K = \frac{V}{cH_c t} \tag{2.4}$$

2.3.2.2 ISO 22282-2 method

The constant-head test can be repeated at different hydraulic heads, for example, H_1, H_2, and H_3. Three constant flow rates are reached as a result. If the test is perfect, the plot of constant flow rates and their corresponding head differences is linear (Figure 2.5). The slope P can be used to calculate the hydraulic conductivity.

$$P = cK \tag{2.5}$$

$$K = \frac{P}{c} \tag{2.6}$$

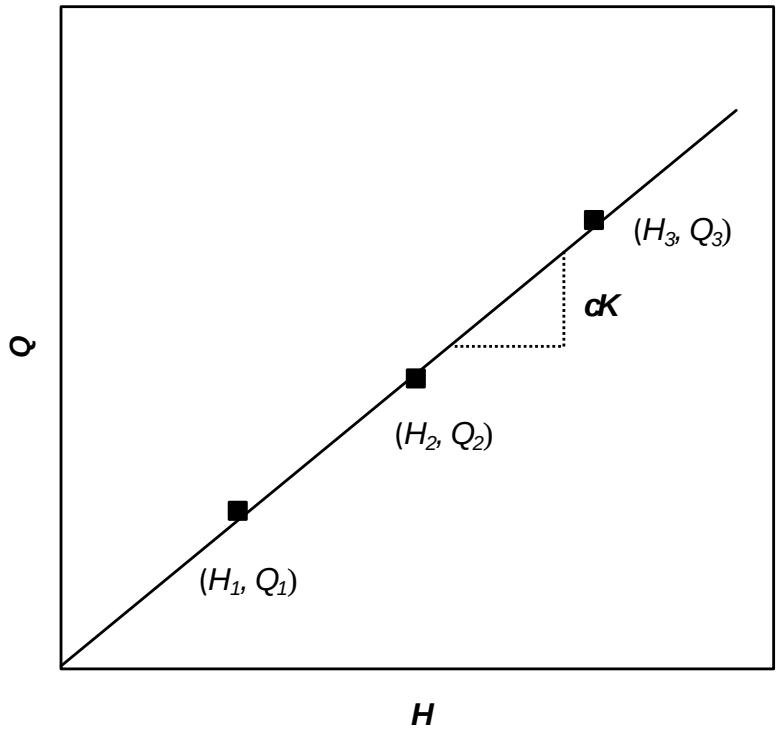

Figure 2.5: Infiltrated water amount depending on the pressure difference

2.3.2.3 Theoretical curve method

According to Cassan (2005), the transient phases including the injection/discharge and recovery of the CH test with a constant flow rate can also be interpreted.

Injection or discharge phase

The flow rate through the wall of the cavity Q_s has found to be related to the applied hydraulic head H as follows:

$$Q_s = cKH \tag{2.7}$$

It is, however, not equivalent to the constant discharge or injection rate Q in transient state. During the test, the variation dH of the water level in the well pipe with an internal cross-section area of S_{inj} during time dt corresponds to the movement of a volume of water:

$$(Q - Q_s)dt = S_{inj}\,dH \tag{2.8}$$

Substituting Equation 2.7 into Equation 2.8, we have:

$$S_{inj}\frac{dH}{dt} + cKH = Q \tag{2.9}$$

It is the differential equation that governs the flow in transient state, which is rewritten as:

$$\frac{dH}{\frac{cKH}{S_{inj}} - \frac{Q}{S_{inj}}} = -dt \tag{2.10}$$

Integrating both sides from time t_i and the head H_i, Equation 2.10 becomes:

$$H = \frac{Q}{cK} + \left(H_i - \frac{Q}{cK}\right)\cdot e^{\left[-\frac{cK}{S_{inj}}(t-t_i)\right]} \tag{2.11}$$

The hydraulic head H of the cavity reaches a limit of $H_p = Q/(cK)$ when t tends to infinity, which indicates that the representative curve of Equation 2.11 has an asymptote parallel to the x-axis. Therefore, the asymptote corresponds to the steady state where the injection/discharge rate is equivalent to the water flow absorbed/supplied by the soil. When the time and head are taken at the time we start the pump, i.e., t_i and H_i equal 0, Equation 2.11 is simplified to:

$$H = \frac{Q}{cK}\left(1 - e^{\left(-\frac{cK}{S_{inj}}t\right)}\right). \quad (2.12)$$

It is observed that the ordinate of the asymptote is still $H_p = Q/(cK)$, and the slope of the tangent at the origin is calculated as Q/S_{inj}.

The sign of the exponential factor in Equation 2.11, $\left(H_i - \frac{Q}{cK}\right)$, determines the position of the curve of Equation 2.11. When $H_i > Q/(cK)$, the curve is above the asymptote, which corresponds to a discharge phase and the recovery of an injection test. The curve is below the asymptote when $H_i < Q/(cK)$, representing the injection phase and the recovery of the discharge test.

Recovery phase

The recovery phase after the steady state represents a test at zero flow after stopping the constant flow. Because $Q = 0$, Equation 2.11 becomes:

$$H = H_i e^{\left[-\frac{cK}{S_{inj}}(t - t_i)\right]} \quad (2.13)$$

where H_i and t_i refer to the water head in the well pipe and the time, respectively, at the moment the pump stops. Obviously, $H_i > Q/(cK)$, the recovery curve represented by Equation 2.11 locates above its asymptote, the abscissa.

With the theoretical curves of the injection/discharge (Equations. 2.11 and 2.12) and its recovery phases (Equation 2.13), the interpretation of the test is then to adjust the theoretical curve on the experimental points of coordinates (H, t) by varying different K values, to find a curve that superposes on the test data.

If the adjustment is unsuccessful, it is because the test is not representative or has been disturbed by clogging or washing. Cassan (2005) illustrated several unsuccessful cases and their solutions.

2.3.2.4 Relative velocity curve method

Another way to interpret the transient state of a CH test with a constant flow rate is based on graphical treatment, called relative velocity curve method (Cassan, 2005).

Injection or discharge phase

It is noted from Equation 2.8 that the relative velocity of the water flow in the well pipe, with respect to the flow rate through the wall of the cavity, is:

$$v = \frac{Q - Q_s}{S_{inj}} = \frac{dH}{dt} \tag{2.14}$$

The ratio Q/S_{inj} represents the maximum instantaneous velocity of the water in pipe, from the start-up of the pumps, even before the water movement into the soil begins. Therefore, the initial velocity $v_i = Q/S_{inj}$ at time $t = 0$ for a zero head. The differential equation (Equation 2.10) can then be written as:

$$v = v_i - \frac{cK}{S_{inj}} H \tag{2.15}$$

where the relative velocity v and the corresponding head H during dt are calculated by two consecutive measurements:

$$H = \frac{H_{j+1} + H_j}{2} \tag{2.16}$$

$$v = \frac{H_{j+1} - H_j}{t_{j+1} - t_j} \tag{2.17}$$

The representative curve of Equation 2.15 indicates the relative speed as a function of the head H, which is a straight line with a slope of cK/S_{inj}, x-intercept of Q/cK and y-intercept *of* v_i (Figure 2.6a). Alternatively, the hydraulic head can also be plotted as a function of the relative velocity (ISO 22282-2, 2012), shown in Figure 2.6b.

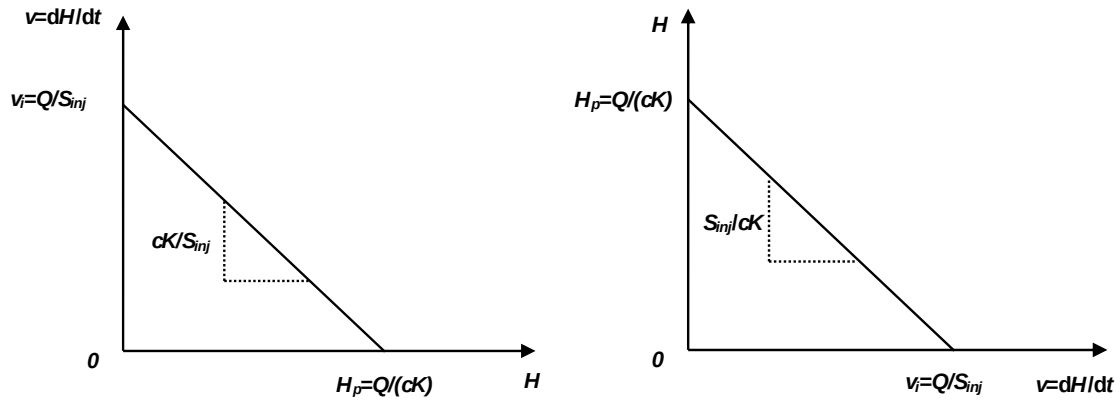

(a) the plot of H versus v (b) the plot of v versus H

Figure 2.6: The relative velocity curve

As a result, it allows the calculation of K from the abscissa value and the slope of the straight line in Figure 2.6. It is necessary to proceed the double evaluations, which should give the same results. If not, it is because the test has been disturbed. When the relative velocity is zero, it means that the discharge/injection flow rate is equal to the flow rate percolating into the soil, thus the abscissa value of the line corresponds to the steady state.

If the test is carried out correctly, the plotted pairs of data are located on a straight line. If the last points are located on an upwards curved graph, it can mean that some particles were washed out. If a clogging has occurred during the test, the last points are located on a downwards curved graph (ISO 22282-2, 2012).

Recovery phase

The study of the recovery curve allows another graphical assessment of the K value. As soon as the pump is stopped, the hydraulic head, which has reached a maximum value of H_p, begins to dissipate and the injection/discharge flow rate becomes zero. As $Q = 0$, the initial velocity $v_i = 0$ in Equation 2.15, we then have

$$v = -\frac{cK}{S_{inj}} H \tag{2.18}$$

Due to the cancellation of the injection/discharge flow, the relative velocity v in Equation 2.18 also refers to the water velocity through the soil. In a range of head from H_i to 0, the velocity

varies within the limits between $-\frac{cK}{S_{inj}}H_i$ and 0. The velocity is therefore always negative, which is indicative of a direction change for the water velocity. But to avoid negative ordinates, the absolute value is normally used:

$$v = \frac{cK}{S_{inj}}H \tag{2.19}$$

Thus, the curve of the *v* versus *H* is, theoretically, a straight line passing through the origin. The *K* value is determined from the slope $\frac{cK}{S_{inj}}$

2.3.2.5 Time-drawdown equation

Injection or discharge phase

If the observation is made only in a single well, during the unsteady state of the pumping test, *T* and *S* are possible to be attained by the drawdown-time curve of Cooper and Jacob (1946). Theis (1935) initially solved the unsteady state flow problems in fully penetrating wells in confined aquifer based on the analogy between groundwater flow and heat conduction (Todd and Mays, 2005),

$$s = \frac{Q}{4\pi T}W(u) \tag{2.20}$$

where *s* is the drawdown, *T* is transmissivity, W(*u*), termed the well function, is an exponential integral function of *u*, which was solved in the 18th century after Euler (Chapuis, 1999a)

$$W(u) = Ei(u) = -\gamma - \ln u + \left(\frac{u}{1\cdot 1!}\right) - \left(\frac{u^2}{2\cdot 2!}\right) + \left(\frac{u^3}{3\cdot 3!}\right) - \left(\frac{u^4}{4\cdot 4!}\right)\cdots \tag{2.21}$$

and the parameter *u* is a function corresponding to the storativity *S*, transmissivity *T*, time *t*, and distance *r* from the pumping well

$$u = \frac{r^2 S}{4Tt} \tag{2.22}$$

A type curve is then obtained by plotting the *W(u)* versus *u* on logarithmic paper. Rewriting Equation 2.22 as

$$\frac{r^2}{t} = \frac{4T}{S}u \tag{2.23}$$

Comparing Equations. 2.20 and 2.23, it is observed that the relation between *s* and r^2/t is similar to that between W(*u*) and *u*. Therefore, the values of *S* and *T* are estimated by the superposition of the drawdown *s* (at time *t* and distance *r*) versus r^2/t to the type curve. The method was included in the US standard ASTM D4106 (2015).

Based on Theis's equation, Cooper and Jacob (1946) provided a simpler graphical method to solve Equation 2.17. For small values of *u*, the drawdown can be approximated by:

$$s = \frac{Q}{4\pi T}\left[-0.5772 - \ln\frac{r^2 S}{4Tt}\right] \tag{2.24}$$

Rewriting and changing to decimal logarithms reduce it to,

$$s = \frac{2.3Q}{4\pi T}\left[\log\frac{2.25Tt}{r^2 S}\right] \tag{2.25}$$

Therefore, a plot of drawdown *s* versus the logarithm of *t* forms a straight line (Figure 2.7a).

When $s=0$, $t=t_i$, we have

$$0 = \frac{2.3Q}{4\pi T}\left[\log\frac{2.25Tt_i}{r^2 S}\right] \tag{2.26}$$

Therefore, $\log\frac{2.25Tt_i}{r^2 S}$ must be 0, and $\frac{2.25Tt_i}{r^2 S} = 1$

resulting in

$$S = \frac{2.25Tt_i}{r^2} \tag{2.27}$$

If $t/t_i=10$, then $\log t/t_i=1$. Therefore, replacing *s* by Δs, the drawdown difference per log cycle of *t*. equation 2.25 becomes

$$\Delta s = \frac{2.3Q}{4\pi T} \tag{2.28}$$

The transmissivity T can be obtained by

$$T = \frac{2.3Q}{4\pi\Delta s} \tag{2.29}$$

where Δs is the slope of the best fitting line of the selected data of the curve for Cooper-Jacob's method. With the known flow rate Q and Δs, the transmissivity T can be calculated. Afterwards, the hydraulic conductivity K can be obtained by the equation:

$$K = \frac{T}{b} = \frac{2.3Q}{4\pi b\Delta s} \tag{2.30}$$

where b is the saturated thickness of the confined aquifer.

This method was mentioned to be allowable when u is less than 0.01 or 0.02 without giving providence. Chapuis (1992a) provided the relative error corresponding to different u and proved the validity of Cooper-Jacob method in the middle zone of the drawdown-time curve. Theis's and Cooper-Jacob's methods can also be applied to the unconfined aquifer if it satisfies the assumption of the confined aquifer.

Recovery phase

The residual drawdown s' is given as

$$s' = \frac{Q}{4\pi T}\left[W(u) - W(u')\right] \tag{2.31}$$

where

$$u' = \frac{r^2 S}{4Tt'} \tag{2.32}$$

and t' is defined in Figure 2.8. The well functions can be approximated for a small r and large t' and Equation 2.31 is written as

$$s' = \frac{2.3Q}{4\pi T}\log\frac{t}{t'} \tag{2.33}$$

We can see that the plot of s' versus log t/t' presents a straight line with the slope of $\frac{2.3Q}{4\pi T}$ Thus, for $\Delta s'$, the s' per log cycle of t/t' (Figure 2.7b), the transmissivity T is expressed as

$$T = \frac{2.3Q}{4\pi\Delta s'} \tag{2.34}$$

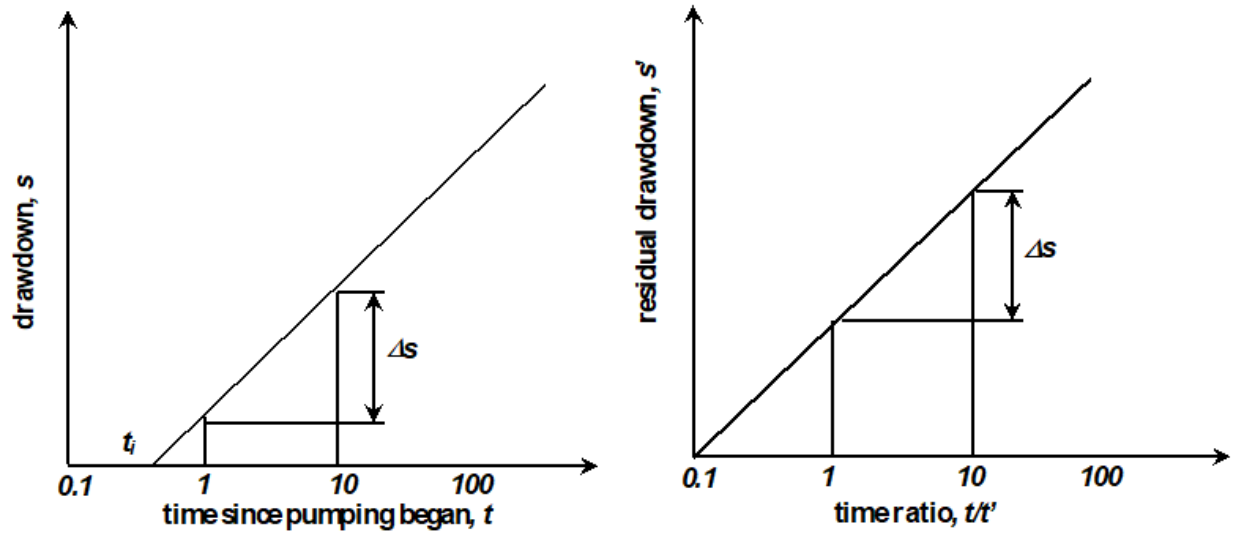

(a) injection or discharge phase (b) recovery phase

Figure 2.7: The time-drawdown plot

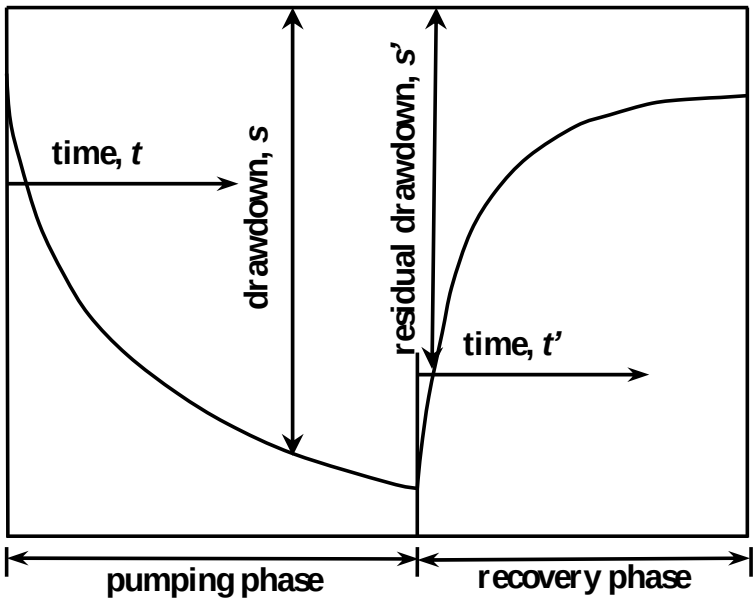

Figure 2.8: Definitions of variables in pumping and recovery phases

2.3.3 Interpretation for constant-head test in clay

For fine-grained soils such as clays, which consolidate or swell during field permeability tests, the *K* values are usually obtained from CH tests performed in piezometers installed in boreholes or driven into place (Chapuis et al. 1990). Equation 2.1 is still applicable to the steady state of the CH test, but the test time can be very long (Mata Mena, 2003). The solutions (Gibson 1963, 1966, 1970; Mieussens and Ducasse, 1977; Wilkinson 1968) yield the hydraulic conductivity, *K*, during steady-state conditions following consolidation; and the coefficient of horizontal consolidation, *C*, during the earlier phase of the test.

Gibson (1963, 1966) analyzed the in situ constant head test for compressible soils of low permeability with a spherical injection zone (Figure 2.9), assuming that the soil is perfectly elastic. The theoretical background of Gibson's interpretation is based on the Terzaghi's consolidation theory (Terzaghi, 1943).

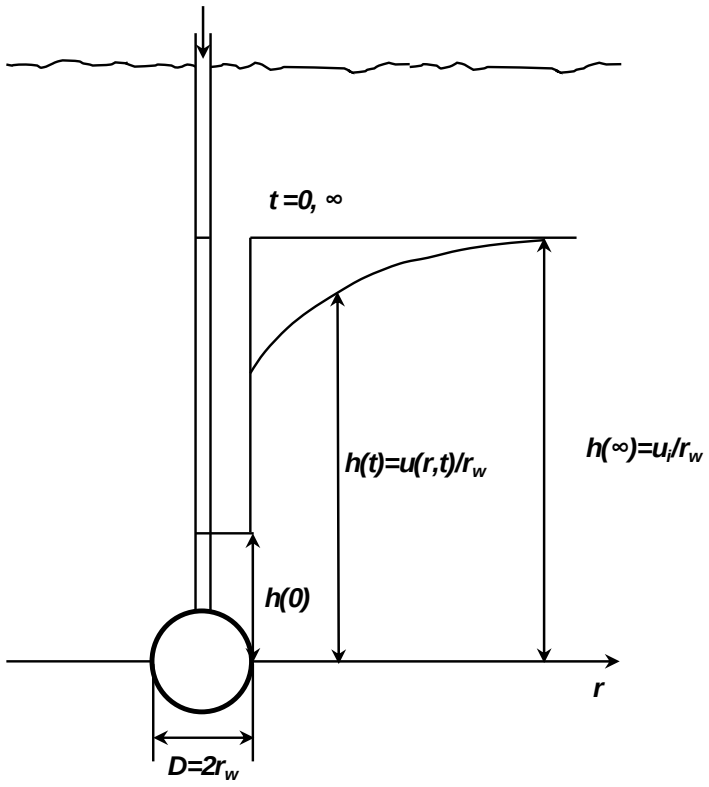

Figure 2.9 The schematic of sphere piezometer in clay

The pore water pressure u (r, t) in clay is governed by the consolidation equation in spherically symmetrical form,

$$C\left(\frac{\partial^2 u}{\partial r^2}+\frac{2}{r}\frac{\partial u}{\partial r}\right)=\frac{\partial u}{\partial t}\text{ , } r > r_w \tag{2.35}$$

At an infinite distance $r = \infty$, the pore pressure is unaffected by the test:

$$u = u_i \tag{2.36}$$

At $t = 0$, $u = u_i$ for $r > r_w$ (2.37)

The water pressure is maintained constant in the porous cavity, therefore,

$$u(r_w, t) = u_i + \Delta u \text{ , } t > 0 \tag{2.38}$$

where Δu is the excess pore water pressure and $\Delta u/\gamma_w$ is the excess water head at the cavity.

The solution of Equation 2.35 with the boundary conditions of Equations. 2.36, 2.37, 2.38 is expressed as

$$u = u_i + \Delta u\left(\frac{r_w}{r}\right) erfc\left(\frac{r - r_w}{2\sqrt{Ct}}\right) \tag{2.39}$$

where C is the coefficient of consolidation (for $\Delta u > 0$) or swelling (for $\Delta u < 0$).

The rate of water flowing through the clay equals that of the water flowing into the pipe, so we have

$$Q(t) = -S_{inj}\frac{dh}{dt} = -4\pi r_w{}^2\frac{K}{\gamma_w}\left(\frac{\partial u}{\partial r}\right)_{r=r_w} = 4\pi r_w K\frac{\Delta u}{\gamma_w}\left(1+\frac{1}{\sqrt{\pi T}}\right) \tag{2.40}$$

where T is the time factor, equal to ct/r_w^2. The flow rate becomes constant when the time is infinite,

$$Q(\infty) = 4\pi r_w{}^2\frac{K}{\gamma_w}\Delta u \tag{2.41}$$

In steady state, u diminishes radially according to the expression:

$$u = u_i + \left(\frac{r_w}{r}\right)\Delta u \tag{2.42}$$

Several plots of the *r* and *t* variation of *u* were provided numerically by Gibson (1963) as shown in Figure 2.10. From Equation 2.40, we see a straight line by plotting Q (t) against $t^{-1/2}$, and the K and C can be obtained from the intercept on the Q-axis and the slope P of this straight line.

$$K = \frac{Q(\infty)\gamma_w}{4\pi r_w \Delta u} \tag{2.43}$$

$$C = \frac{Q(\infty)r_w}{f\sqrt{\pi}} \tag{2.44}$$

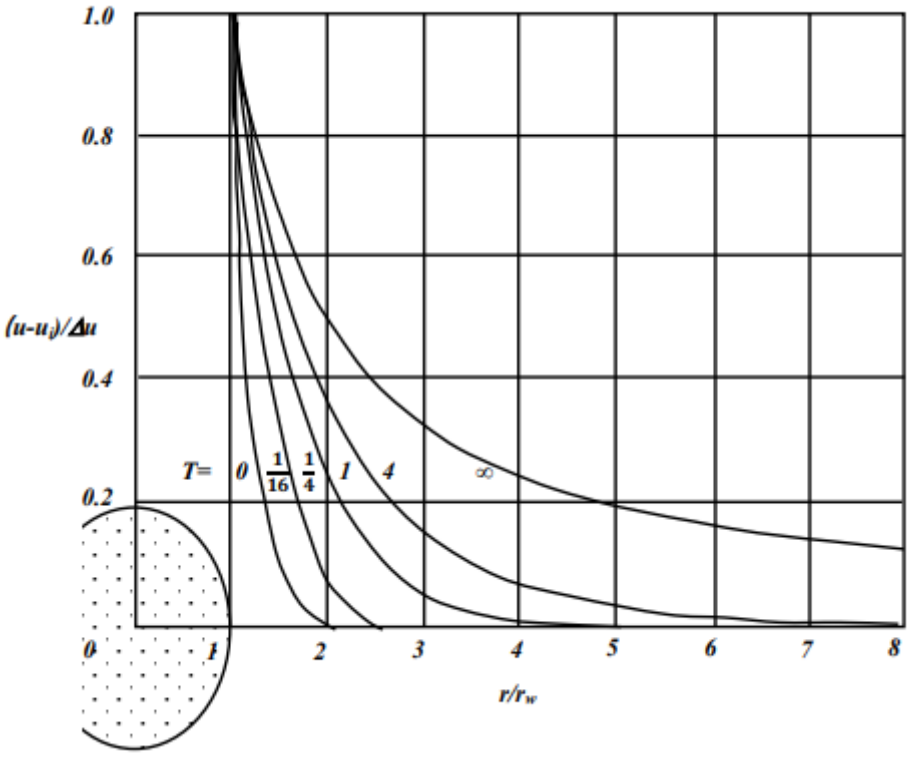

Figure 2.10: Variation of pore water pressure with time around an ideal spherical cavity

Considering the limitations of the isotropic soil and spherical shape of the cavity, Wilkinson (1968) and Mieussens and Ducasse (1977) extended the solution to cylindrical piezometers and analyzed the anisotropic permeability of soils. The inelastic property of soil was also taken into consideration (Gibson, 1970). Tavenas, Diene and Leroueil (1990) carried out a finite-element analysis to evaluate various shape factors in previous literature. Gibson's interpretation method

(Gibson, 1963) was then used by Bromhead (1996) to indicate the effect of performing tests on spherical piezometers in finite extent soil zones.

2.3.4 Interpretation for variable-head test

The interpretation methods of the variable-head test were classified into three groups according to the influence of soil matrix deformation (Chapuis, 1998). The methods of Cooper et al. (1967), Papadopulos, Bredehoeft and Cooper (1973), Nguyen and Pinder (1984), Hyder, Butler, McElwee and Liu (1994) yield both *S* and *T* by considering the aquifer as fully elastic formation. Other researchers like Lefranc (1936, 1937), Hvorslev (1951), Bouwer and Rice (1976), and Chapuis et al. (1981) neglected the deformation of aquifer because it is very small, providing only the local *K* value. The first type was proved analytically and numerically to be inaccurate when applying to the incompressible materials (Chapuis et al., 1990; Chapuis and Chenaf, 2002). The third group is to interpret the *K* values for aquitard with consideration of its elasticity.

The method of Nguyen and Pinder (1984) provided the value of *T* and *S* for the partially penetrating wells in the confined aquifer, using two slopes of plotted graph related to water level variation and time. The analytical analysis, however, was proved to be incorrect by Butler and Hyder (1994). Several other methods for the variable-head test interpretation were introduced by Chapuis (1999a). The most commonly used methods are described in following sections.

2.3.4.1 Cooper et al. method

Cooper et al. (1967) assumed that the solid skeleton of the confined aquifer is elastic with no delay in the elastic response. They proposed the interpretation method for VH test involved in a well screened through the entire thickness of a confined aquifer.

The differential equation that governs the nonsteady radial flow in the confined aquifer is

$$\frac{\partial^2 h}{\partial r^2} + \frac{1}{r}\frac{\partial h}{\partial r} = \frac{S}{T}\frac{\partial h}{\partial t},\ r > r_w \tag{2.45}$$

$$h(r_w + 0, t) = H(t),\ t > 0$$

$$h(\infty, t) = 0,\ t > 0$$

Due to the continuity of water flow, the flow rate through the water injection zone is equal to that through the well pipe:

$$2\pi r_w T\left(\frac{\partial h}{\partial r}\right)_{r_w+0} = \pi r_c^{\,2}\frac{\partial H}{\partial t},\ t > 0 \tag{2.46}$$

$$h(r,0) = 0,\ r > r_w$$

$$H(0) = H_i = \frac{V}{\pi r_c^{\,2}}$$

where r_c is the radius of the casing and $r_w = D/2$ is the radius of the screen or water injection zone. Cooper et al. (1967) provided a solution for $h(r, t)$ by analogy with a heat flow problem:

$$H = \frac{8H_i a}{\pi^2}\int_0^\infty e^{-\beta u^2/\alpha}\frac{du}{u\Delta(u)} \tag{2.47}$$

where $\alpha = S\frac{r_w^{\,2}}{r_c^{\,2}}$, $\beta = T\frac{t}{r_c^{\,2}}$, and $\Delta(u) = \left[uJ_0(u) - 2\alpha J_1(u)\right]^2 + \left[uY_0(u) - 2\alpha Y_1(u)\right]^2$

Values of H/H_i computed by numerical integrating the above equation versus β represents a family of type curves. Each curve refers to one value of the parameter α. Cooper et al. (1967) presented five type curves of α from 10^{-1} to 10^{-5}, and Papadopulos et al. (1973) extended the range of α to 10^{-10} (Figure 2.11). The T and S values are obtained by matching the test data plot of H/H_i versus t with one of the type curves.

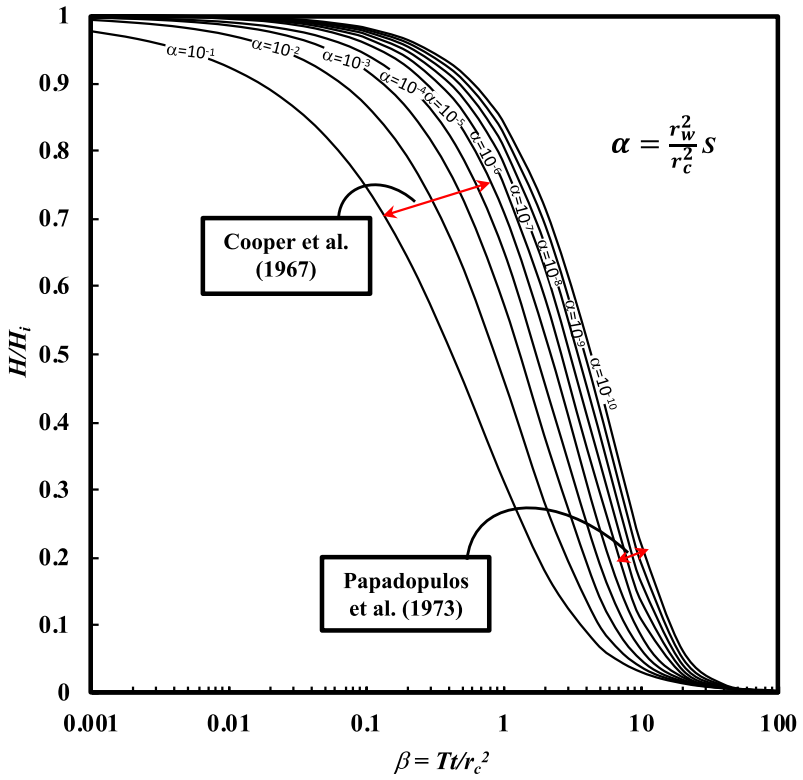

Figure 2.11: Functions of α and β.

2.3.4.2 Hvorslev's method

Hvorslev (1951) proposed a solution to deal with the variable-head test data, known as the semi-log graph method. The flow rate in the soil (Q_s) is equal to the flow rate into the pipe (Q_{inj}), based on Equation 2.1, we have

$$Q_{inj} = Q_s = cKH \tag{2.48}$$

The water velocity in the well pipe which has an inner area of S_{inj} is dH/dt. Thus:

$$Q_{inj} = -S_{inj}\frac{dH}{dt} \tag{2.49}$$

where $S_{\text{inj}} = \pi r_c^2$ is the internal cross-sectional area of the pipe. Combining Equation 2.48 and 2.49 gives:

$$\frac{dH}{dt} = -\frac{cKH}{S_{inj}} \tag{2.50}$$

Integrating leads to Hvorslev's solution, in which the hydraulic head is generally in a logarithmic form:

$$\ln\left(\frac{H_1}{H_2}\right) = -\frac{cK}{S_{inj}}(t_1 - t_2) \tag{2.51}$$

where H_1 and H_2 are the head differences at times t_1 and t_2, respectively

The test data are plotted as ln H on the y-axis and time t on the x-axis in the Hvorslev's graph. If the test is good, the data should yield a straight-line with a slope of $P_1 = -\frac{cK}{S_{inj}}$. Therefore,

$$K = -P_1 \cdot \frac{S_{inj}}{c} \tag{2.52}$$

2.3.4.3 Bouwer and Rice's method

Based on Thiem's equation, Bouwer and Rice (1976) derived two empirical equations on the well geometry property to determine the K value of the unconfined aquifer from a rising-head test. The falling-head test was supplemented afterwards, and the equations involving the shape factor were also applied in the calculation of the hydraulic conductivity in confined aquifer receiving water from recharge or compression from the upper confining layer (Bouwer, 1989).

Based on the Thiem equation, the flow into the well with an applied hydraulic head of H can be expressed by

$$Q = 2\pi KL \cdot \frac{H}{\ln\left(\frac{R_0}{r_w}\right)} \tag{2.53}$$

Where R_0 is the radius of influence over which H is dissipated, evaluated by making an electrical analogy.

Combining the above equation with 2.50 yields:

$$\frac{dH}{H} = -\frac{2KL}{r_c^{\,2} \ln\left(\frac{R_0}{r_w}\right)} dt \tag{2.54}$$

which can be integrated to

$$\ln\left(\frac{H_1}{H_2}\right) = -\frac{2\pi LK}{S_{inj}\ln\left(\frac{R_0}{r_w}\right)}\left(t_1 - t_2\right) \tag{2.55}$$

which is very similar to the formula 2.51 of Hvorslev's solution, but with a coefficient (shape factor) *c* defined by:

$$c = \frac{2\pi L}{\ln\left(R_0 / r_w\right)} \tag{2.56}$$

For the partially penetrating well, the two empirical formulas for $\ln(R_0/r_w)$ were obtained based on the electrical analogs in steady-state conditions:

$$\ln\left(R_0 / r_w\right) = \left[\frac{1.1}{\ln\left(d / r_w\right)} + \frac{A + B\ln\left(b - d\right)/r_w}{L / r_w}\right]^{-1} \tag{2.57}$$

If $b \gg d$, the effective upper limited of $\ln[(b\text{-}d)/r_w]$ is suggested as being 6. When $b = d$, the well becomes fully penetrated and Equation 2.57 changes to:

$$\ln\left(R_0 / r_w\right) = \left[\frac{1.1}{\ln\left(d / r_w\right)} + \frac{C}{L / r_w}\right]^{-1} \tag{2.58}$$

where *d* is the distance from water level to the bottom of the water injection zone, *b* is the saturated thickness of the unconfined aquifer. *A*, *B* and *C* are three dimensionless coefficients, determined by functions of L/r_w (Figure 2.12).

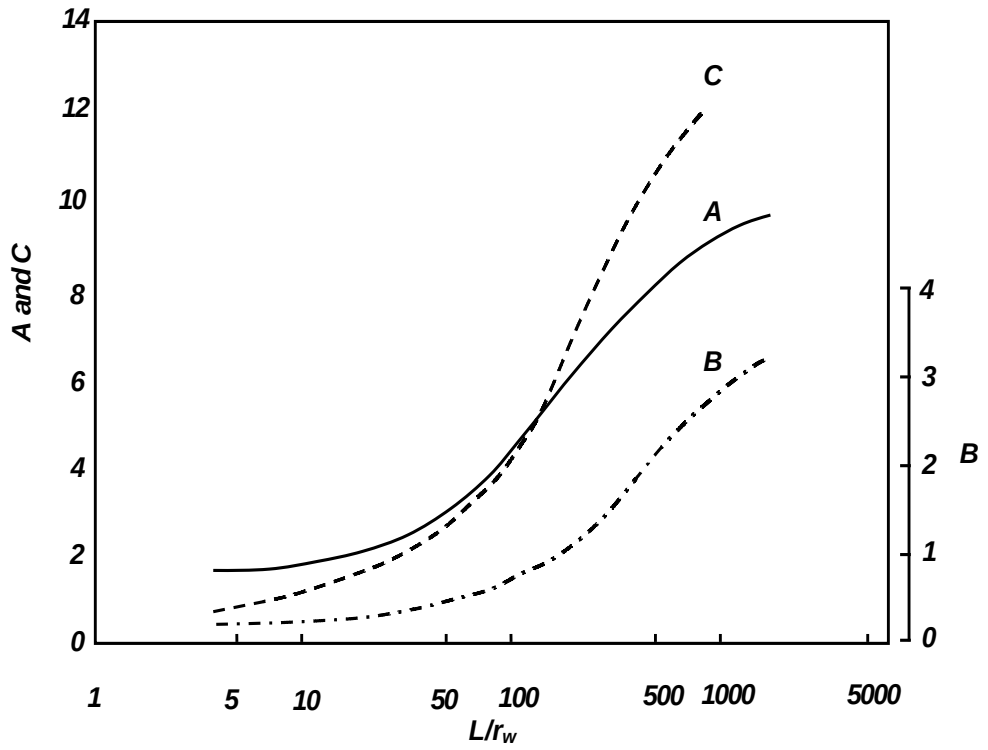

Figure 2.12: Graph of the coefficient *A*, *B*, and *C* versus L/r_w for the Bouwer and Rice equation (1976)

2.3.4.4 Velocity graph method

In practice, the Hvorslev's semi-log plot is not always straight as theory (Figure 2.13 from Chapuis, 2015). It is due to the error on the piezometric level (PL), H_0, which may result from several error sources (Chapuis, 2009a). Chapuis et al. (1981) removed the H_0 to correctly estimate the real piezometric level (PL) and plotted velocity graph to calculate the *K* value. The method has been verified to be correct (Chapuis 1998, 2001, 2015) and retained in the standards CAN/BNQ 2501-135 (2014) in combination with Hvorslev's semi-log graph to interpret the variable rising- and falling-head tests.

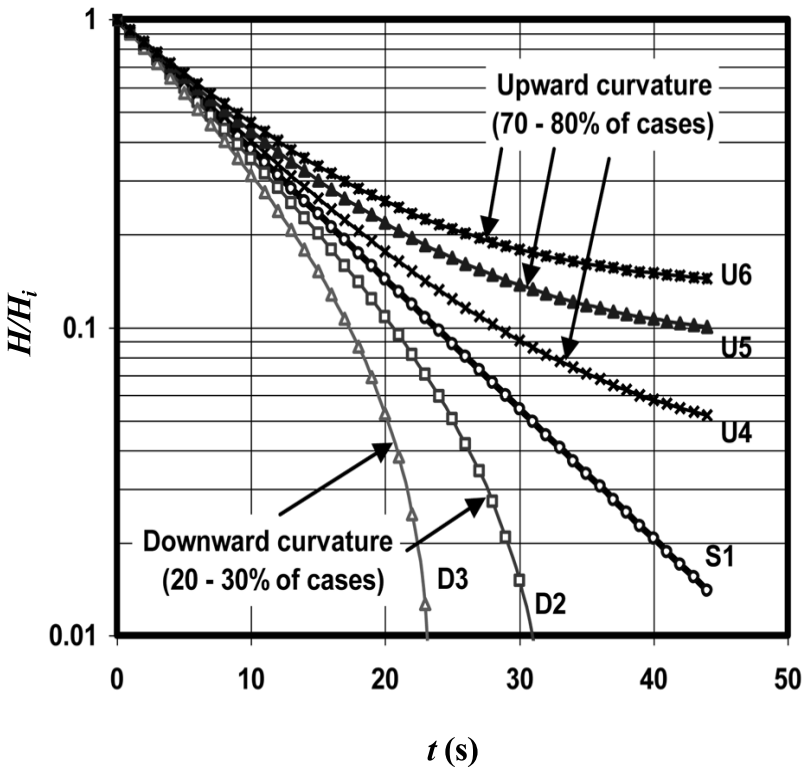

Figure 2.13: Curved semi-log graphs (from Chapuis, 2015).

From Equation 2.50 we know that the by plotting the water level velocity dH/dt in the pipe versus the mean H value, $(H_j+H_{j+1})/2$, during dt should yield a straight line. However, the true H value is frequently not accurately known. Thus, the real value H_r is written as

$$H_r = H - H_0 \tag{2.59}$$

Substituting Equation 2.50 into 2.59 yields:

$$H = -\frac{S_{inj}}{cK}\frac{dH}{dt} + H_0 \tag{2.60}$$

Thus Equation 2.60 represents a straight line with a slope of $P_2 = \frac{S_{inj}}{cK}$ and an intercept on H-axis of H_0 (Figure 2.14). The K value can be calculated as:

$$K = \frac{1}{P_2}\cdot\frac{S_{inj}}{c} \tag{2.61}$$

Then, once the H_r for the test has been found with the velocity graph, the curved Hvorslev's semi-log graph can be corrected to a straight line and yield an accurate K value.

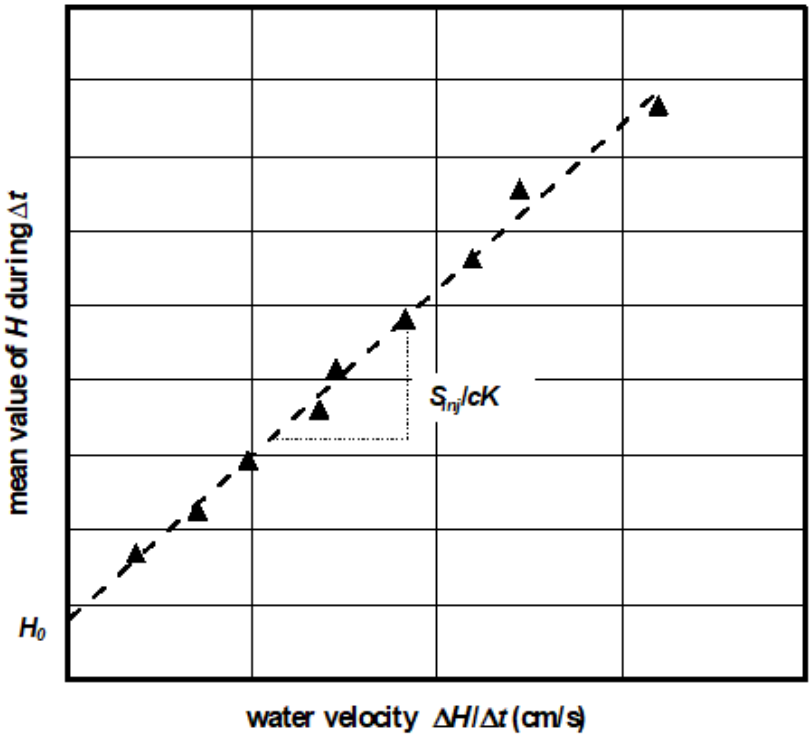

Figure 2.14: Velocity graph

The velocity graph method eliminates the systematic errors caused by hydraulic fractures, short circuit, PT calibration, etc. for overdamped VH test data, which are then corrected so as to contain only a small random error (Chapuis, 2009a). It also removes the early data affected by dynamic effects that should be discarded for the best-fit methods in underdamped slug test (Chapuis, 2012b), where the shape of the velocity plot is spiral. However, the data selection may be user-dependent.

Chiasson (2005, 2012) provided an alternative, unbiased *Z-t* method, to obtain the piezometric error H_0 and optimized Hvorslev's semi-log plot by the linear least square method in the spreadsheet. H_0 in Equation 2.60 is first set to be the variable in the process. And then it is determined when the coefficient of determination R^2 of the best fit line of ln (H-H_0) versus t reaches closest to 1, which indicates the best degree of fit. After the correction of H_0, the curved semi-log becomes straight.

2.3.5 Shape factors

The shape factor (intake factor) required in the equations of the CH and VH tests relates to the geometry of the injection zone, also called intake zone, filter pack, cavity or lantern (from French), the boundary conditions, and the anisotropy of the soil (Mena, 2003; Ratnam, Soga and Whittle, 2001). The determination of shape factors of spherical, cylindrical, circular disc/flush bottom shaped (L = 0), tapered cavities (injection zones) were studied by analytical, electrical analog, and numerical methods in the previous literature. They will be presented chronologically in the following sections. The sphere and cylindrical cavities are the most commonly seen shapes. The circular disc piezometer is often used in earth dams, under pavements, or on the faces of retaining walls (Brand and Premchitt, 1980b). The tapered piezometer is of the Bishop type (Bishop, Kennardand Penman, 1961; Brand and Premchitt, 1980b).

The commonly used shape factor for the circular disc/flush bottom piezometer (L = 0) was proposed by a few electric analog experiments (Harza, 1935) and a graphical approximation to build the radial flow nets (Taylor, 1948), cited as the case 4 in Hvorslev (1951):

$$c = 2.75D \tag{2.62}$$

Dachler (1936) derived a complete formula for the cylindrical injection zone replaced by a semi-ellipsoid with an equivalent surface area, which represents a well casing/piezometer extended at an impervious boundary (case 7 in Hvorslev, 1951). The expression is

$$c = \frac{2\pi L}{\ln\left[\frac{2L}{D} + \sqrt{1+\left(\frac{2L}{D}\right)^2}\right]} \tag{2.63}$$

where L and D are the length and diameter of the water injection zone, respectively. It is applicable to the upper and lower halves of the zone.

The above equation was extended to the entire injection zone represented by an ellipsoid as (case 8 in Hvorslev (1951)):

$$c = \frac{2\pi L}{\ln\left[\frac{L}{D} + \sqrt{1+\left(\frac{L}{D}\right)^2}\right]} \tag{2.64}$$

which is simplified for large values of *L/D* to

$$c = \frac{2\pi L}{\ln(2L/D)} \qquad L/D > 4 \tag{2.65}$$

The formula of shape factor approximating the cylindrical zone by a sphere of an equal surface was presented by Schneebeli (1954):

$$c = 2\pi D\sqrt{\frac{L}{D} + \frac{1}{4}} \quad 1 \le L/D \le 8 \tag{2.66}$$

These two equations were developed before or at the beginning of the century as mathematical solutions of the Laplace equation (Chapuis, 1989,1999b), verified by electrical analogs (Hvorslev, 1951; Mandel, 1939; Schneebeli, 1966; Taylor, 1948).

The formula of shape factor for small spherical injection zones was solved from the Laplace equation which governs the steady state flow in porous media (e.g., Gibson, 1963; Lefranc, 1937), expressed as:

$$c = 2\pi D \tag{2.67}$$

which is the case 1 in Hvorslev (1951). With the known shape factor *c*, applied head difference H_c and constant flow rate *Q*, the *K* values can be calculated for many points at different depths of the soil layer. Once a *K* value had been determined at a point, Lefranc (1937) installed a cylindrical cavity into the same point and apply the same *Q* and measured the corresponding H_c. The shape factor of the cylindrical injection zone is expressed as

$$c = \frac{Q}{KH_c} \tag{2.68}$$

These operations need to be repeated at different points to obtain the average value of *c*, which was considered to be exact.

Luthin and Kirkham (1949) provided the *c* values by experimental measurements in an electrolytic tank. When $L = 0$,

$$c = 2.5D \tag{2.69}$$

Kallstenius and Wallgren (1956) proposed a simple formula for a spherical piezometer (of any shape) as

$$c = 2\sqrt{\pi S} \tag{2.70}$$

where A is the surface area of the injection zone. The equation is the same as 2.63 for the spherical piezometer. It was suggested that a piezometer of any shape could be replaced by a spherical piezometer with the same area S. Therefore, the shape factor for cylindrical and circular disc piezometers can be expressed as (presented by Brand and Premchitt, 1980a using Equation 2.70)

$$c = 2\pi\sqrt{LD} \qquad \text{for cylindrical cavity} \tag{2.71}$$

which has a difference within ±5% from Equation 2.67 when $4 \leqslant L/D \leqslant 10$.

$$c = \pi D \qquad \text{for circular disc} \tag{2.72}$$

Wikinson (1968) firstly used finite difference techniques to propose an expression of shape factor for the cylindrical injection zone by equalizing its volume to an ellipsoid, which is

$$c = \frac{3\pi L}{\ln\left[\frac{1.5L}{D} + \sqrt{1+\left(\frac{1.5L}{D}\right)^2}\right]} \tag{2.73}$$

The natural logarithm in Equations. 2.64 and 2.73 were also written as log by some researchers (Brand and Premchitt, 1980a, b; Wilkinson, 1968). The symbol ln is used in the thesis to refer the natural logarithm, to avoid confusion between the natural and common (base 10) logarithms.

Using an electric analog model, Smiles and Youngs (1965) measured the shape factor for cylindrical injection zone directly in a small range of L/D from 0 to 4. When $L/D = 0$,

$$c = 2.8D \tag{2.74}$$

Al- Dhahir and Morgenstern (1969) solved the finite difference problems using the Gauss-Siedel successive over-relaxation technique (Forsythe and Wasow, 1960), to numerically analyze the shape factor for cylindrical piezometers in a porous medium. The medium was considered to be infinite with a diameter of $50D$. The results were within about 5% of those obtained experimentally by Smiles and Youngs (1965) for $0 \leqslant L/D \leqslant 4$.

Raymond and Azzouz (1969) analyzed the shape factors for injection zones of cylindrical shape through a similar numerical method, whereas the average results were only around 70% of those of Al-Dhahir and Morgenstern (1969). There were no details about the methods they used.

Bouwer and Rice (1976) used an electrical analog to provide *c* values as shown in Equation 2.56. It yields systematic differences compared to the Hvorslev's shape factor because the former was derived from an incorrect electrical analog, verified by numerical simulations (Chapuis, 2009b).

Lowther (1978) noted the discrepancy of shape factors between the case 7 of Hvorslev (1951) when reaching the limit of $L = 0$, $c = 2\pi D$, and the case 3, $c = 2.75\,D$, for the circular disc injection zone, which should be identical. It is due to the approximating nature of the Hvorslev's expression (Youngs, 1980).

Brand and Premchitt (1980a) reviewed several theoretical and numerical shape factors for the cylindrical piezometers and used the same techniques as Smiles and Youngs (1965) and Al-Dhahir and Morgenstern (1969) to carry out the expression for shape factor in infinite soil (with a diameter of 300*D*):

$$c = \frac{2.4\pi L}{\ln\left[\frac{1.2L}{D} + \sqrt{1 + \left(\frac{1.2L}{D}\right)^2}\right]} \tag{2.75}$$

When $L/D \geqslant 4$, the equation is simplified to:

$$c = 7D + 1.65L \tag{2.76}$$

Similarly, the shape factors for circular disc and tapered piezometers were presented (Brand and Premchitt 1980b) as:

$$c = 2.63D \qquad \text{for circular disc piezometer} \tag{2.77}$$

$$c = \frac{2.4\pi L}{\ln\left[\frac{1.2L}{D_a} + \sqrt{1 + \left(\frac{1.2L}{D_a}\right)^2}\right]} \qquad \text{for the tapered piezometer} \tag{2.78}$$

where D_a is the average diameter

Randolph and Booker (1982) proposed an analytical solution for a cylindrical probe by approximating the cylindrical zone to an ellipsoid, which yielded similar results to those provided by Al-Dhahir and Morgenstern (1969) for the cylindrical probe with closed ends. The existence of a singular velocity field at the locations where the Dirichlet-type boundary condition alters to the Neumann-type boundary condition along the same cylindrical boundary was noted by the authors, which is an important contribution (Selvadurai, 2004).

Chapuis (1989) compared the previously mentioned shape factors derived by various computational methods. Compared to the Hvorslev's shape factor, they have differences up to 40% for large *L/D* ratios and over 100% for small *L/D* ratios (Chapuis, 1989; Chapuis et al., 1990). The source errors for such differences were examined and analytical equations for the shape factors were given for cavities having either a pervious or an impervious bottom.

A finite element method was employed by Tavenas et al. (1990) to assess the previously-developed formula for shape factors. The derived numerical values of shape factor showed good agreement to those proposed by Randolph and Booker (1982) and Al-Dhahir and Morgenstern (1969).

Lafhaj and Shahrour (2000) used the boundary element method to evaluate the shape factor numerically. The infinite medium was defined to be a lateral boundary distance of 100*D* and a distance of 50*D* between the injection zone and the water table. The shape factors augmented with the increase of the lateral boundary distance and reached an invariable value, in agreement with Hvorslev's shape factors for injection zones with an impermeable bottom. The authors also determined the shape factor through the electric analogy method (Lafhaj and Shahrour, 2002b). A plastic tube simulated the impervious well casing, connected with a zinc cylinder representing the cavity. They were placed in the medium (a water tank) where an aluminum plate was used to model the water table.

Ratnam, Soga and Whittle (2001) used the finite element method ABAQUS to improve the Hvorslev's solutions of the shape factors for the screened portion between double packers and the cylindrical injection zone of a cased borehole. The equations were given by curve-fitting techniques as:

$$c = 0.5691L + 5.2428D\sqrt{\frac{L}{D}} \qquad \text{for double packers} \qquad (2.79)$$

$$c = 1.1872L + 2.4135D\sqrt{\frac{L}{D}} + 3.1146D \qquad \text{for a borehole casing} \qquad (2.80)$$

The second equation is in consistent with Hvorslev's solution when $1 < L/D < 3$.

Selvadurai (2003) analytically studied the shape factor of spherical and circular disc injection zone located in transversely isotropic porous media. The general expression of the shape factor for spherical zone was written as

$$c = 4\pi D \frac{\sqrt{\lambda - 1}}{\ln\left(\frac{\sqrt{\lambda} + \sqrt{\lambda - 1}}{\sqrt{\lambda} - \sqrt{\lambda - 1}}\right)} \qquad \lambda > 1 \qquad (2.81)$$

$$c = 4\pi D \frac{\sqrt{1 - \lambda}}{2\cot^{-1}\left[\frac{\sqrt{\lambda}}{\sqrt{1 - \lambda}}\right]} \qquad \lambda < 1 \qquad (2.82)$$

where λ is the ratio of horizontal to vertical hydraulic conductivities. When λ infinitely approaches 1, the above equations become the classical Equation 2.67. The shape factor for the circular disc zone in an isotropic medium is:

$$c = 4D \qquad (2.83)$$

In a similar way, the solutions of the shape factor for a cavity of either prolate or oblate spheroid located in transversely isotropic medium were also provided by Selvadurai (2004).

Foroutan (2002) developed numerical estimates for the shape factor of cylindrical injection zones via the finite element method PLAXIS, where the boundary size of $90D$ was considered to be infinite. Their method was calibrated by the analytical solution of Selvadurai (2003) and yielded a simplified formula of shape factors for transversely isotropic media:

$$c = a\left(\frac{b}{\sqrt{\lambda}} + \frac{L}{D}\right) \qquad (2.84)$$

where a and b are constants, approximated as 1.85 and 3.5 respectively.

Mathias and Butler (2006) disagreed with Youngs (1980) on the reason why the shape factors in case 7 ≠ case 3 and case 8 ≠ case 4 (Hvorslev 1951) for the circular disc/flush bottom cavity where $L = 0$. Two improved equations for cases 7 and 8 were given as

$$c = \frac{2\pi R}{\sinh\left[\arctan h(R/L)\right]\ln\left\{\coth[\frac{1}{2}\arctan h(R/L)]\right\}} \tag{2.85}$$

$$c = \frac{2\pi D}{\sinh\left[\arctan h(D/L)\right]\ln\left\{\coth[\frac{1}{2}\arctan h(D/L)]\right\}} \tag{2.86}$$

which corresponds to Equations. 2.63 and 2.64. The authors also proposed a semianalytical solution for the shape factor of double-packer permeameters (Mathias and Butler 2007).

Silvestri, Bravo-Jonard and Abou-Samra (2011) developed an analytical solution for the shape factor of a flush bottom piezometer in an infinite isotropic soil medium, which was analyzed numerically to be a simplified expression:

$$c = 2.8D \tag{2.87}$$

which is very close to Equation 2.62 of case 4 cited by Hvorslev's (1951), same as that presented by Smiles and Youngs (1965) and has differences up to 11% compared to Luthin and Kikham (1949) and Ratnam et al. (2001).

The analytical solution of shape factors for the open-ended cylindrical piezometers was presented by the expression (Silvestri, Abou-Samra and Bravo-Jonard, 2012)

$$c = 3.79D\left(\frac{L}{D}\right)^{0.725} + 2.8D \qquad 0 \leqslant L/D \leqslant 16 \tag{2.88}$$

Silvestri, Bravo-Jonard and Abou-Samra (2013) explained that the discrepancy between the derived shape factors from Hvorslev (1951) and Mathias and Butler (2006) is due to the different definitions of the aspect ratio. The discrepancy reduces when $L/D \leqslant 4$.

Klammler, Hatfield, Nemer and Mathias (2011) generated a series of non-dimensional charts of shape factors for a single screened probe or double packers of various boundary conditions through a trigonometric interpolation method. Based on the method, Klammler, Nemer and

Hatfield (2014) investigated the non-ideal screens of different slottings and various lengths and their combined effects on the shape factors.

2.4 Error sources in measurements of field permeability tests

Under ideal test conditions, the CH test should have a horizontal drawdown in equilibrium and the semi-log and velocity plot of the overdamped VH test data should yield a straight line, in accordance with the theory. In practice, however, upward and downward curves are frequently obtained for the semi-log graph (Chapuis 1998, 2015, 2017), the velocity graph may be scattered or curved (Zhang and Chapuis, 2018), and the water levels during CH tests do not reach stabilization (Zhang et al., 2018a, b). The theoretical solutions were developed based on many assumptions, summarized by several researchers (e.g., Chapuis et al., 1990; Hvorslev, 1951). (1) The groundwater flow respects Darcy's law. (2) The friction losses in the pipe are negligible due to the slow water flow. (3) Soil and water are incompressible. (4) The time lag is negligible. (5) Soil is homogeneous and isotropic. (6) There are no impervious or recharge boundaries close to the test. (7) Boundary conditions are not modified by the test. (8) The well (or casing) is perfectly sealed. (9) The geometry of water injection zone is known and do not change during the test. (10) The soil near the injection zone remains unmodified during drilling or test operation. (11) The filter materials of the injection zone do not mix with the natural soil. (12) Head losses in the water injection zone during the test are negligible. Once the assumptions are not satisfied, potential sources of error in field tests may occur, which have been discussed by some researchers (Brillant, 1966; Bjerrum et al., 1972; Chapuis et al., 1990; Hvorslev, 1951; Weber, 1968; Wilkinson, 1968).

Hydraulic fracturing is a commonly-used technique to free the oil or natural gas from low-permeability rock to the well, which is somewhat controversial because it may contaminate the groundwater. The hydraulic fracture test was used in clays to determine the in-situ lateral stresses and study the fracture mode (e.g., Bjerrum and Andersen 1972; Bjerrum, Nash, Kennard and Gibson, 1972; Lefebvre, Philibert, Bozozuk and Paré, 1981). In groundwater wells, the hydraulic fracturing is due to high hydraulic head difference applied for a test, which simply implies the increased water flow in the surrounding soil rather than a systematic mechanical fracture in soil (Chapuis, 1988). It is difficult to imagine the cracks in granular soils as in rocks and clayey soils (Lefebvre et al. 1981). The excessive water head or overquick water flow, however, may damage

the aquifer formation and affect the accuracy of derived hydraulic parameters, which needs to be avoided. A statistical study of hydraulic fracturing in different granular soils was presented (Chapuis et al., 1981) and a rule of thumb to determine the maximum value of applied head difference was provided (Chapuis, 1988, 2001; Chapuis et al., 1981; Chapuis et al., 1990). The phenomenon may be detected through a curved velocity graph. The slope is relatively flat corresponding to a large K value at the beginning and becomes steeper, refers to a smaller K value, when the applied hydraulic head decreases (Chapuis, 1988).

It is envisioned that the MW, piezometer or borehole casing must be sealed in the full length above the water injection zone (Freeze and Cherry, 1979). If it is not perfectly sealed or simply partially sealed, there is a leakage through pipe joints and between the pipe and adjacent soils, which may cause a preferential flow between the upper and lower aquifer layers, called hydraulic short circuit (Chapuis et al., 1981). This vertical hydraulic communication may cause undesirable contaminant transfer in the preserved aquifer, imprecise measurement of piezometric level, time lag and soil permeability, and incorrect regional assessment of groundwater resources (Chapuis, 1988; Chesnaux and Elliott, 2011; Hvorslev, 1951). Chapuis (1988) employed the velocity graph method to check if there is a vertical hydraulic connection in the aquifers. Instead of being a straight line, the velocity plot appears as two or three straight parts with different slopes. At the beginning of the test, the first straight section yields a piezometric error of $H_0 \neq 0$. The straight portion for small head differences corresponds to a hydraulic short circuit. The final water level of the velocity plot returns to 0. The piezometric error H_0 can be also used to correct the drawdowns of pumping tests in inadequately sealed wells. The corrected transmissivities presented more consistent compared to those without piezometric correction (Chapuis and Sabourin, 1989). The hydraulic connection can be also detected by proper tracer tests (Meiri, 1989), pumping and recovery tests (Chapuis and Chenaf, 1998), and falling-head tests (Richard, Chesnaux, and Rouleau, 2016; Richard et al., 2014). The influence of errors caused by leakage can be minimized by strict control of drilling operations as required by standards CAN-BNQ 2501-135 (2014) and 2501-130 (2014): driving the entire piezometer, surrounding the screen a proper filter pack, and sealing the above portion tightly.

The time lag was categorized into hydrostatic and stress adjustment types by Hvorslev (1951). The former refers to the time for water flow from or to the piezometer until reaching an

equilibrium, which may be minimized by reducing the applied or discharged water volume and enlarging the injection zone. The latter is the time that water flows from or to the soil, which also involves the consolidation or swelling of the soil structure. For the coarse-grained soils, the time lag can be negligible. It is not the same case, however, for the compressible soils like clay, where the time lag can cause serious errors (Gibson, 1963). Therefore, the time lag was taken into account in the interpretation of field permeability tests and pore water pressure measurements in clay materials (Gibson, 1963, 1966; Wilkinson, 1968).

The performance of the well screen and filter pack plays a significant role in acquiring the accurate hydraulic conductivity. Well development is necessary to remove the deposits during borehole drilling and fine particles from the aquifer material. The development process for the MWs is much less severe than for pumping wells, and thus the potential of clogging is higher (Baptiste and Chapuis, 2015). Additionally, there might be soil remolding during the drilling and washing operations, and the filter material may mix with the adjacent natural soil. More than 65% monitoring wells installed in North America since the late 1970s were poorly installed or developed (Nielsen and Schalla, 2005). These damaged or partly clogged wells cause errors in the calculated K values. During the test, a strong outward water flow from well to the aquifer may cause the soil clogging by sedimentation of fine particles, which increases the time lag, and a strong inward flow may carry out the fine particles from the surrounding filter material or soil (Hvorslev, 1951).

The well losses may be significant for a production well due to its large flow rate, the tests of small-scale use relatively low flow rate so that the well loss is small (Klammler et al., 2014). As a result, head losses in the water injection zone during the test may be negligible. However, the water flow may still generate turbulence and bubbles along the well pipe and the screen, which results in the non-linear (quadratic) head losses (Clark and Turner, 1983; Weight and Sonderegger, 2001). The clogging of the screen and filter pack also lead to extra head losses.

The piezometric level is normally assumed to be the water level of the river or lake when the real seepage condition in sediments are unknown before drilling (Chapuis et al., 1990). However, there is a difference H_0 between the real piezometric level and the assumed one. If $H_0 \neq 0$, then the H_0 is the piezometric error made in evaluating the local piezometric level for the test (Chapuis et al., 1981; Schneebeli, 1954). The piezometric error can be caused for several reasons: a

preferential seepage in the vicinity of the borehole, a too short equilibration time before slugging, transducer displacement during slugging or a very long time-lag for an aquitard (Chapuis, 1999b, 2009a; Chapuis and Sabourin, 1989). The large errors were demonstrated numerically due to internal erosion of natural soils around the casing during drilling operations or development, and improper sealing of the piezometer (Chapuis and Sabourin, 1989). All systematic errors for overdamped variable-head test data can be corrected so that data contain only a small random error by the velocity graph method (Chapuis, 2009a).

Some other sources of errors are summarized. Various interpretation methods may yield discrepancies in K values and some methods including visual fit and data selection are usually user dependent (Chapuis, 2012b; Chiasson, 2012). The early data are easily affected by water splashing or air pressure variation, which thus should be excluded (Chapuis, 2012b). Different choices of shape factors also yield potential errors. Most pressure transducers are not correctly calibrated, which may yield systematic and random measurement errors (e.g., Chapuis, 2009a, 2012b). Water evaporation and vapor condensation, instrument damage by extreme temperatures, gas bubbles in the pipes and soils may also have an influence on the piezometric level measurements (Hvorslev, 1951). The local variations in permeability, undetected impervious boundary to the test, and the modified boundary conditions during the test also cause potential errors (Chapuis et al., 1990).

2.5 Numerical code-Seep/W

Seep/W is a finite element software that solves groundwater seepage problems, developed by Geo-Slope International Ltd. It mathematically simulates the real physical process of groundwater flowing through porous media, where seepage through unsaturated soils can also be incorporated into the numerical model (GEO-SLOPE International Ltd., 2012). The numerical results via the code have been validated to be trustworthy for a variety of saturated and unsaturated cases under steady or unsteady state, from one to three dimensions (Chapuis, Chenaf, Bussière, Aubertin and Crespo, 2001).

2.5.1 Theory

The code is formulated based on Darcy's law:

$$v = Ki \tag{2.89}$$

where v is the Darcian velocity, i is the hydraulic gradient, the isotropic hydraulic conductivity K is constant in saturated medium but varies in the conditions of unsaturated flows with the changes in volumetric water content and pore water pressure. The code computes the Darcian velocity rather than the actual average (linear) velocity.

The general governing equation is Richards' conservation equation:

$$K\nabla^2 h + Q = \frac{\partial \theta}{\partial t} \tag{2.90}$$

where h is the total head, Q is the boundary flux, which can be a well or source term, θ is the volumetric water content, and t is the time. The equation indicates that the flow entering and leaving an elemental volume at a point in time is equal to the change in storage of the soil system.

Under steady-state conditions, the equation reduces to:

$$K\nabla^2 h + Q = 0 \tag{2.91}$$

which implies that the flow entering and leaving a unit volume does not change. For constant total stresses, and vertical strain only, m_w is defined as the slope of the volumetric water content θ versus the pore water pressure u_w:

$$m_w = \frac{\partial \theta}{\partial u_w} \tag{2.92}$$

in which u_w can be expressed as:

$$u_w = \gamma_w (h - z) \tag{2.93}$$

where γ_w is the unit weight of water, and z is the elevation. Substituting Equation 2.93 into Equation 2.92 gives:

$$\partial \theta = m_w \gamma_w \partial (h - z) \tag{2.94}$$

The specific storativity S_s and m_w are related by:

$$S_s = m_w \gamma_w \tag{2.95}$$

For constant total stresses, vertical strain, and assumed elastic behaviour, Equations. 2.94 and 2.95 are substituted into Equation 2.90 and the governing equation becomes,

$$K\nabla^2 h + Q = S_s \frac{\partial h}{\partial t} \tag{2.96}$$

This equation is used in groundwater science, for example for pumping tests in confined aquifers. It was shown to be incorrect for slug tests and pulse tests (Chapuis, 2017).

In Seep/W, the Galerkin method of weighed residual was applied to the governing differential equation, to derive the finite element transient seepage equation, abbreviated as:

$$[K]\{H\} + [M]\{H\},t = \{Q\} \tag{2.97}$$

where [*K*] is element characteristic matrix, {*H*} is the vector of nodal heads, [*M*] is the element mass matrix, *t* is the time, and {*Q*} is the element applied flux vector.

The term {*H*}, *t* is zero for a steady-state analysis, and the finite element equation becomes:

$$[K]\{H\} = \{Q\} \tag{2.98}$$

which is the abbreviate finite element form of Darcy's law.

In an axisymmetric analysis,

$$\begin{aligned} [K] &= \int_A \left([B]^T [C] R\right) dA \\ [M] &= \int_A \left(\lambda \langle N \rangle^T \langle N \rangle R\right) dA \\ [Q] &= q \int_L \left(\langle N \rangle^T R\right) dL \end{aligned} \tag{2.99}$$

where [*B*] is the gradient matrix, [*C*] is the element hydraulic conductivity matrix, *R* is the circumferential distance from the symmetric axis, the equivalent element thickness, <*N*> is the vector of interpolation function, λ is storage term for a transient seepage equals to $m_w\gamma_w$, *A* is a designation for summation over the area of an element, and *L* is a designation for summation over the edge of an element.

For a transient analysis, the time integration of the finite element equation is completed by a finite difference approximation method. The code uses the Backward Difference Method to derive a simplified finite element equation:

$$(\Delta t[K]+[M])\{H_e\} = \Delta t\{Q_e\}+[M]\{H_i\} \quad (2.100)$$

where Δt is the time increment, H_e is the head at end of time increment,H_i is the head at the initiation of time increment, and Q_e is the nodal flux at end of the time increment. The equation indicates that the initial conditions must be known to solve for a transient analysis.

The element characteristic [*K*] and mass matrix [*M*] are then evaluated using Gaussian numerical integration by sampling the element properties at specific points and summed together.

2.5.2 Application

Seep/W is a powerful numerical code that is capable to simulate various problems. The seepage through the dike under steady- and unsteady state is one of the applications (Chapuis and Aubertin, 2001). Seep/W is able to be integrated with CTRN/W to solve the problems on groundwater contamination and wastewater treatment (Ardejani et al., 2007). It was also incorporated with a bank stability model in Slope/W to study the bank collapse by seepage erosion (Chu-Agor, Wilson and Fox, 2008). To study the effect of vadose zone on the leakage rates in landfill barrier systems, the moisture flow regime and steady-state leakage rates were simulated for cases of the unsaturated zone in different thicknesses (Çelik, Rowe and Ünlü, 2009). The centrifuge test model of a buttressed embankment was built using the code, of which the numerical results under various conditions were compared with the test results to explain the seepage characteristics of the embankment (Jin, Choo, Kim and Kim, 2014). Meanwhile, the numerical analysis on seepage characteristics via the code was applied in other fields, such as dams (e.g., Guo, Yu, Dong and Deng, 2007; He, Meng and Liu, 2008), pavements (e.g., Ariza, 2002, Mahboub, Liu and Allen, 2003), etc.

In addition, Seep/W can be used in the numerical analysis for aquifer tests. It is useful to evaluate the significance of an individual parameter by keeping alternatives unchanged and varying the single parameter. The independence of slug test results on the storativity in slug tests was verified numerically (Chapuis, 1998, Chapuis and Chenaf, 2002), by setting varied storativities to the model. It was also proven theoretically (Chapuis, 2017). The field permeability tests under other conditions were studied as well (Chapuis, 2005a; Chapuis and Chenaf, 2003), and the numerical value of the shape factor under steady state was presented (e.g., Chapuis, 2005a). The code could be used in the study of constant-head pumping test under different conditions such as considering

well capacity or tidal effects (Chapuis, Bélanger and Chenaf, 2006; Chapuis and Chenaf, 2003; Chapuis, Chenaf, Acevedo, Marcotte and Chouteau, 2005b). A laboratory variable-head test in a rigid-wall permeameter was simulated numerically as well (Chapuis, 2009c).

Meshing is a critical issue to be focused during numerical simulation. A selection for the appropriate finite element size is problem-dependent, which takes practice and experience to be ideal (GEO-SLOPE International Ltd., 2012). If the mesh is not well created, different element sizes provide different solutions. However, the final solution must be independent of the mesh size (Chapuis, 2010). The influence of grid size in numerical simulation of seepage in different cases have been studied by Chapuis (2010a, 2012c, d and e), which recommended that the elements of important details must be fined sufficiently and a verification model is needed to guarantee the validity of the obtained solution.

CHAPTER 3 ARTICLE 1: FIELD PERMEABILITY TESTS: IMPORTANCE OF CALIBRATION AND SYNCHRONOUS MONITORING FOR BAROMETRIC PRESSURE SENSORS

Accepted by Geotechnical Testing Journal, in publication

by

Lu Zhang[1], Robert P. Chapuis[1*], and Vahid Marefat[1]

[1] Department of Civil, Geological and Mining Engineering, École Polytechnique, P.O. Box 6079, Station CV, Montreal, QC, Canada, H3C 3A7

* Corresponding author: Phone: +514 340 4711 ext. 4427 – e-mail: robert.chapuis@polymtl.ca

Submitted for publication to the

November 2016 – Revised June 2017 and September 2017

ABSTRACT

Pressure transducers (PTs) and an atmospheric pressure transducer (APT) were used to register test data during two types of permeability tests performed in 14 wells monitoring a confined aquifer installed in the lab, and a field rising-head test in clay. The constant-head tests were performed using a peristaltic pump and thus functioned as constant flow rate tests until stabilization of the water level in the well riser pipe. The rising-head tests were started by the sudden removal of a "slug" of water. The paper presents first the method used to calibrate the transducers, in order to assess their systematic calibration error (offset) values. Then, it quantifies the influence of synchronized monitoring for the (PT-APT) pair, on short- and long-term test data, which had never been done before. The results indicate that the pair calibration cannot be neglected and the synchronized monitoring is important for all tests, except maybe for a short-duration variable-head test. For most tests however, the barometric fluctuation with time plays a significant role.

Keywords: barometric sensor, calibration, permeability test, rising-head, constant-head, hydraulic conductivity

3.1 Introduction

The in-situ hydraulic properties of aquifers and aquitards are critical for many groundwater and geotechnical problems. The hydraulic conductivity K may be assessed by several types of field permeability tests, which may provide different values. Monitoring wells installed in a large sand-box are used herein to carry out variable and constant-head tests in a confined aquifer. In addition, a long-duration rising-head field test in an aquitard is analyzed. All tests are performed within a material where the pore water pressure is greater than the atmospheric pressure, p_{atm}.

For all tests examined here, the water level positions versus time were registered by an absolute pressure transducer (PT) and an atmospheric pressure transducer (APT). Using small-size pressure transducers for water level measurements was initially proposed by Shuter and Johnson (1961), because traditional water level measuring devices (floats and acoustic devices) had limitations in wells of diameter smaller than 10 cm. Afterwards, different types of PTs, based on different physical methods, were designed and evaluated by researchers (e.g. Clark et al., 1983; Holbo et al., 1975; Keeland et al., 1997; MacVicar and Walter, 1984). Combined with electronic data recorders, the PTs have been developed to collect continuous water level or pressure data from wells (Freeman et al., 2004). A PT linked to a data logger or display device can be used in an open well and is needed for a test in a closed well. This recording system can provide more frequent and accurate measurements than manual measuring (ASTM D4044, 2015).

Two types of PTs are commonly used for water level monitoring, the absolute and gauged sensors. The absolute PT measures the total pressure, thus the sum of pressure exerted by a water column plus p_{atm}. Therefore, the p_{atm} value must be subtracted in order to obtain the height of water column. The gauged PT is vented to the atmosphere and p_{atm} is applied on the negative side of the pressure sensing device, thus allowing a direct measurement of water pressure or water column height (ISO, 2009). The gauged PT provides more accurate measurements in shallow water; however, it may respond slowly and incompletely to small variations in p_{atm} at greater depth, at the end of a long vented tube (Chapuis and Duhaime, 2017). The small-diameter vented cable must be free of kink and nick for the gauged sensor, and a wellhead may be required for certain models. The idea of a vented tube is fine but in practice, the small tube may not function well because of high humidity in air inside, leading to condensation and gas bubbles, which inhibit or delay the transmission of variations in p_{atm}. Therefore, for groundwater monitoring, a

gauged PT is usually more complex to install, transport and maintain than an absolute sensor, especially with long cables. This explains why absolute PTs are most frequently used for groundwater monitoring. The absolute PT can be easily suspended by a wire or cord, which is less costly and nearly maintenance-free, and it provides reliable measurements for long-term water level monitoring. Therefore, absolute PTs were deployed for the permeability tests of this paper.

The transducers used herein (PTs and APT) have data logging systems installed inside them. They convert a water column or a barometric pressure into a water height. They can provide rapid measurements of water level variation and can be programmed to register data at a specified rate.

A poor calibration influences the accuracy of the collected data. The evaluation of the accuracy of a single sensor has been widely discussed in observation of the water level variation. The commonly-used linear calibrations have been discussed by some researchers (e.g., Down and Williams, 1989; Keeland et al., 1997). Freeman et al. (2004) and ISO (2009) were considered as guides for submersible PTs. They proposed a temperature-corrected transducer calibration which could reduce residual error to 0.03% of full-scale output or less, and suggested that users should recalibrate the PTs and determine their performance before using them in the field. ASTM D4050 (2014) stipulates that the single PT should be checked before using it in the field by raising and lowering a measured distance in the well. Also, a verification of the sensor readings periodically with a steel tape is required (ASTM D4050, 2014).

Although the importance of calibration of PT alone has been well recognized, few papers have quantified the importance of calibrating the PT-APT pair, the importance of the APT calibration for the PT data. For an absolute PT used in field tests, the true water column is obtained by subtracting the measured barometric pressure from the measured total pressure. The drawdown for a constant-head test, and the change in water column for a variable-head test, are often obtained by the following direct subtraction: current PT reading at current time t minus the initial PT reading for the water level at rest before the test. However, this direct subtraction normally does not take into account the change in air pressure during the test. The importance of synchronous calibration for the pairs of PT(t) and APT(t) data is often neglected by practitioners. Chapuis (2009a) delineated that the p_{atm} fluctuation is one of the reasons to affect the accuracy of

the readings of the pressure sensor. The noteworthy variations in barometric pressure have been mentioned and an industry-wide standard should be developed (Sorensen and Butcher, 2011).

The expression "constant-head field test" is used for a test performed by continuously adding water into the well to keep a constant water column above the initial water level. This test is common in granular soils (e.g., Avci, 1994; Cardenas and Zlotnik, 2003; Lafhaj and Shahrour, 2002a; Lefranc 1936, 1937), and clay soils (Wilkinson, 1968; Tavenas et al., 1990). It could also be conducted by discharging a constant flow rate from the well until the hydraulic head reaches equilibrium. The in-situ constant-head tests herein are performed with a peristaltic pump by discharging water at a constant rate from the monitoring well. The tests must reach steady state. Drawdowns are registered by a PT-APT pair. This single well test is interpreted by the Lefranc method which has been included in the French standard (AFNOR NF P94-132, 1992) and Canadian Standard (CAN/BNQ 2501-135, 2008, 2014).

Compared to the continuous withdrawal from the monitoring well, the variable-head permeability tests are started with a water level sudden drop or rise in the well riser casing. The "instantaneous" water column variation was caused by adding a solid rod (mechanical slug) and then leaving it immobile under water in the well riser pipe. Afterwards, the solid slug was rapidly removed, which caused an initial rapid water drop, and then the water level raised until reaching equilibrium (rising-head test). The PT and APT were synchronized and programmed to take readings with a 2-second interval as the water recovery is rapid in the granular aquifer. In the low permeability clay layer the reading interval was 15 minutes for a long-term rising head test. Different test types yield different results, even for the same test conditions; different interpretation methods provide different K values (Chapuis 1998, 2015, 2019). Herzog (1994) reported differences of two orders of magnitude for K values. Various interpretation methods of the variable-head test data have been developed for partially and fully penetrated wells in confined and unconfined aquifer (e.g., Bouwer and Rice, 1976; Bouwer, 1989; Chapuis et al., 1981; Chiasson, 2005; Cooper et al., 1967; Hvorslev, 1951; Papadopulos et al., 1973). The Hvorslev's method is used herein to interpret the rising-head test data because it was proved experimentally, numerically and analytically to be the correct method (Chapuis, 2015, 2017; Chapuis and Chenaf, 2002; Chapuis et al., 1990). If the semi-log graph of the Hvorslev method is curved or if the data are inaccurate, the velocity graph (Chapuis et al., 1981) and the Z-t optimization method (Chiasson, 2005), if the data are inaccurate, are used to obtain the real

piezometric level (PL) for the test. All data are analyzed with the three diagnostic graphs (Chapuis, 2015). After the piezometric level correction, the corrected semi-log graph is used to calculate the *K* value.

This paper first describes the calibration method for different PT-APT pairs to assess their accuracy and then, it examines how the change in barometric pressure, during a test, influences the test data and the resulting *K* value. After that, the influence on the recovery of a long-term rising-head test in clay is also presented. In addition, the *K* values obtained from the constant-head tests are compared with those from the rising-head tests.

3.2 Theory of interpretation methods

The interpretation of constant- and variable-head tests is carried on with the Lefranc method presented in CAN/BNQ (2008, 2014), which employs the solution of Hvorslev (1951). The classical equations of the constant- and variable-head tests express the equivalence between the flow rate in the soil (Q_{soil}) and the flow rate into the pipe (Q_{inj}):

$$Q_{inj} = Q_{soil} = cKH \tag{3.1}$$

where *c* is the test shape factor, *H* the water column or applied hydraulic head difference, and *K* the hydraulic conductivity.

The constant-head test has a constant flow rate, and thus the *K* value for a constant-head test could be expressed as Equation 3.2 when the hydraulic head difference H_c becomes constant,

$$K = \frac{Q}{cH_c} \tag{3.2}$$

For the analysis of a variable-head test, the riser pipe, of inner diameter *d*, has an internal cross section area $S_{inj} = \pi d^2/4$ and the water velocity in the riser pipe is *dH/dt*. Thus,

$$Q_{inj} = -S_{inj}\frac{dH}{dt} \tag{3.3}$$

Combining Equations 3.1 and 3.3 gives:

$$\frac{dH}{dt} = -\frac{cKH}{S_{inj}} \tag{3.4}$$

Integrating Equation 3.4 leads to the solution of Hvorslev (1951), in which the hydraulic head is generally in a logarithmic form:

$$\ln\left(\frac{H_1}{H_2}\right) = -\frac{cK}{S_{inj}}(t_1 - t_2) = -\frac{K}{C}(t_1 - t_2) \tag{3.5}$$

where H_1 and H_2 are the differences in total head at times t_1 and t_2, respectively, and $C = S_{inj}/c$.

The test data are plotted as ln H versus time t in the semi-log graph. If the test is good, the data should yield a straight-line, which depends upon two parameters, the assumed PL position and the sought K value. Then, according to Equation 3.5, the slope of the straight line should be:

$$P_1 = \frac{\ln(H_1/H_2)}{(t_1 - t_2)} = -\frac{K}{C} \tag{3.6}$$

Therefore,

$$K = -P_1 \cdot C \tag{3.7}$$

The semi-log graph, however, usually presents a concaved (most often) or convex (less often) shape due to some errors in estimating the piezometric level. The correction can be made by the velocity graph or the *Z-t* method. The velocity graph method was derived from Equation 3.4 and has been verified to be correct in estimating the real PL position and the K value by plotting the water level velocity $\Delta H/\Delta t$ in the pipe versus the mean value of the assumed difference in hydraulic head $(H_i+H_{i+1})/2$ (Chapuis et al., 1981; Chapuis, 1998, 2005a).

According to Equation 3.4 the plotted data of velocity during a time interval dt versus the mean H value during the same time interval should yield a straight line. The true H value is frequently not accurately known (the PL position is assumed), and the real value H_r is the difference between the assumed H value by the user, and the error H_0 on the piezometric level, which may result from several sources of errors, including the PT and APT incorrect calibrations (Chapuis, 2009a):

$$H_r = H - H_0 \tag{3.8}$$

Combining Equations 3.4 and 3.8 yields:

$$H = -\frac{S_{inj}}{cK}\frac{dH}{dt} + H_0 \tag{3.9}$$

Thus Equation 3.9 should yield a straight line with a slope of:

$$P_2 = \frac{S_{inj}}{cK} = \frac{C}{K} \tag{3.10}$$

Therefore, the hydraulic conductivity can be also obtained as follows,

$$K = \frac{C}{P_2} \tag{3.11}$$

The intercept of Equation 3.9 with the *y*-axis for a null velocity is the piezometric level error. Then, once the PL position has been found with Equation 3.9, the method of Hvorslev (1951), which is the integral of the velocity graph method, can be used to confirm the previously found *K* value.

The *Z-t* method is used as an alternative to correct the semi-log graph of Hvorslev (1951), based on the linear least squares method in statistics to estimate the unknown piezometric correction (Chiasson, 2005). The value of H_0 in Equation 8 is first set to be the variable in the process, and then obtained when the coefficient of determination R^2 of the best-fit line of ln (H-H_0) versus t reaches its highest value, close to 1. After the correction of H_0, the curved semi-log plot becomes straight, and the slope of the straight line provides the hydraulic conductivity using Equation 3.7. The *Z-t* method is computer-based and thus accurate and rapid. The manual data selection affects the PL correction value in plotting the velocity graph. The two PL corrections resulting from the velocity graph and the *Z-t* method should be close if the registered data of water level variation are accurate and properly selected.

Two well-known formulas for the shape factor were derived at the end of the 19th century from solutions of the Laplace equation, based on the approximation shape of the cylindrical injection zone, either a sphere of equal surface or an ellipsoid (Chapuis, 1989). The simplified ellipsoid formula was given by Hvorslev (1951) as,

$$c = \frac{2\pi L}{\ln\left(2L/D\right)} \qquad L/D > 4 \tag{3.12a}$$

Whereas the complete ellipsoid formula is (e.g., Dachler, 1936):

$$c = \frac{2\pi L}{\ln\left[\frac{L}{D} + \sqrt{1 + \left(\frac{L}{D}\right)^2}\right]} \tag{3.12b}$$

These equations were derived analytically after using a few assumptions. Duhaime and Chapuis (2009) used numerical methods and found that a better approximation for a cylindrical cavity is:

$$c = \frac{2.2\pi L}{\ln\left[\frac{L}{D} + \sqrt{1 + \left(\frac{L}{D}\right)^2}\right]} \tag{3.12c}$$

The sphere equation has been developed as,

$$c = 2\pi D\sqrt{\frac{L}{D} + \frac{1}{4}} \qquad 1 \le L/D \le 8 \tag{3.13}$$

where L and D are the length and diameter of the filter pack, respectively.

3.3 Test site description and materials

3.3.1 Large sand box installed with monitoring wells

Small monitoring wells (MWs) were installed in a sand tank which consists of three layers: unconfined sand aquifer, sand-bentonite aquitard, and confined sand aquifer. Each layer has been prepared to be fairly homogeneous and isotropic, thus expected to yield little variations in hydraulic properties (Chapuis and Chenaf 2002, 2003b). The stainless steel sand box tank is 3.05 m long, 2.44 m wide and 1.22 m high. It contains, from the bottom to the top, a 38-cm thick confined sand aquifer, a 20-cm thick aquitard, and a 50-cm thick unconfined sand aquifer. The two ends of each aquifer are coarse sand around full width slotted plastic pipes connected to constant-head reservoirs. There are four reservoirs, 24 monitoring wells (MW) in the confined aquifer (see Figure 3.1), and 22 MWs in the unconfined aquifer. Depending on the imposed heads in the external reservoirs, each aquifer can have either a null gradient or a constant horizontal gradient.

The same uniform sand was used for the two aquifers. Its sizes d_{10} and d_{60} are 0.116 and 0.46 mm, respectively, and thus, the coefficient of uniformity $C_U = d_{60}/d_{10} = 4$. In the confined aquifer

the sand was statically compacted with light loads: its average dry density is 1640 kg/m^3 (Chapuis and Chenaf, 2002, 2003b). The aquitard material is a sand-bentonite mix that contains 8% bentonite, with increased bentonite content along the walls to provide a good seal by taking advantage of its swelling capacity (Chapuis, 1990).

This study presents results from monitoring wells installed in the confined aquifer. These monitoring wells have 15-cm long screens that begin at 11.3 cm from the steel bottom. The pipes have an internal diameter of 33.8 mm, and an external diameter of 42.5 mm. They were buried in the sand during its placement and developed by slight overpumping. Their slots are 0.25 mm wide, and their open area is about 2%.

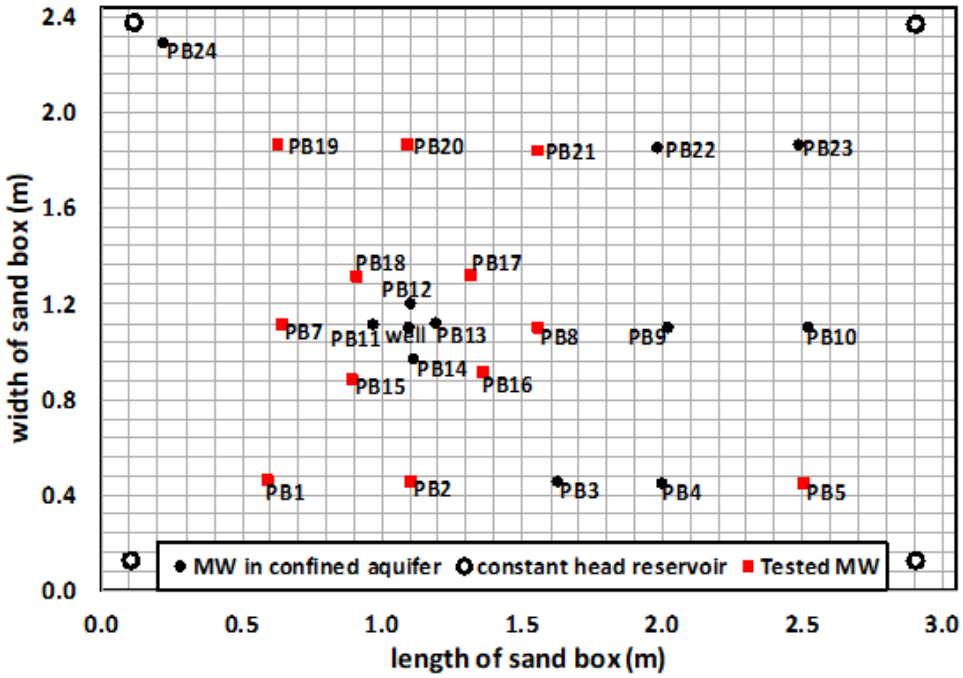

Figure 3.1: Plan of monitoring wells (MWs) installed in the sand box.

3.3.2 Lachenaie clay site and monitoring wells

Results are presented for a long-term rising-head permeability test, which was conducted in a monitoring well installed in Lachenaie clay. The nine (9) study sites were presented by Duhaime, Benabdallah and Chapuis (2013) and Marefat, Duhaime and Chapuis (2015). They cover an area of 50 km^2 in Lachenaie region near Montreal, Canada. At each site the intact body of clay, up to 25 m thick, is located between two more permeable layers: an upper sand layer or fractured clay

layer up to 5 m thick and a till layer up to 7 m thick below. The till rests upon shale bedrock. At each test site 2 monitoring wells named AH and AB were installed at the upper and lower third of the non-fissured clay layer respectively. The rising-head permeability test for this study was conducted within the AH monitoring well in site 1. This monitoring well has a 53-cm long screen, which was installed within a saturated fine sand filter. Its diameter and length are respectively D = 114 and L = 914 mm. The riser pipe has an internal diameter d = 52.5 mm.

3.3.3 Pressure transducers

A pressure transducer (PT) is used to monitor the fluctuations with time of the water level in the solid pipe. The absolute PT measures the total force acting on its sensor, and the measurements are retrieved from the data logger in the sensor. The water column height above the sensor is obtained by subtracting, from the PT reading, the barometric pressure reading of an atmospheric pressure transducer (APT). Figure 3.2 displays the principle of the pressure transducer. Five types of PTs were used in the project, and named A, AA, B, C, and D, to avoid citing commercial names. A single APT was used to calibrate each of the PTs. The type A and AA are of the same mode but with different full scales (FS). The FS range varies between 1.5 and 10 m, and the accuracy is 0.1% or 0.05% of its FS. The recording intervals are user dependent, which can be programmed differently corresponding to the type of the test and the permeability of the tested material.

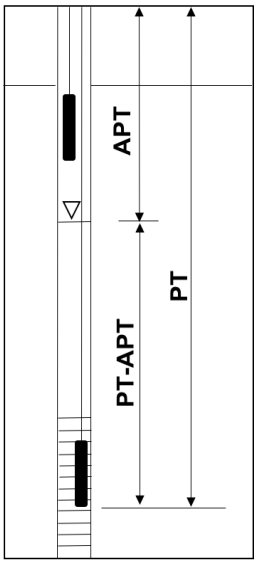

Figure 3.2: Pressure transducer principles.

3.3.4 Other required apparatuses

To measure the water level manually, a water level meter with appropriate sensitivity to water is necessary. A bailer or a mechanical slug is needed to change rapidly the water level in the well pipe for a variable-head test. For the constant-head test, a peristaltic pump is needed to keep the discharge or injection flow rate constant. In addition, a stopwatch and a graduate cylinder are used to measure and verify the flow rate from the peristaltic pump. The USB cable of the pressure transducer and a computer equipped with data extraction software are also required.

3.4 PT-APT pair calibration and monitoring

A recent calibration of the single pressure transducer is needed before putting it into use due to several widely-known reasons: (1) Each PT is unique: different transducers of the same or different manufactures provide deviated readings under the same conditions at the same time; (2) the offset value is not zero: transducers would have some drift in the recordings; (3) transducers are service-time-dependent: the range of the drift becomes greater and the systematic error becomes larger after a long time use.

The significance of the calibration for a PT-APT pair was rarely discussed. The accuracy of PTs is usually 0.1% and rarely 0.05% FS (full scale). If FS is 5 m, then the PT accuracy is ±5 mm or ±2.5 mm. The APT accuracy is usually ±5 mm. The ensuing accuracy for the water column (PT–APT) is thus ± 10 mm or ±7.5 mm, which are theoretical values. The user must be aware that the PT and APT were not calibrated as the same time in the plant where they were manufactured. Also, within the plant the air pressure depends upon the outside atmospheric pressure and also ventilation and air conditioning. Therefore, it differs from the outside atmospheric pressure. As a result, if the (PT–APT) difference is checked in the air, for example at the user's desk, a value between -10 cm and +10 cm may be found, whereas it should be zero because the PT on the user's desk is not under water (Chapuis, 2009a). This finding, which is a systematic calibration error, was confirmed by Sorensen and Butcher (2011), and Von Asmuth, Maas, Bakker and Petersen (2008). As a result, most often the physical water column height is known with an accuracy of ±10 mm or ±7.5 mm (random error) for a PT-APT pair, but with a much larger systematic error of ±10 cm, or even ±30 cm, depending on FS. In addition to these errors (random and systematic), the APT may be incorrectly compensated for temperature variation,

which is important for long duration slug tests in aquitards (Cain III, Davis, Loheide II, and Butler Jr., 2004; McLaughlin and Cohen, 2011). The resulting accuracy and the systematic error should be taken into account in any analysis of water level measurements.

Additionally, the synchronized monitoring of a PT-APT pair, which is frequently used for pumping tests, is not systematic for field permeability tests, because:

a) It is considered for a pumping test that the air pressure should be measured if the test lasts one or more days (Kruseman and de Ridder, 1994). This indicates that the PT readings must be corrected by the atmospheric pressure which varies with time, APT(t), if the test duration is longer than one day. However, barometric pressure p_{atm} may vary greatly within one day or even one hour. This should be investigated.

b) The manufacturer may suggest or the user may be using a linear interpolation for barometric compensation, especially when the PT and APT have different sampling speeds. However, this procedure fails to provide accurate compensation because it assumes a straight-line fluctuation between two sampling times.

c) Many users of PTs and APTs for permeability tests make only a single correction from an initial APT reading, which is incorrect, and yields time-variable errors on the water level data. In this project, we define the systematic piezometric reading error δ_0 as the mean value of $[\mathrm{PT}(t) - \mathrm{APT}(t)]_{\mathrm{air}}$. To ensure the accuracy of analysis for groundwater field tests, this systematic error should be known, and thus the calibration of each PT-APT pair is essential. The synchronized monitoring of the PT-APT pair is also crucial to the field permeability tests, because any change in barometric pressure affects the accuracy of the results.

3.5 In situ permeability test manipulation

The constant-head tests were performed by discharging a single constant flow rate from the riser pipe until reaching a stable water level. After the pump stopped, the water level in the riser pipe slowly returned to the pre-test static water level. The equilibrium state during pumping and the post-test static water level were checked by measuring with a water level meter. The discharge rate was 100 ml/min, the pumping total duration was 50 minutes, and 10 minutes were allowed for recovery. All discharge rates were automatically controlled by the peristaltic pump which had been calibrated before the test. It was monitored manually as well using a burette and a stopwatch

in case the real rate deviated from the value shown on the pump display. The PT registered the water level variation every 15 seconds during the test, and the APT recorded the air pressure change synchronously to provide accurate recordings for water levels.

The rising-head test was achieved by a sudden removal of a volume of water from the well and subsequently recording the water level rise versus time. The test process was quite rapid in granular soils. The recovery took around 1 to 2 minutes when the rising-head test was performed in the large sand box; the pressure transducer recorded the water level variation with an interval of 2 seconds. All rising-head tests were repeated (duplicated) to confirm the results. For the low-permeability Lachenaie clay, the recovery of the rising-head test was very slow: the pressure transducer was programmed to register once per 15 minutes. The nearly full recovery of this rising-head test in clay lasted two months.

3.6 Test results

3.6.1 Calibration of PT-APT pairs on user's desk

The air pressure in the laboratory (which differs from the outside atmospheric pressure) was always taken into account because a fluctuation of a few centimeters may have a significant impact on the water level data. The barometric pressure in the field is able to greatly change due to the change in local weather.

The difference between the PT and APT data at time t in the air, thus $[PT(t) - APT(t)]_{air}$, were obtained for each PT-APT pair. An example of this difference with two transducers in the air (on a desk) is plotted in Figure 3.3, to assess the systematic error for this pair. The mean systematic error, δ_0, which is the mean value of $[PT(t) - APT(t)]_{air}$, is δ_0 = -4.6 ± 0.5 cm for this pair, where ± 0.5 cm defines the total range of all measured values.

For the A series of three transducers, the errors δ_0 were -2.7, -7.7 and -11.3 cm. These errors were found to be stable with time. The errors δ_0 of the AA series were between -2.8 cm and -1.3 cm. For the B series, the errors δ_0 were between -3.4 cm and 0 cm, but they took initially some time to decline and gradually reach a stable level with a random fluctuation of ±1 cm. For the C series, the errors δ_0 were nearly stable with time. For most transducers of the C series the error δ_0 was between -2.9 cm and +7.6 cm, except that C3 had an error δ_0 of +17.2 cm. These transducers

were not used for the field permeability tests reported in this paper. For the D series, the errors δ_0 were roughly stable with time, and they were between -5.7 and +4.0 cm.

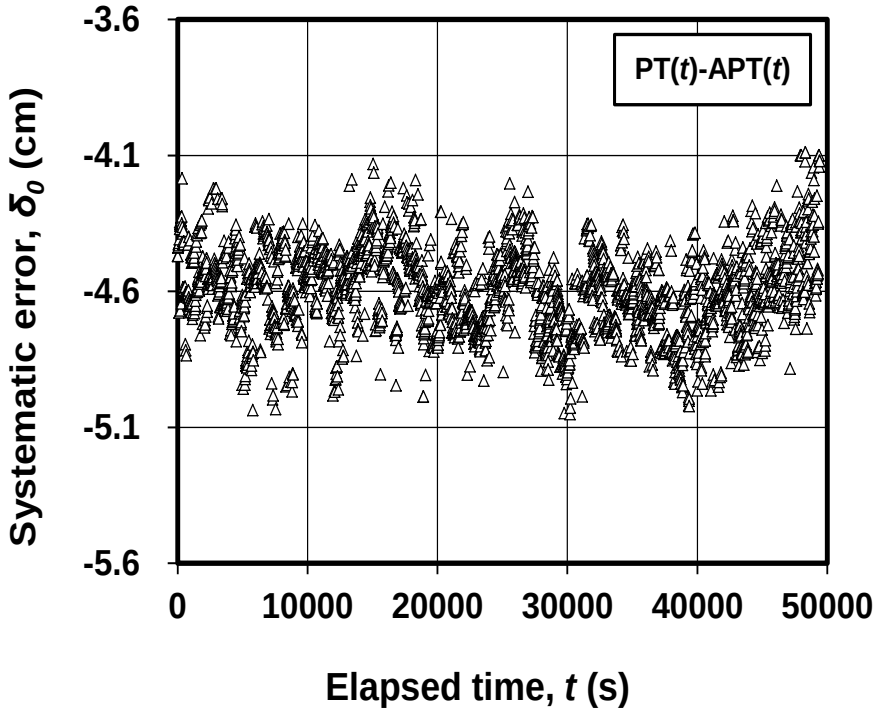

Figure 3.3: Example of $[\mathrm{PT}(t) - \mathrm{APT}(t)]_{\mathrm{air}}$ data for a pair of transducers.

The examples of errors which have been previously given are for pairs made with only one barometric transducer (the same one for all pairs). It is reminded here that a correction must be defined for each pair formed by a PT and an APT.

For constant- and variable-head tests, the water level change within the MW riser pipe was monitored with a PT-APT pair. The apparent water column for the test, at a time t, is $H(t)$, whereas the really active water column is $H_r(t)$, the two being related by:

$$H(t) = \mathrm{PT}(t) - \mathrm{APT}(t) = H_r(t) + \delta_0 \tag{3.14}$$

The smaller the systematic error of the (PT-APT) pair, the better the test data for water column measurement. It is clear that to ensure the accuracy of the test data, a barometric transducer is of significant necessity for any field permeability test. In other words, the systematic error of the pair of transducers should be subtracted from the original results, in order to obtain the actual water level in the riser pipe.

3.6.2 Influence of barometric synchronous monitoring on in-situ tests

3.6.2.1 Short term tests

For the sandy confined aquifer at lab scale, the recovery in the variable-head tests almost finished in less than 2 minutes, during which the barometric pressure fluctuation did not affect much on the results. Hence, the barometric synchronous monitoring could be neglected for the variable-head test in relatively high-permeable soils.

Constant-head tests were performed in monitoring wells of the confined aquifer at lab scale. Two sets of constant-head test data versus time t are plotted in Figure 3.4 for monitoring well PB8. One plot gives the variation in water column, as PT(t) – APT(t), between 80 and 87.5 cm (see the left ordinate). The other plot is obtained when a single barometric correction is used (see right ordinate, for the plot ending near 85 cm), which is:

$$H(t) = \mathrm{PT}(t) - \mathrm{APT}(pre-test) \tag{3.15}$$

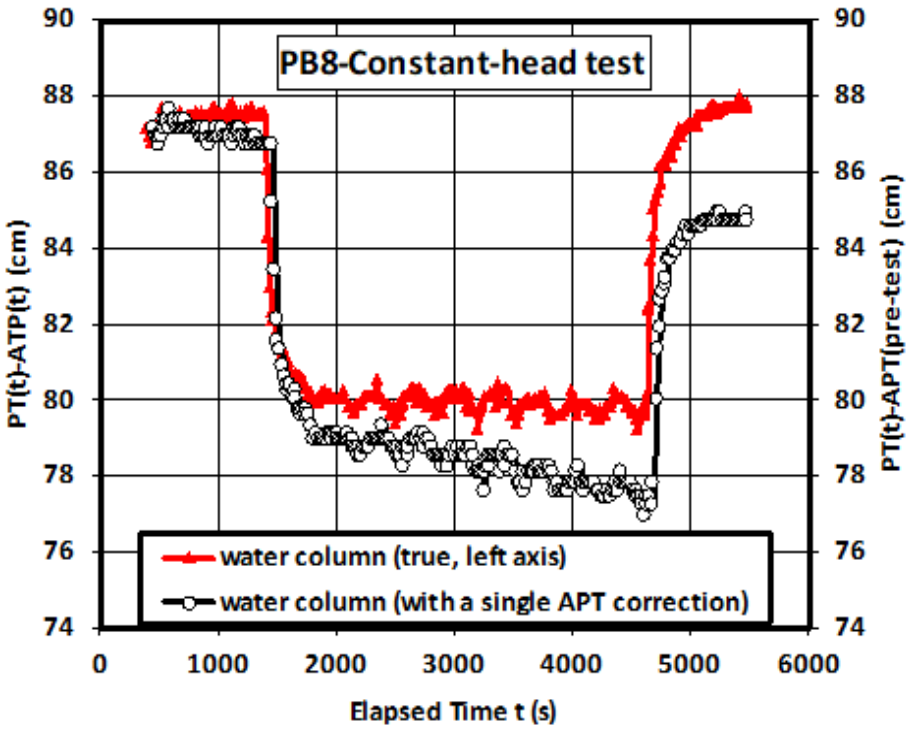

Figure 3.4: Influence of f barometric pressure fluctuation on constant-head test.

The two plots differ only by using either a variable or constant APT value. As mentioned before, according to experience, many users of PTs and APTs make a single barometric correction (some pre-test APT values) for field permeability tests, which is shown here to be incorrect.

In Figure 3.4, it is clear that the water column calculated with a single barometric correction (the [PT(*t*) – APT(*pre-test*)] plot) is around 87 cm before starting the test, whereas it is about 85 cm after the test, 2 cm below the pre-test value. However, physically, and this was verified with a measuring tape from the top of the pipe, the water level in the monitoring well had returned to its initial position. Therefore, the plot means that the atmospheric pressure (APT) has varied by about 2 cm during the test. When the constant-rate pumping started, the water level rapidly dropped by about 9 cm in about 4 minutes, as shown in the plot of water column with a single APT correction, and then seemed to slowly decrease with time until the end of pumping at 4600 seconds: apparently, this "constant-head" test never reached stabilization, i.e., a constant drawdown. This conclusion would be incorrect because the atmospheric pressure variation of 2 cm of water is responsible for this apparent decline in water level, which is clear between 1800 and 4600 seconds (Figure 3.4).

The [PT(*t*) – APT(*t*)] plot, in which the atmospheric correction varies with time helps to reach a different conclusion: the water column has stabilized rapidly, 4-5 minutes after starting the constant-rate pumping. The water column was constant before and after the test at approximately 87.5 cm, and it has stabilized at about 80 cm while pumping.

This example clearly shows that using a PT without a barometric correction that varies with time, at the same sampling rate as the pressure transducer (PT), may yield errors in interpreting the data of a constant-head test. For the example in Figure 3.4, one may consider that the test was incomplete because there was a declining trend in the water column. This may be misinterpreted, for example, as a need to have had a longer duration test.

After a long pumping time, e.g., during groundwater sampling in a monitoring well, the water column given by Equation 3.14 may stabilize, simply because the atmospheric pressure decreased and finally stabilized, for example 15 cm below that prevailing before the test. However, if this change in p_{atm} is ignored, the calculated K value is erroneous. For the case of Figure 3.4, the true

stabilized drawdown is about 7.5 cm, but an incessant change in atmospheric pressure of 15 cm would yield an apparently stabilized drawdown of (7.5 + 15) cm, an error of 300% for the stabilized drawdown, thus a 300% error on the calculated *K* value. This simple example, which may occur during a groundwater sampling test, is illustrating that we need to pay more attention to the importance of correction for the atmospheric pressure variation.

3.6.2.2 Long Term Test

In-situ permeability tests in aquitards can last several weeks, and thus the variation in patm is more important than for short duration tests in aquifers. Figure 3.5 presents two data sets of total pressure and atmospheric pressure in 5 days, which were selected from the recovery curve of a rising-head test in Lachenaie clay during a period of two months. The PT data decrease with time as they would for a falling-head test, but in this case it was a rising-head test. This seems abnormal. Let us examine now the APT data to try to understand why.

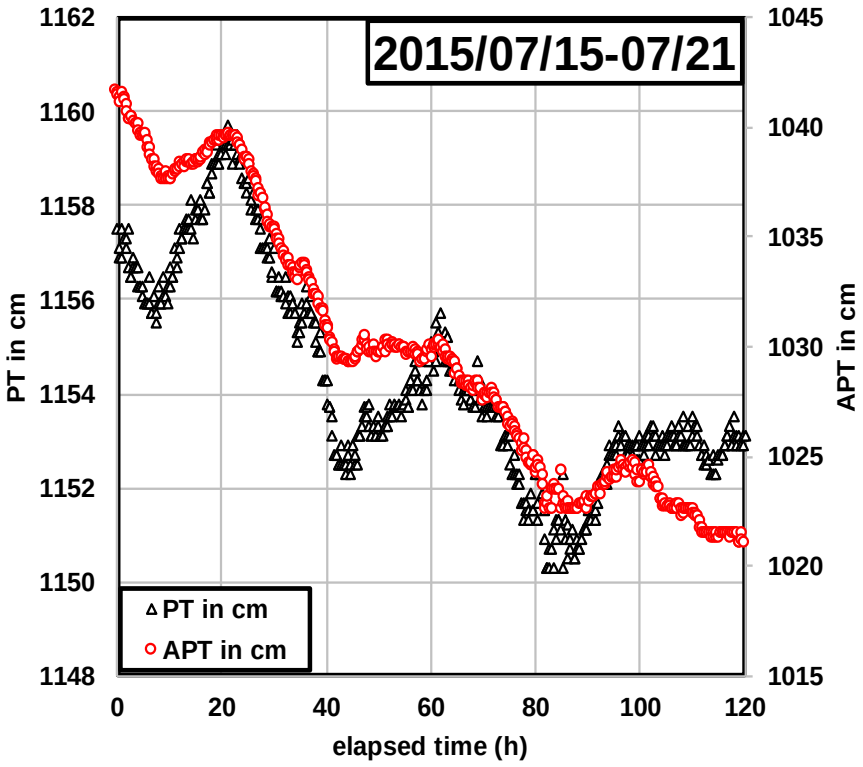

Figure 3.5: Five days of PT and APT data for the rising-head test in Lachenaie clay.

Apparently, the variation trends of the PT follow that of the APT, and the turning points are exactly at the same time. From t = 0 to 120 h, the atmospheric pressure varies from 1041.6 cm to

1021.1 cm and has a large difference 20.5 cm compared with the 4.6 cm decrease in total pressure. The data for [PT(t) – APT(t)] give the real water level variation in Figure 3.6: they have a rising trend instead of seemingly falling trend of Figure 3.5, in accordance with the recovery phase of the rising-head test. The differences between the two plots (Figure 3.6) clearly show the importance of the synchronization of the PT-APT pair for measuring water level variations.

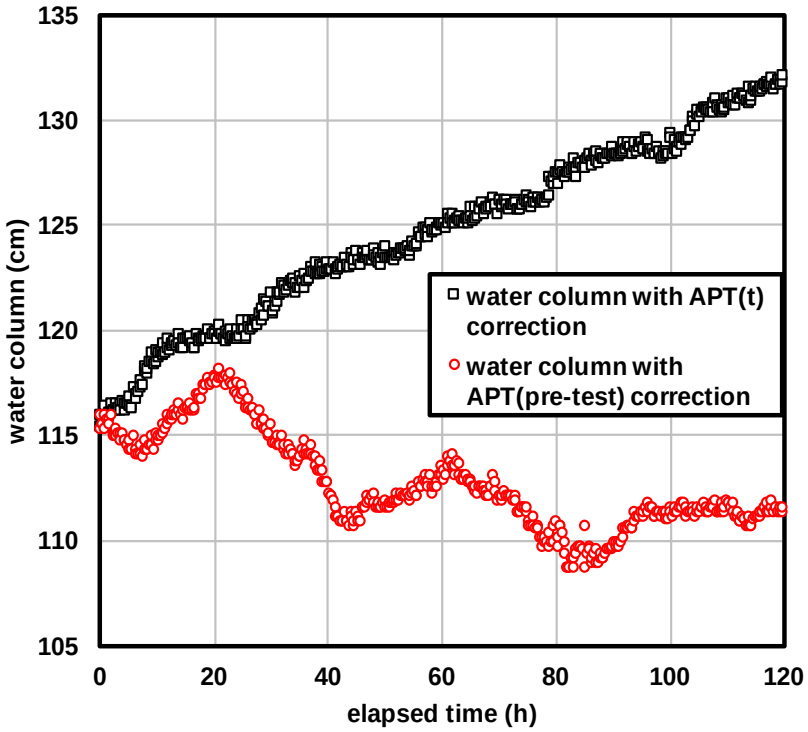

Figure 3.6: Influence of barometric pressure fluctuation on long-term rising-head test data.

3.6.2.3 Examples of test data analyses

The K values of the rising-head tests were calculated for 14 monitoring wells of the confined aquifer in the laboratory sand tank. Here, to give an example, we present only one set of test data for monitoring well PB21, the relationship between ln (H_r) and the elapsed time t (Figure 3.7).

There is no injection zone (filter pack) around the monitoring well. The diameter of the MW is 4.25 cm, and the length of the screen is 15 cm. The ratio of the length to diameter, L/D, is 3.53 which is in the range of $1 \leqslant L/D \leqslant 8$. Equation 3.13 gives the shape factor, c = 51.91cm. For each monitoring well, the K value obtained from the two batches of rising-head tests are very close. The values presented in the second column of Table 3.1 are the mean values of the two

batches of tests, between 4.97 x 10^{-3} cm/s to 9.02 x 10^{-3} cm/s, and have an average value of 7.13 x 10^{-3} cm/s. The lowest local *K* is 30% lower and the highest local *K* value is 26% higher compared with its mean value.

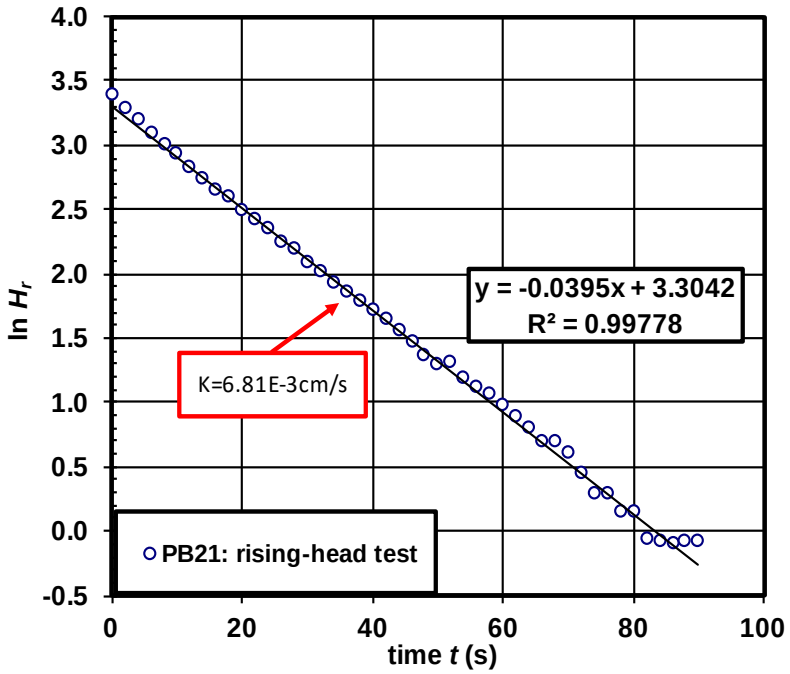

Figure 3.7: Semi-log graph of a rising-head test in PB21

The constant-head tests give an average *K* of 5.06 x 10^{-3} cm/s for the confined sand tank aquifer. The highest local *K* value is 6.08 x 10^{-3} cm/s at PB22 and 20% higher than the average *K* value (Table 3.1). The lowest *K* value is 4.40 x 10^{-3} cm/s for PB2, 13% lower than the average *K* value. It appears that the local hydraulic conductivity at each single well does not vary in a wide range. Therefore, the confined sand tank aquifer appears to be fairly homogeneous, an essential condition for a research project.

Table 3.1: Local hydraulic conductivities for MWs of the two types field permeability tests

MW no.	rising-head cm/s	constant-head cm/s
PB1	7.33E-03	5.84E-03
PB2	6.06E-03	4.40E-03
PB5	4.97E-03	4.46E-03
PB7	7.60E-03	5.35E-03
PB8	7.51E-03	4.54E-03
PB15	8.04E-03	5.00E-03
PB16	9.02E-03	5.62E-03
PB17	7.55E-03	5.21E-03
PB18	8.88E-03	5.13E-03
PB19	6.12E-03	4.46E-03
PB20	7.19E-03	4.71E-03
PB21	6.73E-03	5.08E-03
PB22	6.94E-03	6.08E-03
PB23	5.91E-03	5.00E-03

The *K* values obtained by rising- and constant-head tests are not equal but relatively close for each monitoring well. The largest deviation occurs at the MW PB 18, where the rising-head test provides a *K* value of 8.88 x 10^{-3} cm/s and the constant-head test gives a value of 5.13 x 10^{-3} cm/s for *K*. The narrow distributions of *K* values were analyzed using the modal decomposition method (Chapuis, 2016; Chapuis, Dallaire and Saucier, 2014): they are unimodal with low variances μ of 0.115 and 0.157 for the constant-head and variable-head tests respectively (Figure 3.8). This indicates a good homogeneity of the confined aquifer. Though the two types of testing methods yield different *K* values, the difference is small. The slightly lower *K* values given by the constant-head tests may be due to a reduced influence of the zone adjacent to the well screen. As a constant-head tests involves a larger soil volume than a rising-head tests, it is less likely to be influenced by some unavoidable remolding along the screen. This possible explanation will have to be verified using other field tests and numerical simulations.

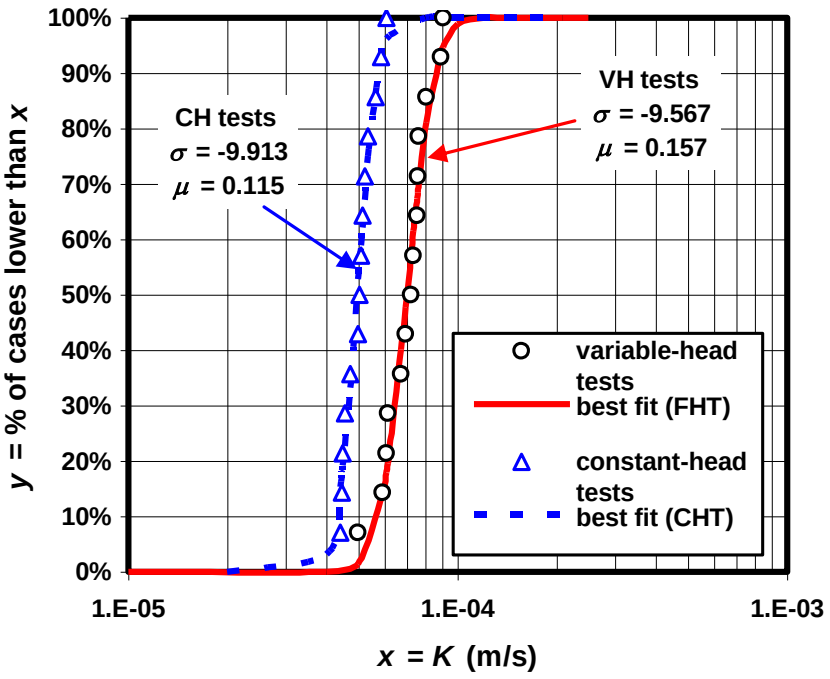

Figure 3.8: Analysis of the distribution of the *K* values obtained with the variable-head and constant-head tests performed in 14 monitoring wells of the large sand box.

Let us examine now the data of the long-term rising-head test performed in the Lachenaie clay. The semi-log graph with the synchronous APT correction is presented in Figure 3.9. It appears as a straight line after a piezometric correction of 20.4 cm. The dispersion of field data around the straight line is increasing with time, as recently explained in Chapuis and Duhaime (2017). For this test, however, the error bars were not added in Figure 3.9 because they would mask the plot.

For the Lachenaie test, the length and the diameter of the filter pack are 11.4 and 91.4 cm, respectively. The ratio of the length to diameter, *L/D*, is 8.02, which is in the range of $L/D > 4$. Equation 3.12 gives the shape factor, c = 206.96 cm. The *K* value was calculated as 6.28 x 10^{-8} cm/s, which is typical of the low permeability Lachenaie clay. The other test data with a single APT correction appear also in Figure 3.9: they present a zigzag, which makes it difficult to calculate the *K* value.

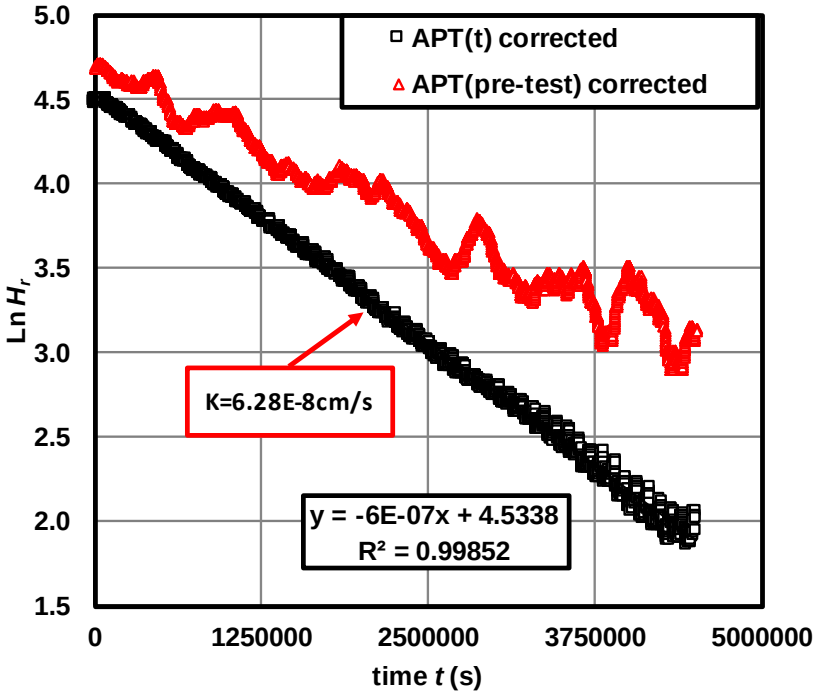

Figure 3.9: Semi-log graph of the rising-head test in Lachenaie clay

3.7 Summary

When a pressure transducer (PT) and an atmospheric pressure transducer (APT) are in the air, the difference [PT(t) – APT(t)] should be zero in theory, and it should not vary with time t. A plot of this quantity versus time should yield a mean value of zero and the fluctuations around zero should give the accuracy of this PT-APT pair. In practice, however, the mean difference is rarely zero, but it defines a systematic calibration error for the PT-APT pair.

Five different types of PTs (for a total of 32 PTs) were verified using a single APT pressure sensor. The 32 pairs yielded differences which were not equal to zero. The calibration yielded a zero calibration error between -11 and +17 cm. This is a systematic error for the measured values of all water columns which are used to calculate the K value as given by a field permeability test.

A simple test protocol (transducers in the air on the desk) is needed to assess the systematic error and the PT-APT pair accuracy. Each PT user must first select the appropriate range of measurement, for example 0-3 m for a field permeability test. The systematic error of the PT-APT pair must be documented to obtain the calibration error and the PT-APT pair accuracy.

Later on, for a field test, the correction for air pressure should not be done with a single APT value for some pre-test time. The air pressure varies continuously during any field hydraulic test (or even laboratory test). Therefore, the PT and APT must be synchronized, in order to collect data at the same times. These data are then used to derive the values of the water column using the difference [PT(t) – APT(t)], where the barometric correction varies synchronously with time t. This procedure is essential to obtain reliable test data before doing any data interpretation.

An example has been given to show the important influence of the air pressure variation within the laboratory (air conditioning and ventilation) during a constant-head test, which lasted for less than one hour. It would have yielded a misunderstanding on the equilibrium state and an erroneous K value if only a single barometric correction had been considered. More significant influence has been observed in the recovery plot of a rising-head test in clay lasting for 5 days. The large variation of 20.5 cm in barometric pressure was able to reverse the trend of water level and plot an inaccurate recovery curve, as if it were a falling-head test whereas it was a rising-head test. Thus, it is important to use the APT synchronously with the PT.

Two batches of rising-head tests were performed on 14 monitoring wells (MWs) in a laboratory sand tank to ensure the validity of the test data: they yielded nearly identical results. The test data were interpreted by the Hvorslev's method, whereas the velocity graph and the Z-t method were both used to correct the piezometric level error. The presented K values are the mean values of the two batches, ranging from 4.97×10^{-3} cm/s to 9.02×10^{-3} cm/s and having an average value of 7.13×10^{-3} cm/s. The constant-head tests were conducted on the same MWs, and the local K values varied between 4.40×10^{-3}cm/s and 6.08×10^{-3}cm/s, giving an average value of 5.06×10^{-3} cm/s.

Comparing with the derived average K of the confined aquifer, the local K values for all monitoring wells differ from the rising-head test values by 1% to 30%, and differ from the constant-head test values by 0% to 20%. It is found that the constant-head tests have a smaller range of variation, probably because they test larger volumes than variable-head tests, in a homogenized sand aquifer; hence they are considered to yield more reliable K values. The rising- and constant-head tests provide different K values, but these are very close. As a result, the values derived from the two testing methods are acceptable and may be used to assess the aquifer permeability.

When a single APT correction was used for a rising-head test lasting for two months in Lachenaie clay, its semi-log graph presented many bends, which could not be interpreted by the conventional methods. The synchronized APT calibration removed these bends and provided a smooth curve for the semi-log graph. The semi-log graph was successfully linearized by a piezometric correction of 20 cm, and yielded a K value of 6.28×10^{-8} cm/s for the tested non-fissured Lachenaie clay.

CHAPTER 4 ARTICLE 2: FIELD PERMEABILITY TESTS WITH INWARD AND OUTWARD FLOW IN CONFINED AQUIFERS

Submitted to Geotechnical Testing Journal (in revision process)

by

Lu Zhang[1], Robert P. Chapuis[1*], and Vahid Marefat[1]

[1] Department of Civil, Geological and Mining Engineering, École Polytechnique, P.O. Box 6079, Station CV, Montreal, QC, Canada, H3C 3A7

* Corresponding author: Phone: +514 340 4711 ext. 4427 – e-mail: robert.chapuis@polymtl.ca

November 2017-Revised July 2018

ABSTRACT

Field permeability tests gave the local hydraulic conductivities (*K*) at three different sites. Constant-head (CH) and variable-head (VH) tests were performed using 33 monitoring wells (MWs) installed in confined aquifers. Each test method was conducted with either an inward flow from aquifer to pipe or outward flow from pipe to aquifer, which makes a number of four types of tests: discharge and injection tests (CH), and rising- and falling-head tests (VH). The MWs were developed soon after their installation to remove the fine particles close to screen areas. The article first explains various test results at different sites. For MWs in a perfect condition, two opposite flows should yield equivalent *K*-values. However, the tests with inward flow and outward flow gave different *K*-values, which is due to some clogging of the screen or internal erosion of the filter pack. In addition, the *K* (CH tests), frequently lower than the *K* (VH tests), are more accurate because the CH test lasts more time and has a larger influence radius. The paper also provides recommendations for estimating reliable *K*-values for a confined aquifer.

Keywords: field permeability test, constant-head, variable-head, outward flow, inward flow

4.1 Introduction

Hydraulic conductivity of granular soil is normally estimated by tests at three scales: constant and falling head permeability test through a permeameter in the laboratory (ASTM D2434, 2006; ASTM D5084, 2016), field permeability tests in single wells (AFNOR NF P94-132, 1992;

ASTM D4044, 2015; CAN/BNQ 2501-135, 2014), and injection or withdrawal test (pumping test) with a control well and several piezometers or observation wells (ASTM D4050, 2014). For the homogeneous aquifer, the scale effect is insignificant and can be neglected (Dallaire, 2004; Chapuis et al., 2005a). The field permeability tests are selected because they can be achieved simply in a single monitoring well (MW).

The field permeability tests consist of generating a water flow with a constant or variable water head into a cavity of a given shape, named cavity/water injection zone, at the bottom of a borehole and observing the variations of the water level (Cassan 2005). These two test methods: constant-head (CH) and variable-head (VH) tests in cased borehole were proposed by the French engineer Lefranc (1936, 1937), and are known as the Lefranc test. These reliable test methods to obtain the local *K*-values, when the pumping test is not available, were included in several textbooks (Cassan 1980, 2005; Monnet 2015) and the French, International and Canadian standards (AFNOR NF P94-132 1992, 2000; ISO 22282-2 2012; CAN/BNQ 2501-135 2014). The CH test is also used to assess the groutability of the soil or rock (Cambefort 1987; Bell 2004) and the anisotropy coefficient of the aquifer (Cassan 2000; Lafhaj and Shahrour 2004).

Two ways are available to perform a CH test. The first one is to add or remove water continuously to maintain a constant water level in the well casing until the flow rate becomes nearly constant (Cassan 2005; Monnet 2015). However, it is easier to do the test with a constant flow rate, which is the second way to achieve a constant head difference, sometimes also called a constant-rate test (Cassan 2005; ISO 22282-2 2012). Even though the two manipulations are different, the CH test must reach a steady state at the end where the pumping flow rate equals the flow rate into the water injection zone.

Besides the cased boreholes, the CH and VH tests can also be conducted in driven permeameters (Chapuis and Chenaf 2010) and MWs (e.g., Chapuis 1998). The VH test performed in a groundwater well is usually known as a slug test by hydrogeologists. However, in geotechnical engineering, it is frequently called a variable-head (VH) test (e.g., Hvorslev 1951; Cassan 2005; Chapuis 1999; Chapuis and Chenaf 2003a; Monnet 2015; Reynolds 2015).

Each of the CH and VH tests may be conducted with two opposite water flows: water could be injected into or discharge from the well riser pipe. We call "inward flow" the case of water flow

from aquifer to well pipe (water withdrawal from the well). Similarly, "outward flow" means water from pipe to aquifer (water injection into the pipe).

Constant-head (CH) test with opposite water flows are termed injection and discharge tests herein. They are achieved by injecting and discharging water, respectively, in the riser pipe at a constant rate until the hydraulic head in pipe reaches equilibrium (steady state). The test is interpreted by the Lefranc method (AFNOR NF P94-132, 1992; CAN/BNQ 2501-135, 2014) which requires a known shape factor *c* for the water intake zone. It is noted that the term constant-head (injection/extraction) test was also used to describe the constant hydraulic head created by varied injection/pumping rate (e.g., Cardenas and Zlotnik, 2003; Wilkinson, 1968).

A variable-head (VH) test, also known as slug test, starts with a sudden change of water level in the well riser pipe. This can be achieved by a quick injection (falling-head test) or removal (rising-head test) of water, and the subsequent water level response is recorded over time. Several ways to initiate a VH test are discussed in ASTM D4044 (2015). The interpretation method used herein for the falling- and rising-head tests is the solution of Hvorslev (1951), whereas the velocity graph method (Chapuis et al., 1981) and *Z*-*t* method (Chiasson, 2005) are used to correct the incorrectly assumed piezometric level.

All tests were conducted in MWs: the performance of the well screen and filter pack plays a significant role in the relationships between head, time and flow rate, used to derive the hydraulic conductivity. Well development is necessary to remove the deposits during borehole drilling and fine particles from the aquifer material. The development process for the MWs is much less severe than for pumping wells, and thus the potential of clogging is higher (Baptiste and Chapuis, 2015). It is estimated that more than 65% of MWs installed in North America since the late 1970s were poorly installed or developed (Nielsen and Schalla, 2005). These damaged or partly clogged wells have the potential to yield inaccurate *K*-values.

To evaluate the performance of a well, a step-drawdown test can be conducted to evaluate the skin effect, which refers to the linear well loss caused by the improvement or damage during drilling and completion of the well (Kruseman and de Ridder 1994). A positive skin indicates a reduced permeability at the wellbore due to clogging from drilling debris or biofouling, etc. Conversely, a negative skin may be caused by over-pumping, which cleans out the surrounding fine particles, yielding a value of hydraulic conductivity higher than that of the formation

(Driscoll, 1986; Paul, 1987; Yang and Gates, 1997). Even if a well was developed after it was installed, the conditions of the well screen and filter pack may change after several tests. According to Hvorslev (1951), during a test, if an outward flow displaces sediments at the bottom of the pipe, clogging of the well screen may occur and thereby decrease the apparent permeability, *K*, of soil. Also, erosion may appear in the natural soil against the filter pack resulting from an inward flow washing away fine particles, and hence a higher apparent *K* is obtained.

The difference in *K*-values, which might be caused by the inward and outward flows, was mentioned in Hvorslev (1951). However, few researches have addressed experimentally the problem. The variable falling- and rising-head tests should yield equal *K*-values if the MW is in perfect condition, because the physical mechanisms of the two types of the VH-test are identical except for the opposite direction of water flow. The standards recommend performing the VH or slug test by generating either a water level rise or fall (CAN/BNQ 2501-135, 2014; ASTM D4044 2015). And normally, researchers analyze the VH-test results of a single flow direction (e.g., Bouwer and Rice, 1976; Chapuis, 1998, 2005b; Chapuis et al., 2007; Cooper et al., 1967). The two types of CH tests, discharging and injecting water, were considered the same way (ASTM 4050 2014). All of these indicate that the practical results of the two ways to conduct the CH- and VH-tests have been rarely compared by researchers and practitioners in the same MW.

Additionally, the CH-test is usually performed in pervious materials and the VH-test is recommended for low permeability materials to shorten the test time (CAN/BNQ 2501-130, 2014; CAN/BNQ 2501-135, 2014). However, the VH-test may be also conducted in high permeability aquifers, because the rapid water level changes can be efficiently recorded by a pressure transducer (PT). The two commonly used test methods may yield some difference in *K*-values; however, few people apply both of them to the same well. They may improve the reliability of *K*-values by duplicating the same test, but neglect to compare either the two test methods or the two types of tests with opposite flows in the same MW.

In this article, four types of tests were performed in three different confined aquifers equipped with MWs: a sand aquifer in a large sand box in the laboratory, a sand aquifer and a fractured rock aquifer respectively in Sorel and Lachenaie in Quebec, Canada. A total number of around 150 tests were conducted in 33 MWs, including duplicate tests to verify the accuracy of results.

Table 4.1 summarizes the four types of tests and the number of tested MWs. Various situations occurred at different test sites and their *K*-values are first presented and discussed. By comparing the results of the two opposite flow paths in CH- and VH-tests, the possibility of the well clogging and/or erosion in filter pack are checked. Inward and outward flows have different effects on erosion and clogging around the well screen. In addition, the article quantifies the difference in *K*-values between the CH- and VH-tests, and provides recommendations for the choice of test method.

Table 4.1: Summary of test types and numbers

flow direction		inward flow	outward flow
test type	CH tests	discharge test	injection test
	VH tests	rising-head test	falling-head test
sand box		14 MWs, 4 types of tests/MW	
Sorel		15 MWs, 4 types of tests/MW	
Lachenaie		4 MWs, 4 types of tests/MW	

4.2 Interpretation methods

The CH-tests are interpreted by the Lefranc method (CAN/BNQ 2501-135, 2014; Lefranc, 1936, 1937). The hydraulic conductivity *K* can be expressed as

$$K = \frac{Q}{cH_c} \tag{4.1}$$

where Q is the constant flow rate of the CH-test, H_c is the constant hydraulic head difference between pre-test and steady state, and c is the shape factor.

Cooper and Jacob (1946) provided an approximation under transient state, derived from the Theis type-curve method (1935), to determine the transmissivity T and storativity S of confined aquifers. The Cooper-Jacob's s-log t method is used to interpret the test data for CH-tests that do

not reach the steady state. The drawndown s is plotted versus the logarithm of time $\log t$ since the pumping starts. The equation is expressed as

$$s = \frac{2.303Q}{4\pi T}\log\left(\frac{2.25Tt}{r^2 S}\right) \tag{4.2}$$

A straight line is drawn through the time-drawdown data plot. The data of early and late times should be excluded for the Cooper-Jacob method because it may cause misinterpretation. The transmissivity can be determined by

$$T = \frac{2.303Q}{4\pi\Delta s} \tag{4.3}$$

where Δs is the increment of drawdown for one log-cycle of time for the straight line. For the saturated aquifer, the hydraulic conductivity is,

$$K = \frac{T}{b} = \frac{2.303Q}{4\pi b\Delta s} \tag{4.4}$$

where b is the thickness of the saturated aquifer.

The Hvorslev's solution (Hvorslev, 1951) is used to interpret the VH-tests data, in which the hydraulic head is in a logarithmic form:

$$\ln\left(\frac{H_1}{H_2}\right) = -\frac{cK}{S_{inj}}\left(t_1 - t_2\right) \tag{4.5}$$

where $S_{inj} = \pi d^2/4$ is internal cross section area of the well pipe, d is the internal diameter, H_1 and H_2 are the hydraulic head differences at times t_1 and t_2, respectively. Equation 4.5 yields a straight line when $\ln H$ is plotted on the y-axis and t is plotted on the x-axis.

Thus, the hydraulic conductivity is

$$K = -P_1 \cdot \frac{S_{inj}}{c} \tag{4.6}$$

in which P_1 is the slope of the straight semi-log graph.

In most cases, however, the semi-log graph appears as a concaved (most often) or convex (less often) shape due to the sign of the piezometric error (Chapuis, 2017). The velocity graph method (Chapuis et al., 1981) is applied to correct the piezometric level:

$$H = -\frac{S_{inj}}{cK}\frac{dH}{dt} + H_0 \tag{4.7}$$

where d*H*/d*t* is the water velocity, the piezometric error H_0 is the difference between the apparent *H*-value and the true value H_r. The H_0-value can be obtained from the intercept with the *y*-axis of the straight velocity plot, which may result from several sources of errors (Chapuis, 2009a).

Therefore, the hydraulic conductivity can be also expressed as

$$K = \frac{1}{P_2} \cdot \frac{S_{inj}}{c} \tag{4.8}$$

where P_2 is the slope of the straight velocity graph. When the variable-head test data set is large, a five-step procedure should be followed to obtain the accurate *K* value (Chapuis 2009b).

An alternative to find the H_0-value is the *Z-t* method (Chiasson, 2005). It uses the unbiased estimator on the linear least squares method in statistics, which makes the best-fit line of ln (H-H_0) versus *t*. The process can be simply achieved by a spreadsheet. The *Z-t* method is more rapid and precise compared to the traditional velocity plot, because it is independent of the manual data selection. However, it lacks a few advantages of the velocity graph method, like identifying hydraulic fracturing (Chapuis, 1992b), clay consolidation, or leakage in buried pipe (Chapuis, 2010b), etc. Additionally, the *Z-t* method should be used in combination with the velocity graph method as it is only valid when the velocity plot is linear (Chiasson, 2012). The two PL corrections resulting from the velocity graph and the *Z-t* method for the material with high hydraulic conductivity should be close for a good test.

Two well-known formulas for the shape factor come from solutions to the Laplace equation, based on the approximated shape of the cylindrical injection zone (Chapuis, 1989). The complete ellipsoid formula is given by Dachler (1936), which was simplified by Hvorslev (1951) as,

$$c = \frac{2\pi L}{\ln(2L/D)} \qquad \text{if } L/D > 4 \tag{4.9}$$

The sphere equation of shape factor can be expressed as,

$$c = 2\pi D\sqrt{\frac{L}{D}+\frac{1}{4}} \qquad \text{if } 1 \le L/D \le 8 \qquad (4.10)$$

where L and D are the length and diameter of the water intake zone, respectively.

4.3 Test site description

4.3.1 The sand box installed with monitoring wells

The stainless-steel sand box has dimensions of 3.05 m x 2.44 m x 1.22 m. It consists of a 38-cm thick confined sand aquifer at the bottom, overlying by a 20-cm-thick aquitard, and a 50-cm thick unconfined sand aquifer on the top. A total number of 24 MWs were installed in the confined aquifer and named PB1 to PB24. The plan of the sand box installed with MWs is shown in (Zhang et al., 2018a). Each layer was controlled to achieve uniformity in material density and hydraulic properties. Four reservoirs, connected to the slotted plastic pipes at both ends of the sand box, keep constant head boundaries in aquifers. The controlled total heads in the reservoirs yield either no gradient or a constant horizontal gradient in each aquifer.

The aquifer material is homogeneous sand with d_{10} = 0.116 mm and d_{60} = 0.46 mm, and the coefficient of uniformity $C_U = d_{60}/d_{10}$ = 4. The sand was statically compacted with light loads, and the average dry density is 1640 kg/m^3 (Chapuis and Chenaf, 2002). A sand-bentonite mix that contains 8% bentonite was used for the aquitard material. An increased bentonite content along the walls provides a good seal due to its swelling capacity (Chapuis, 1990).

Fourteen MWs installed in the confined aquifer were available for the tests. They have internal and external diameters of 33.8 and 42.5mm, respectively. They were buried in the sand during its placement and developed by slight over-pumping. The pipes have 15 cm long screens that begin at 11.3 cm from the bottom of the sand box. The slots of the screens are 0.25 mm wide, and their open area is about 2%. There is no filter pack around the screen. Both CH- and VH- tests were conducted in the MWs. Figure 4.1 presents a schematic of the constant-head test in the sand confined aquifer.

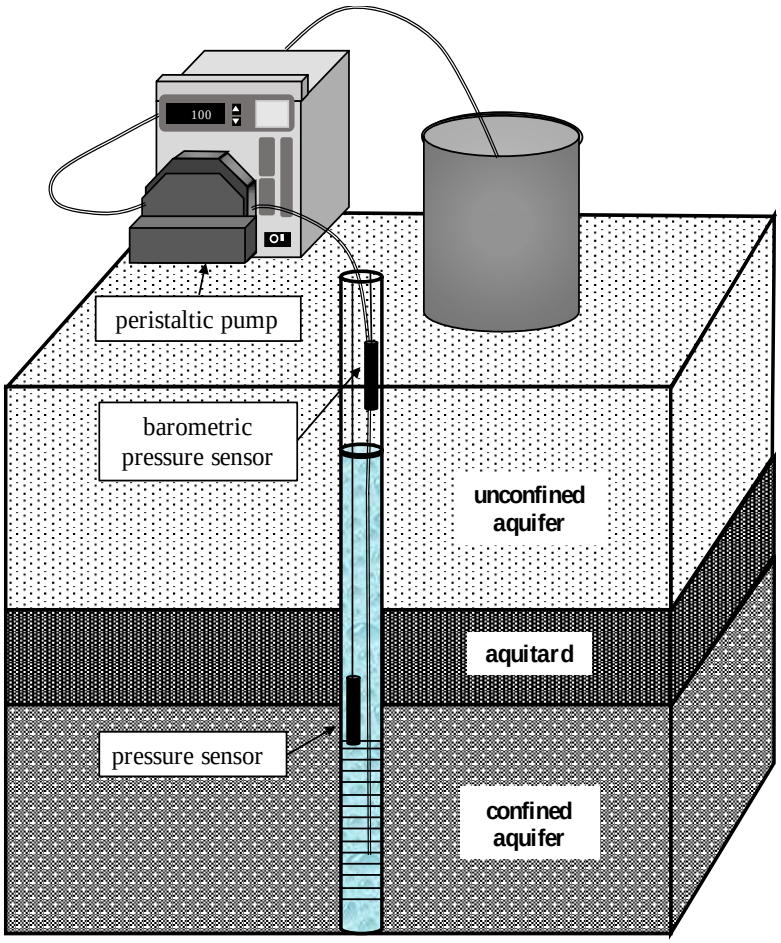

Figure 4.1: Schematic of the CH test in MW installed in the sand tank.

4.3.2 Sorel site installed with MWs

The test site is located in Sorel-Tracy, a city situated approximately 100 km northeast of Montreal, and about 2 km away from the Saint Lawrence River. The site is nearby large lagoons used for the municipal wastewater treatment with a total area of 320 000 m^2 (Chapuis et al., 2014). The test site is relatively flat and has an area of 150 m x 150 m. It is part of a wide floodplain at the confluence of the Richelieu River and the St. Lawrence River. A pumping well and 44 MWs were installed in two steps. The average distance between two MWs is 30 m except in the area around the pumping well. The MWs are named as (x, y) based on their positions (Figure 4.2).

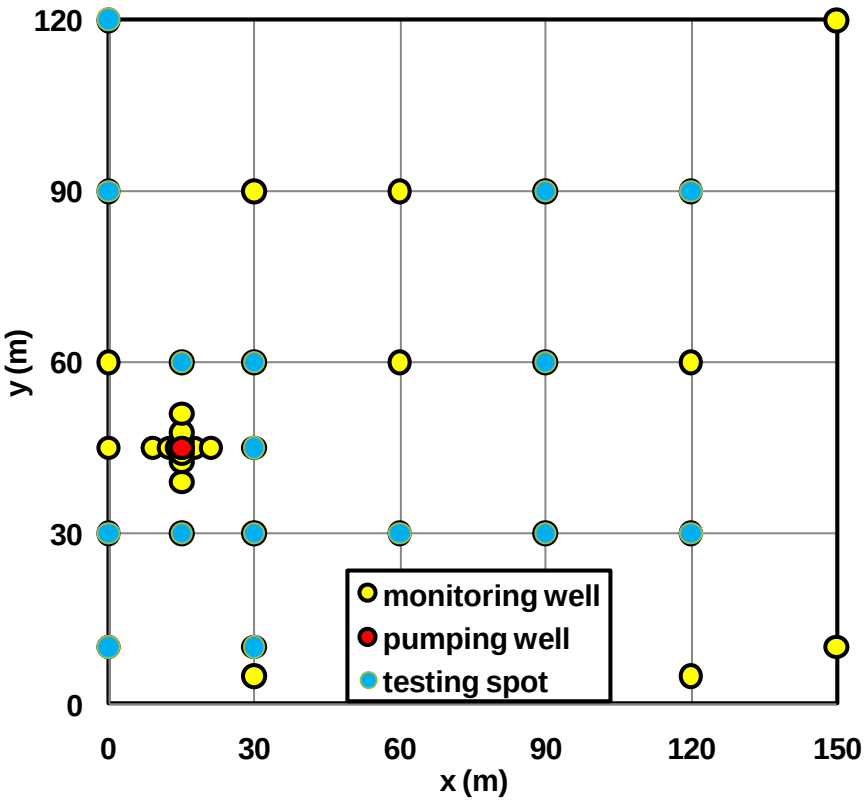

Figure 4.2 Plan view of the Sorel site.

According to the hydrogeological characterization study (Dallaire 2004), the Sorel site is highly stratified. The stratigraphy includes many thin layers of fine sand, which was deposited in low velocity water, and silty clay, which settled in ponds. All layers are 1 to 2 cm-thick. In the pumping well area, there is an unconfined aquifer about 2-m-thick, followed by a layer containing more clayey silt, and the underlying layer is mostly a stratified confined aquifer. Detailed cross sections of the site were displayed by Dallaire (2004). Information about the soil samples and their modal decomposition to retrieve the different layers can be found in Chapuis et al. (2014).

The average diameter of the filter pack is 10 cm for the first installed MWs and 9 cm for the second installation. The length of the filter pack ranges from 0.49 to 1.88 m, resulting in different shape factors. The slots of the MWs screens are 0.254-mm-wide and 6.5-mm-spaced. The MW pipes have an internal diameter of 34.5 mm and an external diameter of 42.2 mm. The results of 15 MWs installed in the Sorel site are presented for constant discharge and injection tests, and variable rising- and falling-head tests.

4.3.3 Lachenaie site installed with MWs

The Lachenaie sites are located around the city of Lachenaie, in southwestern Quebec, Canada. They cover an area of 50 km^2 (Duhaime et al. 2013; Marefat et al. 2015). According to previous studies (GSI Environnement 2001), the stratigraphy of the area is relatively homogeneous. A few sites have a thin topsoil layer, less than 20-cm-thick, which covers a sand layer containing fine to coarse sand with traces of silt. The sand may be up to 3.5-m-thick and it overlies the Champlain clay layer. The clay layer may be up to 30-m-thick in certain areas. Below the clay, there is a till layer up to 5-m-thick resting upon the clayey shale bedrock. All the boreholes have penetrated the shale rock by a depth over 6 m. Planar and cross-sectional views of the site and MWs were presented in Benabdallah (2010).

In total, there were nine study sites in the Lachenaie area, but not all of them are presently available. At each test site three types of MWs named AH, AB and R were installed at the upper and lower third of the non-fissured clay, and the rock layer, respectively. The field permeability tests for this study were conducted within the rock using the MW-R of sites 1, 2, 6, and 9. The MW pipe was sealed with bentonite against the entire length in clay. The MW has a 6-m-long screen, surrounded by a saturated filter pack in its full length. The filter pack of the MW consists of three filter materials: sand no 3, 0, and 00, which were evenly placed in stages from bottom to top of the annular space around the screen (Benabdallah 2010). The sand no. 00 is the finest, to avoid the bentonite particles moving into the filter pack (Baptiste and Chapuis 2015). The lengths of the filter pack for the four sites are slightly different (Table 2). The MW riser pipe has an internal diameter of 51 mm.

4.4 Field permeability tests manipulation

A pair of absolute pressure transducers (PT) and barometric pressure transducers (APT) was used synchronously to collect test data. The true water column height above the sensor is given by the subtraction of PT and APT readings, which refers to the water level measurement when using the sensor as the reference. The PTs had a full scale of 10 m and an accuracy of ±1.0 cm, whereas the APTs had an accuracy of ±0.5 cm, which are the theoretical values given by the manufacturer. The actual accuracy varies with time as well as with different sets of pressure transducers (Zhang

et al. 2018). The time intervals set for the pair of transducers are 15-s and 2-s for the CH and VH tests, respectively.

The CH discharge tests were performed by pumping water at a constant rate from the riser pipe until reaching a stable water level in the pipe. After the pump stopped, the water level in the riser pipe slowly returned to the pre-test static water level. The CH injection tests were conducted with an opposite pumping flow. Water was injected into the MW at a constant rate equal to the discharge rate. The water level increased to reach a stabilized state, and equilibrium. And the water finally recovered to the pre-test water level after the pump stopped. The water levels of pre-test, steady state, and post-test were also verified manually with a water level meter.

The discharge and injection rates for the CH tests in the sand box were around 100 ml/min. For the tests conducted in Sorel site, the discharge and injection rates ranged from 371 to 600 ml/min. The pumping rates for Lachenaie sites 1 and 6 were 328 and 421 ml/min, respectively. The test duration was around 50 minutes, and 10 to 15 minutes were allowed for recovery. The duration was adjustable depending on the manual measurement of the water level. All discharge rates were automatically controlled by the peristaltic pump and calibrated with a burette and stopwatch before and during the test. The injection rate could not be calibrated during the test.

For the sand box and Sorel site, a rod was firstly inserted into the water in the MW to start the falling-head tests, whereas the rising-head tests were started by the quick extraction of the rod from the well. The water level return to its initial level was registered with time. The rising-head tests in Lachenaie site were performed by the extraction of a bailer, to lower the water level. The water level recovery was very rapid in granular soils and a few MWs in fractured rock. Conversely, the falling-head test was achieved by a sudden increase in hydraulic head by a quick insertion of a water volume into the well. Some duplicate falling- and rising tests were conducted to ensure the accuracy of the results.

4.5 Field Permeability Test Results and Analysis

4.5.1 Shape factors

According to the *L/D*-values the shape factors of the MWs installed in the sand box are 51.91 cm, calculated by Equation 4.10. The shape factors for other MWs are computed by Equation 4.9.

They have different values due to various diameters and lengths of the filter pack. Table 4.2 lists the internal diameters and shape factors of all MWs in the three sites.

Table 4.2 Useful parameters to calculate the hydraulic conductivities for the three sites

test site	internal diameter of pipe	diameter of water injection zone	length of water injection zone	shape factor
	d (cm)	*D* (cm)	*L* (cm)	*c* (cm)
sand box	3.38	4.25	15.00	51.91
Sorel 1st installation	3.45	10.00	49.20-144.50	135.20-269.90
Sorel 2nd installation	3.45	9.00	92.10-187.80	191.69-316.24
Lachenaie site1	5.08	9.60	605.00	785.95
Lachenaie site2	5.08	9.60	633.00	814.70
Lachenaie site6	5.08	9.60	638.00	819.82
Lachenaie site6	5.08	9.60	599.00	779.76

4.5.2 Large sand box

The water level in injection and discharge tests changed rapidly in the first few minutes, and then became stable in most cases, except for PB1 and PB19. These are located close to the steel wall of the sand box, an impervious boundary: here, the water level continued to decrease after the rapid drop (upper plot in Figure 4.3). The injection test data is a mirrored plot, and thus is not presented herein. There is no systematic error caused by the barometric pressure change because the PT-APT pair was previously calibrated (Zhang et al., 2018a).

The upper plot in Figure 4.3 shows that the water level rapidly drops from 83.9 to 78.2 cm within the first 3-minute discharge, followed by a linear reduction to 75.0 cm after 50-min pumping. It gives a hydraulic head difference of 8.9 cm and the water level does not stabilize. Since the MW PB1 is very close to an impervious boundary, the aquifer recharge is slower than the well discharge. As a result, the water level of the CH test keeps falling, which is verified by the decrease of water level in the adjacent constant-head reservoir.

A correction was then made during the discharge test: the water pumped out from the MW was injected synchronously into the reservoir at the same rate, to keep the constant head in the confined aquifer. For the injection test, the water injected into the pipe was pumped from the

reservoir. The corrected test indicates that the hydraulic head reaches equilibrium shortly (lower plot in Figure 4.3). The new H_c = 6.1 cm was used to calculate the *K*-value for PB 1. The *K*-value (discharge test) for PB1 calculated by Equation 4.1 is 5.26 x 10^{-5} m/s instead of the previous erroneous value of 3.61x 10^{-5} m/s.

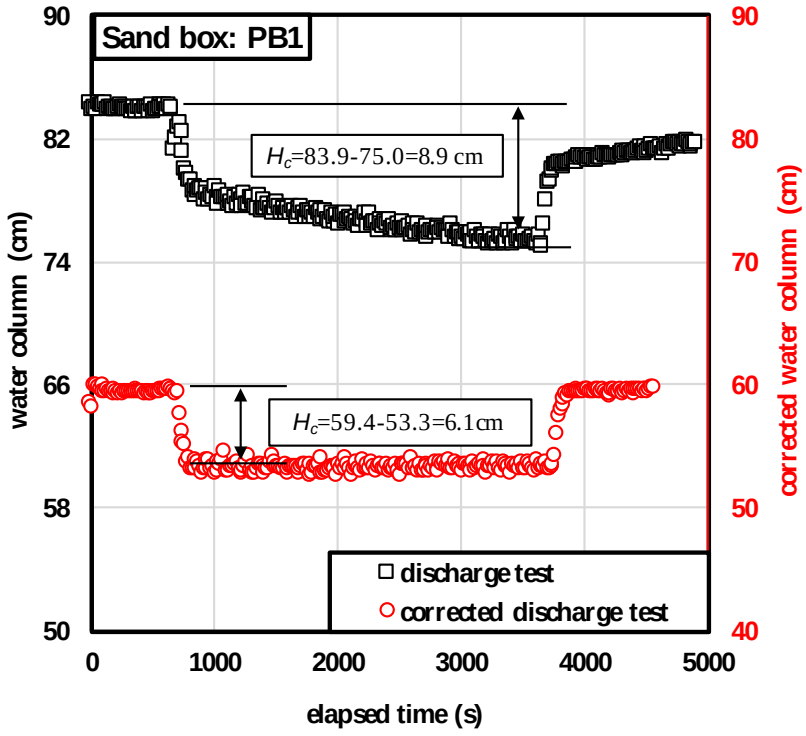

Figure 4.3: Influence of impervious boundary on CH discharge test in PB1.

The *K*-value (discharge test) for all tested MWs ranges from 4.40 x 10^{-5} to 6.08 x 10^{-5} m/s, with a mean value of 5.06 x 10^{-5} m/s. The *K*-value (injection test), with an opposite flow direction, yields a range of 4.12 x 10^{-5} - 5.95 x 10^{-5} m/s. The mean *K*-value is 5.08 x 10^{-5} m/s.

The plots of water column versus time for all VH tests have a normal shape like Figure 4.5. The *K*-value (falling-head test) varies between 4.53 x 10^{-5} and 8.17 x 10^{-5} m/s, and have an average value of 6.43 x 10^{-5} m/s. The rising-head tests give *K*-values from 4.97 x 10^{-5} to 9.02 x 10^{-5} m/s, and 7.10 x 10^{-5} m/s in average. The complete *K*-values for all tests are presented in Table 4.3.

4.5.3 Sorel site

Four types of field permeability tests performed in Sorel and yielded good results. Figures 4.4-4.5 give the water column change with time of CH and VH tests, respectively, for the MW (30,10).

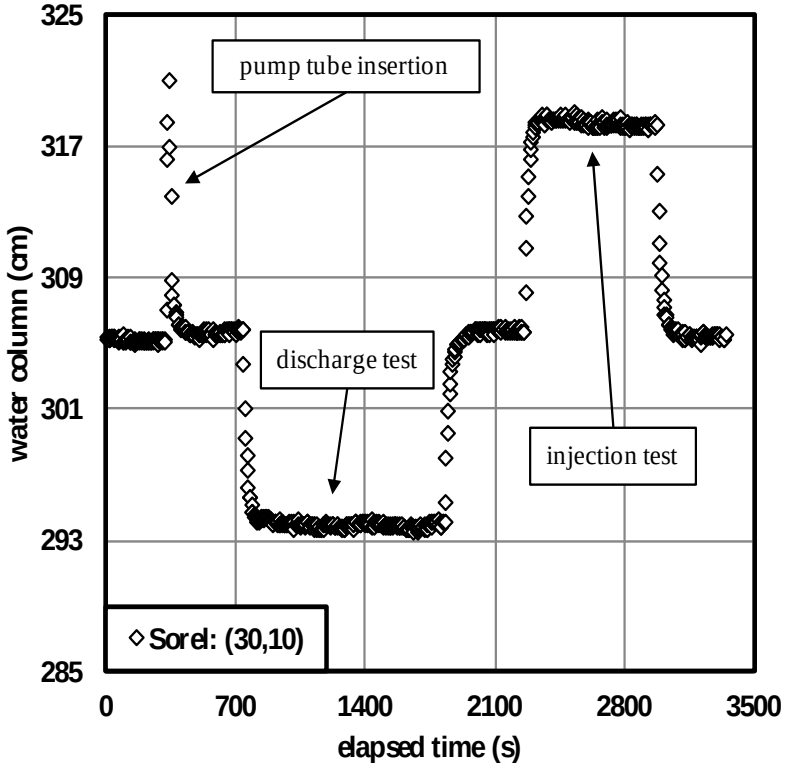

Figure 4.4: Two types of CH test results in MW (30,10).

It is observed from Figure 4.4 that the water column drops fast from 305.7 to 294.4 cm in 1 min after the pumping starts. And then it decreases slowly to the equilibrium level, 293.9 cm. The H_c-value is 305.7 - 293.9 = 11.8 cm for the discharge test. The following injection test also has a quick water level change in 1 min, rising from 305.8 to 318.3 cm, which yields an H_c-value of 12.5 cm, higher than the H_c-value of the discharge test. According to Equation 4.1, the hydraulic conductivity is inversely proportional to the hydraulic head difference, because the pumping rate and shape factor do not change for the two types of tests. Thus, the K (injection test) is 2.26×10^{-5} m/s, slightly lower than the K (discharge test) of 2.39×10^{-5} m/s. For all tested MWs in Sorel, the K (injection test) varies from 7.45×10^{-6} to 4.37×10^{-5} m/s, with an average value of $1.72 \times$

10^{-5} m/s. The *K* (discharge test) is between 7.58 x 10^{-6} and 5.23 x 10^{-5} m/s, with an average of 1.94 x 10^{-5} m/s.

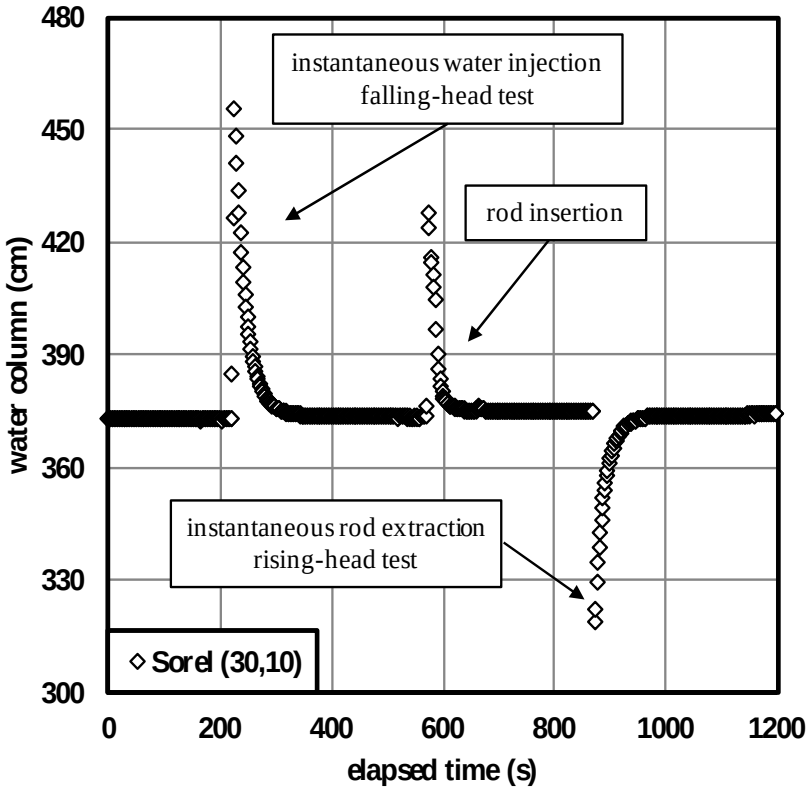

Figure 4.5: Two types of VH test results in MW (30,10).

Figure 4.5 presents the data plot of the falling- and rising-head tests, which started with initial water heads of 82.6 and 55.6 cm, respectively. The water column data in 100 s of each test was selected to plot the semi-log graph. With the PL corrections of 1.13 and 1.04 cm, the semi-log plot of the falling- and rising-head test became straight lines with slopes of -0.0496 and -0.0516, respectively. The *K* (falling-head test) by Equation 4.6 is 2.09 x 10^{-5} m/s, and the *K* (rising-head test) is 2.17 x 10^{-5} m/s. The *K* (rising-head test) for all tested MWs in Sorel ranges from 9.29 x 10^{-6} to 6.23 x 10^{-5} m/s, and the mean is 2.23 x 10^{-5} m/s. The falling-head tests yield *K*-values between 8.64 x 10^{-6} and 5.49 x 10^{-5} m/s, and have an average *K* of 2.03 x 10^{-5} m/s. The *K*-values for other MWs are listed in Table 4.3.

4.5.4 Lachenaie site

The MWs of the Lachenaie sites presented more diversity than those of the two other sites. The results of the CH and VH tests for each site are in different situations. The shapes of the plots varied from one site to another. Figure 4.6 displays the results of discharge and injection tests for site 1, which tended to reach equilibrium, but not rapidly. Therefore, the time-drawdown method (Cooper and Jacob, 1946) was also used to estimate the *K*-values for the two types of CH tests (Figure 4.7). Figure 4.8 displays the VH test plots of site 2 that did not stabilize rapidly. The VH test plots in site 9 show very quick variations in water level in Figure 4.9. Site 6 is the only case that has good results and normal plots of CH and VH tests as Figures 4.4-4.5, and hence its analysis is not repeated in the section.

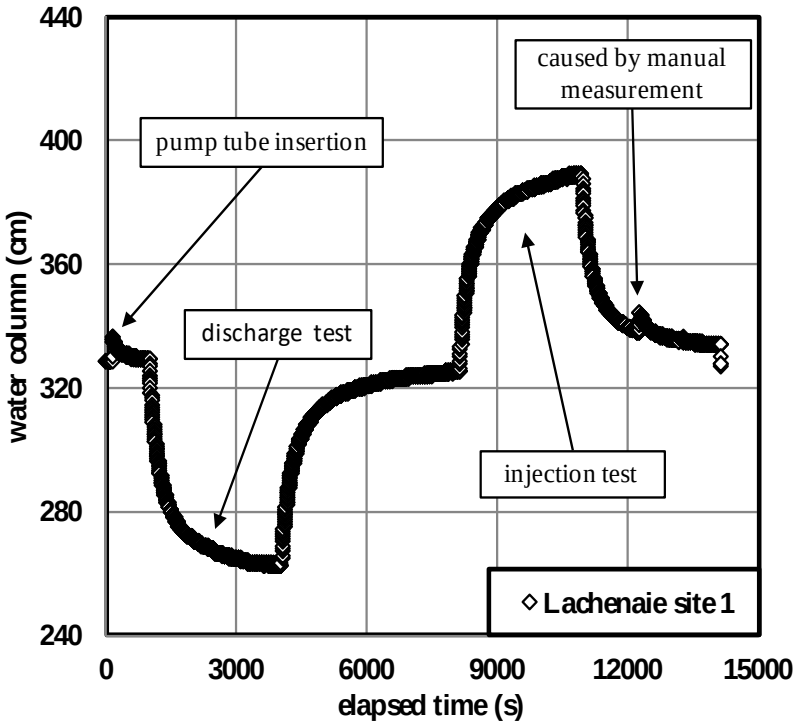

Figure 4.6: Two types of CH test results in site 1.

The injection and discharge rate was 327.5 ml/min for site 1. During the first 13 minutes after the pump starts to discharge water from the pipe, the water level quickly dropped from 329 to 273 cm, and then reduced nonlinearly to 262 cm at a lower speed. After the constant discharge of around 50 minutes, the water level almost reached steady state. The injection test yielded a mirrored plot with the same trend. The phenomena resulted from the too high pumping rate we

specified. If we use the deepest water level of the discharge test and the highest water level of the injection test to represent the stabilized water level, the assumed H_c of the discharge and injection tests are 67 and 65.5 cm, respectively. The derived K-values are 1.04 x 10^{-6} m/s for the discharge test and 1.06 x 10^{-6} m/s for the injection test. When the pumping rate was decreased to 113 ml/min, the tests reached equilibrium in only 30 min, and gave K (discharge test) = 1.17 x 10^{-6} m/s and K (injection test) = 1.09 x 10^{-6} m/s, which are very close to the previous values.

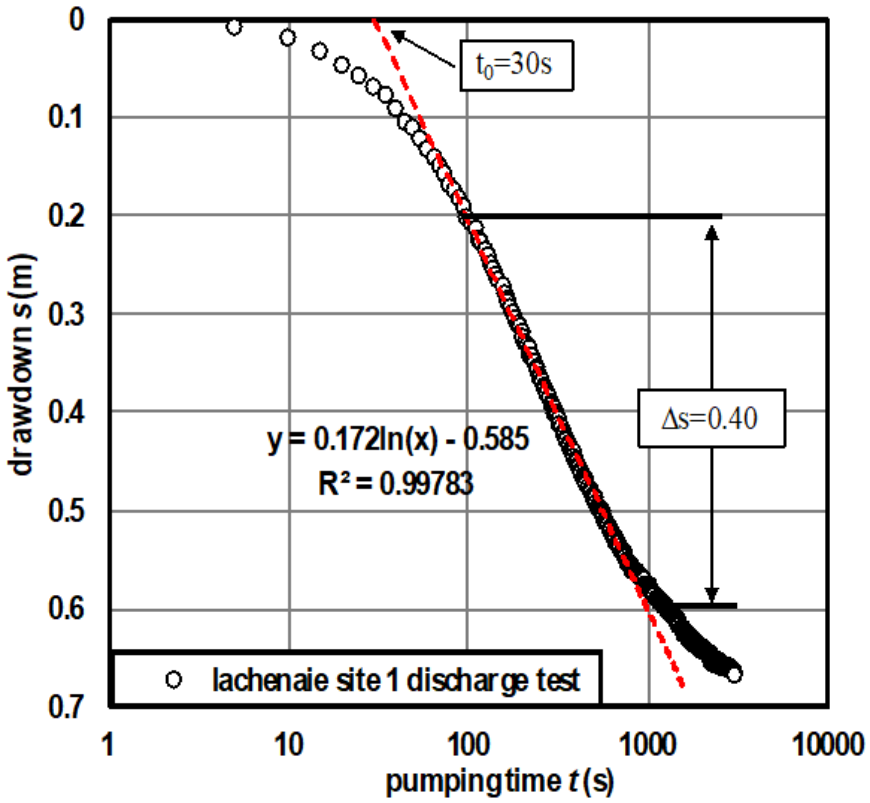

Figure 4.7: Time-drawdown interpretation of discharge test site 1.

Figure 4.7 displays the plot of drawdown s on the y-axis and log t on the x-axis. The straight line is the best fit of the linear part of the plot. The Cooper-Jacob approximation is not valid at early times because the Thesis solution cannot be linearized, and the discharged water comes from the well casing rather than the aquifer (Chapuis and Chenaf, 2003b). The late time data indicates the influence of the boundaries on drawdown, and thus are excluded. The value of Δs is calculated to be 0.4 m. According to Equation 4.4, the K (discharge test) = 4.20 x 10^{-6} m/s, and the K (injection test) = 4.70 x 10^{-6} m/s, are about 3 times larger than that by the Lefranc's method.

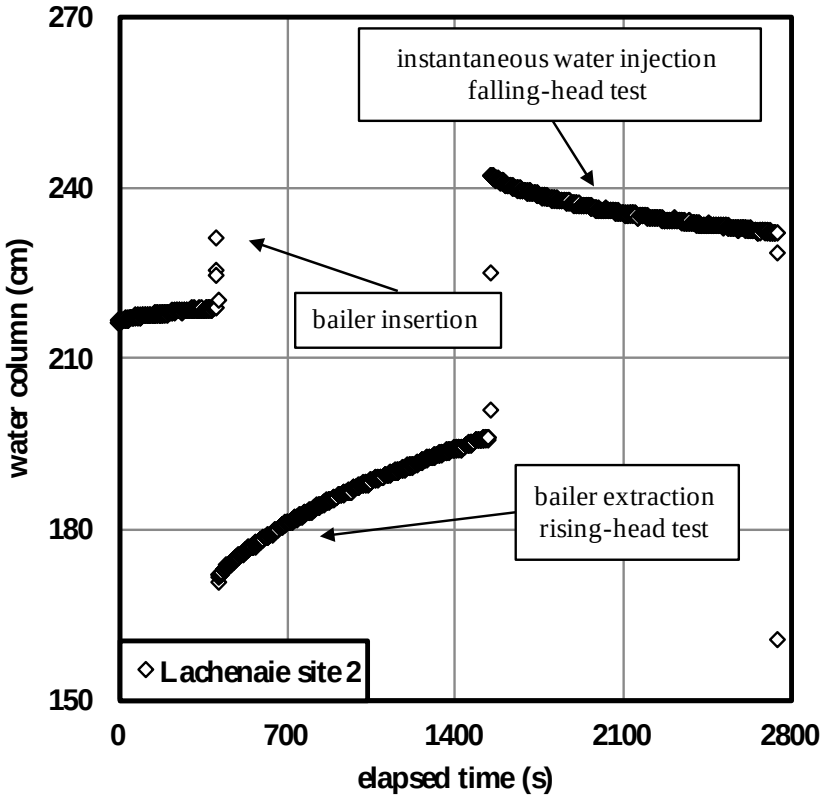

Figure 4.8: Two types of VH test results in Lachenaie site 2.

Figure 4.8 presents a rising-head test followed by a falling-head test conducted in site 2. Compared to Figure 4.5, the rising-head test does not have an instant water level rise: the water level slowly increases from 170.7 to 196 cm after around 20 min, while the pre-test water level was 218.5 cm. A water height of 22.5 cm is still needed to be recovered, which may take another extra 20 minutes or more. The water head drop in the falling-head test is also very slow. As the rising-head test does not return to the pre-test water level, the insertion of a 46-cm water column generates an initial water head of 23.5 cm with reference to the pre-test water level. The PL corrections are 3.5 and 10.0 cm for the rising- and falling-head tests, respectively. The *K* (rising-head test) is 1.76×10^{-7} m/s, and the *K* (falling-head test) is 2.76×10^{-7} m/s.

It is noteworthy that if the reference of pre-test water level for the falling-head test were specified as the end water level of the rising-head test, 196 cm, the initial water head for the falling-head test would be 46 cm, and the PL error becomes 32.5 cm. However, the *K*-value obtained by the corrected semi-log plot is still 2.76×10^{-7} m/s, which equals the previous value.

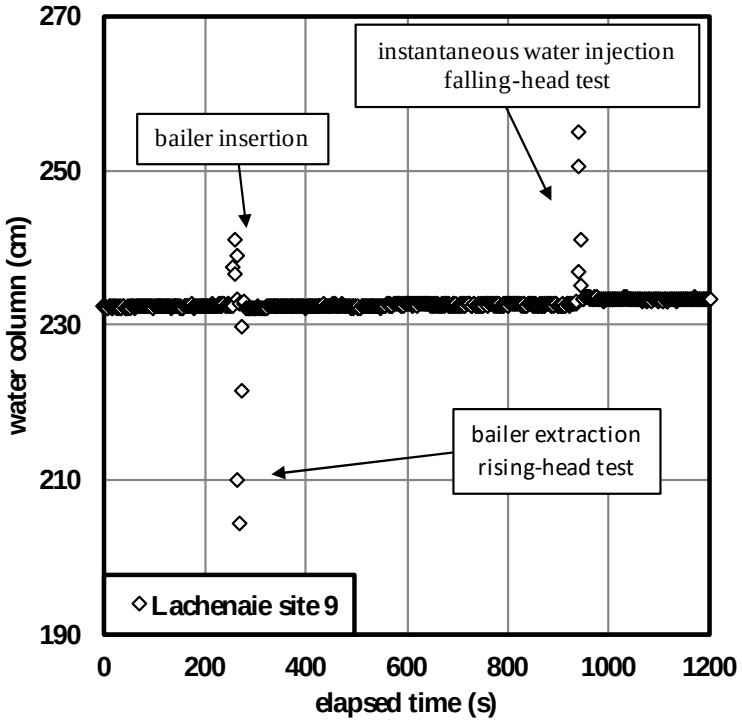

Figure 4.9: Two types of VH test results in site 9

Unlike the slow recovery of VH tests in site 2 (Figure 4.8), VH tests are very rapid in site 9 (Figure 4.9). It is observed that the rising-head test with an initial water head of 28 cm took only 8 seconds and the initial water head of 23 cm of the falling-head test fully dropped in 10 seconds. The very quick recovery of the two types of VH tests indicates that the local permeability of site 9 is much higher than that of site 2. After interpretation by the optimized Hvorslev's method, the *K*-values of rising- and falling-head tests are 2.24×10^{-4} and 1.68×10^{-4} m/s, respectively. For better data accuracy, the recording interval of the pressure sensor should be reduced to 0.5 s.

The CH test is not shown for site 2, because its permeability is relatively low, and the CH test takes a lot of time. The discharge test failed for site 9: the drawdown linearly decreased and never reached stabilization when the discharge rate was 480 ml/min, which is the up limit of the peristaltic pump we used. The CH test data of site 6 were also interpreted by the time-drawdown method, which gave the *K* (discharge test) of 1.16×10^{-6} m/s, and *K* (injection test) of 1.50×10^{-6} m/s. The other unmentioned *K*-values are listed in Table 4.3. Compared to the sand box and Sorel site, the *K* values in Lachenaie sites are more scattered, which may be due to the heterogeneity of the rock.

Table 4.3: Hydraulic conductivities from each MW of the confined aquifers in three sites

MW no.	injection test K m/s	discharge test K m/s	falling-head test K m/s	rising-head test K m/s
sand box				
PB1	4.40E-05	5.84E-05	6.91E-05	7.33E-05
PB2	4.59E-05	4.40E-05	5.17E-05	6.06E-05
PB5	4.12E-05	4.46E-05	5.29E-05	4.97E-05
PB7	4.94E-05	5.35E-05	7.02E-05	7.60E-05
PB8	5.18E-05	4.54E-05	6.58E-05	7.51E-05
PB15	5.18E-05	5.00E-05	7.03E-05	8.04E-05
PB16	5.95E-05	5.62E-05	7.71E-05	9.02E-05
PB17	5.10E-05	5.21E-05	6.69E-05	7.55E-05
PB18	5.26E-05	5.13E-05	8.17E-05	8.88E-05
PB19	5.44E-05	4.46E-05	5.74E-05	6.12E-05
PB20	5.63E-05	4.71E-05	6.12E-05	7.19E-05
PB21	4.79E-05	5.08E-05	6.07E-05	6.73E-05
PB22	5.63E-05	6.08E-05	7.04E-05	6.95E-05
PB23	4.87E-05	5.00E-05	4.53E-05	5.48E-05
Sorel site				
(0,10)	1.28E-05	1.86E-05	1.95E-05	2.40E-05
(0,30)	1.87E-05	2.18E-05	2.50E-05	2.85E-05
(0,90)	7.45E-06	7.58E-06	8.92E-06	9.29E-06
(15,30)	1.27E-05	1.33E-05	1.46E-05	1.50E-05
(15,60)	8.23E-06	8.36E-06	9.54E-06	1.01E-05
(30,10)	2.26E-05	2.39E-05	2.16E-05	2.79E-05
(30,30)	1.03E-05	1.30E-05	1.49E-05	1.27E-05
(30,45)	8.45E-06	9.10E-06	8.64E-06	9.36E-06
(30,60)	1.36E-05	1.40E-05	1.31E-05	1.28E-05
(60,30)	2.16E-05	2.32E-05	2.17E-05	2.51E-05
(90,30)	9.35E-06	9.69E-06	1.12E-05	1.17E-05
(90,60)	2.80E-05	2.89E-05	3.14E-05	3.35E-05
(90,90)	1.32E-05	1.47E-05	1.60E-05	1.72E-05
(120,30)	4.37E-05	5.23E-05	5.49E-05	6.23E-05
(120,90)	2.69E-05	3.24E-05	3.32E-05	3.53E-05
Lachenaie site				
1	1.06E-06	1.04E-06	1.53E-06	1.22E-06
2	--	--	2.76E-07	1.76E-07
6	4.28E-06	3.81E-06	3.26E-06	2.84E-06
9	--	--	1.68E-04	2.24E-04

4.6 Comparison of Tests with Inward and Outward Flows

The *K*-values of the tests with outward flow are plotted on the *x*-axis, and inward flow on the *y*-axis for the sand box and Sorel (Figures 4.10-4.11). The diagonals of the quadrate graph of Figures 4.10-4.11 represent that *K* (tests with outward flow) = *K* (tests with inward flow), which indicates the ideal result in theory. The two plots in each graph represent the CH and VH tests, respectively. In other words, *K* (falling-head test) on the *x*-axis is plotted versus *K* (rising-head test) on the *y*-axis, and *K* (injection test) on the *x*-axis is plotted versus *K* (discharge test) on the *y*-axis. The differences of each two types of tests are also plotted in lower rectangular graphs. The test data of Lachenaie site are not plotted herein due to their limited number and specific issues.

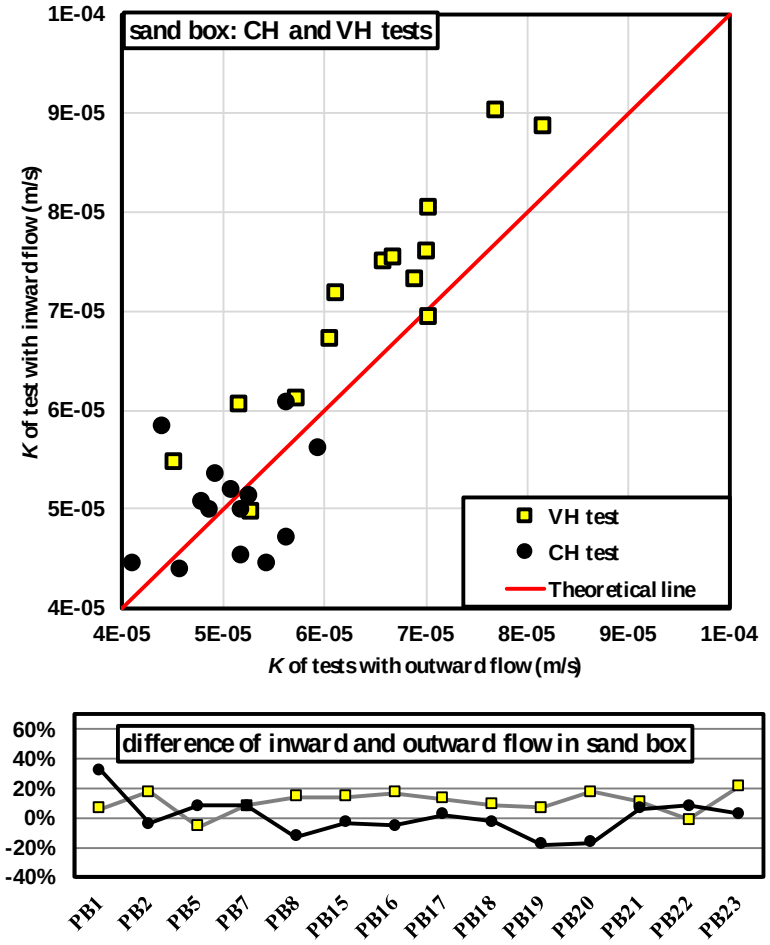

Figure 4.10: The *K* comparison of tests with outward and inward flows in the sand box.

The square spots above the theoretical line indicate that the *K* (rising-head test) is greater than the *K* (falling-head test), and vice versa. Eleven out of twelve MWs in the sand tank yielded higher *K*-values for the rising-head test compared to the falling-head test, giving an increase from 6% to 21%. The circular spots represent the *K* of constant-head tests. Half of the MWs had larger *K* (discharge test) than *K* (injection test), and the other half comparisons gave opposite results. The highest difference is 32.7%.

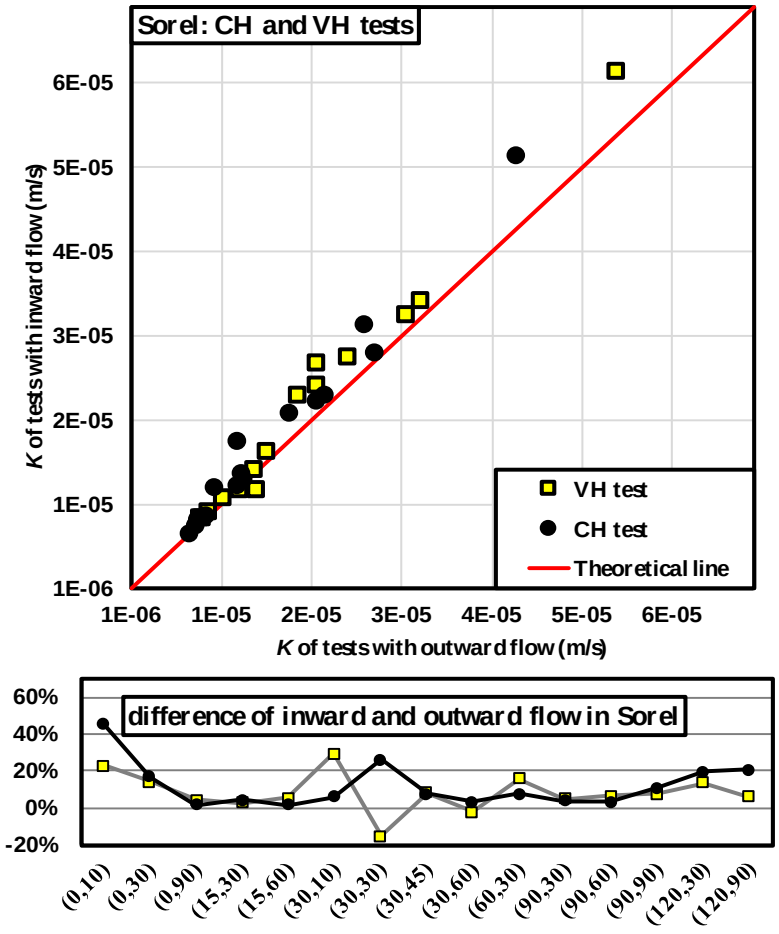

Figure 4.11: The *K* comparison of tests with outward and inward flows in Sorel

The two types of tests in Sorel seem to have nearly identical results in Figure 4.11 due to the scale of *K*-values. The fact is that the rising-head tests in 13/15 MWs provided *K*-values 3% to 29% higher than those of the falling-head tests. Only MWs (30, 30) and (30, 60) are different, their *K* (rising-head test) are 15% and 2% lower than the *K* (falling-head test), respectively. All *K* (discharge tests) are higher than the *K* (injection tests), the difference ranging from 1.6% to 45%.

Contrary to most cases in sand box and Sorel, the *K* (discharge tests) are 2% and 11% lower than the *K* (injection tests) for sites 1 and 6, respectively. Their *K* (discharge tests) values, interpreted by the time-drawdown method, are 10% and 22% smaller than their *K* (injection tests). Meanwhile, the *K* (rising-head tests) for sites 1, 2, and 6 are lower than the *K* (falling-head tests), by 13%, 20% and 36%. Only the site 9 has a *K* (rising-head test) that is 33% higher than its *K* (falling-head test).

It is observed from the three sites that most *K*-values of the tests with inward flows are not equivalent to those of the tests with outward flows as expected in theory for perfect MWs. All rising-head tests gave higher *K*-values, either in the sand box or Sorel. Moreover, all discharge tests in Sorel, and half of them in the sand box, gave *K*-values greater than the *K*-values of injection tests. The difference can be explained by some clogging of the screen slots (by solids or tiny gas bubbles) or/and erosion in the filter pack, as explained in Hvorslev (1951).

A falling-head test or an injection test in the MW produces an outward flow from the pipe into the aquifer. This outward flow may carry sediment in suspension within the pipe into the screen slots or the injection zone, and it may also create small gas bubbles, resulting in some clogging in the inside screen or in the filter material. The interpretation of the field permeability tests provide the local hydraulic conductivity *K* (test), which depends upon *K* (screen) and *K* (filter pack) and *K* (soil) (Baptiste and Chapuis, 2015). The decrease of *K* (screen) or/and *K* (filter material) can yield a reduced apparent *K*-value for the soil if the screen clogging is ignored. On the other hand, the inward water flow generated by a rising-head test or a discharge test may carry fine particles from the surrounding filter pack or even the aquifer material into the pipe, and may dislodge tiny gas bubbles from the screen slots, which thereby facilitates the inward flow and increases the apparent hydraulic conductivity of the test.

Meanwhile, if the particles carried by the inward flow are equal to or larger than the screen slot size, they may cause clogging on the outside opening of the MW screen slots. This explains the rare occurrence of lower *K* in rising-head tests. The discharge test lasts longer and thus has higher potential to bring the particles to clog against the screen, which explains why the *K* (discharge tests) in the sand box has higher frequency to yield lower values than the *K* (injection tests), compared to the VH tests. Most often, fine soil particles may settle at the bottom of the pipe, which could contribute to the further clogging in the screen or filter pack with the outward flow.

Unlike the very long pipes in Sorel, the MWs pipes in the sand box can be easily checked. A long rod was inserted down to the bottom of the pipes in the sand box, and fine particles were seen covering the end of the rod, which demonstrated the presence of loose sediments at the bottom of the MW pipe.

Because the confined aquifer in Lachenaie site is shale rock instead of sand, no fine particle from aquifer material could be displaced to clog the screen and filter pack. The smaller *K* (discharge test) and *K* (rising-head test) in sites 1, 2 and 6 indicate that some clogging is caused by the inward flow and occurs on the outside of the well screen. The local hydraulic conductivity for site 9 is 2 orders of magnitude higher than that at other three sites, which provides an easier path for the outward water flow that carries fine particles of the filter pack, and thus to block the void spaces in the shale. Therefore, its *K* (rising-head test) is larger than the *K* (falling-head test).

The differences lower than 10% are small enough to be viewed as negligible. After excluding those values, the maximal difference is 45% in Sorel (between 1.28×10^{-5} and 1.86×10^{-5} m/s), which may be acceptable in practice. As a result, despite slight clogging or erosion, the screens and filter packs in the three sites have shown relatively good performance.

4.7 Comparison of CH and VH tests

The *K*-values from the CH and VH tests for each MW in the sand box and the Sorel site are plotted in two radar charts (Figures 4.12-4.13). The labels outside the chart boundary represents the MW numbers. The *K*-values are located on the radar axis in logarithm. The comparison of *K*-values for the CH and VH tests is based on the water flow direction. In other words, the injection and falling-head tests, which have outward flows, are compared. And the discharge test is compared to the rising-head test.

All MWs, except PB23, show that the VH tests including both rising- and falling-tests yield larger *K*-values than the two types of CH tests (Figure 4.12). The differences between *K* (rising-head test) and *K* (discharge test) range between 5.4% and 57%. And the *K* (falling-head test) is greater than the *K* (injection test) by 9.5% - 73%. The *K* (falling-head test) of PB 23 is 4.53×10^{-5} m/s, which is 7% lower than the *K* (injection test). In Figure 4.13, 26/30 comparisons provide higher *K* (VH test) values than the *K* (CH test) values. The difference of tests with outward flows ranges from 0.3% to 52%, and the tests with inward flows have a difference between 3% and

31%. Several *K*-values from CH tests are from 2.2% to 8.7% lower than those of the VH tests. A difference lower than 10% could be viewed as negligible. Additionally, the round shape of plots in Figure 4.12 illustrates that the confined aquifer in sand box is relatively homogeneous, while the confined aquifer in Sorel is less homogeneous as shown by a more irregular plot in Figure 4.13.

The screens and filter materials of the tested MWs were found properly designed, and no important head loss in the screen and the filter pack was observed according to last section. However, the VH tests yielded larger *K*-values than the CH tests, and the differences were greater than the comparison described in last section. For a MW with filter pack, the selected filter material must be more permeable than the aquifer material. During development, a natural filter zone will be formed at the interface between the filter pack and the natural soil (Figure 4.14). If there is no filter pack around the screen as it is the case in the sand box, the MW is developed after installation and only a natural filter zone is formed against the screen. Normally, the fine particles in created filter zones are washed away, which yields a filter zone with higher permeability (K_{23}) than the aquifer (K_3). The experimental quantification of the development results is explained and quantified in Wendling, Chapuis and Gill (1997).

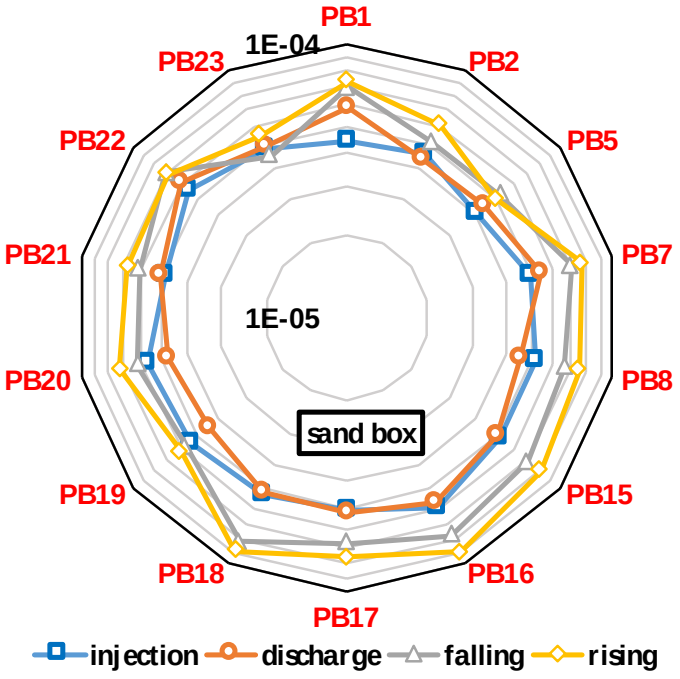

Figure 4.12: The *K* (m/s) comparison of VH and CH tests in sand box

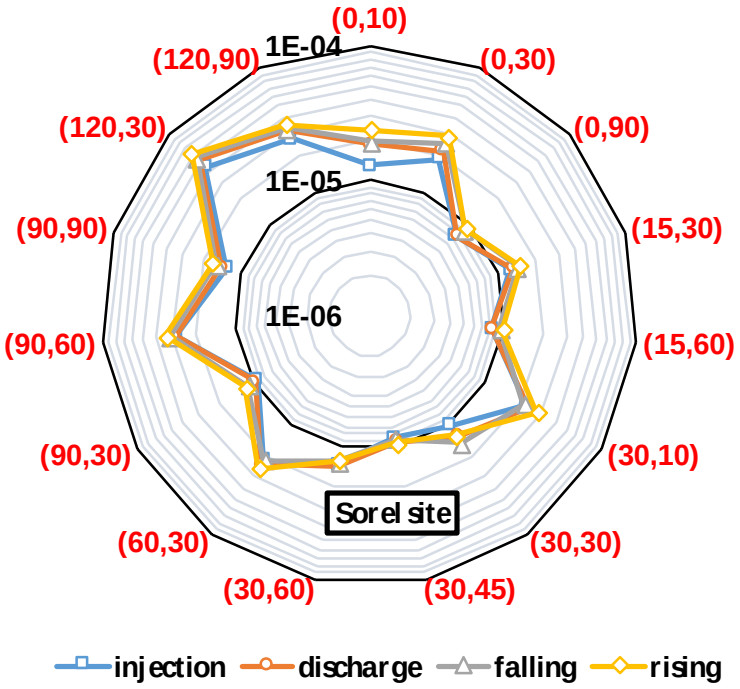

Figure 4.13: The *K* (m/s) comparison of VH and CH tests in Sorel

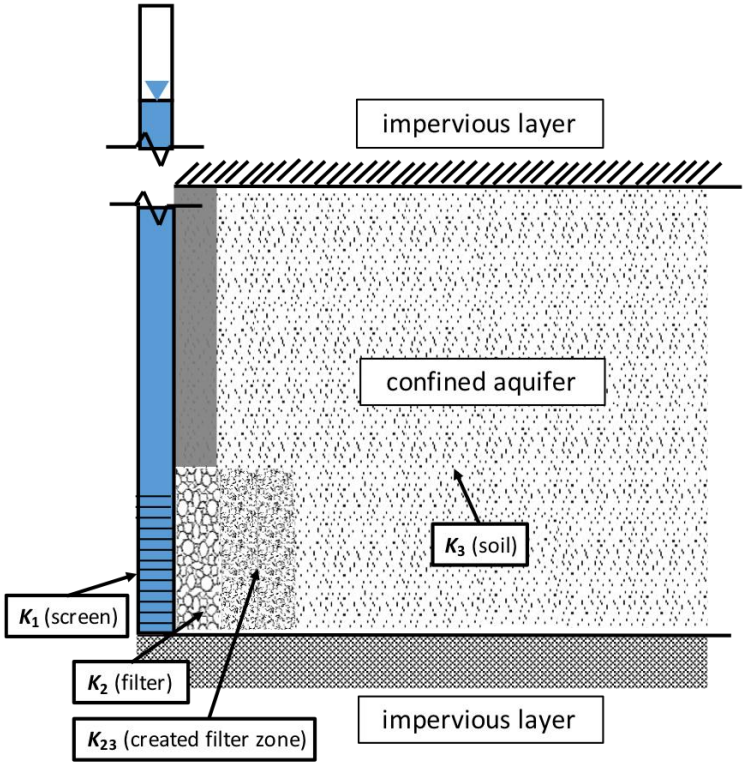

Figure 4.14: The sketch of created filter zone

The VH test has a short duration and its influence radius is small. Therefore, the K_{23} (filter zone) contributes significantly to the apparent *K*-value of the VH test. By comparison, a CH test has a long duration, and thus a larger influence radius than the VH test. The apparent *K* (CH test) is computed from the hydraulic head difference in steady state, and thus is less affected by the locally high K_{23} (filter zone). As a result, a CH test provides a slightly lower *K*-value than a VH test, which is more representative of the *K* (soil). If the K_1 (screen) and K_2 (filter material) are not large enough, only limited range of *K*-values can be measured for the aquifer (Baptiste and Chapuis, 2015).

It is also observed oppositely that a few CH tests give higher *K*-values than the VH tests. The *K* (injection test) of the MW in site 4 of Lachenaie, for example, is 24% higher than the *K* (falling-head test), and its *K* (discharge test) has an increase of 25% compared to the *K* (rising-head test). In these cases, fine particles are transported with either inward or outward water flow, and may be trapped in the water intake zone only during the VH test, and cause partial clogging of the screen or filter material. The contribution of filter pack, created filter, and aquifer material caused a reduced *K*-value for the VH test.

4.8 Summary

Two field permeability testing methods, constant-head (CH) and variable-head (VH), were conducted in 33 MWs. The tested MWs monitor confined aquifers in three sites: a large sand box, Sorel, and Lachenaie. Each test method consists of two types of test with opposite water flows. The water columns for the four types of tests were registered by a pressure transducer (PT) synchronized with an atmospheric pressure transducer (APT). The recording intervals were 15 s for the discharge and injection tests, and 2 s for the rising- and falling-head tests. Duplicate tests were performed for the VH tests in MWs in the sand box to verify the test results.

The article indicates that the tests with inward and outward flows can be used to assess the conditions of the well screen and filter pack when testing a MW. Most results imply that inward flow (discharge/rising-head) yields an increased apparent *K*-value as compared to outward flow (injection/falling-head). The outward seepage from the pipe to the aquifer may displace fine sediments already in the MW and create tiny gas bubbles that block parts of openings in the screen slots or the voids of the filter pack, which yield a decreased apparent *K*-value. The inward

flow generated by a water discharge test may wash off fine particles and tiny gas bubbles from the filter pack or the water intake zone, which facilitates the inward flow and results in an increased apparent *K*-value. The minority of lower *K*-values of the test with inward flow occurs mostly in CH tests. In these cases, if fine particles carried by the inward flow are larger than the screen slots, they are blocked outside the screen, which causes the reduced *K*-values. The difference in *K*-values between two water flows was lower than 10% for some MWs, which is negligible, and could reach up to 45%, which is acceptable. Therefore, the screens and filter packs of the three sites were in good condition.

Some practical recommendations are provided for the practitioners while conducting a CH test. For a confined aquifer, normally, the hydraulic head of a CH test increases or decreases rapidly in the first few minutes and then reach the equilibrium state after pumping at a constant rate. The recovery time is also short. Sometimes however, even if the MW has a good performance, the CH test may not yield good results. This could be examined and corrected in several ways: (1) a pair of PT and APT must be calibrated and monitored synchronously, to remove the systematic error caused by barometric pressure variations; (2) the discharge or injection rate needs to be adjusted appropriately by trial-and-error tests, either to shorten the test time or succeed in a test by reaching steady-state in preferably less than 20 min; (3) the tested well close to the impervious boundary requires special treatment, such as to provide enough aquifer recharge for the discharge test in PB1 (sand box).

Additionally, some useful suggestions for the choice of test method are given herein. The sudden water level change of the VH tests was initiated in a few seconds and the tests lasted 1-2 min in sand aquifers, and longer in materials with lower permeability. Due to its shorter duration compared to the CH test, the VH tests can be used in preliminary judgement of the permeability for an unknown layer. If the *K*-value is smaller than 10^{-6} m/s it is not wise to perform a CH test based on our results because the test duration is much too long, even with a small flowrate. If the *K*-value is in the range of 10^{-4} m/s, a discharge or injection rate of a few hundred of cm^3/min may be used for the CH test, whereas for a VH test the recording interval for the PT and APT should be 1 s or 0.5 s.

A VH test has a smaller zone of influence than a CH test, and hence is more likely to be affected by the created filter zone when the screen and filter pack are in good condition. As a result, a VH

test yields a higher *K*-value than the CH test in most cases. If both the CH and VH tests are carried out in the same MW, and the two yield different *K*-values, the *K* (CH tests) are deemed to be more representative, because they are derived from a larger influence area in steady state. If the situation does not allow a CH test (too low *K*-value), it is recommended to perform both VH tests (falling-head and rising-head) with inward and outward flows as a mean to check the condition of the screen and filter pack.

CHAPTER 5 ARTICLE 3: PLAUSIBLE VARIABLE-HEAD TESTS INITIATED WITH CONTINUOUS PUMPING IN MONITORING WELLS

Accepted by the 71st Canadian Geotechnical Conference

by

Lu Zhang[1] and Robert P. Chapuis[1*]

[1] Department of Civil, Geological and Mining Engineering, École Polytechnique, P.O. Box 6079, Station CV, Montreal, QC, Canada, H3C 3A7

* Corresponding author: Phone: +514 340 4711 ext. 4427 – e-mail: robert.chapuis@polymtl.ca

April 2018

ABSTRACT

The variable-head (VH) test is initiated by suddenly injecting or withdrawing a volume of water and recording the water level recovery in the monitoring well (MW). A slug or solid rod is added to displace water, which yields a falling recovery of water level. For a rising-head test, a slug of water is removed by extracting the sunk rod or a bailer. A pump can also be used to either inject or remove water, but it is more difficult to practise because it must be conducted very quickly. Seven real and numerical tests in aquifers were considered to be variable-head tests. However, the water recovery in the MW occurred after 15- to 40-min pumping, which are actually constant-head (CH) tests. The paper proves that the interpretation methods for the VH test are applicable to the recovery data of CH test. Five tests have different K_{CH} and K_{VH} values, and present curved or scattered velocity plots instead of straight lines, which is indicative of poorly installed MWs.

5.1 Introduction

The variable-head (VH) or slug test, is frequently used to assess the hydraulic properties of the aquifer because it is easy and fast to apply in the field. It is initiated by a sudden increase or

decrease of water volume, which corresponds to a falling- or rising-head test, respectively (ASTM D4044, 2015; CAN/BNQ 2501-135, 2014). The falling recovery of water level can be caused by inserting a slug or solid rod to displace water. A volume of water is removed by extracting the sunk rod or a bailer, which starts the rising-head test. If a pump is used to add or remove water in the pipe, the addition or removal must be conducted quickly. As a longer pumping duration represents a constant flowrate test (ISO 22282-2, 2012), also known as a constant-head (CH) test (Cassan, 2005, CAN/BNQ 2501-135, 2014).

The paper was inspired by an inquiry from a field practitioner asking why the velocity graphs he plotted did not display straight lines for several VH tests. The so-called VH tests, however, were found to be the recovery phases after groundwater sampling, which pumps water constantly for a period of time, rather than the real VH tests.

Therefore, the first question is that if we can use the interpretation methods of VH test to deal with the recovery data of the CH test. If yes, the second question is that does the velocity plot still present a straight line for a good CH recovery test.

The paper first presents the theoretical evidence to apply the interpretation methods of VH tests on the recovery data of CH tests. A total number of five examples that have curved or scattered velocity plots are presented subsequently. The K_{CH} is used to refer the hydraulic conductivity calculated by the interpretation method of CH test. It is determined through the provided constant flowrate Q and hydraulic head difference H_c. Meanwhile, the test data are analyzed by the interpretation methods of VH tests: Hvorslev's semi-log plot (Hvorslev, 1951), velocity graph (Chapuis et al., 1981), and *Z-t* method (Chiasson, 2005). The yielded hydraulic conductivity is termed K_{VH}. The values of K_{CH} and K_{VH} are then compared. In addition, another two CH tests performed in MWs of good conditions are analyzed in the same way. The results are compared with those of the five previous tests.

5.2 Theoretical solutions

5.2.1 Interpretation of hydraulic conductivity

In a CH test, the constant discharge/injection rate Q generates a constant hydraulic head difference H_c when the test reaches equilibrium. With the knowledge of the shape factor

$c=2\pi L/\ln(2L/D)$ (Hvorslev, 1951), where L and D are the length and diameter of the immersed filter pack, we know from the Lefranc's solution (Lefranc, 1936, 1937) that the flow rate through the water injection zone, Q_s, has found to be related to the applied hydraulic head H_c as follows:

$$Q_s = cKH_c \tag{5.1}$$

where $Q_s = Q$ in steady state. The saturated hydraulic conductivity K in the aquifer is interpreted by

$$K = \frac{Q}{cH_c} \tag{5.2}$$

If the recovery of CH test is considered as a VH test with a rising/falling water level in the MW, the K value can be determined from the Hvorslev's semi-log plot, expressed as

$$\ln\left(\frac{H_1}{H_2}\right) = -\frac{cK}{S_{inj}}\left(t_1 - t_2\right) \tag{5.3}$$

where the hydraulic heads H_1 and H_2 at respective times t_1 and t_2 appear as a straight line if there is no piezometric error, and S_{inj} is the internal area of the MW. Therefore,

$$K = -P_1 \cdot \frac{S_{inj}}{c} \tag{5.4}$$

in which P_1 is the slope of the straight line represented by Equation 5.3. If a piezometric error H_0 exists, the semi-log plot can be upward or downward curved (Chapuis 1998, 2015, 2017). The H_0 value is estimated by either the velocity graph (Equation 5.5) or the Z-t methods (Chiasson, 2005). The detailed calculation processes of the two methods were presented by Zhang et al. (2018 a, b)

$$H = -\frac{S_{inj}}{cK}\frac{dH}{dt} + H_0 \tag{5.5}$$

The K value is expressed as

$$K = \frac{1}{P_2} \cdot \frac{S_{inj}}{c} \tag{5.6}$$

where P_2 is the slope of the straight velocity plot referred by Equation 5.5.

5.2.2 Theoretical examination

The section explains why the interpretation methods of VH test can be used for the CH test in theory. Cassan (2005) presented the interpretation of transient state of the CH test. In the transient phase, $Q_s \neq Q$, and the relative flow rate in the pipe is Q - Q_s. Therefore, the variation of the water level dH in the well pipe with an internal area of S_{inj} during the time dt corresponds to the movement of a volume of water:

$$(Q - Q_s)dt = S_{inj}\,dH \tag{5.7}$$

Substituting Equation 5.1 into Equation 5.7, the equation can be rewritten as:

$$\frac{dH}{\frac{cKH}{S_{inj}} - \frac{Q}{S_{inj}}} = -dt \tag{5.8}$$

which is the differential equation that governs the flow in transient state. Integrating both sides from time t_i to t and from head H_i to H, the equation becomes

$$H = \frac{Q}{cK} + \left(H_i - \frac{Q}{cK}\right) \cdot e^{\left[-\frac{cK}{S_{inj}}(t - t_i)\right]} \tag{5.9}$$

The hydraulic head difference H of the injection zone reach a limit of $H_c = Q/(cK)$ when t tends to infinity, which indicates that the representative curve of Equation 5.9 has an asymptote parallel to the x-axis. Therefore, the asymptote corresponds to the steady state where the Q is equivalent to Q_s. When the time and head are recorded at the time we start the pump, i.e., t_i and H_i equal 0, Equation 5.9 is simplified to:

$$H = \frac{Q}{cK}\left(1 - e^{\left(-\frac{cK}{S_{inj}}t\right)}\right). \tag{5.10}$$

It is observed that the ordinate of the asymptote is still $H_c = Q/(cK)$, and the slope of the tangent at the origin is calculated as Q/S_{inj}.

The recovery phase after the steady state, which represents a test at zero flow after the constant flow is stopped. Because $Q = 0$, Equation 5.9 becomes:

$$H = H_i e^{\left[-\frac{cK}{S_{inj}}(t-t_i)\right]} \tag{5.11}$$

where H_i and t_i refer to the water head in the well pipe and the time, respectively, at the moment the pump stops. Equation 5.11 can be rewritten as:

$$\ln\left(\frac{H}{H_i}\right) = -\frac{cK}{S_{inj}}(t-t_i) \tag{5.12}$$

which is the same as the Hvorslev's semi-log plot represented by Equation 5.3.

The relative velocity of the water flow in pipe from Equation 5.7 is

$$v = \frac{Q-Q_s}{S_{inj}} = \frac{dh}{dt} \tag{5.13}$$

The ratio Q/S_{inj} represents the maximum instantaneous velocity of the water in pipe, from the start-up of the pumps, even before the water movement into the soil begins. Therefore, the initial velocity $v_i = Q/S_{inj}$ at time $t = 0$ for a zero head. The differential equation (Equation 5.8) is written as:

$$v = v_i - \frac{cK}{S_{inj}}H \tag{5.14}$$

where the relative velocity v and the corresponding head difference H during dt are calculated by the two consecutive measurements:

$$H = \frac{H_{j+1}+H_j}{2} \text{ and } v = \frac{H_{j+1}-H_j}{t_{j+1}-t_j}.$$

As soon as the pump is stopped, the hydraulic head, which has reached a maximum value of H_c, begins to dissipate and the injection/discharge flow rate becomes zero. As $Q = 0$, the initial velocity $v_i = 0$ in Equation 5.14, we have

$$v = -\frac{cK}{S_{inj}}H \tag{5.15}$$

which can be transformed into the Equation 5.5 of velocity graph by adding the piezometric correction.

Therefore, Equations 5.12 and 5.15 prove that the VH test methods of Hvoslev and velocity graph can be used to interpret the recovery phases of a CH discharge/injection test, groundwater sampling, and pumping test.

5.3 Examples of poorly installed wells

The examples 1 to 5 present the recovery data after groundwater sampling. The first three tests were performed in a sand aquifer, whereas the examples 4 and 5 were in a till (silty sand) layer. The flow rates, steady-state head differences, shape factors and inside cross-sectional areas of MWs are summarized in Table 5.1. The information of Q and H_c are missing for examples 4 and 5. The tests are interpreted by the CH test method firstly, and then compared with the VH test methods. We use K_{VH1}, K_{VH2}, and K_{VH3} to refer the K_{VH} values estimated from the semi-log graph, velocity graph and optimized semi-log graph by *Z-t* method, respectively.

Table 5.1: Several information of the examples.

examples	pumping rate Q (cm^3/s)	head difference H_c (cm)	internal area S_{inj} (cm^2)	shape factor c (cm)
1	181.0	179.5	20.3	384.6
2	540.7	220.4	20.3	545.6
3	83.8	3.7	20.3	473.2
4	--	--	5.1	538.8
5	--	--	5.1	538.8
6	7.6	15.7	9.3	221.6
7	609	100	21.2	244.1

5.3.1 Example 1

The MW has a 305-cm long screen but only 225 cm were immersed before the sampling and testing. The data was collected during recovery after 38-min pumping at a rate of 10.86 L/min (see Figure 5.1), which generated a constant head difference of 179.5 cm. The hydraulic conductivity K_{CH} is 2.6×10^{-3} cm/s. The semi-log and velocity graphs are plotted in the same graph on primary and secondary axes, respectively.

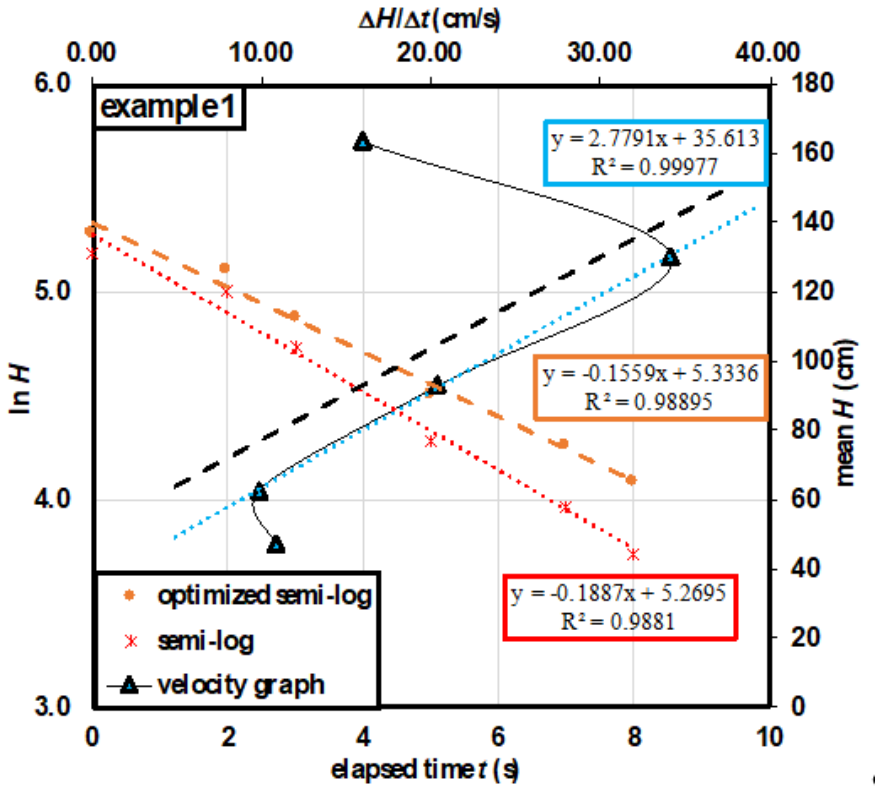

Figure 5.1: Example 1 in sand, L = 225 cm, D = 11.4 cm

It is observed from Figure 5.1 that the test data pass through a nearly straight semi-log graph, which yields K_{VH1} of 9.9 x 10^{-3} cm/s. The velocity graph appears scattered instead of straight, and the R^2 of its best fit (the black dashed line) is 0.3, which provides an incorrect K_{VH2} of 2.0 x 10^{-2} cm/s. We selected the three points that form a linear line (the blue dotted line) to calculate the piezometric error H_0 and K'_{VH2}, which are 35.6 cm and 1.9 x 10^{-2} cm/s. However, the Z-t method gives a different H_0 of -17.6 cm. And the optimized hydraulic conductivity of K_{VH3} = 8.2 x 10^{-3} cm/s, which is considered to be the most accurate compared to the other K_{VH} values. It is obvious that the three K_{VH} values are different and the value of K_{VH3} is 213% larger than K_{CH}.

5.3.2 Example 2

The screen of MW is also 305 cm in length and 360 cm was immersed. The groundwater was sampled at a rate of 32.44 L/min during 32 min, which reached a constant head difference of 220.4 cm. The calculated K_{CH} is 4.5 x 10^{-3} cm/s. The recovery test data are illustrated in semi-log and velocity graphs in Figure 5.2.

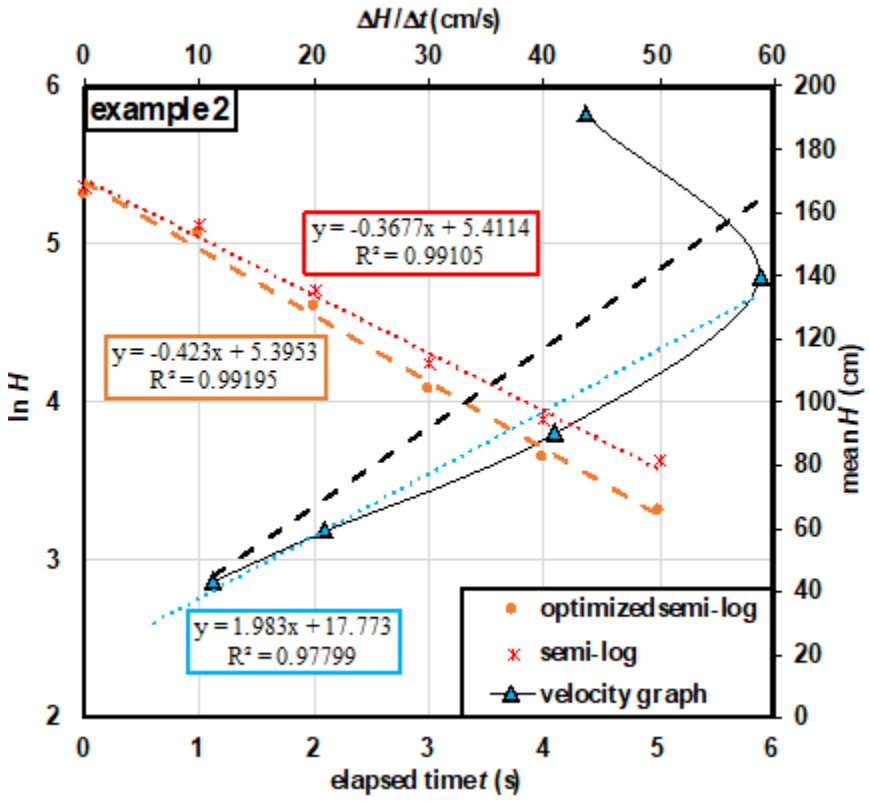

Figure 5.2: Example 2 in sand, L = 360 cm, D = 11.4 cm

The semi-log plot is also a straight line, giving a K_{VH1} of 1.4 x 10^{-2} cm/s. The optimized one is more accurate, from which the K_{VH3} is equal to 1.6 x 10^{-2} cm/s with a peizometric correction of 10.3 cm. The velocity graph appears a similar shape to that of the Figure 5.1, but without the last point being abnormal. It also has a bad linear fit (the black dashed line) with R^2 = 0.6, which determines a K_{VH2} of 1.5 x 10^{-2} cm/s. The last four points of the velocity graph has a better linear fit, where K'_{VH2} = 1.9 x 10^{-2} cm/s. We can see that the K_{VH} and K_{CH} values are not in the same order. The K_{VH3} is greater than K_{CH} by 249%.

5.3.3 Example 3

The length of MW screen is 305 cm, and 298 cm was immersed. Compared to the examples 1 and 2, a smaller H_c of 3.7 cm was generated due to a lower Q of 5.03 L/min. The estimated K_{CH} is 4.8 x 10^{-2} cm/s. The water level started to recover after 15-min discharging, which were registered against time (plotted in Figure 5.3).

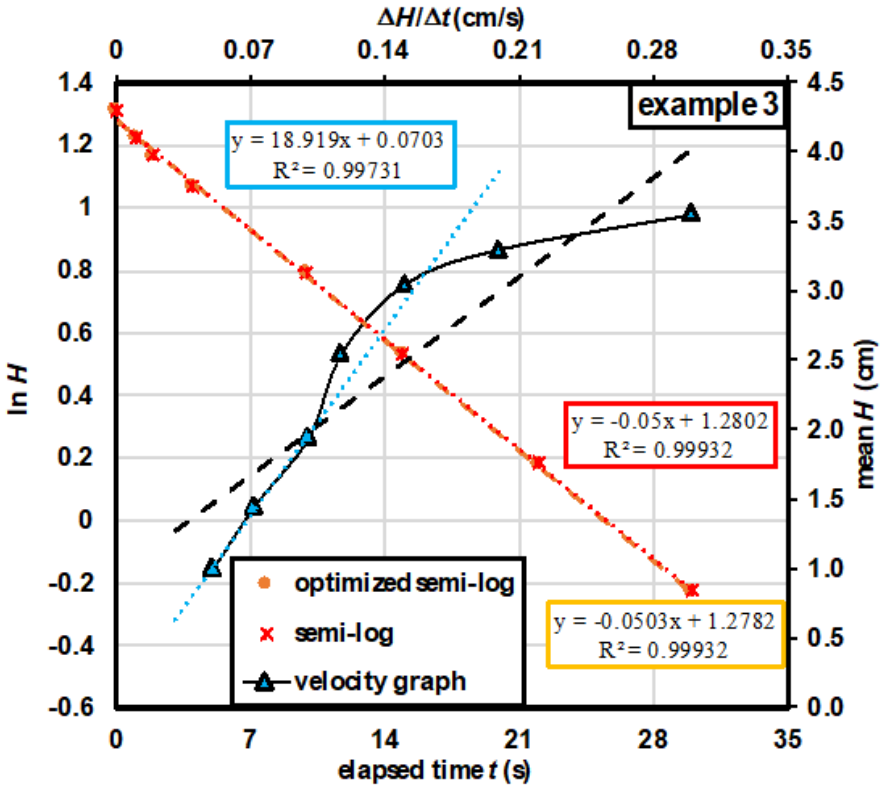

Figure 5.3: Example 3 in sand, L = 298 cm, D=11.4 cm

In this case, the semi-log plot is perfectly linear and no piezometric error exists according to the *Z-t* method. Therefore, $K_{VH1} = K_{VH3} = 2.1 \times 10^{-3}$ cm/s. However, the velocity graph is downwardly curved and has a best fit line (the black dashed line), of which $R^2 = 0.8$ and $K_{VH2} = 4.2 \times 10^{-3}$ cm/s. The last three points pass through a straight portion that yield a K'_{VH2} of 2.3×10^{-3} cm/s, which is similar to the K_{VH1} and K_{VH3} values. However, the K_{VH3} is 95% lower than K_{CH}.

5.3.4 Example 4

The screen of the MW is 367 cm in length. There was a very long pumping duration before the recovery, but no information about the pumping rate and time were provided. Thus, the K_{CH} is unknown, and only K_{VH} values are obtained from the recovery data.

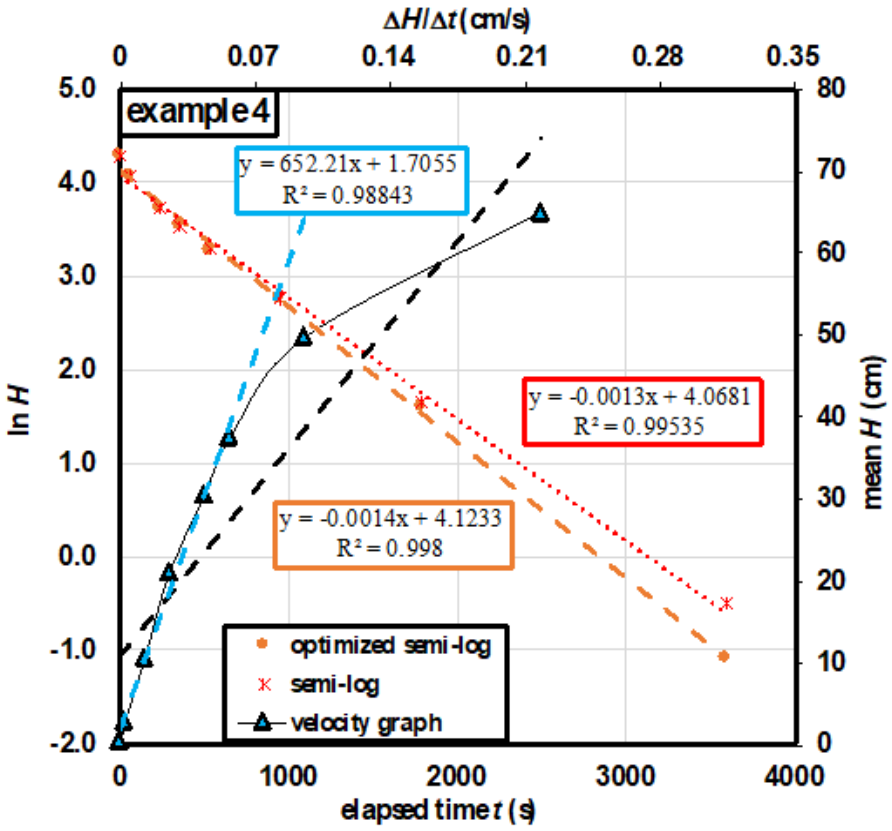

Figure 5.4: Example 4 in till, L = 367 cm, D = 10.16 cm

In Figure 5.4, the original and optimized semi-log graphs are close, and thus yield similar K_{VH1} and K_{VH3} of 1.2 x 10^{-5} cm/s and 1.4 x 10^{-5} cm/s, respectively. The entire velocity data has a linear fit of R^2 = 0.8, giving K_{VH2} = 3.2 x 10^{-5} cm/s. From the straight portion of the late velocity data, a more accurate K'_{VH2} of 1.4 x 10^{-5} cm/s is obtained, which is equivalent to the optimized K_{VH3}.

5.3.5 Example 5

The same information was provided for this example as the example 4. Thus, the K_{CH} is unknown, and only the recovery data are plotted in Figure 5.5.

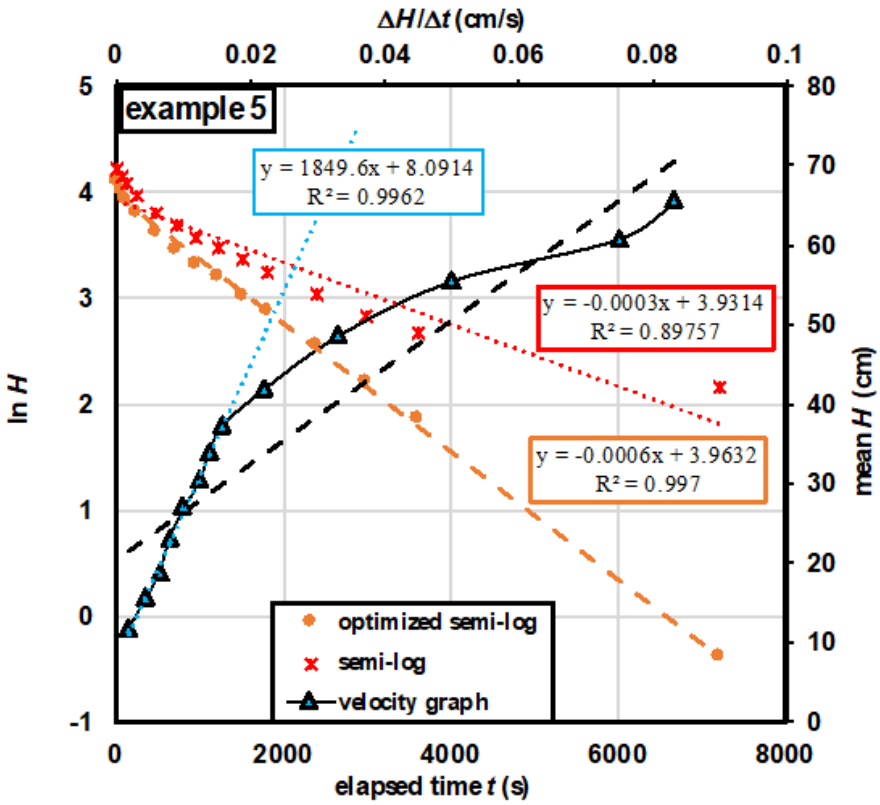

Figure 5.5: Example 5 in till, L = 367 cm, D = 10.16 cm

The original semi-log plot in Figure 5.5 presents a larger curvature compared to other examples, thus its K_{VH1} is the most inaccurate one, 2.8 x 10^{-6} cm/s. It was optimized to be straight by *Z-t* method, which has a K_{VH3} value of 5.7 x 10^{-6} cm/s. The shape of the velocity graph is similar to that of the example 4, from which K_{VH2} = 1.6 x 10^{-5} cm/s. The K'_{VH2} value is 5.1 x 10^{-6} cm/s from the straight portion of the velocity graph, which is close to the K_{VH3}.

5.3.6 Discussion

The five examples illustrate that the original semi-log graphs are approximately straight except that the example 5 has an obvious upward curvature. They are optimized by the *Z-t* method in a spreadsheet to determine more accurate K_{VH3} values compared to the K_{VH1} values. Even though with the optimization, the K_{VH3} values of examples 1 and 2 are over 200% higher than the corresponding K_{CH} values, and K_{VH3} of example 3 is 95% lower than its K_{CH} value.

Additionally, the shapes of velocity graphs are divided into two types: being scattered in examples 1 and 2, and downwardly curved in examples 3 to 5 instead of straight lines. The K_{VH2}

values determined by the entire velocity graph differ from the K_{VH3} values. The early data of the velocity plot refers to the recovery in pipe, therefore the straight portions of the late data which represents the recovery in aquifer are used to derive the H_0 and K'_{VH2}. In examples 3, 4 and 5, the derived H_0 values are close to those determined by the *Z-t* method, and the values of K'_{VH2} are very close to the K_{VH3} values. It is, however, not the case for examples 1 and 2. The reason might be the large pumping rate of the first two examples. The high flow rate may cause turbulence close to the screen, which enhances the energy dissipation, and thus generates a more important head loss and a large dewatering of the screen during pumping. Additionally, the K'_{VH2} from the straight portion is approximately equal to K_{VH3}, but still greatly differ from the K_{CH} values for example 3.

Based on the known condition of examples 1 and 3 that the screens were partially immersed, the deviations between the K_{CH} and K_{VH} values and the abnormal velocity plots are believed to be due to the poorly installed monitoring wells. However, this needs to be checked. Therefore, the results of CH recovery tests in another two MWs in good conditions are provided in the following section.

5.4 EXAMPLES of good wells

5.4.1 Example 6

It is a CH test conducted in the MW installed in a sand confined aquifer in Sorel. The MW was proved to be in good condition (Zhang et al., 2018b). The H_c is 15.7 cm, generated by a constant flow rate of 0.45 L/min, which yields a K_{CH} of 2.2×10^{-3} cm/s. The screen was entirely immersed during the test. The semi-log and velocity graphs of the recovery data collected after 17-min pumping are plotted in Figure 5.6.

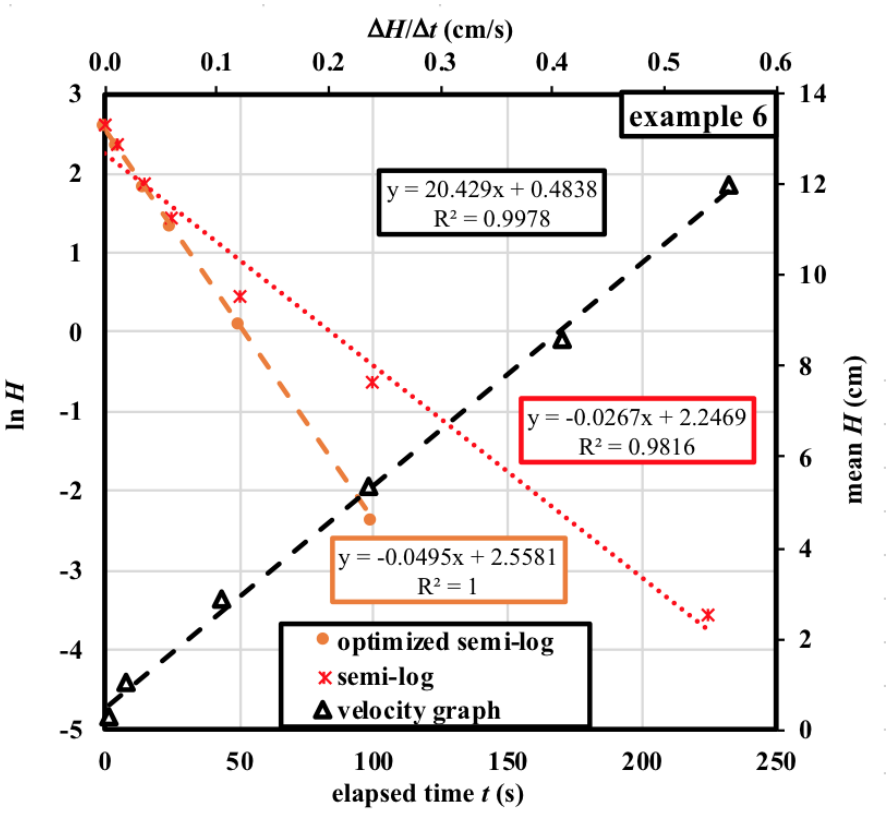

Figure 5.6: Example 6 in sand, L = 114 cm, D = 9 cm.

The semi-log graph is slightly curved, and K_{VH1} = 1.1 x 10^{-3} cm/s. After optimization, the K_{VH3} has a value of 2.1 x 10^{-3} cm/s, which is very close to the previously calculated K_{CH}. The velocity plot is a straight line with an intercept on y-axis of 0.48 cm, which is close to the H_0 of 0.45 achieved by the *Z-t* method. And the K_{VH2} from the velocity graph is 2.1 x 10^{-3} cm/s, equivalent to K_{VH3}.

5.4.2 Example 7

Example 7 presents a CH test in the MW in a sand unconfined aquifer modelled with the numerical code, and thus the well is in good condition during a pumping period of 30 min. The screen was entirely immersed during the test. The H_c is 100 cm, generated by a constant pumping of 36.5 L/min. The yielded K_{CH} is 2.5 x 10^{-2} cm/s.

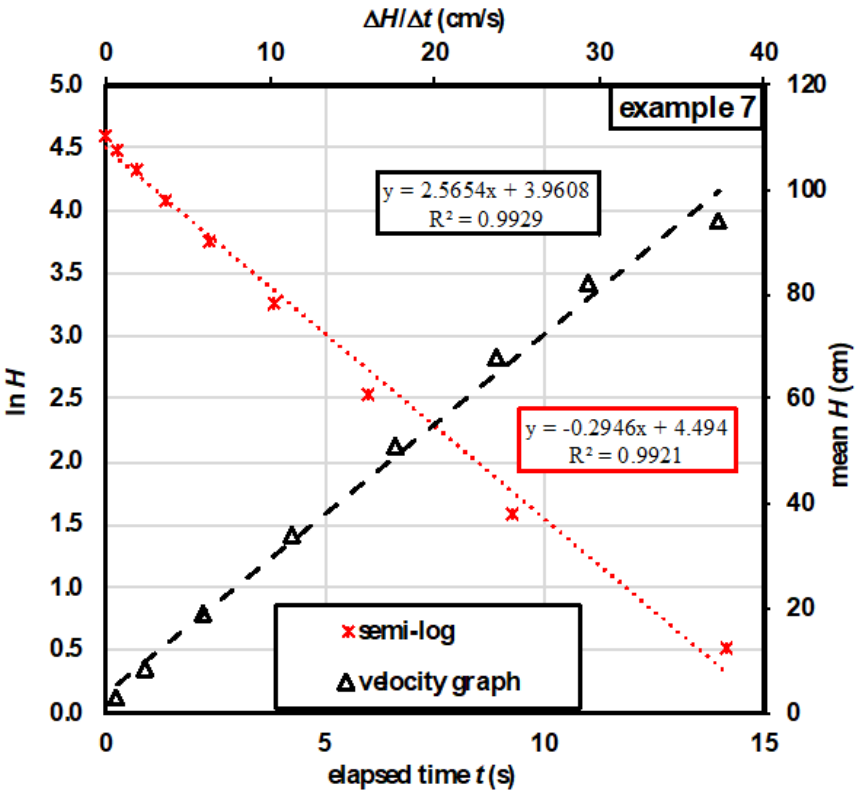

Figure 5.7: Example 7, L = 100 cm, D = 15.24 cm.

The semi-log and the velocity graphs in Figure 5.7 are straight lines. No optimization is needed for the case. The K_{VH1} = K_{VH3} is 2.5 x 10^{-2} cm/s, equivalent to the K_{CH}. The K_{VH2} is 3.2 x 10^{-2} cm/s, close to the K_{CH} value. It is noted that although the flow rate is higher compared to the examples 1 and 2, the velocity plot is not scattered, because the hydraulic conductivity of the sand in example 7 is one order higher than that in examples 1 and 2, and thus higher flow rate is needed to generate the head difference.

5.5 Summary

A total number of seven-group recovery data of CH tests are analyzed as if they were VH tests. They seem like plausible VH tests with water level changing smoothly back to the initial level, however, there are long pumping durations before the recovery (not a sudden water volume change). Therefore, the paper first theoretically proved that the Hvorslev's semi-log and velocity plots used to interpret the VH test also apply to the CH recovery test.

If the MW is perfectly installed and the CH test operation is good, the velocity graph of the recovery data appears to be straight, and the yielded K_{VH} values are close to the K_{CH} value, like what was obtained with good examples 6 and 7.

Table 5.2: Elements of comparison for the seven examples.

example no.	1	2	3	4	5	6	7
flow rate	high	high	low	low	low	low	high
semi-log plot	straight	straight	straight	straight	slightly curved	slightly curved	straight
velocity plot	scattered	scattered	curved	curved	curved	straight	straight
K_{CH} (cm/s)	2.62×10^{-3}	4.50×10^{-3}	4.79×10^{-2}	--*	--*	2.18×10^{-3}	2.50×10^{-2}
K_{VH1} (cm/s)	9.94×10^{-3}	1.37×10^{-2}	2.14×10^{-3}	1.22×10^{-5}	2.77×10^{-6}	1.13×10^{-3}	2.54×10^{-2}
K_{VH2} (cm/s)	1.99×10^{-2}	1.49×10^{-2}	4.21×10^{-3}	3.24×10^{-5}	1.57×10^{-5}	2.06×10^{-3}	3.17×10^{-2}
K_{VH2}' (cm/s)	1.90×10^{-2}	1.87×10^{-2}	2.26×10^{-3}	1.44×10^{-5}	5.09×10^{-6}	2.06×10^{-3}	3.17×10^{-2}
K_{VH3} (cm/s)	8.21×10^{-3}	1.57×10^{-2}	2.15×10^{-3}	1.36×10^{-5}	5.68×10^{-6}	2.09×10^{-3}	2.54×10^{-2}
K_{VH3}/K_{CH}	3.13	3.49	0.04	--	--	0.96	1.02
comments	1-5: non-straight velocity plot and $K_{CH} \neq K_{VH3}$ indicates poorly-installed MWs * The flow rates were unknown, and thus K_{CH} could not be calculated.					6-7: good MWs	

The examples 1, 2 and 3 show approximately straight Hvorslev's semi-log plots, but the derived K_{VH1} values from the original plot have around 1 order difference from the K_{CH} value. After the optimization of the semi-log graph, the K_{VH3} values of examples 1 and 2 are still greatly different from the corresponding K_{CH} values.

Two shapes of velocity graphs were observed in the poorly installed/test MWs. They are either scattered for examples 1 and 2 or downwardly curved for examples 3-5, which are difficult to analyze. In all cases, the values of K_{VH2} interpreted directly from the linear fitting lines of the entire velocity plots deviate from the K_{VH3} values. The H_0 and K'_{VH2} are obtained from the straight portion formed by late data. For examples (3-5) which have low flowrates, there are two results that need to be noted. Firstly, the H_0 values are similar to those estimated through the *Z-t* method. Secondly, the K'_{VH2} values are very close to the K_{VH3} values. However, these two results are false for the examples 1 and 2. The scattered shapes of the velocity graphs and discordant results are considered to be due to the high pumping rate, which may have created high parasitic head losses against the screen. All results of the MWs are gathered in Table 5.2.

In summary, the interpretation methods of VH tests are applicable to the recovery phase of CH tests based on the theoretical and experimental examinations. They can be used in combination with the Lefranc's solution for steady state, to check the general performance of the screen by comparing the K_{VH} with the K_{CH}. Even if the Hvorslev's plot seems to be linear, it is recommended to optimize the original semi-log graph and plot the velocity graph. If a great difference between K_{VH} and K_{CH}, and the velocity is not straight, it must be indicative of poor design or installation of the well or improper manipulation of the test, e.g., the screen is partially immersed, the water is dewatering down to the screen, the head losses is important close to the screen, etc.

CHAPTER 6 NUMERICAL VALUES OF SHAPE FACTORS FOR FIELD PERMEABILITY TESTS IN UNCONFINED AQUIFERS

6.1 Introduction

The shape factor, *c*, is a factor related to the shape and dimension (Hvorslev, 1951), the position (Bouwer and Rice, 1976, 1989) of the well point or the water injection zone, and the boundary conditions. It serves as a critical parameter in the calculation of hydraulic conductivity *K* for aquifers, which is interpreted from field permeability test data. Researchers proposed different theoretical, electrical analog, and numerical methods to deduce the shape factor in unconsolidated materials (Al-Dhahir and Morgenstern, 1969; Brand and Premchitt, 1980a, 1980b, 1982; Chapuis, 1989; Kallstenius and Wallgren, 1956; Klammler et al., 2014; Lafhaj and Shahrour, 2002b; Lowther, 1978; Mathias and Butler, 2007; Randolph and Booker, 1982; Ratnam el al., 2001; Raymond and Azzouz, 1969; Selvadurai, 2004; Silvestri et al., 2011, 2012, 2013; Smiles and Young, 1965; Tavenas et al., 1990; Wilkinson, 1968;). Two famous equations for the shape factor were provided by Hvorslev (1951) and Bouwer and Rice (1976). The latter, however, yields a higher *c* value due to its unrealistic assumptions (Chapuis, 2009b).

The code Seep/W (GEO-Slope International Ltd., 2012) enables us to quantify the shape factor numerically. Unlike other numerical codes on groundwater seepage, it allows the capillary retention curves $\theta(u)$ and unsaturated hydraulic conductivity functions $K(u)$ to be independent, which models the monitoring well adequately (Chapuis, 2009c). Its reliability was examined for various cases, from one- to three-dimensions (Chapuis et al., 2001). A variety of problems, such as seepage through dikes (Chapuis and Aubertin, 2001), the vadose zone effect on the leakage rates in landfill barriers (Çelik et al., 2009), the seepage characteristics of the buttressed embankment using a centrifuge test model (Jin et al., 2014) were solved via the code. Integrated with other codes, it was also applied to study hydraulic short-circuits, groundwater contamination and slope collapse by seepage erosion (e.g., Ardejani et al., 2007; Chesnaux, Chapuis and Molson, 2006; Chu-Agor et al., 2008).

The numerical simulation for the variable-head (VH) test by the code was initially presented by Chapuis (1998). The negligible role of storativity for the simulated VH tests (Chapuis and Chenaf, 2002), the pipe storage capacity effect and tidal influence on pumping test results were

discussed for the confined aquifer (Chapuis and Chenaf, 2003b; Chapuis et al., 2006). For unconfined aquifers, the double line effect while dewatering down to the screen in the VH test, and the unusual drawdown curves of the pumping test were also analyzed numerically (Chapuis, 2005a; Chapuis et al., 2005b). The numerical value of shape factor was determined for the steady-state conditions of the constant-head (CH) test in either confined or unconfined aquifers (Chapuis, 2005a; Chapuis and Chenaf, 2002; Chapuis et al., 2007). For aquifer models with given geometries, the smaller numerical *c* values compared to the Hvorslev's *c* value were due to a reduced flow rate caused by the model finite size (Chapuis, 2005a; Chapuis and Chenaf, 2002).

However, several problems still wait to be solved. Firstly, if no information is available about the influence radius of the well, increasing the boundary radial distance will significantly increase the computation time because unsaturated drainage takes a very long time. However, in field conditions, the pumping rate for a CH test will be small and one may suspect that the influence radius will be small, but how much? Thus, we need to specify an appropriate boundary radial distance for the numerical test model. Secondly, the shape factor values in the literature were obtained for steady-state conditions only, thus for a CH test, not a VH test. In practice, CH and VH tests are performed. Unfortunately, in the calculation of shape factors, a biased electrical analogy was used (Chapuis, 2009b), and no attention was paid to transient conditions preceding steady-state in the CH test. Furthermore, the shape factor values deduced from numerically simulated VH tests have never been presented and compared with those used for the CH tests. In addition, we are curious about how many parameters would affect the numerical results of the two types of tests.

To provide practical answers, two series of axisymmetric unconfined aquifer models equipped with monitoring wells (MWs) were studied because unconfined aquifers have a high potential for being contaminated, and MWs in unconfined aquifers are frequently tested using CH or VH tests. The MW pipe of the first series of models had a screen but no filter pack. In the second series, the pipe screen was surrounded by a filter pack. Field permeability tests of two types (CH and VH) were conducted numerically in the MWs, and the numerical *c* values were calculated. The CH test reached steady-state after a transient condition, which lasted a long time depending upon the radius of influence and the unsaturated hydraulic properties of the tested soil. The VH test was totally in transient condition.

Each series of models investigated four variables: 11 distances of the boundary (R), 4 lengths (L) for the injection zone, 3 positions of the water injection zone, and 15 types of soils, thus 15 sets of water retention curves (WRC) and saturated hydraulic conductivities (K_{sat}) for the unconfined aquifer. Three parameters were kept constant when one parameter was varied. The unconfined aquifer was homogeneous and isotropic, and its unsaturated parts were fully defined with the use of capillary retention and unsaturated hydraulic functions, $\theta(u)$ and $K(u)$.

The influences of the four variable parameters on numerical c values are analyzed. The c differences derived from CH and VH tests of each series are discussed. The result of the transient analysis of the CH test is compared with that of its steady-state analysis. The numerical c values are also compared with the theoretical values by equations of Hvorslev (1951) and Bouwer and Rice (1976).

6.2 Field permeability tests modelisation

6.2.1 Unconfined aquifer models

They are axisymmetric (r, z) models, the z-axis being the central vertical axis of the monitoring well. The MW is installed in the unconfined aquifer located between elevations 0 and 4 m. Before the tests, the water table was 1 m below ground level, at elevation 3 m. The MW is a schedule 40 2-inch pipe, which have internal and external diameters of 5.2 and 6.0 cm, respectively, and a wall thickness of 0.4 cm. The riser pipe extends up to z = 4.2 m and has a 1-m long screen located at the bottom, without a filter pack (the first series).

The screen is surrounded by a filter pack of 15.24 cm (6-inch borehole) in external diameter in the second-series model. The filter pack extends from z = 0 to 1 m. The screen is 0.8 m long between z = 0.1 and 0.9 m. The annular space around the solid pipe above the filter pack is sealed using bentonite pellets.

The initial R for the two series of models is 3 m. In addition, other 10 boundary radial distances, 2, 4, 5, 8, 10, 20, 40, 60, 80, 100 m, were studied for models either with or without a filter pack to study the influence of R on the numerical c values.

For the first series that has a screen but no filter pack, the lengths of the partially penetrated screened portions are 1m, 2m, and 3m, respectively. The pipe with a 4-m screen was also

analyzed as a fully penetrating MW. The filter packs of the second series similarly range from 1 to 4 m in lengths, and the screens are 0.1 m shorter than the filter packs at both ends. Furthermore, the water injection zones of the two series were located at top (T), middle (M), and bottom (B) positions in the aquifer. The various lengths and positions of the water injection zone were termed 1m-B, 1m-M, 1m-T, 2m-B, 2m-M, 2m-T, 3m-B, 3m-T, and 4m. Figures 6.1a and 61b present schematics of the dimensions and positions of the two series of water injection. zones.

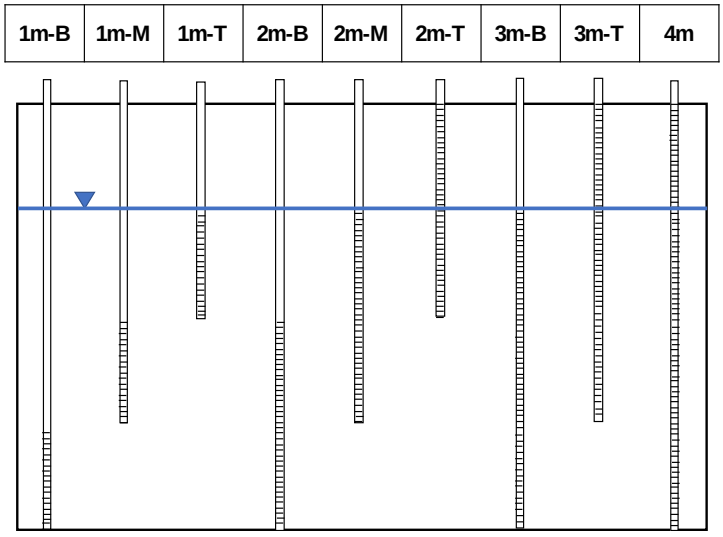

(a) Screen only

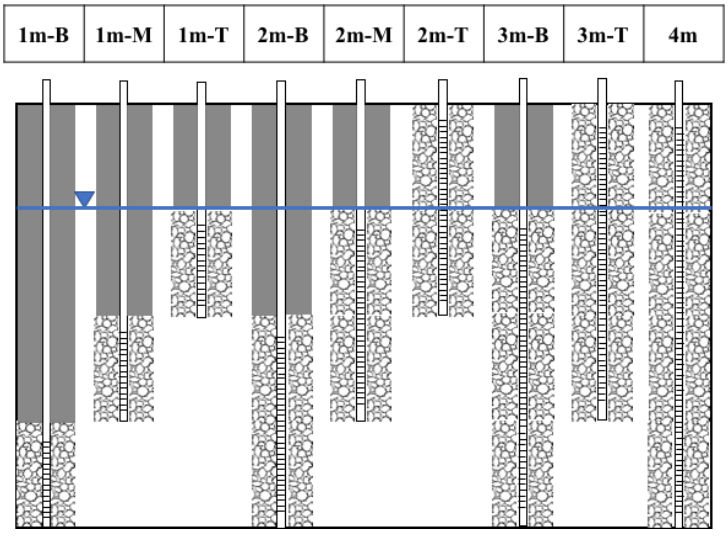

(b) With a filter pack

Figure 6.1: Different lengths and positions of two series of water injection zones.

A global mesh size of 10 cm was used to run the model. The mesh was refined to 1 cm close to the water injection zone and in the unsaturated soil volume where the pore water pressure is negative. The refined regions were mixed quad and triangle mesh, and the pipe was generated as rectangular meshes. The large element size was used where hydraulic head varies lightly. The element size of the bottom saturated zone and the far saturated boundary were increased up to 30 cm when R exceeds 20 m, in order to reduce the computation time. The mesh of the model was generated properly, so that the final solution was independent of the element size, i.e., the model provided accurate results.

6.2.2 $K(u)$ and $\theta(u)$ functions

In the unconfined aquifer model, the pipe, filter pack and granular soil are homogeneous and isotropic, and the unsaturated behaviors were taken into account. The pipe inside is very permeable with a saturated K_{pipe} of 100 m/s, which was considered as a "reservoir" element and has two independent $K(u)$ and $\theta(u)$ functions (Chapuis, 2009c). The $\theta(u)$ declines from θ_s = 0.9 to θ_r =0.15 as the pore water pressure u drops from 0 to -1 kPa. It means that the internal section of the MW, which stores water, represents 75% (0.90 – 0.15) of the external section. The drop of u from 0 to -1 kPa could provide a rapid convergence (Chapuis, 2009c).

The aquifer material No. 0 has a porosity n of 0.38 (void ratio e of 0.613) and effective size d_{10} of 0.145 mm. Its saturated hydraulic conductivity is obtained from the predictive equation $K_{sat}\,(\text{cm/s}) = 2.4622\left(\frac{d_{10}^2 e^3}{1+e}\right)^{0.7825}$ (Chapuis, 2004), which is 2.61 x 10^{-4} m/s. The filter material has a saturated K value of 1.74 x 10^{-2} m/s and is much more pervious than the aquifer material. The materials have constant K values in saturated zones where the pore water pressure is positive.

Besides No. 0 sand, the other 14 types of soils, ranging from coarse sand to silt, were collected from previous research (Haverkamp, Zammit and Bouraoui, 1997; Leij, Alves, Van Genuchten and Williams, 1996; Mbonimpa, Aubertin and Bussière, 2006; Mualem, 1976) to study the impact of different materials on numerical shape factors. The soils have different grain size distributions and saturated hydraulic conductivities between 1.45 x 10^{-7} and 2.31 x 10^{-4} m/s (Table 6.1), which were named from No. 1 to 14.

Table 6.1: Basic soil geotechnical and hydraulic parameters

No.	granular materials	K_{sat} (m/s)	n --	d_{10} (cm)	C_u --	e --	ed_{10} --
0	Sand for initial model	2.61×10^{-4}	0.380	0.1450	--	0.613	0.0889
1	Code 1460 Berlin coarse sand	2.91×10^{-5}	0.297	0.0224	--	0.422	0.0095
2	Code 1461 Berlin coarse sand	2.31×10^{-4}	0.373	0.0224	--	0.595	0.0133
3	Code 1462 Berlin medium sand	1.16×10^{-4}	0.430	0.0144	--	0.754	0.0108
4	Code 1463 Berlin medium sand	8.01×10^{-5}	0.399	0.0144	--	0.664	0.0095
5	Code 1465 Berlin fine sand	4.63×10^{-6}	0.384	0.0028	4.5	0.623	0.0017
6	Code 1466 Berlin fine sand	2.48×10^{-5}	0.414	0.0062	1.8	0.706	0.0044
7	Code 1467 Berlin loamy sand	1.27×10^{-6}	0.312	0.0028	14.2	0.453	0.0012
8	Code 2221 Riverwash sand	1.45×10^{-4}	0.328	0.0054	8.7	0.488	0.0026
9	Code 4650 Plumhof sand	1.13×10^{-6}	0.380	0.0090	--	0.613	0.0055
10	No. 2002 Silt	1.45×10^{-7}	0.442	0.0002	122.0	0.792	0.0002
11	No. 4118 Sand	1.81×10^{-4}	0.342	0.0156	--	0.520	0.0081
12	No. 8 Sand Grenoble 1	2.87×10^{-5}	0.430	0.0143	--	0.754	0.0108
13	No. 9 Sand Grenoble 2	1.48×10^{-4}	0.408	0.0100	--	0.689	0.0069
14	No. 11 Sand Grenoble 4	6.33×10^{-5}	0.385	0.0210	--	0.626	0.0132

Note: Code 1460 to 4650 sand (Leij et al., 1996), No 8 to No11 sand (Haverkamp et al., 1997), No. 2002 silt and No 4118 sand (Mualem, 1976).

The water retention curve (WRC) is a critical material function that defines the unsaturated soil behaviour. The air entry value (AEV), residual suction u_r (kPa), and residual volumetric water content θ_r were predicted by the best-fit equations (Chapuis, Masse, Madinier and Duhaime, 2015) based on known d_{10} (mm) and e. The WRCs of coarse soils were then obtained by substituting the derived parameters into the LN fit (Kosugi, 1994). The method is valid when the product of e and d_{10} is larger than 0.0005.

For finer soils of No. 5, 6, 7, 8 and 10 which have $ed_{10} < 0.0005$, their $\theta(u)$ functions were estimated by the modified Kovacs (MK) method (Aubertin, Mbonimpa, Bussière and Chapuis, 2003). The MK model redefined some key parameters that had not been well defined in the original Kovacs (Kovács, 1981) model. The modifications focus on the statistical function used to describe the pore-size distribution of the media in the capillary component, and the constitutive parameters based on the basic soil properties (Aubertin et al., 2003). The suction unit is cm water and must be converted to kPa (1 kPa = 10.197 cm water) for the code. The model can be applied to a large range of materials from coarse sand to fine-grained soils. Compared to the best-fit equation (Chapuis et al., 2015), however, it provides a slowly decreasing residual water content instead of a constant one, which is less realistic for coarse materials.

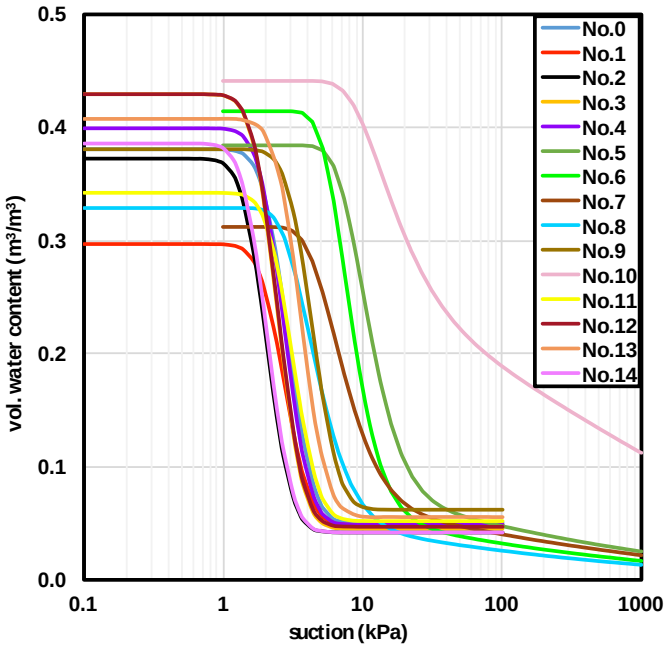

Figure 6.2: *θ(u)* functions of the aquifer materials.

The *K(u)* functions were estimated by the van Genuchten's closed form equation (Van Genuchten, 1980) embedded with the code, based on known *θ(u)* functions. The corresponding *θ(u)* and *K(u)* of each soil must give close AEVs, as presented in Figures 6.2 and 6.3.

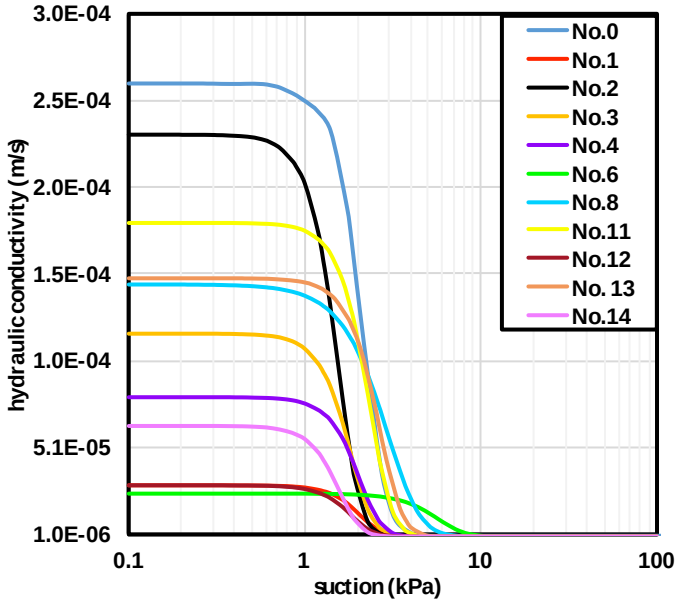

(a) Aquifer materials with $K_{sat} > 10^{-5}$ m/s

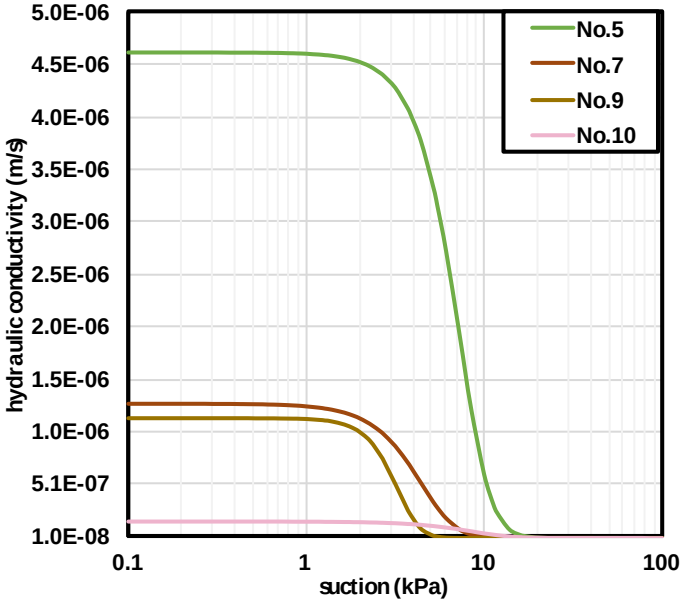

(b) Aquifer materials with $K_{sat} < 10^{-5}$ m/s

Figure 6.3: Corresponding *K(u)* functions of aquifer materials.

6.2.3 Boundaries for field permeability tests

The CH test, for the steady-state analysis, had a far boundary with a hydraulic head of 3 m, and the head at the screen and in the riser pipe was h = 4 m, which represents the steady state of a CH injection test that has a head difference of 1 m. A constant flow rate Q in pipe and aquifer will be found by the numerical analysis. An alternative way of modelling the CH test was to keep the far boundary of h = 3 m, and apply this constant injection Q in the MW to create a constant head difference of 1 m.

The transient analysis of the CH test started with an initial equilibrium state, which is a steady-state analysis, by specifying h = 3 m everywhere. The next step was the transient analysis of an injection process with and h (far boundary) = 3 m, and the boundary conditions for screen of either h = 4 m, or Q = const. The test durations vary with different boundary radial distances and aquifer materials, and thus should be determined by trial and error for each model. In the field, the CH test duration is usually around 20-30 min. However, a 5-h-duration was identically used for all numerical CH tests, which is less practical but helps to compare the seepage in different models synchronously. In all cases, 100 time steps were applied to shorten the computation time greatly, which had been verified to yield same results as the calculation of 1000 time steps.

The simulation of the VH test was in three steps. The initial equilibrium condition was assumed with known piezometric level 3 m in the entire model. The water level in the pipe was then raised by 1 m in 1 s, implemented by imposing a boundary function of the total head h versus time t on the screen, and h = 3 m on the far boundary. The final step kept h (far boundary) = 3 m and removed the boundary condition on screen, which started the falling-head test.

6.3 Shape factors equations

The numerical shape factor of the water injection zone given by CH tests, for either steady-state or transient analysis, can be calculated from the equation of Lefranc (1936, 1937):

$$c = \frac{Q}{KH_c} \tag{6.1}$$

where K is the hydraulic conductivity, Q is the constant flow rate through the screen, obtained from the numerical result, and H_c is the applied hydraulic head difference.

For the transient analysis of VH tests, the numerical value of the shape factor is derived from the equation of Hvorslev (1951):

$$c = \frac{\ln\left(H_1/H_2\right)}{\left(t_1 - t_2\right)} \cdot \frac{S_{inj}}{K} \tag{6.2}$$

where H_1 and H_2 are the hydraulic head differences at times t_1 and t_2, respectively, and $[\ln(H_1/H_2)]/(t_1-t_2)$ is the slope of the Hvorslev's semi-log graph, S_{inj} is the internal cross-section area of MW pipe. For field tests, if the semi-log graph is not a straight line, the velocity graph method (Chapuis, 1998, 2017; Chapuis et al., 1981) or the *Z-t* method (Chiasson, 2005) is used to straighten the plot and extract the systematic error on water columns, which may be due to 4 or 5 sources of field errors. However, for numerical tests, there is no such systematic error.

The formulas for the theoretical shape factor were derived from the solutions of the Laplace equation, based on approximate shapes of the cylindrical injection zone, either a sphere of equal surface or an ellipsoid (Chapuis, 1989), in an infinite medium. The complete ellipsoid formula was given by Dachler (1936):

$$c = \frac{2\pi L}{\ln\left[\frac{L}{D} + \sqrt{1 + \left(\frac{L}{D}\right)^2}\right]} \tag{6.3}$$

where L and D is the length and diameter of the water injection zone, respectively. It was simplified by Hvorslev (1951) as,

$$c = \frac{2\pi L}{\ln\left(2L/D\right)} \qquad \text{if } L/D > 4 \tag{6.4}$$

The sphere formula is expressed as,

$$c = 2\pi D\sqrt{\frac{L}{D} + \frac{1}{4}} \qquad \text{if } 1 \le L/D \le 8 \tag{6.5}$$

Bouwer and Rice (1976) assumed that the Thiem equation could be used in the unconfined aquifer with partially penetrated well, and then made an electrical analogy, which provided a shape factor:

$$c = \frac{2\pi L}{\ln\left(R_0 / r_w\right)} \tag{6.6}$$

where R_0 is the radius of influence and $r_w = D/2$ is the external radius of the water injection zone. This equation is similar to Equation 6.4. Two empirical formulas for $\ln(R_0/r_w)$ were obtained based on the electrical analogs in steady-state conditions:

$$\ln\left(R_0 / r_w\right) = \left[\frac{1.1}{\ln\left(d / r_w\right)} + \frac{A + B\ln\left(b - d\right)/ r_w}{L / r_w}\right]^{-1} \tag{6.7}$$

$$\ln\left(R_0 / r_w\right) = \left[\frac{1.1}{\ln\left(d / r_w\right)} + \frac{C}{L / r_w}\right]^{-1} \tag{6.8}$$

where d is the distance from water level to the bottom of the water injection zone, b is the saturated thickness of the unconfined aquifer. A, B and C are three dimensionless coefficients, functions of L/r_w defined by Bouwer and Rice (1976).

6.4 Theoretical values of shape factors

The two known theoretical shape factors are independent of the aquifer radial distances and materials. The Hvorslev shape factor depends only upon the dimensions of the water injection zone. The Bouwer and Rice's equation, however, needs to additionally take into account the injection zone position. The shape factors of injection zones with lengths of 1, 2, 3, 4 m were computed, considering their different positions. The diameter of injection zone for the MW without filter pack is equal to the external diameter of the screen, which was 6 cm. For the case that has a filter pack around the screen, the injection zone had a diameter of 15.24 m (6-inch borehole). The Hvorslev's and Bouwer and Rice's c values for the two series are presented in Table 6.2, where the Bouwer and Rice's c values of 1m-B, 2m-B, 3m-B and 4m were calculated by Equation 6.8, and the others by Equation 6.7 due to the different positions of the injection zone.

Table 6.2: Theoretical shape factors

injection zone	lengths (*L*) & positions	1m-B	1m-M	1m-T	2m-B	2m-M	2m-T	3m-B	3m-T	4m
no filter pack *D*=0.06m	Hvorslev	1.79	1.79	1.79	2.99	2.99	2.99	4.09	4.09	5.14
	Bouwer and Rice	1.90	2.39	2.76	3.60	4.29	5.01	5.29	6.26	6.93
with a filter pack *D*=0.1524m	Hvorslev	2.44	2.44	2.44	3.85	3.85	3.85	5.13	5.13	6.35
	Bouwer and Rice	2.55	3.33	3.99	4.67	5.73	6.96	6.82	8.16	8.87

It is observed (Table 6.2) that the Bouwer and Rice's *c* in the two series is always higher than the Hvorslev's *c*. This happens because in their electrical analog the authors confused the water table with a constant-head boundary, which yielded a higher flow rate compared to the realistic problem, thus producing a higher shape factor (Chapuis, 2009b).

6.5 Influences of the four variables on numerical shape factors

6.5.1 Boundary radial distance influence on shape factor

6.5.1.1 First series: no filter pack

The numerical *c* values derived from the three types of numerical analyses were plotted together with the theoretical *c* values versus *R* in Figure 6.4. The CH steady-state flow rates *Q* in pipe decreased steadily with the increase of the boundary radial distance *R* from 2 to 100 m due to the decline in radial gradients. Due to their proportional correlations, the derived *c* values steadily decrease in the lin-log plot, from 1.84 to 1.36 m (Figure 6.4). The numerical *c*-curve intersects with the constant Hvorslev's *c* of 1.79 m at *R* = 2.6 m. The CH transient *c* is equal to the CH steady-state *c* when *R* is no greater than 8 m. Beyond this range, the two types of shape factors

become different and the former finalizes at a constant value of 1.59 m starting from R = 20 m. The Bouwer and Rice's c value is 1.90 m, greater than the CH and Hvorslev's c values.

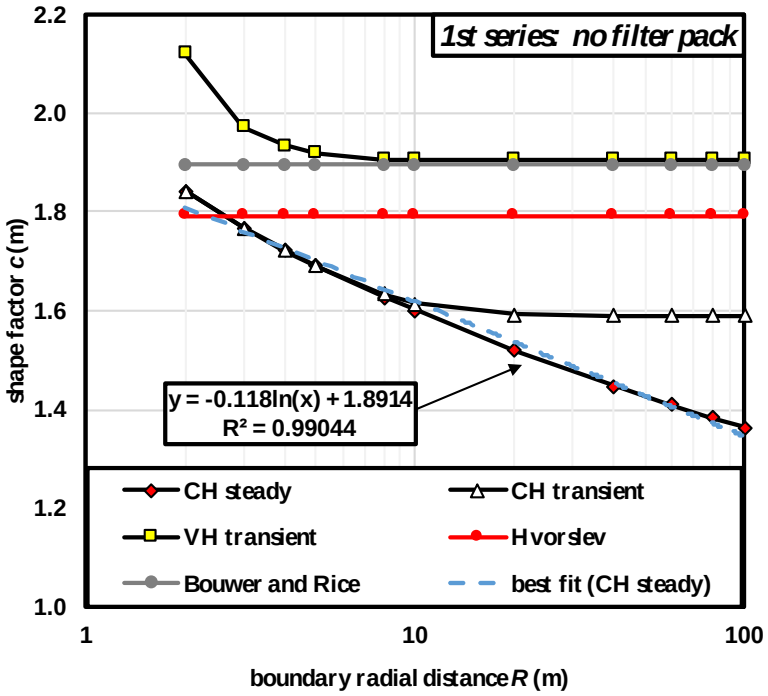

Figure 6.4: Shape factors versus boundary radial distance (no filter pack).

For the VH test, R does not have the same influence on the shape factor because the VH test is quite rapid and modifies the hydraulic head within a small volume around the well (Figure 6.5). In Figure 6.4, the numerical c for the VH test has a narrow range from 1.91 to 2.12 m. It starts at the highest value for a small R value and then drops to a constant value of 1.91 m from R = 8 to 100 m. In addition, the transient water table positions at r = 3 cm at various times were compared with the steady water table positions for models of different boundary radial distances (Figure 6.6). The water tables under steady-state analysis of aquifer models yield a log-linear line with increased R. For the CH transient plots, the water tables are at z = 3 m at the beginning (t = 0 s) everywhere. They then rise along with the elapsed time up to 5 h in all cases of boundary radial distances from 2 to 100 m. It is also observed that the transient water table of 5 h deviates from the steady-state water table when R > 8 m.

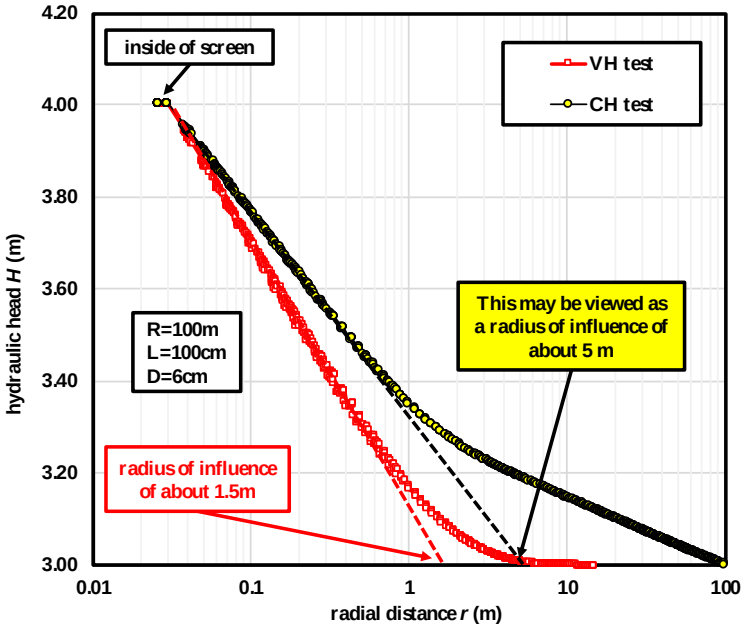

Figure 6.5: Examples of variation of the hydraulic head versus distance.

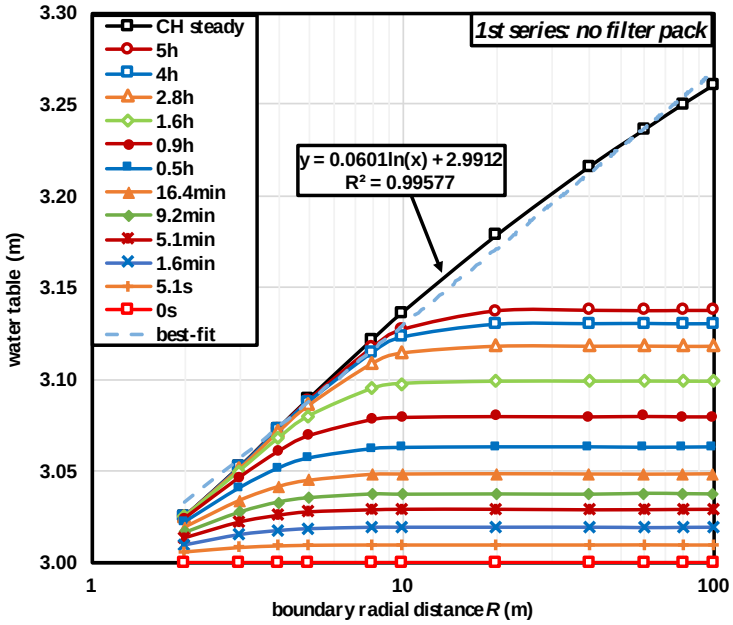

Figure 6.6: CH steady and transient water tables at r = 0.03 m versus boundary radial distance.

6.5.1.2 Second series: with a filter pack

The addition of a filter pack increases the diameter of the injection zone from 0.06 to 0.1524 m. Figure 6.7 presents all types of c values for the second series. The CH steady-state Q decreased

from 6.43 x 10^{-4} to 4.38 x 10^{-4} m^3/s when R increases from 2 to 100 m. The c value consequently reduces from 2.46 to 1.68 m. Similar to the results of the first series, the CH steady-state and transient c values become different when R > 8 m, but the difference is that they equal the Hvorslev's c when R = 2.1 m instead of 2.6 m. The CH transient c value becomes an invariable of 2.03 m from R = 20 m. The VH-test shape factor drops from 2.88 to 2.47 m for boundary radial distances below 8 m, which has a constant value of 2.47 at further distances. The Bouwer and Rice shape factor is 2.55 m, slightly higher than the Hvorslev's shape factor of 2.44 m.

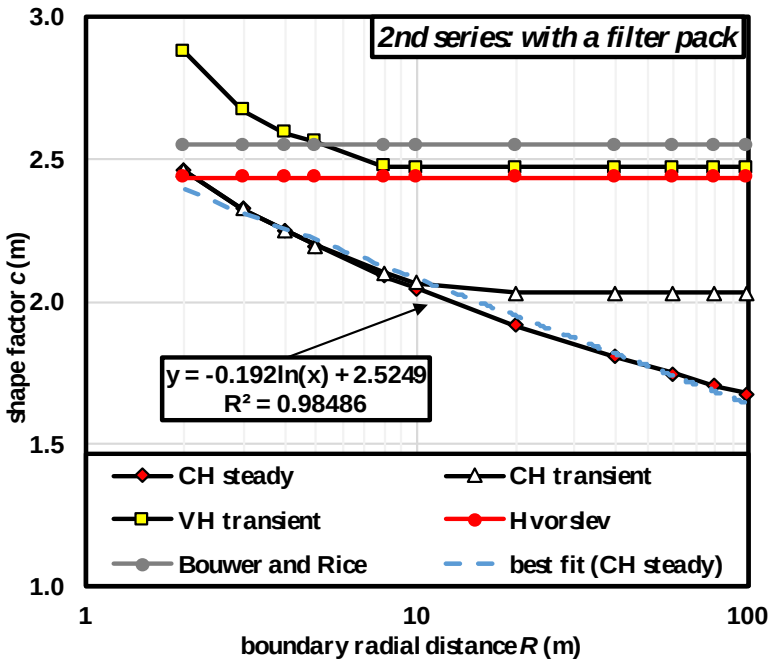

Figure 6.7: Shape factors versus boundary radial distances (with a filter pack).

The water tables of the two numerical analyses for the CH tests were plotted in Figure 6.8. The plots of water tables at r = 7.62 cm (interface between the soil and the filter pack) versus R of the second-series models have similar relationship in comparison with the first series. The steady water table also appears as a straight line.

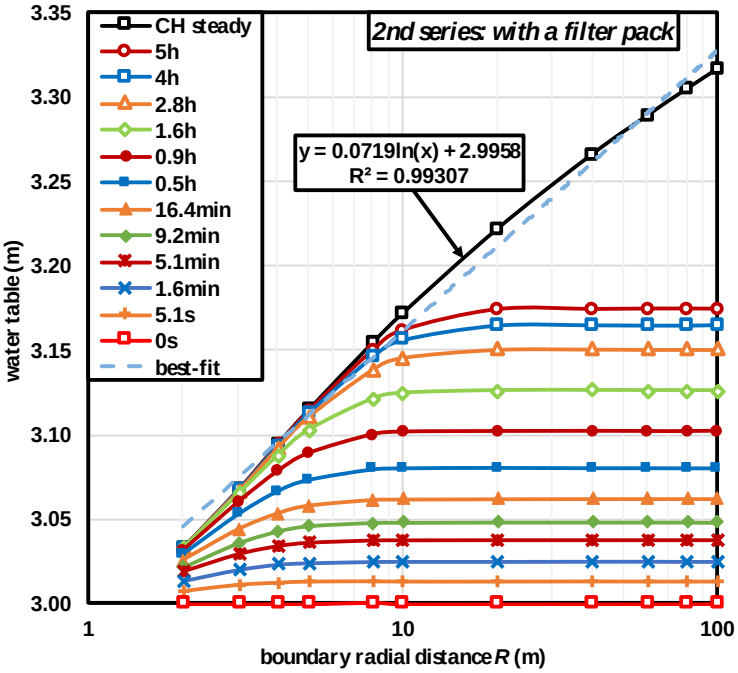

Figure 6.8: CH steady and transient water table at r = 0.0762 m (interface between soil and filter pack) versus boundary radial distance R

6.5.1.3 Discussion

Compared to the first-series models, all shape factors take greater values and the water tables during the test are higher for the second series due to the increased diameter of water injection zone, i.e., the addition of the filter pack.

Theoretically, the final results of the CH-test in transient and steady-state analyses should be the same if the former reaches equilibrium, because the two test models are identical in geometry, material and boundary condition except that the transient analysis is time-dependent. In transient analysis, the flow rate is decreasing in pipe and increasing in aquifer with elapsed time. The two flow rates become equivalent when steady state is reached.

In our case, the final results including the flow rate, water table, and contours are different for the two analyses when R exceeds 8 m. The reason is that the specified 5-h-test-duration is not long enough for numerical models of large boundary radial distances to reach equilibrium. Consequently, the Q (pipe) is larger than instead of equivalent to the Q (aquifer), hence, the derived CH-test transient c values are greater than the CH-test steady c. We subsequently ran

each numerical model of the first series for a time long enough to have a Q (pipe) value varying by less than 1% (Figure 6.9). The same curves with test times in log-scale are also plotted to make those of smaller radial distances clearer to see. It should be noted that the curves seem to decrease faster after around 1000 s (Figure 6.9b) but this is due to the time log scale, the real variation of Q with time being much slower than it seems to be in Figure 6.9b.

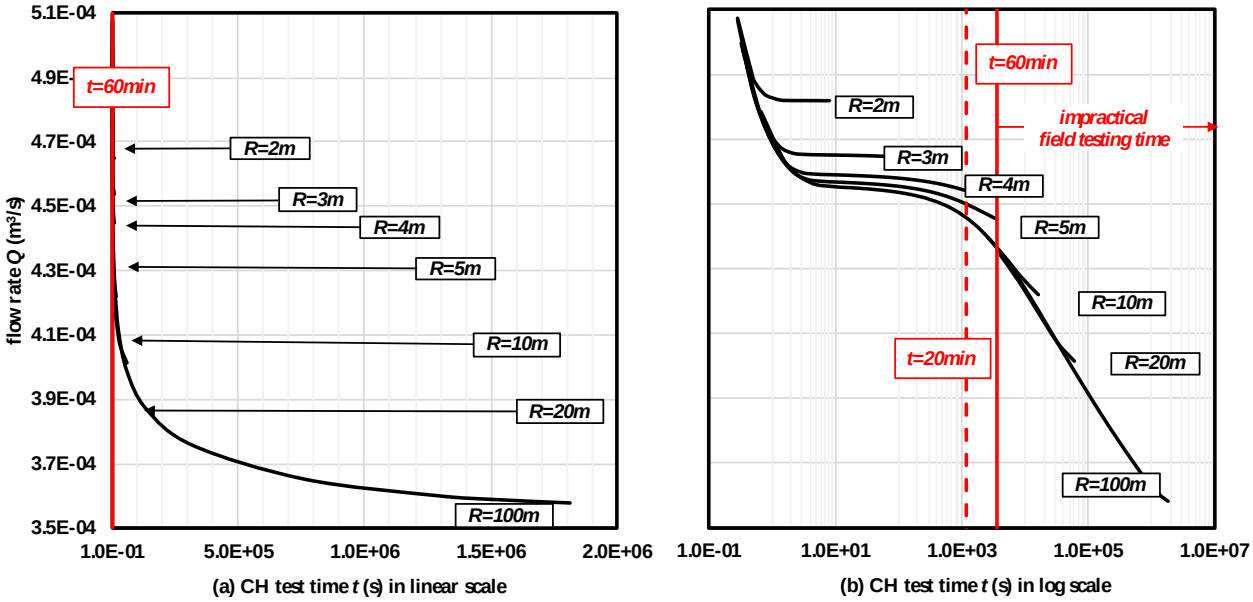

Figure 6.9: Flow rate Q variations in pipe with CH test time t in linear and log scale.

The curves in Figure 6.10 are the hydraulic head (H) variations with time when the CH tests were conducted with a constant flow rate. The tests were stopped when the H (pipe) has a variation less than 1%. If we stop the tests after 2 min, for example, the post-test stabilized hydraulic heads differ from the theoretical equilibrium of 4 m by 0.01-5.4% (R = 2-100 m). The numerical shape factors are slightly different compared to the tests stopped after 20 min, because the specified boundary condition of constant Q (pipe) needs a few minutes to become constant. This is more representative of real field testing conditions. For any boundary radial distance, R, the hydraulic head seems to be stable between 2 and 20 min, usually the longest duration of field tests. Thus, stopping a field tests after a few minutes seems justified, but the numerical analyses indicate that the time t and the R value still have some influence on the hydraulic head, which changes only a little as compared to the change in the first two minutes.

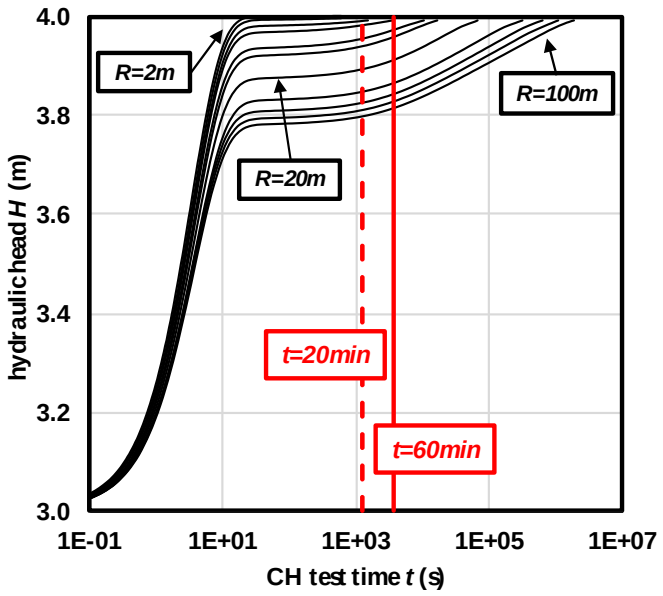

Figure 6.10: Hydraulic head *H* variations in pipe with CH test time *t*.

When the *Q*- or *H*- value reached 99% of the steady-state value, the tests were considered to reach equilibrium, and the corresponding times were defined as the test durations. Figure 6.11 shows the durations of CH tests that were simulated in two ways for different boundary radial distances (black plots). The first boundary condition has a constant *H* difference, and the second has a constant *Q* on the screen. The two ways provide approximately equivalent results, which follow a power function, except for *R* = 2 and 3 m. The reason is that when *R* is smaller than 4 m, the tests reach the set equilibriums faster than when the boundary radial distance is larger. When *H* reaches 3.99 m, it varies from the head difference of 1 m by 1%. Figure 6.10 shows that it is difficult to obtain accurate test duration for *R* = 2 and 3 m because the *H* plot is nearly horizontal when *H* variation < 1%. If we extrapolate the plot, the two test durations at *R* = 2 and 3 m (the two red points) represent the time to reach the equilibrium where where *Q* and *H* values reached 99.5% of the steady-state values.

It is observed from Figures 6.9-6.11 that the test duration, for *R* values exceeding 5 m, exceeds 1 h, which is impractical for field tests. Normally, the CH test takes 20 min maximum based on field experience. Therefore, the boundary radial distances of 2-4 m are the most representative of field conditions. In this range, the difference between the numerical and theoretical shape factors is less than 10% (Figure 6.12). The range of appropriate boundary radial distance maybe different for the second series, but can be analyzed in the same way, and thus is not presented here.

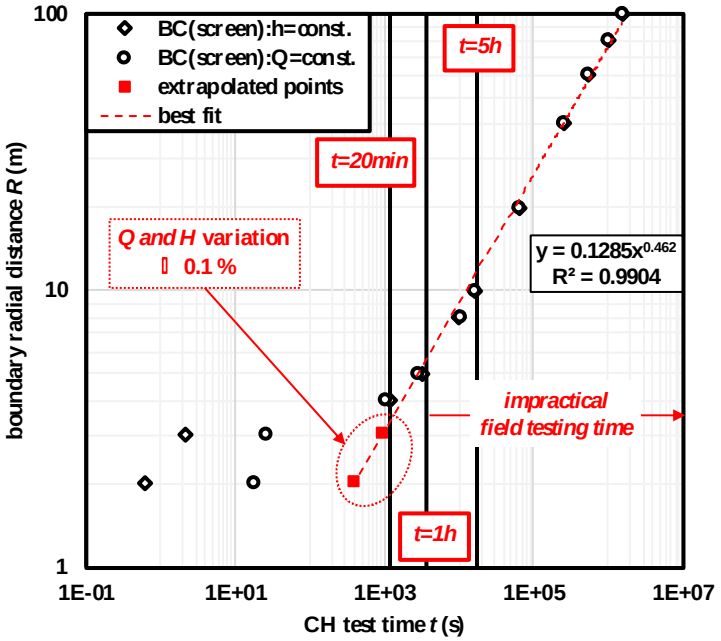

Figure 6.11: CH test times by two simulating methods versus boundary radial distances.

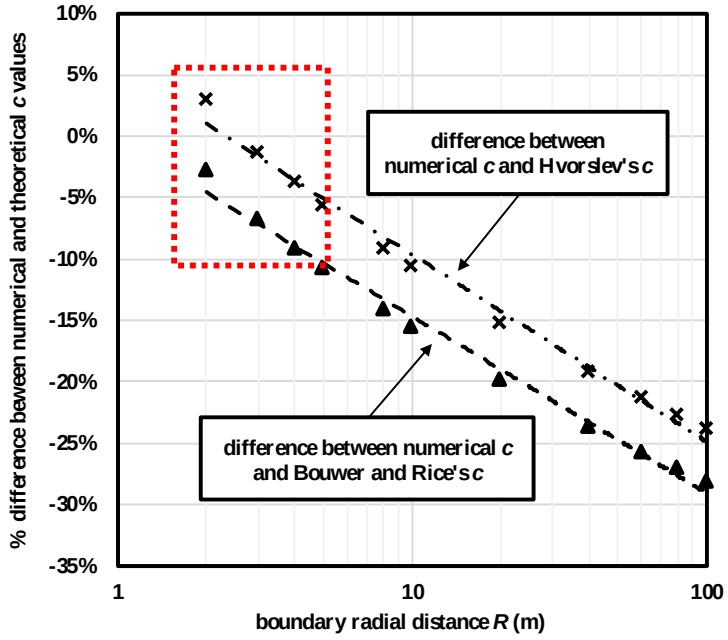

Figure 6.12: Percentage differences between theoretical and numerical shape factors versus boundary radial distances (no filter pack).

The two series of VH tests were influenced similarly by the extended radial distance: they reduced from R = 2 to 8 m and kept constant at further distances. The second series has a filter pack and it yields c values closer to the Hvorslev's c values compared to that of the first series.

At first sight, the shapes of the plots for VH and CH transient shape factors (Figures 6.4 and 6.7) seem similar. However, they represent different meanings: the decreased part from R = 2 to 8 m of the CH transient plot presents steady numerical c values, but the VH plot shows the sensitive c values affected by the varied R. When R > 8 m, the flat part of the VH plot indicates a stable shape factor, whereas the CH transient plot becomes horizontal due to the insufficient test time.

Then the problem arises, "What boundary radial distance should we define for the aquifer model to get correct shape factors or numerical results?" The answers are different for the two types of field permeability tests. For the CH-test model, the first step is to build several trial models with different boundary radial distances, and the second step is to find the one that has similar test duration as the field test. For the VH-test model, the R at which the c value starts to become constant can be chosen as the appropriate R. For different geometries of aquifer models, the representative R may change.

6.5.2 Water injection zone dimension and position influence on shape Factor

6.5.2.1 First series: no filter pack

The different lengths and positions of water injection zones were analyzed for the first-series models with boundary radial distances of 3 m. The theoretical and numerical c values are displayed in Figure 6.13. The Hvorslev's shape factors are 1.79, 2.99, 4.09, and 5.14 m for injection zone lengths of 1, 2, 3, and 4 m, respectively. They do not depend on the position of the water injection zone. Bouwer and Rice's method yield the highest c values. They grow from 1.90 to 6.93 m corresponding to the increased length (from 1 to 4 m) and the rising positions (from lower to upper part of aquifer) of the injection zone. The VH-test c values seem to follow the trend of the Bouwer and Rice's c, ranging from 1.97 to 6.13 m, which are 9 to 49% larger than the Hvorslev' c values. The CH steady and transient shape factors are identical and superpose in the plot. They are close to the Hvorslev's c values but somewhat differ from one another. The c of 1m-M is 13% higher than the Hvorslev's c value, which is the greatest difference.

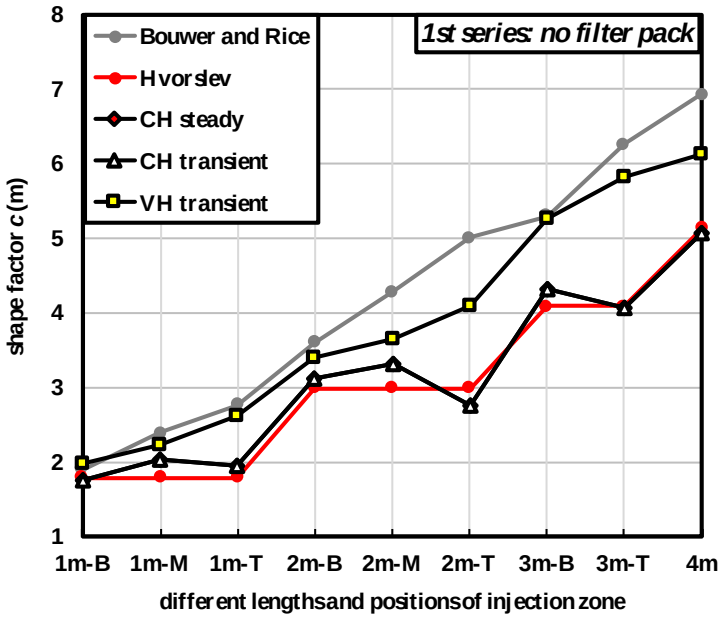

Figure 6.13: Shape factors with regard to different injection zones (no filter pack).

6.5.2.2 Second series: with a filter pack

The shape factor values for the second-series models are presented in Figure 6.14. The Hvorslev's *c* values are 2.44, 3.85, 5.13, and 6.35 when the lengths of filter packs are respectively 1, 2, 3, and 4 m. The numerical *c* values of CH tests under two analyses are equivalent and deviate from the Hvorslev's *c* in the same way as the first-series models do. The largest deviation occurs in model 1m-M, which is 12% higher. The Bouwer and Rice's *c* values are the highest in most cases except the 3m-B, ranging from 2.55 to 8.87 m. The *c* values of VH test increased with the position of the water injection zone from 2.67 to 7.62 m, which are between 6 and 66% higher than the Hvorslev's *c* values.

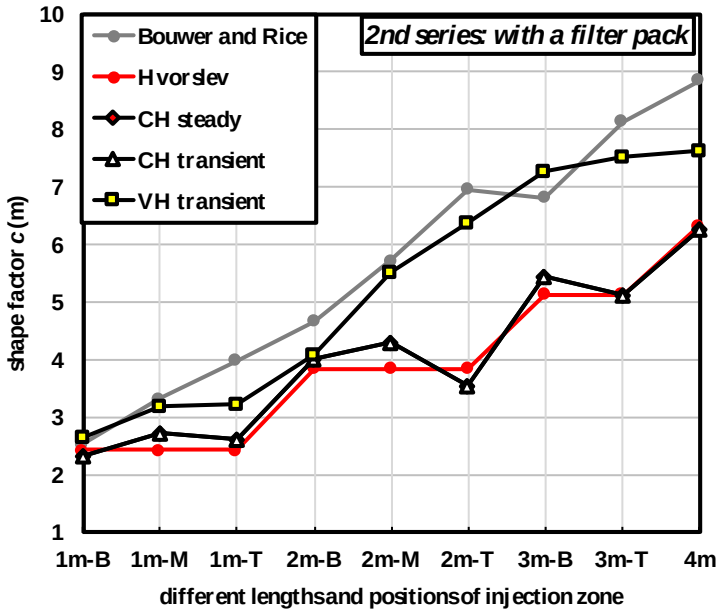

Figure 6.14: Shape factors with regard to different injection zones (with a filter pack).

6.5.2.3 Discussion

For each series of models, the shape factors increase when the lengths of the screen or filter pack increase. The second-series models yield higher *c* values than the first series due to the larger diameter of the water injection zone. The CH-test *c* values for the two series are close to the Hvorslev's *c* values but have slight discrepancies, which is due to the equivalent boundary radial distance defined for altered water injection zones. For each water injection zone, the corresponding *R* should be customized. The VH-test shape factor values approach those of Bouwer and Rice's *c*, therefore are higher than those of the CH tests. Based on the discussion in previous section, a numerically defined *R* value of 3 m is too small for the VH-test models, especially for the water injection zones with 3- or 4-m lengths.

6.5.3 Material influence on numerical shape factors

6.5.3.1 First series: no filter pack

The initial No. 0 sand was replaced by No. 1 to 14 soils that are coarse, medium, fine, loamy sand and silt. The numerical *c* values of models with the 14 aquifer materials are compared with the theoretical shape factors in Figure 6.15. The numerical shape factors of CH tests are 1.77 - 1.78

m, 1% smaller than the Hvorslev's *c* value of 1.79 m when *R* is 3 m for the two series of models. They are also equivalent to that of the initial model with No. 0 sand (1.77 m), which indicates that the aquifer material has no effect on them. The VH test shape factors, ranging from 1.84 to 2.08 m, are more easily affected by the material properties. They are 3 to 16.4 % higher than the Hvorslev's *c* when *R* = 3 m. When *R* increases to 10 m, the VH test *c* values stabilize and decrease by 2-4%.

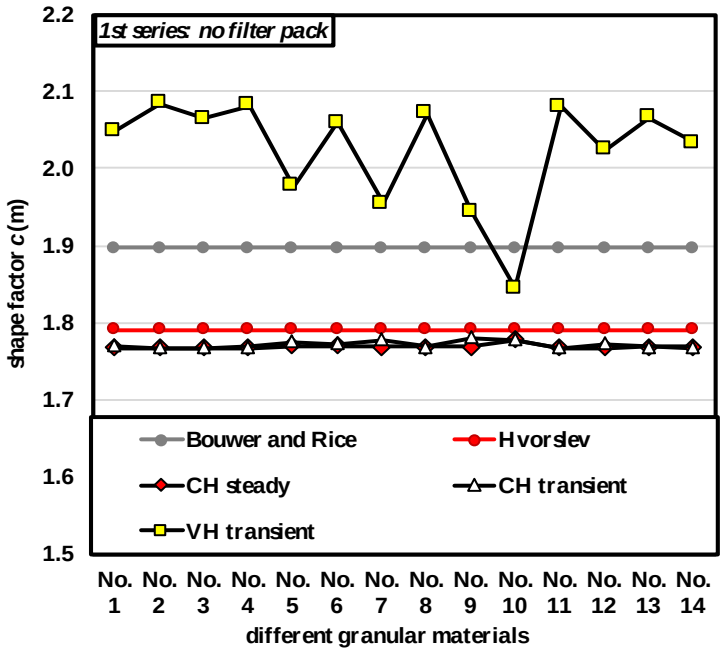

Figure 6.15: Theoretical and numerical shape factors with regard to different materials (no filter pack).

6.5.3.2 Second series: with a filter pack

The filter material is the same for the 14 different aquifers. It has a much higher hydraulic conductivity than those of aquifers. Figure 6.16 presents the *c* values in the same order as the first series. The CH tests of steady-state and transient analyses yield the lowest shape factors values between 2.33 and 2.37 m (nearly constant), 3-5 % less than the Hvorslev's *c* when *R* = 3 m. Similar to the first series, the *c* values of the VH tests vary with the aquifer material. They are between 2.4 to 2.8 m, which increase by 0-15 % compared to the Hvorslev's *c* when *R* = 3 m.

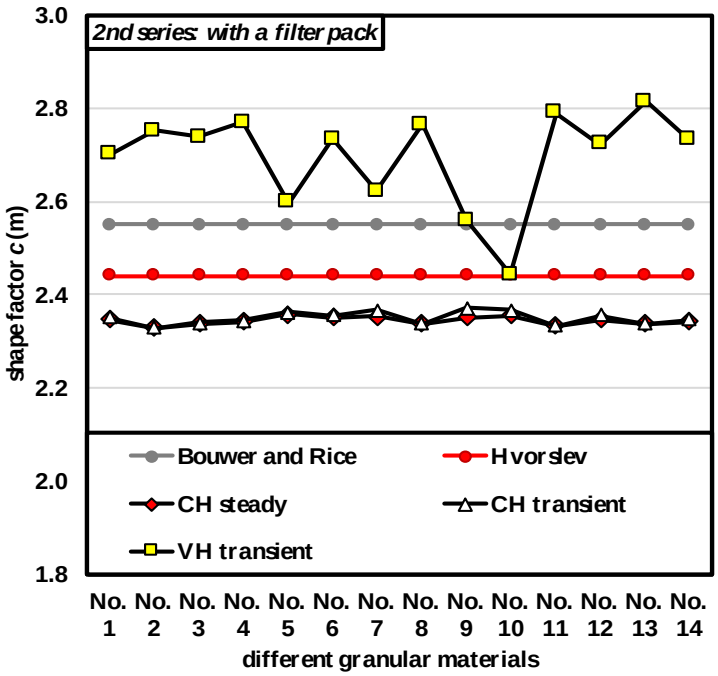

Figure 6.16: Theoretical and numerical shape factors with regard to different materials (with a filter pack).

6.5.3.3 Discussion

The second-series models yield greater *c* values because of the filter pack. The two types of numerical analyses for the CH test gave very close shape factor values for each aquifer material, which implies that the test with a transient analysis reached stabilization for all models with *R* of 3 m. Although the CH transient analyses give nearly constant *c* values for different materials, the time to reach equilibrium for coarser sand is shorter than that for finer sand or silt due to its higher hydraulic conductivity. Figure 6.17 presents the duration of test time versus the aquifer material K_{sat} value. The test is considered as completed when the *Q*- or *H*- value reached 99% of the steady-state value. Thus, aquifer models with different materials need to be defined with different test times and boundary radial distances, which is also a trial-and-error process.

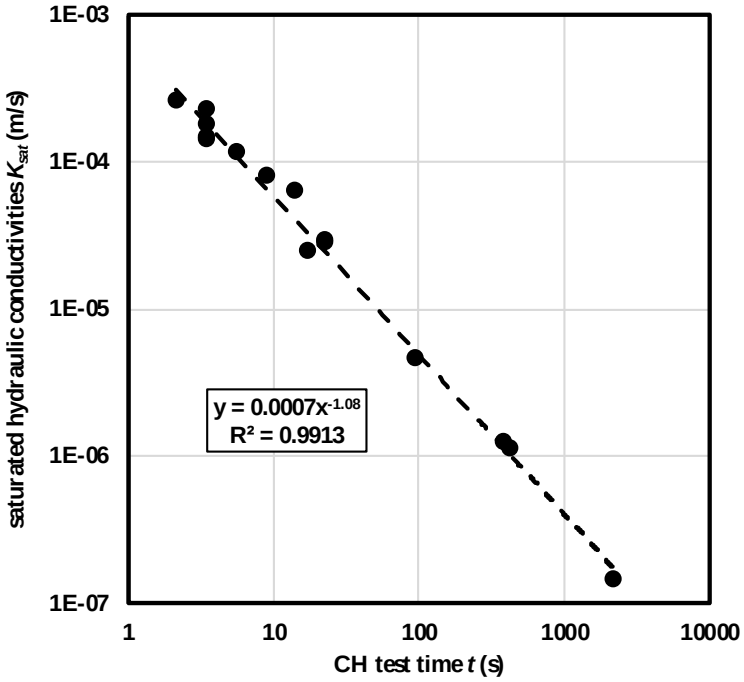

Figure 6.17: Relationship between saturated hydraulic conductivities and CH test time (no filter pack).

The two series of VH-test c values have similar variation trend and show higher sensitivity to different aquifer material properties. The recovery phases of the VH tests were considered to be completed when the water in pipe returned to 3.002~3.004 m, which is around 0.1% different from the pre-test water level (3 m). The recovery time for the first-series model was 27 s for No. 2 Berlin coarse sand, which has the highest K_{sat}, and reached 15 h for the No. 10 silt which is the least permeable. The second-series of VH tests had similar relationship between the test time and the saturated hydraulic conductivity. The only difference is that the second-series VH test of each aquifer material used less time to recover than the corresponding first series due to its high permeable filter pack. The relationship between K_{sat} and VH test time follows a power function (Figure 6.18), from which the VH test time can be deduced for any aquifer material with given K_{sat}.

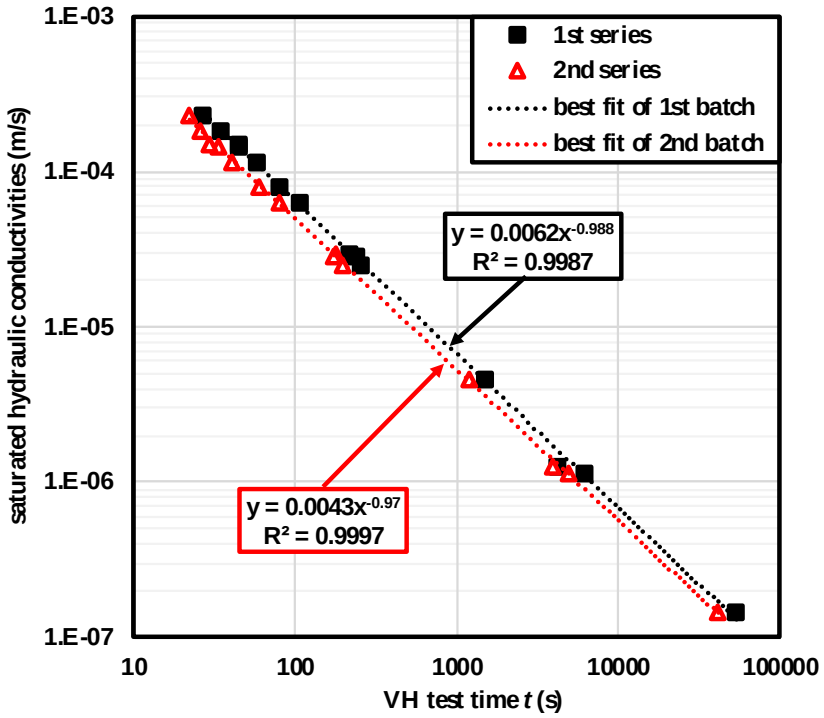

Figure 6.18: Relationship between saturated hydraulic conductivities and VH test time (1st series = no filter pack; 2nd series = filter pack).

When we plot the VH-test *c* values with their corresponding K_{sat} values (Figure 6.19), a linear relationship between the *c* values and log K_{sat} was found. The two series of VH-test shape factors increase nearly in parallel with the increase of the K_{sat} values. The small deviation is due to the slightly different post-test water level (3.002-3.004 m) used in test interpretation. The exact post-test water level is 3 m, which is the initial water level specified in the aquifer. The average difference of the two series VH-test *c* values in Figure 6.19 is 0.67 m, which is close to the Hvorslev's *c* difference between the first and second series: 2.44 – 1.79 = 0.65 m.

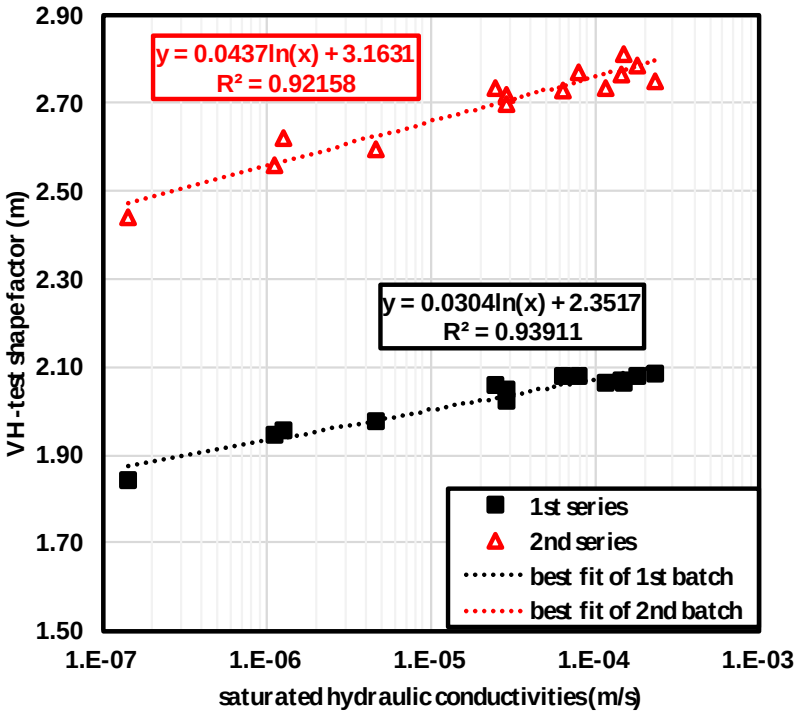

Figure 6.19: Relationship between saturated hydraulic conductivities and VH-test shape factor (1st series = no filter pack; 2nd series = filter pack).

6.6 Summary

The CH and VH tests in unconfined aquifers were numerically simulated using the code Seep/W, from which the numerical values of shape factors were calculated. The CH tests were modelled in steady-state and transient conditions. Each condition was simulated by applying the boundary condition of either a constant head difference or a constant flow rate on screen, which corresponds to the two different ways to conduct the CH test in the field. The steady-state analysis for the CH test results in an equivalent flow rate in pipe and aquifer, which yield a numerical CH steady *c* value. This value is not influenced by aquifer materials for the two-series models, the first with a screen only and the second with a screen surrounded by a filter pack. When the length and diameter of the water injection zone were increased, its shape factor increased. For the fixed length and diameter, the shape factor varies slightly with the rising position of water injection zone, and thus a reduced distance to the unsaturated zone. Among all the variables, the boundary radial distance has the largest influence on the numerical results (up

to 35% for the second series when R = 100 m). The c values decline due to the logarithmically reduced radial gradient. Specifying a large boundary radial distance in a numerical model poorly represents the field conditions and largely increases the computation time.

The shape factors of the CH test with transient analysis are influenced by the material type and altered dimensions and positions of the water injection zone in the same way as the steady-state analysis are, when the equilibrium of the test is reached (test duration is long enough). If not, the c values become invariable rather than decreasing. It indicates one of the differences between the two types of CH-test simulation: the transient analysis requires a much longer computation time. Therefore, if the two types of numerical analyses for the CH test model give different shape factors for each aquifer material, one needs either to apply a longer test time or a smaller boundary radial distance. The test time, however, should be in a realistic range.

Another difference is that the change of hydraulic head and flow rate at any time during the CH test can be known by the transient analysis, which is its superiority compared to the steady-state analysis. If your interest is the steady-state flow rate, to derive the shape factor, or to check the K value, a CH steady-state analysis is the right choice. It is simple and time-saving. If you target at studying the seepage at different times during the test, you need a CH transient analysis. Less permeable materials and larger boundary radial distances need longer testing times, and vice versa. In this case, a long testing time may represent unrealistic field testing conditions, but an inadequate accuracy for a very small pumped flow rate also represents impractical field testing conditions. It is important to note that materials that have a K_{sat} value lower than 10^{-6} m/s are not suitable for a CH test (Zhang et al., 2018b), and those with test duration exceeding 1 hour are uneconomic for field constant-head tests (Figures 6.10-6.11). These are practical recommendations field CH tests.

The VH-test shape factors are affected by the boundary radial distance in a different way. The c values decline first, and then stabilize at larger distances. The invariable numerical c value of the second-series water injection zone is closer to Hvorslev's c values than that of the first series, but the differences are always smaller than 5%. Therefore, in practice, the test may be interpreted using the c value of Hvorslev (1951) with confidence, even if the numerical c-values present a linear small variation ith log K_{sat} for the two series of VH tests.

The recovery time of the VH test and the CH test duration are shorter for the high permeability aquifer material. The two parameters, K_{sat} and t, follow a power function relationship. The functions can be used to deduce the CH and VH test times for any material with a given K_{sat} for a certain series of models.

The boundary radial distance of the aquifer model needs to be carefully specified because it may cause unrealistic results. Several practical recommendations for modelling the CH tests are summarized. The first step is to build several trial models with different radial distance, for example 1, 3, and 5 m (based on the size of the model). The second step is to find the test time that reaches stabilization for each model by observing the variation of flow rate or hydraulic head in transient analysis. And then compare the test duration with the one in practice, to determine a proper range of R values. The radial distance also depends upon the aquifer material properties. A test time is firstly specified as a start, and then adjusted to the proper one by trial and error. The R value of the VH-test model is where the c value starts to be constant.

Additionally, the models with different aquifer materials were built with a single filter material with a much higher permeability. If the screen slots were poorly selected, and if the filter material is changed, the shape factor is changed and also, there is a maximum K_{sat} value that may be correctly measured (Baptiste and Chapuis, 2015) by the tests. When a monitoring well is poorly designed, the complex problem of the resulting shape factor is useless, and it was not investigated for this paper.

CHAPTER 7 GENERAL DISCUSSION

The investigation of several error sources was proposed in the objectives. These are caused by inappropriate calibration of pressure and atmospheric transducers, clogging of the MW screen or erosion of the filter pack during a test, poorly installed MW, imperfect field manipulations and improper boundary radial distances of the numerical aquifer models. They may weaken the reliability of field permeability test, and thus yield inaccurate *K* values. Additionally, different test types and interpretation methods may result in some discrepancies in *K* values. The approaches to check and eliminate these imperfect conditions and their influence on the test results are summarized in this section.

(1) To remove the systematic error caused by barometric variation during the test by calibrating each PT-APT pair on user's desk.

An absolute PT measures the total pressure, equal to the water pressure plus air pressure. An APT registers only the air pressure. When the two types of sensors are put together on user's desk in the air, the difference of PT(t) and APT(t) should be zero in theory and should not vary with time t. In fact, $[PT(t) - APT(t)]_{air}$ normally presents small values fluctuating around zero if the sensors are in good conditions, which is the accuracy of the pair. A total of 32 PTs in five different types were calibrated in this way using an APT. The accuracies of the PT-APT pairs range from ± 6.5 to ± 15 mm, provided by the manufacturer. Each PT-APT pair was started at the same time with identical intervals. It was found that the differences of the 32 pairs were between -11.3 cm and +17.2 cm, which are much larger than the inaccuracies. The large difference defines a systematic calibration error (non-zero offset) for the PT-APT pair. Besides, the difference of several PT-APT pairs presents variations against time. Thus, a test protocol was proposed to remove the systematic error from the apparent water column data, to assess the accuracy and systematic error of the PT-APT pair. The users should first select the appropriate measurement range of transducers for either the groundwater monitoring or field permeability test. The systematic error of the PT-APT pair must be documented and calibrated. The PT-APT pair that has a small difference for $[PT(t)\text{-}APT(t)]_{air}$ gives a better result for the real water column.

(2) To examine how the synchronous monitoring of a PT-APT pair, during a field permeability test, influences the test data accuracy and the resulting *K* value.

For field permeability tests, the calibration for air pressure should not be done with a single APT value for some pre-test time. As the air pressure changes continuously with time during any field test, the synchronous barometric monitoring of APT for each PT is essential to collect the atmospheric and total pressures at the same times. The real water column $H(t)$ is then derived by [PT(t) – APT(t)].

The procedure is essential to obtain reliable test data before doing any data interpretation. For the sandy confined aquifer at a reduced scale, the recovery in the VH tests lasted less than 2 minutes, during which the barometric pressure fluctuation was so small that it did not affect much on the results. Therefore, the synchronous monitoring of the barometric could be neglected for the VH test in relatively high-permeable soils. In such a case, the head difference could be determined by the direct difference of PT(t) and PT(*pretest*). Two examples were provided to illustrate how the variable barometric pressure significantly affects the interpretation of the test results. The first example is a CH test that lasted less than one hour within the laboratory under normal air conditioning and ventilation. In this short duration, the consideration of only a single barometric correction could yield a misunderstanding on the equilibrium state that the CH test had a declined PL and never reached stabilization. Meanwhile, an erroneous K value was obtained. The second example is a rising-head field test in clay lasting for 5 days, with large fluctuations of the barometric pressure. The variations in air pressure were up to 20.5 cm and had similar trends and turning points as the total pressure, which was able to reverse the trend of water column after the subtraction of APT(t) from PT(t). If these variations were ignored, the rising-head test would be regarded as a falling-head test incorrectly. Thus, it is critical to synchronously monitor each PT-APT pair during the test. Additionally, when a single APT correction was used for the rising-head test, the semi-log graph showed zigzag patterns, which could not be interpreted. The synchronized APT calibration smoothed the semi-log plot, which was then linearized by a piezometric correction of 20 cm. It yielded a K value of 6.28×10^{-8} cm/s, which is representative of the tested non-fissured Lachenaie clay.

(3) To check the conditions of the screen and filter pack by conducting field permeability tests with two opposite flows (i.e., rising- and falling-head tests, discharge and injection tests) in the same MWs.

Two field permeability test methods, CH and VH test, were conducted in 33 MWs installed in the confined sand aquifer in a large sand box, confined sand aquifer in Sorel and confined shale rock aquifer in Lachenaie. Each method of the test was performed with either an inward or outward flow: CH test include discharge and injection tests, and VH tests include rising- and falling-head tests. The $H(t)$ was monitored by a pair of PT-APT with intervals of 15 s and 2 s for the CH and VH tests, respectively. Duplicate tests were performed for the VH tests in MWs in the sand box to verify the test results.

In theory, K (tests with outward flow) is equivalent to K (tests with inward flow) due to their identical test mechanisms. That is, K (falling-head test) = K (rising-head test), and K (injection test) = K (discharge test). However, most tests with outward flows (injection/falling-head tests) yielded apparent K values lower than those of the inward flows (discharge/rising-head tests). The reason is that the outward flow from MW to aquifer could move fine sediments at the bottom of the pipe and create tiny gas bubbles that blocked parts of openings in the screen slots or the voids of the filter pack, which resulted in a decreased K value. Also, the inward flow could wash off fine particles and tiny gas bubbles from the filter pack or the adjacent soil, which facilitated the water flow and yielded an increased K value. Oppositely, a few K values by inward flow tests were lower than those by outward flow tests, which occurred mostly in the CH tests. In such cases, particle sizes larger than the screen slots in the filter pack/adjacent soil were carried by the inward flow and blocked outside the screen openings, which caused smaller K values. The phenomena occurred in Lachenaie sites 1, 2 and 6, however, only the particles from filter pack could be displaced to clog the outside of the screen because the adjacent zone is shale rock. The local K value for site 9 is 2 orders of magnitude higher than that measured at three other sites, because the shale of this site was more fissured. The outward water flow carried fine particles through the filter pack, which then could block void spaces in the shale. It explains why the K (rising-head test) was larger than the K (falling-head test). Although there are some discrepancies in K values between the tests with two water flows, the difference was lower than 10% for some MWs, which is negligible, and could reach up to an acceptable value of 45%. Therefore, the screens and filter packs of the three sites were in good condition.

(4) To find the reason for the discrepancy of K values between CH and VH tests in the same MW by studying the connection of the interpretation methods for the two types of tests.

All CH test data in the three confined aquifers were interpreted by the Lefranc's solution under steady state. The entire VH test is in transient state, and its data were analyzed by the Hvorslev's method, whereas the velocity graph and the *Z-t* method were employed to make the piezometric correction if needed. In the same MW, the VH tests yielded *K* values higher than the *K* values obtained from the CH tests. The inconsistency may be due to the difference in the mechanisms of either the interpretation methods or the tests themselves.

The constant head difference H_c of a CH test is generated by continuously pumping water at a constant rate, and the recovery phase begins after the pump is stopped. The steady-state H_c is used to determine the K_{CH} value. However, for a VH test, the initial head difference H_i is caused by an instantaneous water volume change. The H_i and subsequent H values in transient state of the recovery period are employed to calculate the K_{VH} value. Despite of the different ways that generate a head difference before the recovery, i.e., a sudden water volume change for a VH test and a long pumping duration for a CH test, the thesis proved in theory that the Hvorslev's semi-log and velocity plots used to interpret the VH test are also applicable to the recovery phase of the CH test. For two MWs which were correctly installed and manipulated, the K_{VH} values determined from the recovery data of the CH tests are approximately equal to the corresponding K_{CH} values, and the velocity graphs of the recovery data are straight.

It indicates that the interpretation methods for CH and VH are not responsible for the discrepancies in *K* values. The differences in *K* values for the VH and CH tests are due to the two distinct mechanisms of the test methods. For an MW which has a filter pack, the filter material is selected to be more pervious than the aquifer material. A created filter zone is formed at the interface between the filter pack and the adjacent aquifer material during well development or after many times testing. If there is no filter pack around the screen, only a naturally created filter zone is generated against the screen. The created filter zone possesses a higher permeability than the aquifer because the fine particles in the zones are washed away. The VH test has a smaller influence zone compared to the CH test, and thus is easily affected by the created filter zone even though the screen and filter pack are in good condition. That is why in most cases, the VH test yielded a higher *K* value than the CH test. It also explains why the CH tests had a smaller range of variation in *K* than the VH test in the homogenous sand aquifer in the laboratory.

In addition, the recovery data of the CH tests in five poorly-installed MWs were also interpreted by the VH test interpretation methods. The velocity graphs were either scattered or curved and $K_{CH} \neq K_{VH}$. The scattered shapes of the velocity plots are due to the high pumping rate, which may have created high parasitic head losses against the screen. Therefore, the semi-log and velocity graphs can be used as supplementary methods to compare with the Lefranc's solution, to check the general performance of the screen by comparing the K_{VH} with the K_{CH}. Even though the semi-log graphs appear to be straight, it is recommended to plot the velocity graph and optimize the original semi-log graph. If the velocity is not straight and K_{VH} greatly differs from K_{CH}, it indicates a poorly designed/installed MW or improper test operation, for example, the screen is partially immersed before the test, the aquifer is dewatering down to the screen during the test, the head losses are important close the screen, the pumping rate is too high for a CH test.

(5) To verify the reliability of field hydraulic conductivity by comparing the results of CH and VH tests and provide recommendations for the choice of the test method.

The VH and CH tests provided different *K* values in the same MW, the former frequently yielded higher *K* due to its smaller influence zone, and however, the difference in the two types of *K* values was small. Thus, the values derived from the two testing methods are both acceptable and may be used to assess the aquifer permeability. If the CH and VH tests are performed in the same MW and yield different *K* values, the *K* (CH tests) values are more representative, because they are derived from the tests which have a larger influence area and longer test duration. If a pump is not available or the aquifer has a low permeability, it is recommended to perform the falling- and rising-head tests to examine if the screen and filter pack are in good condition.

The hydraulic head for a good CH test normally rises or declines in the first few minutes and then reach equilibrium. When the pump is shut off, the recovery time is also short. Sometimes, however, the CH tests may have difficulties in reaching equilibrium even if the MW has a good performance. Firstly, the PT-APT pair must be calibrated before each test to determine its systematic error and make sure its non-zero offset does not vary with time. During the test, the sensor pair must be monitored synchronously, to remove the systematic error caused by barometric pressure variations. Secondly, a proper pumping rate should be applied for the CH test, which can be obtained by trial-and-error tests for aquifers with different permeabilities. A low flow rate may generate a too small head difference in the MW pipe. However, a high

discharge or injection rate may cause migration of soilds and hydraulic damage, important head loss along the inside pipe and against the screen, or increase the CH test time. An impervious boundary condition may affect the CH test, and it should be known before the test. If it occurs, the test data for a MW close to an impervious boundary requires extra treatment.

The sudden water level change is initiated in a few seconds and the VH tests last a few minutes in sand aquifers, and longer in less permeable materials. Compared to the CH tests, the VH tests are less time consuming, thus can be carried out as a preliminary step to evaluate the permeability for an unknown layer. The test results indicate that it takes too much time to perform a CH test when the K value is lower than 10^{-6} m/s, even with a small discharge or injection rate. In such cases, a VH test is recommended. When $K > 10^{-4}$ m/s, a constant flow rate of a few hundred of cm^3/min may be used for the CH test, and the recording interval for the PT and APT should be 1 s or 0.5 s for a VH test because the water level in the MW increases or decreases very rapidly.

(6) To simulate the CH and VH tests via numerical code, through which numerical values of shape factors of various cases are evaluated and the proper boundary radial distance of the aquifer model are determined.

Except for the CH and VH tests conducted in real confined aquifers, the two test methods in unconfined aquifers were also presented numerically using the code Seep/W. All tests were conducted in axisymmetric unconfined aquifer models with MWs of two series: one series had a screen and no filter pack; the other had a filter pack around the screen. The CH tests were modelled for the steady-state and transient analyses. CH tests were simulated by two approaches, specifying either a constant head difference or a constant flow rate on the screen as the boundary condition, which corresponds to the two different ways to conduct the CH test in the field. They yielded similar numerical results.

The flow rates in pipe and aquifer are equivalent for the steady-state CH test, which deduced a numerical shape factor c. This value was not affected by aquifer materials for the two-series models, but it increased with the increase of the length and diameter of the water injection zone. When the length and diameter are fixed, the c value has a slight change when the position of the injection zone rises. The boundary radial distance R had an important influence on the c values. The c values declined continuously due to the reduced radial gradient.

The varied aquifer materials and altered dimensions and positions of the water injection zone affected the *c* values of the transient CH test in the same pattern as the steady-state CH test. The prerequisite is that the test must reach equilibrium, which requires a long enough test time. Otherwise, the CH test is incomplete and the *c* values stop declining and become constant. Compared to the numerical simulation of the steady-state CH test, the transient analysis is time-consuming, but it provides a better visualization of seepage property of any point at any time. If the transient analysis of a CH test is complete, the numerical results including the derived *c* values should be the same. Therefore, one needs either to apply longer test time or smaller *R* to the test model if the results of the two analyses are different. However, a long testing time may be unrealistic compared to the corresponding field conditions. The users may choose the proper CH test model based on their own needs.

The VH tests were modelled with the transient analysis. The deduced shape factors were affected by *R* differently. They reduced rapidly at the beginning and stabilized at larger *R* values. The stabilized *c* values of the two series differed by less than 5% from the Hvorslev's *c* values. Besides, the VH test showed more sensitivity to various aquifer materials and altered injection zone positions.

The test times for the CH and VH tests in less permeable materials are longer, and vice versa. The K_{sat} and *t* followed a power function, which could be used to assess the CH and VH test durations for any material with a given K_{sat}. Additionally, specifying a large *R* in a numerical model also largely increases the test and computation times, which poorly represents the field conditions.

Several practical steps to simulate the field permeability tests and define the appropriate *R* values were provided. The trial models with several different *R* values should be first built. The variations of flow rate or hydraulic head in transient CH test are observed to determine the time that is needed to reach steady state. The *R* value of the model for which the determined time is equal to the one in the field is regarded as the representative boundary size. The representative *R* of the VH-test model is determined where the *c* value becomes invariable.

It is not recommended to perform a CH test in materials with a K_{sat} value lower than 10^{-6} m/s. Also, a test duration exceeding 1 hour is uneconomic for CH tests. Some realistic test duration, a

proper flow rate, and an appropriate boundary radial distance must be defined by trial and error processes.

It should be noted that citations in text, captions of tables and figures and equations were adapted, in order to be consistent for the thesis and have a single format. The context of the thesis may have some differences compare to the final published papers.

CHAPTER 8 CONCLUSION AND RECOMMENDATIONS

8.1 Conclusion

The thesis includes the analyses of the calibration of pressure transducers, condition of the MW screen/filter pack, field manipulations and installation, different test types and interpretation methods, and numerical simulation of aquifer models, before and during a field permeability test. It aims at improving the test reliability and the accuracy of hydraulic conductivity by removing or minimizing the errors occurred in these analyses. Based on the purpose of the research, the conclusions are summarized below:

- The PT and APT yielded different measurements when they were put on user's desk to register the air pressure under the same condition. Unlike the theory of $[PT(t) - APT(t)]_{air} = 0$, the non-zero difference of PT(t) and APT(t) was much larger than the accuracy provided by the manufacturer and sometimes varied with time. The large difference indicates the systematic calibration error for the PT-APT pair, which affects the accuracy of water column measurements. Therefore, it must be removed before either a groundwater monitoring or field permeability test. A simple test protocol was proposed to remove the systematic error: (1) select the appropriate measurement range of PT and APT; (2) record and calibrate the systematic error of each PT-APT pair; (3) choose the pair that has a smaller difference of $[PT(t)-APT(t)]_{air}$.
- Due to the continuous variations in air pressure during any field tests, the inappropriate monitoring of a PT-APT pair can cause great errors in the interpretation of a field permeability test and thus yield an inaccurate K value. The inappropriate monitoring includes monitoring the PT with a single APT (*pretest*) value, and unsynchronized monitoring of the PT-APT pair. The direct subtraction of PT(t) and PT (*pretest*) may also lead to mistakes because the change of atmospheric pressure during the test is ignored. The test results indicated that the synchronous monitoring of the barometric could only be neglected for the VH test in relatively high-permeable soils. For the CH tests in sand or the long-duration VH tests in clay, a single APT value significantly influence the accuracy of the test results and resulting K values. Thus, the synchronous barometric

monitoring of APT for each PT must be implemented to collect the atmospheric and total pressures. The real water column $H(t)$ is then derived by [PT(t) – APT(t)].

- The CH and VH test were performed with either an inward or outward flow. In theory, for either a CH or VH test, K (outward flow) = K (inward flow) because their test mechanisms are identical. In practice, however, most K (outward flow) < K (inward flow), because the outward flow generated by an injection/rising-head test may move fine sediments at the MW bottom and create tiny gas bubbles, which blocks parts of the screen openings or voids of the filter pack. The inward flow created by a discharge/falling-head test may wash off fine particles and tiny gas bubbles from the filter pack or the adjacent soil, which facilitated the water flow and resulted in an increased K value. However, in a few cases, the K (inward flow) < K (outward flow). It is due to that the inward flow moves particles that have larger sizes than the screen slots, the outside screen openings are blocked. As a result, the conditions of the screen and filter pack can be simply checked by conducting the field permeability tests with two opposite flows in the same MWs. The discrepancies in K values between the tests with two water flows were all acceptable for the three sites, which indicates that the screens and filter packs are in good condition.
- In the same MW, the K (VH tests) values were always larger than the K (CH tests). The discrepancy is found to be caused by the different test mechanisms. A created filter zone is formed at the interface between the filter pack and the adjacent aquifer material during well development or after many times testing. If there is no filter pack, a naturally created filter zone is generated against the screen. The created filter zone is usually more permeable than the aquifer because the fine particles in the zones are washed away. The VH test has a smaller influence zone than the CH test, as a result, it is easier to be affected by the created filter zone even though the screen and filter pack are in good condition and thus presents a higher K value.
- The different interpretation methods are not responsible for the different K values obtained from the CH and VH tests in the same MW. Theoretically, the Hvorslev's semi-log and velocity graphs used to interpret the VH test were proved to be applicable to the recovery phase of the CH test. Experimentally, the two VH-test interpretation methods

were used to analyze the real test data and the derived K_{VH} values are equivalent to the K_{CH} values (calculated by the Lefranc's solution) for the MWs correctly installed and manipulated, and the velocity plots of the recovery data are straight. However, for the poorly-installed MWs or poorly-manipulated tests, the velocity graphs were either scattered or curved and the $K_{CH} \neq K_{VH}$. Therefore, for a CH test, the semi-log and velocity graphs can also be employed together with the Lefranc's solution, to indicate the general condition of the design/installation of an MW.

- The thesis provides some practical recommendations for selecting the test method. The VH and CH test results imply that the two test methods are both acceptable, however, if they are performed in the same MW, the K (CH tests) values are more representative, because they are derived from the tests which have a larger influence area and longer test duration. A VH test is recommended if a pump is not available or the aquifer has a low permeability ($K < 10^{-6}$ m/s), which is necessary to be done with inward and outward flows to examine if the screen and filter pack are in good condition. Additionally, it is more efficient than a CH test, thus can be functioned as a preliminary test to evaluate the permeability for an unknown layer. When $K > 10^{-4}$ m/s, a CH test needs a relatively large flow rate (a few hundred of cm^3/min) to create an obvious head difference, and a VH test requires a small recording interval (1 s or 0.5 s) because the water level in the MW varies very rapidly.

- A good CH test reaches equilibrium in a few minutes and has a short recovery time. When the CH test shows difficulties in achieving a stabilization, several steps should be checked: (1) the PT-APT pair must be correctly calibrated before the test and synchronously monitored during the test; (2) the discharge/injection rate should be a proper value based on several trial-and-error tests for different aquifers; (3) the impervious boundary should be at a far distance from the tested MW so that it does influence the test results.

- Numerical ways to model field permeability tests and to deduce the shape factor in unconfined aquifers were presented, under steady- and transient-states, with partly unsaturated seepage. The CH test simulated by specifying either a constant head difference or a constant flow rate on screen as the boundary condition yields similar

numerical results. The numerical results of the CH tests with transient and steady-state analyses are the same when the transient analysis reach equilibrium. The transient analysis is much more time-consuming, however, provides a better visualization of seepage property of any point at any time than the steady-state analysis. Therefore, one needs either to apply longer test time or smaller boundary radial distance to the test model if the results of the two analyses are different. However, a long testing time may be unrealistic compared to the corresponding field conditions. The users may choose the proper CH test model based on their own needs.

- The influences of four variables (the radial distance of the external boundary, dimensions and positions of the water injection zone, and aquifer material type) on the numerical *c* values were studied. For a CH test, the *c* value is not affected by aquifer materials and increases with the increase of the length and diameter of the water injection zone. When the length and diameter are fixed, the *c* value has a slight change when the position of the injection zone rises. The VH test is more sensitive to different aquifer materials and varied injection zone positions. The boundary radial distance *R* remarkably affects the numerical *c* value. Therefore, practical recommendations were proposed by reconciling the numerical and realistic test conditions, to determine the representative *R*-value for the test model. Several trial models with different *R* values should be built. The times that reach the steady state were then determined for the models. The *R*-value of the test model that has a time equivalent to the one in field condition is regarded as a representative boundary size. The representative *R* of the VH-test model is determined where the *c* value becomes invariable. The variables influence the two series of models, either with or without a filter pack, in the same way.

- The test times for the CH and VH tests are longer in less permeable materials. The K_{sat} and *t* followed a power function, from which the test duration of the CH and VH tests for any material with a given K_{sat} can be estimated. Specifying a large *R* in a numerical model considerably increases the test and computation times, which poorly represents the field conditions. The test duration exceeding 1 hour are uneconomic for CH tests. A realistic test duration, a proper flow rate, and an appropriate boundary radial distance must be defined by trial and error processes.

8.2 Limitations and Recommendations

As the condition of the screens/filter packs of the three sites was good, the differences of the *K* values between the inward and outward flow tests were relatively small, which made the physical explanation less convincing. If the tests were done with a well screen and/or a filter pack in poor condition, the difference in *K* values would be more important. Therefore, we can plan to install a clogged screen or poor filter material to better prove the phenomena in the future.

The K_{CH} values in the dissertation were mostly by the Lefranc's solution applicable to the CH test data in steady state. It used the time-drawdown method to interpret the pumping phase of the CH tests which did not reach equilibrium. Additionally, it used the Hvorslev's and velocity graph methods to interpret the CH recovery phase, which was compared with the Lefranc's solution. However, these interpretation methods were not applied to all test data. A systematic analysis and comparison of the transient-state results interpreted by different methods and the steady-state results for the CH test are needed to be implemented.

The practical way to numerically evaluate the shape factor for the cylindrical injection zone was presented, via the code Seep/W. The boundary radial distance of the aquifer was considered to be finite in numerical models, whereas the theoretical *c* values were derived for an infinite medium, and no curving-fitting equation was proposed. The numerical shape factor will be analyzed in the infinite medium, from which the proposed equation will be compared with the theoretical solutions previously reviewed. For the second series of models, only a single filter material with a much higher permeability was specified for various aquifer materials. For a low *K* value of the filter material, the shape factors may be different, which has not been checked in the thesis. In addition, the numerical CH and VH tests can also be simulated in confined aquifers.

BIBLIOGRAPHY

AFNOR NF P94-132. (1992). *Essai d'eau Lefranc*. Paris, France: AFNOR.

AFNOR NF P94-132 (2000). *Sols: Reconnaissance et essais - essai d'eau Lefranc*. Paris, France: AFNOR (Replaced by ISO 22282-2).

Al-Dhahir, Z. A., & Morgenstern, N. R. (1969). Intake factors for cylindrical piezometer tips. *Soil Science, 107*(1), 17-21.

Ardejani, F. D., Badii, K., Limaee, N. Y., Mahmoodi, N. M., Arami, M., Shafaei, S. Z., & Mirhabibi, A. R. (2007). Numerical modelling and laboratory studies on the removal of Direct Red 23 and Direct Red 80 dyes from textile effluents using orange peel, a low-cost adsorbent. *Dyes and Pigments, 73*(2), 178-185.

Ariza, P. 2002. *Evaluation of water flow through pavement systems* (Master thesis).

ASTM D2434. (2006). *Standard test method for permeability of granular soils (Constant Head)*. West Conshohocken, PA: ASTM.

ASTM D4044. (2015). *Standard test method (field procedure) for instantaneous change in head (slug) tests for determining hydraulic properties of aquifers*. West Conshohocken, PA: ASTM.

ASTM D4050. (2014). *Standard test method (field procedure) for withdrawal and injection well tests for determining hydraulic properties of aquifers*. West Conshohocken, PA: ASTM.

ASTM D4106. (2015). *Standard test method for (analytical procedure) for determining transmissivity and storage coefficient of nonleaky confined aquifers by the theis nonequilibrium method*. West Conshohocken, PA: ASTM.

ASTM D5084. (2016). *Standard test methods for measurement of hydraulic conductivity of saturated porous materials using a flexible wall permeameter*. West Conshohocken, PA: ASTM.

Aubertin, M., Mbonimpa, M., Bussière, B., & Chapuis, R. P. (2003). A model to predict the water retention curve from basic geotechnical properties. *Canadian Geotechnical Journal, 40*(6), 1104-1122.

Avci, C. B. (1994). Analysis of in situ permeability tests in nonpenetrating wells. *Groundwater, 32*(2), 312-322.

Baptiste, N., & Chapuis, R. P. (2015). What maximum permeability can be measured with a monitoring well? *Engineering Geology*, *184*, 111-118.

Bell, F. G. (2014). *Engineering geology and construction*. CRC Press.

Benabdallah, E. M. (2010). *Mouvement des eaux souterraines et des ions majeurs dans une argile Champlain depuis sa formation* (Doctoral dissertation, École Polytechnique de Montréal).

Bishop, A. W., Kennard, M. F., & Penman, A. D. M. (1960). Pore pressure observations at Selset dam. *Pore pressure and suction in soils*, 91-102.

Bjerrum, L., & Anderson, K. H. (1972). *In situ measurement of lateral pressures in clay*. Proceedings of the 5th European Conference of the I.S.S.M.F.E., Madrid, 1, 11- 20.

Bjerrum, L., Nash, J. K. T. L., Kennard, R. M., & Gibson, R. E. (1972). Hydraulic fracturing in field permeability testing. *Géotechnique*, *22*(2), 319-332.

Bouwer, H., & Rice, R. C. (1976). A slug test for determining hydraulic conductivity of unconfined aquifers with completely or partially penetrating wells. *Water resources research*, *12*(3), 423-428.

Bouwer, H. (1989). The Bouwer and Rice slug test—an update. *Groundwater*, *27*(3), 304-309.

Brand, E. W., & Premchitt, J. (1980a). Shape factors of cylindrical piezometers. *Géotechnique*, *30*(4), 369-384.

Brand, E. W., & Premchitt, J. (1980b). Shape factors of some non-cylindrical piezometers. *Géotechnique*, *30*(4), 536-537.

Brand, E. W., & Premchitt, J. (1982). Response characteristics of cylindrical piezometers. *Géotechnique*, *32*(3), 203-216.

Bredehoeft, J. D., & Papadopulos, S. S. (1980). A method for determining the hydraulic properties of tight formations. *Water Resources Research*, *16*(1), 233-238.

Brillant, J. (1966). La mesure in situ des perméabilités locales. *Géotechnique*, *16*(1), 33-52.

Bromhead, E. N. (1996). Interpretation of constant head in situ permeability tests in soil zones of finite extent. *Géotechnique*, *46*(1), 133-143.

Butler, J. J., & Hyder, Z. (1994). An Assessment of the Nguyen and Finder Method for Slug Test Analysis. *Groundwater Monitoring & Remediation*, *14*(4), 124-131.

Cain III, S. F., Davis, G. A., Loheide II, S. P., & Butler Jr, J. J. (2004). Noise in pressure transducer readings produced by variations in solar radiation. *Groundwater*, *42*(6), 939-944.

Cambefort, H. (1987). Grouts and grouting. *Ground Engineer's Reference Book*, *32*, 1-32.

Canadian Geotechnical Society. (1978). *Canadian foundation engineering manual*. Vancouver, BC: BiTech.

CAN/BNQ 2501-130. (2014). *Soils - Determination of permeability at the end of a casing*. Ottawa, ON: National Standard of Canada.

CAN/BNQ 2501-135. (2008). *Soils - Determination of permeability by the Lefranc method*. Ottawa, ON: National Standard of Canada.

CAN/BNQ 2501-135. (2014). *Soils - Determination of permeability by the Lefranc method*. Ottawa, ON: National Standard of Canada.

Cardenas, M. B., & Zlotnik, V. A. (2003). A simple constant-head injection test for streambed hydraulic conductivity estimation. *Groundwater*, *41*(6), 867-871.

Cassan, M. (1980). *Les essais d'eau dans la reconnaissance des sols*. Paris, France: Eyrolles.

Cassan, M. (2000). Application des essais Lefranc à l'évaluation du coefficient d'anisotropie hydraulique des sols aquifères. *Revue Française de Géotechnique*, (90), 25-43.

Cassan, M. (2005). *Les essais de perméabilité sur site dans la reconnaissance des sols*. Paris, France: Presses des Ponts.

Çelik, B., Rowe, R. K., & Ünlü, K. (2009). Effect of vadose zone on the steady-state leakage rates from landfill barrier systems. *Waste Management*, *29*(1), 103-109.

Chapuis, R. P. (1988). Determining whether wells and piezometers give water levels or piezometric levels. In Collins, A. G., & Johnson, A. I. (Eds.), *Ground-Water Contamination: Field Methods*: *ASTM STP 963* (pp. 162-171). Philadelphia, PA.

Chapuis, R. P. (1989). Shape factors for permeability tests in boreholes and piezometers. *Groundwater*, *27*(5), 647-654.

Chapuis, R. P. (1990). Sand–bentonite liners: predicting permeability from laboratory tests. *Canadian Geotechnical Journal*, *27*(1), 47-57.

Chapuis, R. P. (1992a). Using Cooper-Jacob Approximation to Take Account of Pumping Well Pipe Storage Effects in Early Drawdown Data of a Confined Aquifer. *Groundwater*, *30*(3), 331-337.

Chapuis, R. P. (1992b). Fracturing pressure of soil ground by viscous materials: discussion. S*oils and Foundations*, *32*(3), 174-175.

Chapuis, R. P. (1998). Overdamped slug test in monitoring wells: review of interpretation methods with mathematical, physical, and numerical analysis of storativity influence. *Canadian Geotechnical Journal*, *35*(5), 697-719.

Chapuis, R. P. (1999a). *Guide des essais de pompage et leurs interprétations*. Québec, QC: Ministère de l'environnement.

Chapuis, R. P. (1999b). Borehole variable-head permeability tests in compacted clay liners and covers. *Canadian Geotechnical Journal*, *36*(1), 39-51.

Chapuis, R. P. (2001). Extracting piezometric level and hydraulic conductivity from tests in driven flush-joint casings. *Geotechnical Testing Journal*, *24*(2), 209-219.

Chapuis, R. P. (2004). Predicting the saturated hydraulic conductivity of sand and gravel using effective diameter and void ratio. *Canadian geotechnical journal*, *41*(5), 787-795.

Chapuis, R. P. (2005). Numerical modeling of rising-head permeability tests in monitoring wells after lowering the water level down to the screen. *Canadian geotechnical journal*, *42*(3), 705-715.

Chapuis, R. P. (2005). Using the velocity graph method to interpret rising-head permeability tests after dewatering the screen. *Geotechnical Testing Journal*, *28*(3), 305-312.

Chapuis, R. P. (2009a). Permeability or hydraulic conductivity tests in a monitoring well: why are piezometric level corrections required. *Geotechnical News*, *27*(2), 46-49.

Chapuis, R.P. (2009b). Variable head permeability tests in monitoring wells: comparing the shape factor defined by Bouwer and rice (1976) to the shape factor given by Hvorslev (1951). *Geotechnical News*, *27*(1), 41-43.

Chapuis, R. P. (2009c). Numerical modeling of reservoirs or pipes in groundwater seepage. *Computers and Geotechnics*, *36*(5), 895-901.

Chapuis, R. P. (2010a). Influence of element size in numerical studies of seepage: large-scale or regional studies. *Geotechnical News*, *28*(4), 31-34.

Chapuis, R. P. (2010b). Using a leaky swimming pool for a huge falling-head permeability test. *Engineering Geology*, *114*(1-2), 65-70.

Chapuis, R. P. (2012a). Predicting the saturated hydraulic conductivity of soils: a review. *Bulletin of engineering geology and the environment*, *71*(3), 401-434.

Chapuis, R. P. (2012b). Improved curve fitting methods for underdamped slug tests. *Geotechnical Testing Journal*, *35*(5), 752-761.

Chapuis, R. P. (2012c). Influence of element size in numerical studies of seepage: small-scale details. *Geotechnical News*, *30*(1): 32-35.

Chapuis, R. P. (2012d). Influence of element size in numerical studies of seepage: unsaturated zones, steady-state. *Geotechnical news*, *30*(3): 27-30.

Chapuis R. P. (2012e). Influence of element size in numerical studies of seepage: unsaturated zones, transient conditions. *Geotechnical News*, *30*(4): 34-37.

Chapuis, R. P. (2015). Overdamped slug tests in aquifers: the three diagnostic graphs for a user-independent interpretation. *Geotechnical Testing Journal*, *38*(4), 474-489.

Chapuis, R. (2016). *Extracting Information from Grain Size Distribution Curves*. Montreal, QC: Geotics.

Chapuis, R. P. (2017). Stress and strain fields for overdamped slug tests in aquifer materials, and resulting conservation equation. *International Journal for Numerical and Analytical Methods in Geomechanics*, *41*(18), 1908-1921.

Chapuis, R. P., (2019). Disagreeing evaluations for slug tests in monitoring wells: importance of standards. *Geotechnical Testing Journal*, in print.

Chapuis, R. P., & Aubertin, M. (2001). A simplified method to estimate saturated and unsaturated seepage through dikes under steady-state conditions. *Canadian Geotechnical Journal*, *38*(6), 1321-1328.

Chapuis, R. P., Bélanger, C., & Chenaf, D. (2006). Pumping test in a confined aquifer under tidal influence. *Groundwater*, *44*(2), 300-305.

Chapuis, R. P., & Chenaf, D. (1998). Detecting a hydraulic short circuit along a monitoring well with the recovery curve of a pumping test in a confined aquifer: method and example. *Canadian geotechnical journal*, *35*(5), 790-800.

Chapuis, R. P., & Chenaf, D. (2002). Slug tests in a confined aquifer: experimental results in a large soil tank and numerical modeling. *Canadian Geotechnical Journal*, *39*(1), 14-21.

Chapuis, R. P., & Chenaf, D. (2003a). Variable-head field permeability tests in driven flush-joint casings: physical and numerical modeling. *Geotechnical Testing Journal*, *26*(3), 245-256.

Chapuis, R. P., & Chenaf, D. (2003b). Effects of monitoring and pumping well pipe capacities during pumping tests in confined aquifers. *Canadian geotechnical journal*, *40*(6), 1093-1103.

Chapuis, R. P., & Chenaf, D. (2010). Driven Field Permeameters: Reinventing the wheel? *Geotechnical News*, *28*(1), 37.

Chapuis, R. P., Chenaf, D., Acevedo, N., Marcotte, D., & Chouteau, M. (2005b). Unusual drawdown curves for a pumping test in an unconfined aquifer at Lachenaie, Quebec: field data and numerical modeling. *Canadian geotechnical journal*, *42*(4), 1133-1144.

Chapuis, R. P., Chenaf, D., Bussière, B., Aubertin, M., & Crespo, R. (2001). A user's approach to assess numerical codes for saturated and unsaturated seepage conditions. *Canadian Geotechnical Journal*, *38*(5), 1113-1126.

Chapuis, R. P., Dallaire, V., Gagnon, F., Marcotte, D., & Chouteau, M. (2007). Falling-head permeability tests in an unconfined sand aquifer. *Geotechnical Testing Journal*, *30*(2), 104-112.

Chapuis, R. P., Dallaire, V., Marcotte, D., Chouteau, M., Acevedo, N., & Gagnon, F. (2005a). Evaluating the hydraulic conductivity at three different scales within an unconfined sand aquifer at Lachenaie, Quebec. *Canadian Geotechnical Journal*, *42*(4), 1212-1220.

Chapuis, R. P., Dallaire, V., & Saucier, A. (2014). Getting information from modal decomposition of grain size distribution curves. *Geotechnical Testing Journal*, *37*(2), 282-295.

Chapuis, R. P., & Duhaime, F. (2017). Taking into account data accuracy for interpretation of slug tests in confined or unconfined aquifers. *Geotechnical Testing Journal*, *40*(1), 122-133.

Chapuis, R. P., Masse, I., Madinier, B., & Duhaime, F. (2015). Water-retention curves of coarse soils without organic matter: Improved data for improved predictions. *Geotechnical Testing Journal*, *38*(3), 325-337.

Chapuis, R.P., Paré, J.J., and Lavallée, J.G. (1981). *In situ variable head permeability tests*. Proceedings of the 10th International Conference on Soil Mechanics and Foundation Engineering, Stockholm, 1, 401-406.

Chapuis, R. P., & Sabourin, L. (1989). Effects of installation of piezometers and wells on groundwater characteristics and measurements. *Canadian Geotechnical Journal*, *26*(4), 604-613.

Chapuis, R. P., Soulié, M., & Sayegh, G. (1990). Laboratory modelling of field permeability tests in cased boreholes. *Canadian Geotechnical Journal*, *27*(5), 647-658.

Chesnaux, R., Chapuis, R. P., & Molson, J. W. (2006). A New Method to Characterize Hydraulic Short-Circuits in Defective Borehole Seals. *Groundwater*, *44*(5), 676-681.

Chesnaux, R., & Elliott, A. P. (2011, August). *Demonstrating evidence of hydraulic connections between granular aquifers and fractured rock aquifers*. Proceedings of GeoHydro 2011, Joint Meeting of the Canadian Quaternary Association and the Canadian Chapter of the International Association of Hydrogeologists (pp. 28-31).

Chiasson, P. (2005). Methods of interpretation of borehole falling-head tests performed in compacted clay liners. *Canadian Geotechnical Journal*, *42*(1), 79-90.

Chiasson, P. (2012). Interpretation of Falling-Head Tests in Presence of Random Measurement Error. *ISRN Civil Engineering*, 1, 1-10.

Chu-Agor, M. L., Wilson, G. V., & Fox, G. A. (2008). Numerical modeling of bank instability by seepage erosion undercutting of layered streambanks. *Journal of Hydrologic Engineering*, *13*(12), 1133-1145.

Clark, J. E., Germond, B. J., & Bennett, K. C. (1983). *Aquifer test monitoring by electrical pressure transducer in comparison with the hand-held tape method* (No. DE83-006491). Marietta, GA: Law Engineering Testing Co.

Clark, L., & Turner, P. A. (1983). Experiments to assess the hydraulic efficiency of well screens. *Groundwater*, *21*(3), 270-281.

Cooper, H. H., & Jacob, C. E. (1946). A generalized graphical method for evaluating formation constants and summarizing well-field history. *Transactions American Geophysical Union*, *27*(4), 526-534.

Cooper, H. H., Bredehoeft, J. D., & Papadopulos, I. S. (1967). Response of a finite-diameter well to an instantaneous charge of water. *Water Resources Research*, *3*(1), 263-269.

Dachler, R. (1936). *Grundwasserstromung* (*Flow of groundwater*). Vienna, Austria: Julius Springer.

Dallaire, V. (2004). *Étude des effets d'échelle dans un aquifère alluvionnaire* (Master thesis).

Dhouib, A., Shahrour, I., Lafhaj, Z., & Delfaut, A. (1998). Essais Lefranc pour la mesure de la perméabilité in situ: étude théorique et interprétation pratique. *Revue Française de Géotechnique*, (84), 27-36.

Dowd, J. F., & Williams, A. G. (1989). Calibration and use of pressure transducers in soil hydrology. *Hydrological processes*, *3*(1), 43-49.

Driscoll, F. G. (1986). *Groundwater and wells*. St. Paul, MN: Johnson Filtration Systems Inc.

Duhaime, F., Benabdallah, E. M., & Chapuis, R. P. (2013). The Lachenaie clay deposit: some geochemical and geotechnical properties in relation to the salt-leaching process. *Canadian Geotechnical Journal*, *50*(3), 311-325.

Duhaime, F., and Chapuis, R. P. (2009). *Some numerical experiments with the finite element method to determine the shape factors for field permeability tests*. Proceedings of the 62nd Canadian Geotechnical Conference. Halifax, NS, 1302–1309.

Fetter, C. W. (2001). *Applied hydrogeology*. Upper Saddle River, NJ: Prentice-Hall.

Foroutan, R. (2002). *Intake Shape Factors for Transversely Isotropic Porous Media* (Doctoral dissertation, McGill University Libraries).

Forsythe, G. E., & Wasow, W. R. (1960). Finite-Difference Methods for Partial Differential Equations. New York, NY: Wiley.

Freeman, L. A., Carpenter, M. C., Rosenberry, D. O., Rousseau, J. P., Unger, R., & McLean, J. S. (2004). Use of submersible pressure transducers in water-resources investigations. *US Geological Survey, Techniques of Water-Resources Investigations*, *8*, A3.

Freeze, R.A., and Cherry, J.A. (1979). *Groundwater*. Englewoods Cliffs, NJ: Prentice-Hall.

GEO-SLOPE International Ltd. (2012). *Seepage Modeling with SEEP/W*. Calgary, AB: GEO-SLOPE International, Ltd.

Gibson, R. E. (1963). An analysis of system flexibility and its effect on time-lag in pore-water pressure measurements. *Géotechnique, 13*(1), 1-11.

Gibson, R. E. (1966). A note on the constant head test to measure soil permeability in situ. *Géotechnique*, *16*(3), 256-259.

Gibson, R. E. (1970). An extension to the theory of the constant head in situ permeability test. *Géotechnique*, *20*(2), 193-197.

GSI Environnement (2001). Étude Géotechnique-Agrandissement du Secteur Nord, Lots Parties 77 à 87, 90, 93, 94, 99 et 100-BFI Usine de Triage Lachenaie Ltée (N/D: 293-2549-151). Montreal, QC.

Guo, J., Yu, J., Dong Y., and Deng C. (2007). Analysis of seepage and stability for the clay core dam of LongJing reservoir. *Journal of Engineering Geology, 6.*

Harza, L. F. (1935). Uplift and seepage under dams on sand. *Trans. of ASCE, 100,* 1352-1406.

Haverkamp, R., Zammit, C., Bouraoui, F. (1997). *Grizzly soil data bank, base de données de paramètres caractéristiques des sol*s. Grenoble, France: LTHE.

He, Y., Meng, J., & Liu, X. (2008). Analysis of seepage stability of earth-rock dam with clay core under ascending and descending water table conditions. *Engineering Journal of Wuhan University*, *41*(5).

Herzog, B. L. (1994). *Slug tests for determining hydraulic conductivity of natural geologic deposits*. Proceedings of the Symposium on Hydraulic Conductivity and Waste Contaminant Transport in Soil. Philadelphia, PA: ASTM.

Holbo, H. R., Harr, R. D., & Hyde, J. D. (1975). A multiple-well, water-level measuring and recording system. *Journal of Hydrology*, *27*(3-4), 199-206.

Houti, F. B. *Chapter 5: Les principaux moyens de reconnaissance* (Course note). Retrieved from https://ft.univ-tlemcen.dz/assets/uploads/pdf/departement/gc/houti/Chapitre-5-LES-PRINCIPAUX-MOYENS-DE-RECONNAISSANCE.pdf

Hvorslev, M. J. (1951). *Time lag and soil permeability in ground-water observations* (Bulletin 36). Vicksburg, MS: U.S. Army Engineering Waterways Experimental Station.

Hyder, Z., Butler, J. J., McElwee, C. D., & Liu, W. (1994). Slug tests in partially penetrating wells. *Water Resources Research, 30*(11), 2945-2957.

ISO. (2009). *Hydrometry-Measuring the water level in a well using automated pressure transducer methods* (ISO/TR 23211). Geneva, Switzerland.

ISO 22282-2. (2014). *Geotechnical investigation and testing - Geohydraulic testing - Part 2: Water permeability tests in a borehole using open systems*. Geneva, Switzerland: ISO.

Istok, J. D., & Dawson, K. J. (1991). *Aquifer testing: design and analysis of pumping and slug tests*. CRC Press.

Jin, S. W., Choo, Y. W., Kim, Y. M., & Kim, D. S. (2014). Seepage Characteristics of a Buttressed Embankment with a Low Permeable Foundation: Centrifuge and Numerical Studies. *Transactions of the ASABE, 57*(2), 463-477.

Kallstennius, T., & Wallgren, A. (1956). *Pore water pressure measurement in field investigations*. In Swedish Geotechnical Institute Proc.

Keeland, B. D., Dowd, J. F., & Hardegree, W. S. (1997). Use of inexpensive pressure transducers for measuring water levels in wells. *Wetlands Ecology and Management, 5*(2), 121-129.

Kipp, K. L. (1985). Type curve analysis of inertial effects in the response of a well to a slug test. *Water Resources Research, 21*(9), 1397-1408.

Klammler, H., Hatfield, K., Nemer, B., & Mathias, S. A. (2011). A trigonometric interpolation approach to mixed-type boundary problems associated with permeameter shape factors. *Water Resources Research, 47*(3).

Klammler, H., Nemer, B., & Hatfield, K. (2014). Effect of injection screen slot geometry on hydraulic conductivity tests. *Journal of Hydrology, 511*, 190-198.

Kosugi, K. I. (1994). Three-parameter lognormal distribution model for soil water retention. *Water Resources Research, 30*(4), 891-901.

Kovács, G. (1981). *Seepage hydraulics*. Amsterdam, Netherlands: Elsevier.

Kruseman, G. P., & de Ridder, N. A. (1994). *Analysis and evaluation of pumping test data.* Wageningen, Netherlands: International Institute for Land Reclamation and Improvement.

Lafhaj, Z. (1998). *Détermination de la perméabilité des sols in situ: étude expérimentale et numérique du facteur de forme* (Doctoral dissertation).

Lafhaj, Z., & Shahrour, I. (2000). Use of the boundary element method for the analysis of permeability tests in boreholes. *Engineering analysis with boundary elements*, *24*(9), 695-698.

Lafhaj, Z., & Shahrour, I. (2002a, October) *Interprétation de l'essai Lefranc dans un sol partiellement saturé*. Journées Nationales de Géotechnique et de Géologie de l'Ingénieurs (JNGG), Nancy, France.

Lafhaj, Z., & Shahrour, I. (2002b). Use of the electric analogy for the determination of the shape factor in complex soil conditions. *International Journal of Physical Modelling in Geotechnics*, *2*(4), 39-44.

Lafhaj, Z., & Shahrour, I. (2004). Détermination de l'anisotropie de perméabilité des sols par l'essai Lefranc. *Revue Française de Géotechnique*, (109), 99-103.

Lafhaj, Z., & Shahrour, I. (2006). Influence of the presence of a partially saturated layer on the interpretation in field permeability tests. *Mechanics Research Communications*, *33*(4), 568-575.

Lefebvre, G., Philibert, A., Bozozuk, M., & Paré, J. J. (1981). *Fissuring from hydraulic fracture of clay soil*. Proceedings of the 10th International Conference on Soil Mechanics and Foundation Engineering, Stockholm, 2, 513-518.

Lefranc, E. (1936). Procédé de mesure de la perméabilité des sols dans les nappes aquifères et application au calcul du débit des puits. *Le Génie Civil*, *109*(15), 306-308.

Lefranc, E. (1937). La théorie des poches absorbantes et son application à la détermination du coefficient de perméabilité en place et au calcul du débit des nappes d'eau. *Le Génie Civil*, *111*(20), 409-413.

Leij, F. J., Alves, W. J., Van Genuchten, M. T., Williams, J. R. 1996. *The UNSODA unsaturated soil hydraulic database* (EPA/600/R-96/095). Version 1.0. Cincinnati, OH: US Environmental Protection Agency, National Risk Management Research Laboratory.

Lowther, G. (1978). A note on Hvorslev's intake factors. *Géotechnique*, *28*(4), 465-466.

Luthin, J. N., & Kirkham, D. (1949). A piezometer method for measuring permeability of soil in situ below a water table. *Soil Science*, *68*(5), 349-358.

MacVicar, T. K., & Walter, M. F. (1984). An electronic transducer for continuous water level monitoring. *Transactions of the ASAE*, *27*(1), 105-109.

Mahboub, K. C., Liu, Y., Allen, D. L. (2003). *Seepage analysis and study on slope stability of subgrade pavement under rainfall condition* (KTC-03-32/SPR207-00-1F). Frankfort, KY: Kentucky Transportation Cabinet.

Mandel, J. (1939). Note sur le calcul des infiltrations. *Annales des Ponts et Chaussées, Juillet*, 57-110.

Marefat, V., Duhaime, F., & Chapuis, R. P. (2015). Pore pressure response to barometric pressure change in Champlain clay: Prediction of the clay elastic properties. *Engineering Geology*, *198*, 16-29.

Mata Mena, C. (2003). *Hydraulic behaviour of bentonite based mixtures in engineered barriers: the backfill and plug test at the Äspö Hrl* (Doctoral dissertation).

Mathias, S. A., & Butler, A. P. (2006). An improvement on Hvorslev's shape factors. *Géotechnique*, *56*(10), 705-706.

Mathias, S. A., & Butler, A. P. (2007). Shape factors for constant-head double-packer permeameters. *Water resources research*, *43*(6).

Mbonimpa, M., Aubertin, M., & Bussière, B. (2006). Predicting the unsaturated hydraulic conductivity of granular soils from basic geotechnical properties using the modified Kovács (MK) model and statistical models. *Canadian Geotechnical Journal*, *43*(8), 773-787.

McElwee, C. D. (2001). Application of a nonlinear slug test model. *Groundwater*, *39*(5), 737-744.

McElwee, C. D., & Zenner, M. A. (1998). A nonlinear model for analysis of slug-test data. *Water Resources Research*, *34*(1), 55-66.

McLaughlin, D. L., & Cohen, M. J. (2011). Thermal artifacts in measurements of fine-scale water level variation. *Water Resources Research*, *47*(9).

Meiri, D. (1989). A tracer test for detecting cross contamination along a monitoring well column. *Groundwater Monitoring & Remediation*, *9*(2), 78-81.

Mieussens, C., & Ducasse, P. (1977). Mesure en place des coefficients de perméabilité et des coefficients de consolidation horizontaux et verticaux. *Canadian Geotechnical Journal*, *14*(1), 76-90.

Milligan, V. (1975). *Field measurement of permeability in soil and rock*. Proceedings of ASCE Conference on In Situ Measurement of Soil Properties. Raleigh, NC, 2, 3-36.

Monnet, J. (2015). *In situ tests in geotechnical engineering*. John Wiley & Sons.

Mualem, Y. (1976). A catalogue of the hydraulic properties of unsaturated soils. Development of methods, tools and solutions for unsaturated flow with application to watershed hydrology and other fields. Research Project 442. Haifa, Israel: Technion Israel Inst Technol.

Neuzil, C. E. (1982). On conducting the modified 'slug'test in tight formations. *Water Resources Research*, *18*(2), 439-441.

Nguyen, V., & Pinder, G. F. (1984). Direct calculation of aquifer parameters in slug test analysis. *Groundwater Hydraulics*, 222-239.

Nielsen, D. M., & Schalla, R. (2005). Design and installation of ground-water monitoring wells. In D. M. Nielsen (Ed.), *Practical Handbook of Ground-Water Monitoring* (pp. 639-806). Boca Raton, FL: CRC Press.

Olson, R. E., & Daniel, D. E. (1981). Measurement of the hydraulic conductivity of fine-grained soils. In *Permeability and groundwater contaminant transport*. ASTM International.

Papadopulos, S. S., Bredehoeft, J. D., & Cooper, H. H. (1973). On the analysis of 'slug test'data. *Water Resources Research*, *9*(4), 1087-1089.

Paul, D. G. (1987). *The effect of construction, installation, and development techniques on the performance of monitoring wells in fine-grained glacial tills* (Master thesis).

Randolph, M. F. & Booker, J. R. (1982). *Analysis of seepage into a cylindrical permeameter*. Proceedings of the 4th International Conference on Numerical Methods in Geomechanic, Edmonton, 1, 349-357.

Rat, M., Laviron, F., & Jorez, J. C. (1970). Essai Lefranc. *Bulletin de Liaison des Laboratoires Routiers. No. spécial N*, 56-66.

Ratnam, S., Soga, K., & Whittle, R. W. (2001). Revisiting Hvorslev's intake factors using the finite element method. *Géotechnique*, *51*(7), 641-645.

Raymond, G. P., & Azzouz, M. M. (1969). Permeability determination for predicting rates of consolidation. *In situ investigations in soils and rocks*, 285-293. London: Institution of Civil Engineers.

Reynolds, W. D. (2015). A generalized variable-head borehole permeameter analysis for saturated, unsaturated, rigid or deformable porous media. *Engineering Geology*, *185*, 10-19.

Richard, S. K., Chesnaux, R., & Rouleau, A. (2016). Detecting a Defective Casing Seal at the Top of a Bedrock Aquifer. *Groundwater*, *54*(2), 296-303.

Richard, S. K., Chesnaux, R., Rouleau, A., Morin, R., Walter, J., & Rafini, S. (2014). Field evidence of hydraulic connections between bedrock aquifers and overlying granular aquifers: examples from the Grenville Province of the Canadian Shield. *Hydrogeology journal*, *22*(8), 1889-1904.

Ritchey, J. D. (1986). Electronic sensing devices used for in situ ground water monitoring. *Groundwater Monitoring & Remediation*, *6*(2), 108-113.

Ross, B. (1985). *Theory of the oscillating slug test in deep wells*. Memoirs of the 17th International Congress on the Hydrogeology of Rocks of Low Permeability, 17(2), 44-51.

Schneebeli, G. (1954). *La mesure in situ de la perméabilité d'un terrain*. Comptes-rendus des 3ièmes journées d'hydraulique, *Alger*, 270-279.

Schneebeli, G. (1966). *Hydraulique souterraine*. Paris, France: Eyrolles.

Selvadurai, A. P. S. (2003). Intake shape factors for entry points in porous media with transversely isotropic hydraulic conductivity. *International Journal of Geomechanics*, *3*(2), 152-159.

Selvadurai, A. P. (2004). Fluid intake cavities in stratified porous media. *Journal of Porous Media*, *7*(3), 1-17.

Shuter, E., & Johnson, A. I. (1961). *Evaluation of equipment for measurement of water level in wells of small diameter* (Geological Survey Circular 453). US Dept. of the Interior, Washington, DC.

Silvestri, V., Bravo-Jonard, C., & Abou-Samra, G. (2011). A note on Hvorslevs shape factor for a flush bottom piezometer in uniform soil. *Geomechanics and Engineering*, *3*(2), 109-116.

Silvestri, V., Abou-Samra, G., & Bravo-Jonard, C. (2012). Shape factors of cylindrical piezometers in uniform soil. *Groundwater*, *50*(2), 279-284.

Silvestri, V., Bravo-Jonard, C., & Abou-Samra, G. (2013). A Note on the Validity of Hvorslev's Shape Factors for Well Points and Piezometers. *Geotechnical Testing Journal*, *36*(1), 138-145.

Smiles, D. E., & Youngs, E. G. (1965). Hydraulic conductivity determinations by several field methods in a sand tank. *Soil Science*, *99*(2), 83-87.

Sorensen, J. P., & Butcher, A. S. (2011). Water Level Monitoring Pressure Transducers—A Need for Industry-Wide Standards. *Groundwater Monitoring & Remediation*, *31*(4), 56-62.

Taylor, D. (1948). *Fundamentals of soil mechanics*. Chapman and Hall, Limited.; New York.

Tavenas, F., Diene, M., & Leroueil, S. (1990). Analysis of the in situ constant-head permeability test in clays. *Canadian Geotechnical Journal*, *27*(3), 305-314.

Terzaghi, K. (1943). *Theoretical soil mechanics*. New York, NY: John Wiley & Sons.

Theis, C. V. (1935). The relation between the lowering of the Piezometric surface and the rate and duration of discharge of a well using ground-water storage. *Transactions American Geophysical Union*, *16*(2), 519-524.

Todd, D. K., & Mays, L. W. (2005). *Groundwater hydrogeology*. New York, NY: John Willey & Sons.

Uffink, G. J. M. (1984). *Theory of the oscillating slug test*. Unpublished Research Report. Bilthoven, Netherlands: National Institute for Public Health and Environmental Hygiene.

United States Bureau of Reclamation. (1960). *Earth manual*. First Edition.

United States Bureau of Reclamation. (1990). *Earth manual*. Part 2: A water resources technical publication. Third Edition

Von Asmuth, J. R., Maas, K., Bakker, M., & Petersen, J. (2008). Modeling time series of ground water head fluctuations subjected to multiple stresses. *Groundwater*, *46*(1), 30-40.

Van der Kamp, G. (1976). Determining aquifer transmissivity by means of well response tests: The underdamped case. *Water Resources Research*, *12*(1), 71-77.

Van Genuchten, M. T. (1980). A closed-form equation for predicting the hydraulic conductivity of unsaturated soils 1. *Soil science society of America journal*, *44*(5), 892-898.

Weber Jr, W. G. (1968). In situ permeabilities for determining rates of consolidation. *Highway Research Record*, (243).

Weight, W. D., & Sonderegger, J. L. (2001). *Manual of applied field hydrogeology*. McGraw-Hill.

Wendling, G., Chapuis, R. P., & Gill, D. E. (1997). Quantifying the effects of well development in unconsolidated material. *Groundwater*, *35*(3), 387-399.

Wilkinson, W. B. (1968). Constant head in situ permeability tests in clay strata. *Géotechnique*, *18*(2), 172-194.

Yang, Y. J., & Gates, T. M. (1997). Wellbore skin effect in slug-test data analysis for low-permeability geologic materials. *Groundwater*, *35*(6), 931-937.

Youngs, E. G. (1980). Discussion: A Note on Hvorslev's intake factors. *Géotechnique*, *30*(3), 328-331.

Zhang, L., Chapuis, P. R., & Marefat, V. (2015). *Constant-Head Permeability Tests Performed in Monitoring Wells at Laboratory Scale*. The 68th Canadian Geotechnical Conference. Quebec, QC.

Zhang, L., & Chapuis, P. R. (2018). *Plausible variable-head tests initiated with continuous pumping in monitoring wells*. The 71st Geotechnical Conference. Edmonton, AB.

Zhang, L., Chapuis, P. R., & Marefat, V. (2018a). Field permeability tests: importance of calibration and synchronous monitoring for barometric pressure sensors. *Geotechnical Testing Journal*. In press.

Zhang, L., Chapuis, P. R., & Marefat, V. (2018b). Field Permeability Tests with Inward and Outward Flow in Confined Aquifer. *Geotechnical Testing Journal*. Under review.

Zurbuchen, B. R., Zlotnik, V. A., & Butler, J. J. (2002). Dynamic interpretation of slug tests in highly permeable aquifers. *Water Resources Research, 38*(3).